CRANFIELD UNIVERSITY

**Cesar Celis**

# EVALUATION AND OPTIMISATION OF ENVIRONMENTALLY FRIENDLY AIRCRAFT PROPULSION SYSTEMS

SCHOOL OF ENGINEERING

PhD THESIS

CRANFIELD UNIVERSITY

SCHOOL OF ENGINEERING

DEPARTMENT OF POWER AND PROPULSION

PhD THESIS

Academic Year: 2007-2010

**Cesar Celis**

# EVALUATION AND OPTIMISATION OF ENVIRONMENTALLY FRIENDLY AIRCRAFT PROPULSION SYSTEMS

Supervisors: Dr. Vishal Sethi

Professor Riti Singh

Professor Pericles Pilidis

April 2010

This thesis is submitted in partial fulfilment of the requirements for the degree of Doctor of Philosophy

# Abstract

In this globalised world where the efficient transportation of people and goods greatly contributes to the development of a given region or country, the aviation industry has found the ideal conditions for its development, thereby becoming in one of the fastest growing economic sectors during the last decades. The continuing growth in air traffic and the increasing public awareness about the anthropogenic contribution to global warming have meant that environmental issues associated with aircraft operations are currently one of the most critical aspects of commercial aviation. Several alternatives for reducing the environmental impact of aircraft operations have been proposed over the years, and they broadly comprise reductions in the number of aircraft operations, changes in the type of aircraft, and changes in the aircraft operational rules and procedures. However, since the passenger traffic is expected to increase over the next years, only the last two options seem to be the most feasible solutions to alleviate the problem. Accordingly, the general aim of this research work is to develop a methodology to evaluate and quantify aircraft/engines design trade-offs originated as a consequence of addressing conflicting objectives such as low environmental impact and low operating costs. More specifically, it is an objective of this work to evaluate and optimise both aircraft flight trajectories and aircraft engine cycles taking into account multidisciplinary aspects such as performance, gaseous emissions, and economics.

In order to accomplish the objectives proposed in this project, a methodology for optimising aircraft trajectories has been initially devised. A suitable optimiser with a library of optimisation algorithms, Polyphemus, has been then developed and/or adapted. Computational models simulating different disciplines such as aircraft performance, engine performance, and pollutants formation, have been selected or developed as necessary. Finally, several evaluation and optimisation processes aiming to determine optimum and ‘greener’ aircraft trajectories and engine cycles have been carried out and their main results summarised. In particular, an advanced, innovative gaseous emissions prediction model that allows the reliable calculation of emissions

trends from current and potential future aircraft gas turbine combustors has been developed. When applied to a conventional combustor, the results showed that in general the emission trends observed in practice were sufficiently well reproduced, and in a computationally efficient manner for its subsequent incorporation in optimisation processes. For performing the processes of optimisation of aircraft trajectories and engine cycles, an optimiser (Polyphemus) has also been developed and/or adapted in this work. Generally the results obtained using Polyphemus and other commercially available optimisation algorithms presented a satisfactory level of agreement (average discrepancies of about 2%). It is then concluded that the development of Polyphemus is proceeding in the correct direction and should continue in order to improve its capabilities for identifying and efficiently computing optimum and 'greener' aircraft trajectories and engine cycles, which help to minimise the environmental impact of commercial aircraft operations.

The main contributions of this work to knowledge broadly comprise the following: (i) development of an environmental-based methodology for carrying out both aircraft trajectory optimisation processes, and engine cycle optimisation-type ones; (ii) development of both an advanced, innovative gas turbine emissions prediction model, and an optimiser (Polyphemus) suitable to be integrated into multi-disciplinary optimisation frameworks; and (iii) determination and assessment of optimum and 'greener' aircraft trajectories and aircraft engine cycles using a multi-disciplinary optimisation tool, which included the computational tools developed in this work. Based on the results obtained from the different evaluation and optimisation processes carried out in this research project, it is concluded that there is indeed a feasible route to reduce the environmental impact of commercial aviation through the introduction of changes in the aircraft operational rules and procedures and/or in the aircraft/engine configurations. The magnitude of these reductions needs to be determined yet through careful consideration of more realistic aircraft trajectories and the use of higher fidelity computational models. For this purpose, the computations will eventually need to be extended to the entire fleet of aircraft, and they will also need to include different operational scenarios involving partial replacements of old aircraft with new environmentally friendly ones.

# Acknowledgments

First of all, I would like to extend my gratitude to my supervisors, Dr V. Sethi, Professor R. Sigh, and Professor P. Pilidis, for their dedicated guidance and support throughout the entire research project. I also wish to express my thanks to all Cranfield University's Researchers and Professors, in particular to Professor P. Pilidis and Professor K. Ramsden from the Department of Power and Propulsion, who gave me the opportunity to pursue my PhD degree at Cranfield University.

I am indebted to my mother Crescencia, my wife Antonia Olivania, my brother Juan Luis, and all my family in general for all their love and understanding that I do not know how to describe it in words. But what I do know is that without their support and encouragement, the completion of this project and other ones that I have undertaken in my life could have been in serious risks.

I also want to thank to the Programme Alβan, the European Union Programme of High Level Scholarships for Latin America; and to the Department of Power and Propulsion at Cranfield University, for the funding and support provided for the development of this research project.

Last, but not least, I would like to express my enormous gratitude to all the colleagues and friends that I have met in Cranfield for the beautiful moments shared during all these years of study at Cranfield University. In particular, I would like to extend my gratitude to both Mr. Hasan Zolata, who using commercially available optimisation algorithms produced some of the results showed here, and Mr. Richard Long, for his time and patience during our long discussions about aircraft trajectory optimisation.

Dedicated to my beloved wife Antonia Olivania…

# List of Contents

# List of Figures

# List of Tables

# Notations

| Symbol | Definition | Unit |
|---|---|---|
| A | Flow area | $m^2$ |
| Alt | Altitude | m |
| $A_{noz}$ | Engine nozzle area | $m^2$ |
| $A_s$ | Surface area | $m^2$ |
| a | Speed of sound** | m/s |
| | Oxygen reaction order (depending on oxygen molar fraction)** | - |
| | Constant factor** | - |
| BPR | Bypass Ratio | - |
| b | Degree of non-uniformity | - |
| CAS | Calibrated Airspeed | m/s |
| CDT | Compressor Delivery Temperature | K |
| CDTTO | Compressor Delivery Temperature at Take Off | K |
| COT | Combustor Outlet Temperature | K |
| c | Number of constraints | - |
| D | Drag | N |
| d | Diameter (of soot particles) | nm |
| EAS | Equivalent Airspeed | m/s |
| EI | Emission Index(indices) | g/kg fuel |
| $E_{ac}$ | Aircraft (kinematic) energy | J |
| $E_{path}$ | Path dependent energy | J |
| $E_{req}$ | Required energy | J |
| eval(X) | Evaluation function | - |
| F | Multi-objective function | - |
| FAR | Fuel-air-ratio | kg fuel/kg air |
| FN | Net thrust | kN |
| FPA | Flight Path Angle | deg |
| FPR | Fan Pressure Ratio | - |
| $FN_{req}$ | Net thrust required | N |

| | | |
|---|---|---|
| F1 | Fraction of fuel reaching the near-wall mixing zone | - |
| F2 | Proportion of the swirler and dome air that goes into the PaSR reactor | - |
| F3 | Fraction of the burning gases admitted into the second near-wall reactor | - |
| F4 | Fraction of air initially assigned to the primary zone that goes into the near-wall reactor | - |
| F5 | Fraction of air initially assigned to the intermediate zone that goes into the near-wall reactor | - |
| F* | Target vector (multi-objective function) | - |
| f | Mixture fraction | kg fuel/kg gas |
| $f_{pr}$ | Correction factor | - |
| $f_v$ | Soot volume fraction | $m^3$ soot/$m^3$ |
| f(X) | Objective function | - |
| f* | Target (objective function) | - |
| GS | Ground Speed | m/s |
| GWP | Global Warming Potential | - |
| g | Acceleration of gravity | $m/s^2$ |
| $g_j(X)$ | Inequality constraints (vector) | - |
| HBL | Height of Blade | mm |
| HBLTO | Height of Blade at Take Off (high pressure compressor, last stage) | mm |
| HPCPR | High Pressure Compressor Pressure Ratio | - |
| $H_{cont}$ | Hydrogen content in fuel | % |
| h | Height (or altitude) | m |
| $h_l(X)$ | Equality constraints (vector) | - |
| IAS | Indicated Airspeed | m/s |
| IPCPR | Intermediate Pressure Compressor Pressure Ratio | - |
| k | Reaction rate coefficient** | $(m^3/kg\text{-}mol)^{(React.\ order-1)}/s$ |
| | Number of design variables** | - |
| $k'_{pr}$ | Prompt $NO_x$ parameter depending on ‘P’ (pressure) and ‘a’ (oxygen reaction order) | - |
| L | Lift | N |
| $L_{AS,max}$ | Maximum A-weighted sound pressure level recorded over a period of time | dBA |

| | | |
|---|---|---|
| L/D | Lift-to-Drag ratio | - |
| M | Mach number | - |
| $\overline{M}$ | Molecular weight | kg/kg mol |
| m | Number of inequality constraints** | - |
| | Displacement vector magnitude** | - |
| $\dot{m}$ | Mass flow rate | kg/s |
| N | Particle number density | $1/m^3$ |
| n | Number of moles** | - |
| | Total number of chromosomes** | - |
| OPR | Overall Pressure Ratio | - |
| O* | Vector of non-finite targets | - |
| O(X) | Optimisation factor | - |
| P | Pressure | atm |
| PML | Particulate Mass Loading | $\mu$m/l |
| $P_T$ | Total or stagnation pressure | atm |
| P( )/PDF | Probability Density Function of ( ) | - |
| P( ) | Chromosomes population | - |
| p | Partial pressure** | atm |
| | Number of equality constraints** | - |
| | Parental chromosome** | - |
| p(X) | Penalty term | - |
| q | Dynamic pressure | atm |
| R | Reaction rate** | - |
| | Ground range** | m |
| | Specific gas constant** | $J\,kg^{-1}\,K^{-1}$ |
| $R_e$(X) | Range error factor | - |
| r | Random number | - |
| S | Mixing parameter (‘unmixedness’) | - |
| SFC | Specific Fuel Consumption | mg/(N.s) |
| SN | Smoke Number | - |
| $S_f$ | Rate of soot formation | $m^3$ soot/s |
| T | Temperature | K |
| TAS (or V) | True Airspeed | m/s |
| TET | Turbine Entry Temperature | K |
| TR | Thrust ratio | - |
| T* | Vector of finite targets | - |

| | | |
|---|---|---|
| $T_a(X)$ | Target achievement factor | - |
| t | Time** | S |
| | Generation number** | - |
| $t_{max}$ | Maximum generation number | - |
| $t_{res}$ | Residence time | ms |
| $V_{crit}$ | Critical speed | m/s |
| $V_d$ | Displacement vector | - |
| $V_{NE}$ | Never exceed speed | m/s |
| $V_{stall}$ | Stall speed | m/s |
| W | Rate of soot oxidation** | $m^3$ soot/$m^3$.s |
| | Mass flow rate** | kg/s |
| W' | Rate of soot oxidation | kg soot/$m^2$.s |
| X | Molar fraction** | moles/moles gas |
| | Design vector (k-dimensional)** | - |
| | Chromosome** | - |
| | Ground range** | m |
| x | Number of carbon atoms per fuel molecule | - |
| | Gene | - |
| Y | Mass fraction | kg/kg gas |
| y | Number of hydrogen atoms per fuel molecule | - |
| $\alpha$ | Exploration factor** | - |
| | Standard temperature lapse rate** | °C/m |
| $\beta$ | Spread factor | - |
| $\overline{\beta}$ | Polynomial probability distribution | - |
| $\Delta_{max}$ | Creep mutation maximum size | - |
| $\gamma$ | Creep decay rate** | - |
| | Iteration dependency factor** | - |
| | Ratio of specific heats** | - |
| $\delta$ | Creep size** | - |
| | Delta ratio** | - |
| $\eta$ | Process completion ratio | - |
| $\lambda$ | Range error parameter** | - |
| | Target achievement parameter** | - |
| $\theta$ | OH Collision efficiency** | - |
| | Theta ratio** | - |
| $\rho$ | Density | kg/$m^3$ |
| $\sigma$ | Deviation (standard)** | - |

| | | |
|---|---|---|
| | Sigma ratio** | - |
| $\phi$, PHI | Equivalence ratio | - |
| [ ] | Species concentration | kg mol/m$^3$ |

(**) Depending on context

Subscripts

| Symbol | Definition |
|---|---|
| a | Air |
| amb | Ambient conditions |
| b | Backward |
| cal | Calculated (value) |
| DP | Design Point (conditions) |
| e | Equilibrium |
| f | Fuel**<br>Forward**<br>Final** |
| g | Gas |
| i | Initial |
| MR | Maximum range |
| m | Mean |
| p | Number of objectives or criteria |
| s | Stoichiometric |
| soot | Soot |
| std | Standard |
| t | Total |
| 0 | Initial**<br>Sea level (conditions)** |

(**) Depending on context

# Abbreviations & Formulae

| | |
|---|---|
| AAS | Amsterdam Airport Schiphol |
| ACARE | Advisory Council for Aeronautics Research in Europe |
| APM | Aircraft Performance Model |
| ATC | Air Traffic Control |
| BLX | Blend crossover |
| BOD | Bottom Of Descent |
| BWB | Blended Wing Body |
| CDA | Continuous Descent Approach |
| CD&R | Conflict Detection and Resolution |
| CEA | Chemical Equilibrium with Applications |
| CFD | Computational Fluid Dynamics |
| $CH_4$ | Methane |
| CTOP | Chebyshev Trajectory Optimisation Program |
| CO | Carbon monoxide |
| $CO_2$ | Carbon dioxide |
| CPM | Critical Path Method (for project management) |
| Cryoi | i-esimo cryoplane transition scenario |
| CU | Cranfield University |
| $C_{12}H_{23}$ | Jet-A aviation fuel |
| DOC | Direct Operating Cost |
| DP | Design Point (conditions) |
| DVM | Dynamic Vectored Mutation |
| DZ | Dilution Zone |
| EDA | En Route Descent Advisor |
| EPNdB | Effective Perceived Noise in decibels |
| eSTOL | extremely Short Take Off and Landing |
| FF | Flame Front |
| FMS | Flight Management System |
| FICAN | Federal Interagency Committee on Aviation Noise |
| FICON | Federal Interagency Committee on Noise |
| GA (GAs) | Genetic Algorithm (s) |
| H | Hydrogen |

| | |
|---|---|
| HPC | High Pressure Compressor |
| HPT | High Pressure Turbine |
| $H_2O$ | Water |
| ICAO | International Civil Aviation Organization |
| ICR | Intercooled Recuperated |
| IPC | Intermediate Pressure Compressor |
| IPT | Intermediate Pressure Turbine |
| ISA | International Standard Atmosphere |
| ITD | Integrated Technology Demonstrator |
| IZ | Intermediate Zone |
| JTI | Joint Technology Initiative |
| LB | Lower Bound |
| LDI | Lean Direct Injection |
| LPP | Lean Pre-vaporised Premixed |
| LPT | Low Pressure Turbine |
| LTO | Landing and Take Off (cycle) |
| MAE | Management of Aircraft Energy |
| MADS | Mesh Adaptive Search |
| MDO | Multidisciplinary Design Optimisation |
| MTM | Management of Trajectory and Mission |
| MTOW | Maximum Take Off Weight |
| N | Nitrogen |
| NAP | Noise Abatement Procedure |
| NASA | National Aeronautics and Space Administration |
| NLP | Non-Linear Programming problem |
| NO | Nitric oxide |
| NPDOT | Nonlinear Programming for Direct Optimisation of Trajectories |
| $NO_2$ | Nitrogen dioxide |
| $NO_x$ | Oxides of Nitrogen |
| NW | Near-Wall region |
| $N_2$ | Molecular nitrogen |
| $N_2O$ | Nitrous oxide |
| O | Oxygen |
| OASPL | Over All Sound Pressure Level |
| OD | Off Design (conditions) |
| OEW | Operating Empty Weight |

| | |
|---|---|
| OH | Hydroxyl radical |
| $O_2$ | Molecular oxygen |
| PARTNER | Partnership for AiR Transportation Noise and Emissions Reduction |
| PaSR | Partially-Stirred Reactor |
| PERT | Program Evaluation and Review Technique (for project management) |
| PFR | Plug Flow Reactor |
| PI | Performance Index |
| POLYPHEMUS (Polyphemus) | oPtimisatiOn aLgorithms librarY for PHysical complEx MUlti-objective problemS |
| PSR | Perfectly-Stirred Reactor |
| PSRS | Perfectly-Stirred Reactor Series |
| PZ | Primary Zone |
| RIA | Runway-Independent Aircraft |
| RPKs | Revenue Passenger-Kilometres |
| RQL | Rich-burn Quick-mix Lean-burn |
| SAE | Society of Automotive Engineers |
| SBX | Simulated Binary crossover |
| SEL | Sound Exposure Level |
| SBW | Strut-Braced Wing |
| SGA | ‘Simple’ Genetic Algorithm |
| SGO | Systems for Green Operations |
| $SO_2$ | Sulphur dioxide |
| STOL | Short Take Off and Landing |
| SUS | Stochastic Universal Sampling |
| S/L | Sea Level |
| TERA | Techno-economical Environmental Risk Analysis |
| TO | Take Off |
| TOC | Top Of Climb |
| TOD | Top Of Descent |
| TRACON | Terminal Radar Approach Control |
| TRL | Technology Readiness Level |
| UB | Upper Bound |
| UHC | Unburned Hydrocarbons |
| UML | Unified Modelling Language |

| | |
|---|---|
| VTOL | Vertical Take Off and Landing |
| WingMOD | Boeing multidisciplinary design optimisation tool for aircraft design |
| Wt (s) | Weight (s) |
| $\mathcal{F}$ | Feasible search space |
| $\mathcal{S}$ | Search space |
| $\mathcal{U}$ | Unfeasible search space |

# 1
# General Introduction

This first chapter provides a general introduction to the subject addressed in this research project in an attempt to provide an idea of the general context in which the project was developed. It also deals with the general and specific objectives of the research project, as well as it summarises the main contributions of the same. The specific context and scope of the research, and the methodology followed during the research in order to achieve the objectives initially proposed are also included in this chapter. In addition, an outline of this thesis is also provided.

## 1.1
## Introduction

In a globalised world, in which the efficient transportation of people and goods from one place to another greatly contributes to the development of a given region or country (through the creation and/or development of new business and leisure opportunities, the facilitation of cultural exchanges, and the development of relationships among people and institutions, among others), the aviation industry has found the ideal conditions for its development. These conditions have allowed the aviation industry becomes one of the fastest growing economic sectors during the last decades. The growth in the aviation industry is reflected in the increase in air transport, which has risen at an average annual rate of around 5% over the past 20 years [1]. Market projections associated with this industry indicate this growth will continue over the following years, as illustrated in Figure 1-1, which shows the projected increase (average annual rate of 4.9%) in the Revenue Passenger-Kilometres (RPKs) – the number of fare-paying passengers multiplied by the number of kilometres they fly (i.e., airline passenger traffic) – for the following 20 years.

Environmental issues associated with aircraft operations are currently one of the most critical aspects of commercial aviation [2]. This is a result of both the continuing

growth in air traffic, and the increasing public awareness about the anthropogenic contribution to global warming. Clarke [3] indicates that if reductions in the environmental impact of aircraft operations are to be achieved then either (i) the number of operations must be reduced, (ii) the type of aircraft must be changed, or (iii) the aircraft operational rules and procedures must be changed. However, due to the fact that passenger traffic is expected to increase over the next years (Figure 1-1), it seems unlikely that the number of operations will be reduced. Only the last two options, or a combination of both, seem to be then the most feasible solutions to the problem.

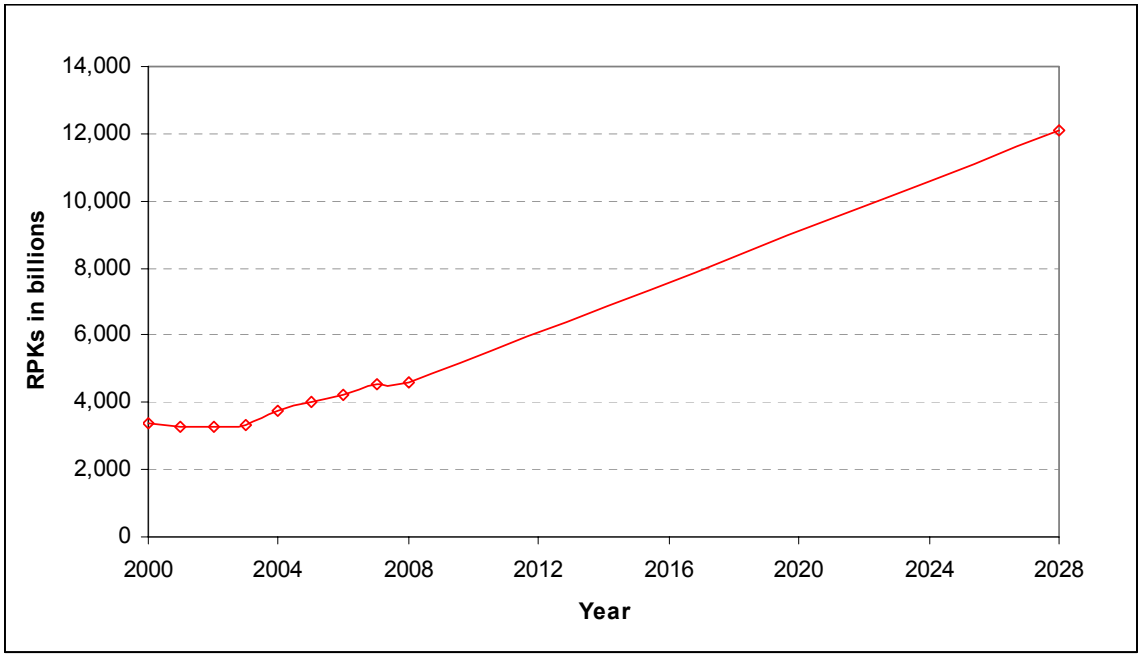


Figure 1-1. Airline passenger traffic projections [1]

This last aspect is emphasised by Clarke [3] considering one of the major contributors to environmental pollution, noise. He highlights that the reduction in source noise produced per unit of thrust that has been achieved each year during the last 50 years has diminished over time and appears to be asymptotically approaching a constant noise level per unit thrust. If it were the case, he concludes, without revolutionary changes in the way that engines are designed, the only alternatives available to the aviation community are either to design aircraft that require lower thrust to move the same payload (addressed through better aerodynamics or lighter aircraft structures), or to determine ways to operate aircraft at lower thrust levels (addressed through changes in flight procedures).

Regarding the change of the type of aircraft (Clarke's second option [3]), in reference [2] it is indicated that the main focus of commercial aircraft design has been on producing airplanes that meet performance goals at minimum operating costs. Environmental performance has been mostly considered, consequently, at the post design analysis phase, during which adjustments have been made to satisfy specific environmental constraints (sequential design approach). Currently, however, due to the gradual tightening of environmental requirements, the cost and complexity of meeting this environmental performance in the post design phase has increased significantly. It has been concluded in reference [2], therefore, that there is a need for integrating environmental considerations at an early stage of the aircraft design process, and for more systematic investigations and quantifications of the trade-offs involved in meeting the associated specific environmental constraints.

Similarly, Green [4] points out that until now the main focus of commercial aircraft design has been on producing aircraft to fly further, faster, higher, and at less cost. However, in the present century, he adds, it is expected that the emphasis be shifted towards increasing safety and, above all, reducing the impact on the environment. The introduction of new configurations of aircraft (mostly related to unconventional and innovative airframe configurations) constitutes an alternative for medium and long term, because, as Brooker [5] highlights, the timescale from new aircraft concepts to be brought to operational readiness is a lengthy one (often several decades). Major changes in aircraft design can only be expected then in 20 to 50 years. One of the novel aircraft concepts extensively studied during the last years is the Blended Wing Body (BWB). This aircraft configuration has received great attention mainly because of its airframe aerodynamic efficiency.

Revising the current aircraft operational rules and procedures (Clarke's third option [3]), with respect to necessary changes or the implementation of new ones, provides an option for reducing the impact of aircraft operations on the environment that may be implemented more readily than changes in aircraft design or component technology. In particular, an analysis of advanced aircraft trajectory technologies to identify 'greener' trajectories (aircraft trajectories with minimum environmental impact) has the potential to contribute to a significant reduction in both fuel consumption and the pollutants emitted (gaseous emissions and noise).

From what was mentioned above (and in accordance with what is highlighted in reference [2]), it is concluded that there is indeed a need for integrating environmental considerations at an early stage of the aircraft/engine design process, and for more systematic investigations and quantifications of the trade-offs involved in meeting specific noise and gaseous emissions constraints. It implies, in turn, the use of multidisciplinary design optimisation (MDO) processes in order to evaluate and quantify aircraft/engines design trade-offs originated as a consequence of addressing conflicting objectives such as low environmental impact and low operating costs.

It is in this general context that the present work has been mainly developed, i.e., considering environmental performance, gaseous emissions in particular, as one of the key aspects in the assessment of different alternatives (including the engine preliminary design) for reducing the impact of aircraft operations on the environment. Thus, the present research project focuses mainly on the development (and/or adaptation) of not only robust computational models capable of rapidly quantifying the level of pollutants emitted by aircraft along their whole mission profile (e.g. gaseous emissions prediction model); but also aircraft trajectory computation algorithms capable of performing efficient trajectory optimisation processes involving multi-criteria optimisation (fuel, emissions, time, etc.), thereby identifying aircraft ‘greener’ mission profiles.

The main contributions of this work to knowledge broadly comprise the following: (i) development of an environmental-based methodology for carrying out both aircraft trajectory optimisation processes, and engine cycle optimisation-type ones; (ii) development of both an advanced, innovative gas turbine emissions prediction model, and an optimiser suitable to be integrated into multi-disciplinary optimisation frameworks; and (iii) determination and assessment of optimum and ‘greener’ aircraft trajectories and aircraft engine cycles using a multi-disciplinary optimisation tool, which included the computational tools developed in this research project. The main results of this research project have been already published (or will appear published) in several scientific journals and international conferences as highlighted in Appendix A.

## 1.2 Context

The critical nature of the problem has meant that currently several organisations worldwide focus their efforts towards large collaborative projects whose main objective is to identify the best alternatives or routes to reduce the environmental impact of aircraft operations. Particular examples of these projects include the PARTNER (Partnership for AiR Transportation Noise and Emissions Reduction) project [6], and the European Clean Sky JTI (Joint Technology Initiative) project [7]. The Clean Sky JTI will demonstrate and validate different technologies thereby making major steps towards achieving the environmental goals set by the Advisory Council for Aeronautics Research in Europe (ACARE). These goals, which are to be realised in 2020, include, among others, reductions in carbon dioxide ($CO_2$) and oxides of nitrogen ($NO_x$) emissions of 50% and 80%, respectively.

Cranfield University (CU) and other partners from the European aviation industry are collaboratively participating in several areas of the Clean Sky project, including the Systems for Green Operations (SGO) Integrated Technology Demonstrator (ITD). The Systems for Green Operations (SGO), one of the six ITDs of the project, concentrates on two key areas: Management of Aircraft Energy (MAE), and Management of Trajectory and Mission (MTM). The main contributions of CU to the SGO ITD relate to the development of computational algorithms not only for the management of aircraft trajectory and mission (i.e., for aircraft trajectory optimisation), but also for the modelling of different disciplines taking part in the optimisation processes, such as aircraft performance, engine performance, and pollutants formation, among others. The results of this research project constitute some of the main contributions of CU to the SGO ITD.

In this sense, the aircraft trajectory optimisation algorithms developed and/or adapted in the present research project constitutes the basis of an industry standard optimisation tool being developed as part of the main activities of the SGO ITD. The development of this tool will take several years, and it is expected that at the end of its development its level of maturity is high, which is reflected in high TRL (Technology Readiness Level) values, i.e., TRL: 5-6 (tool fully functional). This optimisation tool will be eventually deployed by industry and policy-makers to assess different

alternatives that reduce the environmental impact of aircraft operations. The work developed as part of this research project corresponds thus to the initial stages of the development of the referred optimisation tool.

Accordingly, a methodology for optimising aircraft trajectories has been initially devised. Optimisation algorithms have been then developed and/or adapted for carrying out these aircraft trajectory optimisation processes. Computational models simulating different disciplines such as aircraft performance, engine performance, and pollutants formation, have been selected or developed as necessary. Finally, in order to evaluate the performance of the optimisation algorithms developed and/or adapted, simplified aircraft trajectory optimisation processes have been carried out using these algorithms and the computational models selected and/or developed. The main results of these optimisation processes are summarised in this thesis. In addition, in order to show the flexibility of the optimisation algorithms developed/adapted, engine cycle optimisation assessments have been performed, and their main results are presented as well.

## 1.3 Objectives

The main contributions of this work to knowledge broadly comprise the following: (i) development of an environmental-based methodology for carrying out both aircraft trajectory optimisation processes, and engine cycle optimisation-type ones; (ii) development of both an advanced, innovative gas turbine emissions prediction model, and an optimiser suitable to be integrated into multi-disciplinary optimisation frameworks; and (iii) determination and assessment of optimum and ‘greener’ aircraft trajectories and aircraft engine cycles using a multi-disciplinary optimisation tool, which included the computational tools developed in this research project.

The general and specific objectives of the present research project, whose main contributions are highlighted above, included the following:

- In general, to develop a methodology to evaluate and quantify aircraft/engines design trade-offs originated as a consequence of addressing conflicting objectives such as low environmental impact and low operating costs.

- More specifically, to evaluate and optimise both aircraft flight trajectories and aircraft engine cycles taking into account multidisciplinary aspects such as performance, gaseous emissions (environmental performance), and economics, among others.
- To use the different computational tools currently available at Cranfield University, and, when necessary, to develop new computational tools or to introduce modifications to the existing ones, in order to perform the tasks proposed in this project.
- Additionally, to contribute to the adaptation and deployment of the Techno-economical Environmental Risk Analysis (TERA*) techniques, and to participate in the development of projects.

## 1.4 Scope

In this research project, the processes of evaluation and optimisation of aircraft propulsion systems have been performed from two different perspectives: operation and preliminary design. However, both aircraft flight trajectories and aircraft engine cycles have been evaluated and optimised from the point of view of the design and operation of the propulsion system (aircraft engine) only. Thus, it has been assumed that both the optimum aircraft flight trajectories determined, as well as the reference trajectories utilised for the optimisation of the aircraft engine cycles are feasible and safe to fly, even though they represent only theoretical ones. In other words, aspects related to the feasibility of the aircraft operation and its associated safety issues have not been considered in this work. It has been also assumed that only one aircraft is present in the

* TERA is a concept conceived by Cranfield University. As a multi-disciplinary optimisation tool, TERA increases the visibility of the risks and enables the user to compare and rank competing power-plant schemes on a formal and consistent basis.

air space during any given flight, i.e., there are no obstacles (flight corridors, other aircraft, hills, etc.) that might constrain the aircraft flight path unless otherwise explicitly specified. Finally, uncertainties associated with the data used as input in the different computational models utilised have not been considered. The referred uncertainties will be addressed in future as part of the further work to be developed in this research area. Thus, when possible, results are presented in relative terms rather than in absolute terms. This means that the trends in the results obtained are considered more representative than the absolute values.

## 1.5 Methodology

During this research project, initially a set of computational tools currently available at CU has been utilised. However, due to the need of the same, new computational tools have been developed and implemented, and/or modifications to the existing ones have been introduced. This last aspect is particularly important because it improved the degree of reliability of the results obtained from the aircraft/engine simulations. One particular example of these tools constitutes the gaseous emissions prediction model developed, which predicts more accurately emissions trends from current and potential future aircraft gas turbine combustors. Another example constitutes the optimisation algorithms developed and/or adapted, which allowed performing the optimisation processes initially proposed. Finally, in order to determine optimum and 'greener' aircraft trajectories and engine cycles that help to minimise the impact of commercial aircraft operations on the environment, multidisciplinary evaluation and optimisation processes of both aircraft flight trajectories and aircraft engine cycles have been carried out. The main results obtained from these evaluation and optimisation processes are summarised in this thesis.

## 1.6 Thesis Outline

The main results of the present research project which are summarised in this thesis are presented in ten chapters. The first chapter (i.e., current one) provides a

general introduction to the subject addressed in this research project in an attempt to provide an idea of the general context in which the project was developed. It also deals with the general and specific objectives of the research project, as well as it summarises the main contributions of the same. The specific context and scope of the research, as well as the methodology followed during the research in order to achieve the objectives initially proposed are also included in this chapter. In addition, an outline of this thesis is also provided.

An initial literature review related to the state-of-the-art of the different approaches considered so far to reduce the environmental impact of commercial aircraft operations is presented in Chapter 2. In order to facilitate its understanding, the review is presented separately in two parts: one corresponding to those studies that mainly involve new configurations of aircraft, and the other one corresponding to those studies involving the introduction of changes in the aircraft operational rules and procedures. Additionally, a summary of further references reviewed is presented at the end of this chapter.

Chapter 3 describes the development and implementation of a gaseous emissions prediction model, which allows the reliable calculation of emissions trends from current and potential future aircraft gas turbine combustors. Initially the model requirements are established, and the main strategies that can be adopted for combustor emissions prediction are then described. The methodology followed for simulating combustion chambers, and the algorithms utilised for modelling the formation of pollutants inside them are also summarised. The emissions prediction model developed has been verified through simulations of an actual combustor. The main results obtained from these simulations using the model developed are also shown and discussed in this chapter.

Chapter 4 is focussed on optimisation problems and, in particular, on those main aspects that characterise the aircraft trajectory optimisation ones. The first sections discuss general aspects of optimisation, as well as a general classification of the different optimisation problems that can be found in practical applications. Aircraft trajectory optimisation problems are then classified according to their main features. This is followed by a short description of the main numerical techniques that can be utilised for solving this type of problems. Finally, the last sections of this chapter briefly describe part of the past experience on optimisation problems through the presentation

of a summary of some of the research work developed about this subject at both Cranfield University, and other research organisations.

Since the optimisation algorithms utilised in the present research project are based on genetic algorithms, basic concepts associated with this optimisation technique are initially presented in Chapter 5. This is followed by a short description of the main characteristics of the genetic algorithms-based optimiser utilised. The description presented in this thesis highlights the main modifications introduced in the past into a general-purpose genetic algorithms library. The aim of these modifications was both the adaptation of the algorithms for engineering design optimisation problems, and the maximisation of their performance.

Chapter 6 and Chapter 7 describe, in turn, the main results obtained from the processes of evaluation and optimisation of environmentally friendly aircraft propulsion systems. The aircraft propulsion systems have been optimised from two different perspectives: propulsion system operation (Chapter 6) and propulsion system design (Chapter 7). As part of the optimisation of the operation of aircraft propulsion systems (and/or aircraft, in general), aircraft flight trajectories have been optimised considering that the aircraft/engine configurations are unchanged, i.e., aircraft/engine configurations already designed and in operation. From the propulsion system design point of view, the preliminary design of different aircraft propulsion systems has been optimised. In this case, the aircraft flight profile (aircraft trajectory) has been considered fixed.

Finally, Chapter 8 and Chapter 9 of this thesis summarise, respectively, the main conclusions drawn from the work developed during this research project, including some recommendations for further work; and the main references consulted during the research, and for the elaboration of this thesis. This thesis concludes with some appendices (Chapter 10) which provide supporting information for the discussions carried out in its main body.

# 2
# Literature Review

An initial literature review performed in order to have a better understanding of the state-of-the-art of the ways of reducing the environmental impact of aircraft operations is summarised in this chapter. In order to facilitate its understanding, this review is presented separately in two parts: one corresponding to those studies mainly involving new configurations of aircraft (Clarke's second option [3]), and the other one corresponding to those studies mainly involving the introduction of changes in the aircraft operational rules and procedures (Clarke's third option [3]). These second and third options correspond to the alternatives of solution to the problem that represents the environmental impact of aircraft operations, which were identified in reference [3] and highlighted in Chapter 1. Additionally, a summary of further literature reviewed is presented at the end of this chapter.

## 2.1
## New Configurations of Aircraft

The introduction of new configurations of aircraft (mostly related to unconventional and innovative airframe configurations) in order to reduce the aircraft climate impact constitutes an alternative for medium and long term, since as highlighted in reference [5], the timescale from new aircraft concepts to be brought to operational readiness often involves several decades. A first step for the accomplishment of this goal is the inclusion of environmental aspects at the early stage of the aircraft/engine design process. Currently, several well-known academic institutions and research centres worldwide study the feasibility of including environmental performance (i.e., parameters measuring the environmental impact) as an optimisation objective at the aircraft conceptual design stage [2-7]. These studies commonly include the use of multidisciplinary design optimisation processes in which conflicting objectives such as low noise, low gaseous emissions, and low operating costs are addressed in order to

estimate optimal aircraft configurations. For instance, in reference [2], the development of a preliminary design framework, which explores and quantifies trade-offs between aircraft design, operations, and environmental impact, is described. The referred framework includes not only computational models that estimate aircraft noise and engine performance; but also aircraft operational procedures, analysis, and optimisation modules, which were developed in order to assess the relative benefits of different opportunities for improving air transportation.

Diedrich *et al.* [8] describe an integrated design tool developed in order to predict and optimise the performance and costs associated with producing a novel commercial aircraft – the so called 'silent' aircraft – placing noise as the primary design goal. The silent aircraft configuration studied was based upon a BWB aircraft, whose main characteristic relates to its airframe aerodynamic efficiency. The MDO framework utilised (Figure 2-1) included several acoustic models coupled to a set of first-principles and empirically-based aircraft design modules that address design issues related to propulsion, aerodynamics, structures, weight, and flight profiles. During the optimisation process, given the aircraft load (215 passengers) and range (5,000 nm), the maximum take off weight (MTOW) subject to noise constraints was minimised. Although many of the noise components exhibited large reductions in comparison with current aircraft of similar size (Boeing 767-300), the results showed that the design does not achieve the goal of 'an aircraft inaudible outside the airport perimeter', i.e., a 'silent' aircraft.

A three-dimensional airframe design methodology for low noise emissions and high fuel efficiency is presented by Hileman *et al.* [9]. This study, which was also based on a BWB aircraft (Figure 2-2), describes the incorporation of leading edge camber of the centre body to provide cruise pitch trim without large penalties in drag. In order to reduce the noise approach, a reduced approach velocity and an increased distance between the airframe and the observer – steep approach – were utilised. This was obtained through a combination of thrust vectoring, quiet drag generation, and leading edge high-lift devices. The referred design methodology essentially involved the generation of three-dimensional airframes, aerodynamic assessments at cruise conditions (using computational fluid dynamics – CFD), and approach aerodynamic and aero acoustic assessments. Based on the results, the authors of that study concluded that

although the preliminary BWB type airframe design is highly efficient (Mach number times lift-to-drag ratio – ML/D ≈ 18.5), it does not yet fully meet the noise reduction goal – 'silent' aircraft – due to limitations on the low speed, high-lift performance of the fixed geometry outer-wing.

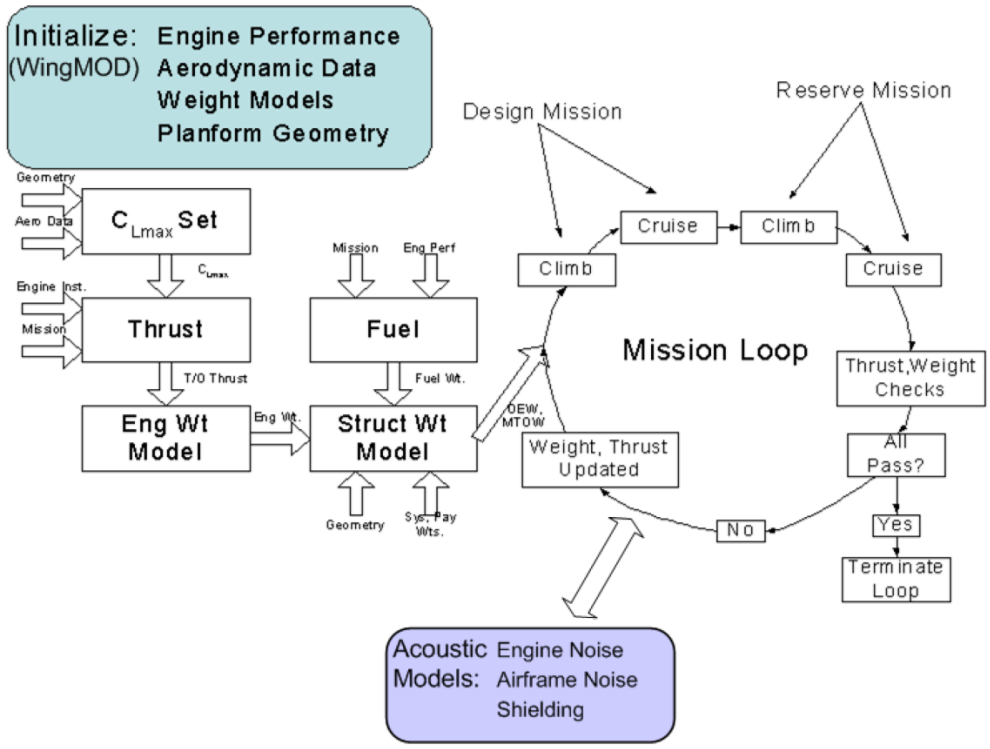


Figure 2-1. Silent aircraft experimental MDO design framework [8]

According to Hileman *et al.* [10], aircraft technology and operational procedures need to be designed in parallel to meet the noise goal of being below ambient noise levels outside the perimeter of a typical urban airport – 'silent' aircraft. Thus, in their work [10] they describe the incorporation of different technologies into a conceptual 'silent' aircraft BWB type design allowing a slow (≈ 60.8m/s) and steep (≈ 3.9°) continuous descent approach (CDA) trajectory with a displaced landing threshold (≈ 1.2km). The results showed that the use of this approach trajectory produces a peak noise level of 61 dBA outside the airport perimeter (Figure 2-3). Among others, the technologies utilised included the use of an all-lifting-body – no flaps, a deployable drooped leading edge, and trailing edge brushes. The authors of this study concluded that the benefits of CDA procedures would be enhanced through the incorporation of steeper approach angles (e.g., 3.9° versus a conventional approach of 3°), displaced landing thresholds, and low engine thrusts. At the same time, they indicated that

although the noise benefits of these 'silent' aircraft technologies and operating techniques could be used in the short term for existing aircraft, the operational consequences of these modified procedures need to be carefully analysed.

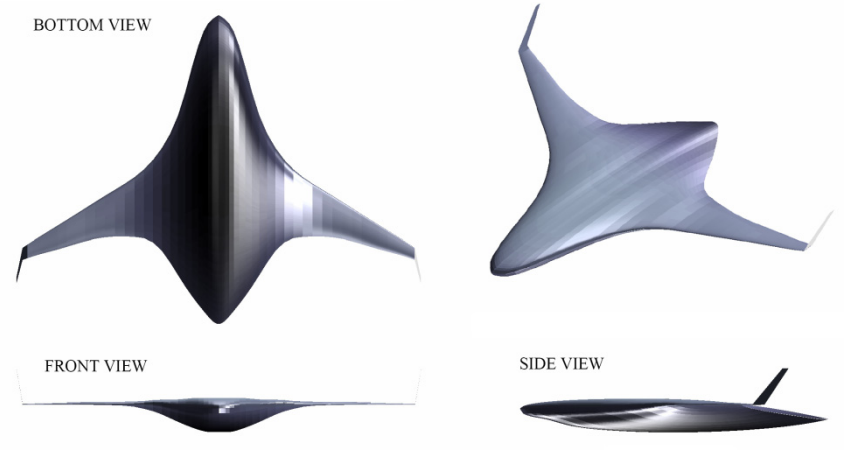


Figure 2-2. BWB Silent aircraft experimental – Three-dimensional view [9]

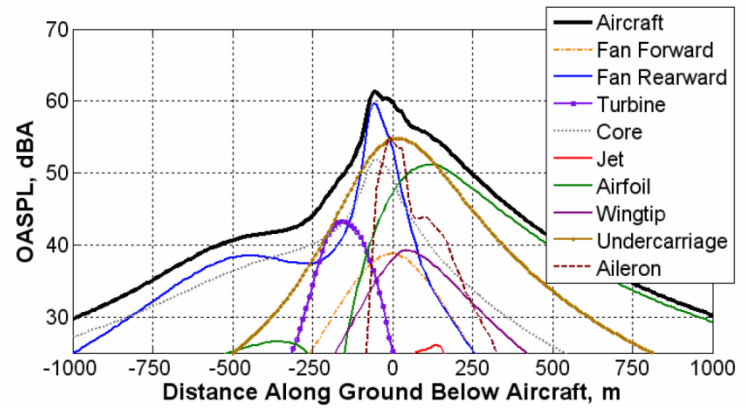


Figure 2-3. Components' noise at airport perimeter (BWB Silent aircraft experimental) [10]

Crichton *et al.* [11] studied the feasibility of obtaining further improvements in jet noise reduction during take off through the use of variable jet area. According to Crichton *et al.*, by continuously modifying the nozzle exit area, the fan can operate at an ideal local location (e.g., away from stall and surge regions). In addition, the take off optimisation can be extended to cover noise sources other than the jet. Thus, they increased the nozzle area at take off relative to the area at top of climb and cruise. Additionally, in order to make full use of a variable area nozzle to reduce jet noise, the fan was operated at part-speed during take off, which in turn allowed larger nozzle increases before obtaining a choked fan. The results showed that when the take off optimisation process is performed considering the jet noise as the only noise source,

noise levels below the ‘silent’ aircraft noise target (60 dBA) can be achieved, even with a relatively high top of climb fan pressure ratio of 1.50. However, when additional noise sources (fan and airframe) are considered, noise levels of about 5 dBA above the ‘silent’ aircraft noise target are obtained.

A study of a distributed propulsion/airframe configuration that provides low-noise short take off and landing (STOL) operations carried out in order to explore the potential benefits from incorporating embedded distributed propulsion systems into a cruise efficient airplane is presented by Kim *et al.* [12]. The study mainly focuses on the use of embedded distributed propulsion for very low noise STOL capability with highly efficient cruise performance. Due to the exponential rise in noise rules, regulations and restrictions, Kim *et al.* indicate that revolutionary airplane concepts are needed in order to meet future traffic demand. Thus a BWB type of airplane using distributed propulsion with 12 small engines was selected as the baseline configuration (Figure 2-4). Some of the results showed that it is possible to achieve a sideline noise of 96.8 EPNdB (Effective Perceived Noise, in decibels), flyover noise of 94.7 EPNdB, and approach noise of 47.7 EPNdB. The approach prediction did not include turbomachinery noise, so according to the authors of the work it is likely to be considerably higher. It was concluded that this type of aircraft have the potential to offer a relatively quieter approach, which would allow the use of smaller and more noise sensitive airports, relieving in turn congestion and enabling the growth of the aviation industry.

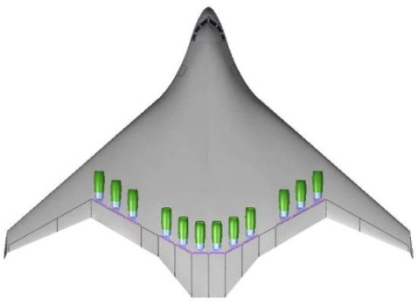

Figure 2-4. STOL aircraft with distributed propulsion [11]

Leifsson *et al.* [13] used a MDO process to optimise the design of aircraft using MTOW as the objective function (to be minimised), while constraining noise at the approach condition. The MDO framework utilised included, essentially, aircraft conceptual design tools and an aircraft noise prediction model (Figure 2-5). The results of this design study, which was performed for cantilever wing and Strut-Braced Wing

(SBW) transport aircraft (payload: 300 passengers, range: 7,700 nm), showed that, by reducing the approach speed alone, only a small reduction in airframe noise is achieved. Even though, in this case, the performance and weight penalty incurred was significant. Thus, it was concluded that, in order to achieve a significant airframe noise reduction, more dramatic changes to the aircraft design are needed, including the re-design of the high-lift devices and the landing gear. The results also indicated that the trailing edge flap can be eliminated without large weight and performance penalties.

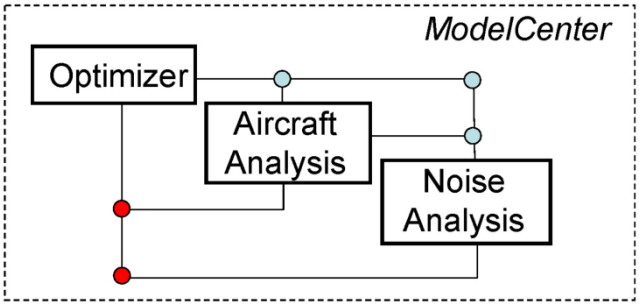


Figure 2-5. Diagram of MDO framework [13]

There are some researchers who consider that runway-independent aircraft (RIA) – vertical take off and landing (VTOL), and extremely short take off and landing (eSTOL) vehicles – could increase passenger throughput at crowded urban airports via the use of vertiports or stub runways. Thus, in references [14-16] studies of simultaneous non-interfering noise abatement procedures (NAPs) for RIA are described. These studies mainly analysed different trajectory optimisation algorithms in order to develop tools that identify (rapidly and efficiently) acceptable NAPs, and evaluate their impact on air traffic and the surrounding communities. The optimisation cost functions utilised included, typically, time, fuel, and noise terms. It was concluded in these studies that the optimisation tools developed might eventually provide airport and airspace designers with a larger number of trajectory options for analysis of potential landing sites, associated traffic procedures, and entry options.

## 2.2 New Aircraft Operational Rules and Procedures

Regarding the aircraft operational rules and procedures, a revision of the current ones with respect to necessary changes or the implementation of new ones provides an

option for reducing the environmental impact of aircraft operations that may be implemented more readily than changes in aircraft design or component technology. However, as discussed above, the introduction of new configurations of aircraft – a possibility for medium and long term – will also result in significant changes on aircraft operations as a whole. In the literature, it is possible to find a number of studies carried out in order to analyze the feasibility of using new (or modified) operational rules and procedures seeking to reduce aircraft climate impact, namely, noise and gaseous emissions. These studies describe typically the development of methodologies and/or computer codes that efficiently estimate optimal procedures to be followed in order to mitigate the environmental impact of aircraft operations.

It is important to highlight that studies regarding this subject have been performed by researchers associated with not only academia and research centres, but also industry. In this sense, in reference [17] different programs currently in development by The Boeing Company including those related to flight efficiency (advanced noise, fuel and time efficient procedures, CDAs, etc.), guidance law (vertical), advanced trajectory technologies (advanced trajectory prediction, trajectory optimisation, trajectory management, etc.), and air transport economics are described. The ultimate goal of these technologies (when implemented) is to relieve crowded airspace and airports in an efficient manner and with a minimum environmental impact. The following paragraphs summarise some of the main studies developed in the past on this area of aircraft operational rules and procedures.

The research work carried out by Visser and Wijnen [18-21] related to optimisation of noise abatement trajectories (departure and arrival) is perhaps the most important one in this category. This is because in the optimisation processes they use indices that are not only generic in nature (e.g. noise footprints), but also site-specific criteria that take into account the population distribution in those areas surrounding the airport. In reference [18], the development of a tool that combines a noise model, a geographic information system, and a dynamic trajectory optimisation algorithm, which allows the analysis and design of noise abatement procedures at any given airport, is described. Due to the fact that the optimisation process involved a compromise between two conflicting requirements, noise and fuel consumption, a composite performance measure, which consisted of a weighted combination of a noise-impact-related criterion

and fuel consumed, was used as its performance index. In order to take into account the dependence of the true noise impact on the population density distribution around the airport, the so-called ‘awakenings’ parameter (i.e., number of people within the exposed community that are expected to awake due to a single event night-time noise intrusion) was utilised as the noise-impact-related criterion. This parameter was estimated as a function of the sound exposure level (SEL), as shown in Figure 2-6.

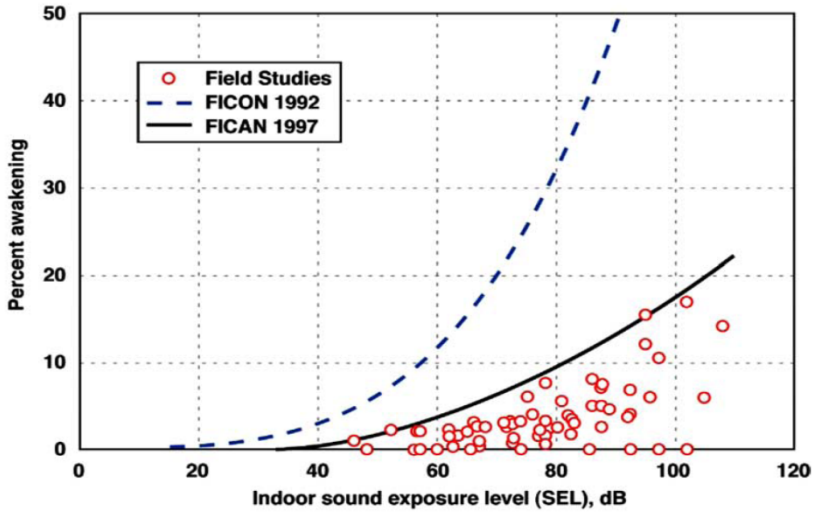


Figure 2-6. FICAN sleep disturbance dose-response relationship [18-21]

In the optimisation processes, essentially routings and flight paths were modified to minimise the noise impact on the surrounding communities, while satisfying different imposed constraints. Results obtained from the optimisation of the departure trajectory of a Boeing 737-300 at Amsterdam Airport Schiphol (AAS) showed that the number of people that awake due to the noise impact reduces from 5042 to 3312 (about 35%) when compared to the reference condition (fuel-optimal trajectory), and that the noise-optimal departure trajectory requires only about 1% more fuel. In particular, it was observed that the noise optimisation process shifts the noise impact from densely populated city areas to more rural regions. The authors of that study concluded that the optimisation concept developed is generic and flexible, since alternative optimisation criteria, additional constrains, or model refinements can be readily introduced.

In reference [19] the same optimisation tool was applied to the design of noise-optimised arrival trajectories considering the same airport and the same type of aircraft. The results indicated that the number of people that awake due to the noise impact reduces from 3166 to 1495 (about 50%) when compared to reference condition (fuel-

optimal trajectory); and that the noise-optimal trajectory requires about 30kg (15%) more fuel, and an additional flight time of about 50s (about 10%), as illustrated in Figure 2-7. Due to limitations from an operational point of view, a modification of the composition of the performance index used in the two works described previously is proposed and utilised in reference [20]. The new performance index incorporates the deviation from a reference flight path instead of a fuel parameter. Thus, an optimised trajectory deviates from the reference track only if this improves the noise impact. The results obtained from the optimisation process of a Boeing 737-300 departure trajectory at AAS showed that, using the modified performance index, noise-optimised trajectories can be generated in a similar way. The possibility of choosing whether the optimisation process should be performed by changing the vertical and/or horizontal flight profile seems to be an additional advantage of the use of this modified performance index.

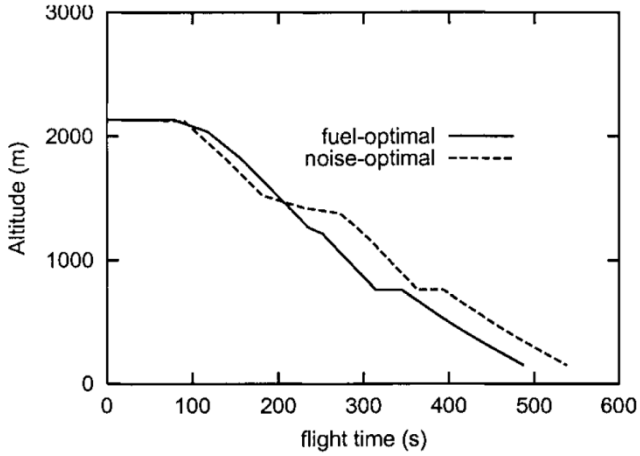


Figure 2-7. Comparison of minimum-fuel and minimum-noise arrival trajectories [19]

The trajectory-synthesis tool initially developed by Visser and Wijnen was extended to include other noise performance criteria [21]. The original performance index (fuel and awakenings) was modified by adding two new parameters: population (population living within a specified noise contour level) and area (total area enclosed within a specified noise contour level). A parametric analysis involving the four weighting parameters in the composite noise performance index was performed by comparing arrival trajectories of a Boeing 737-300 at AAS. From the results, it was concluded that an optimisation process with respect to one particular criterion may lead to a solution that exhibits undesirable performance with respect to the other parameters

considered. Thus, it is indicated that a compromise must be achieved by specifying a sensible combination of the weighting factors used in the performance index.

According to the relationship between aircraft noise exposure and sleep disturbance (dose-response) utilised in the studies carried out by Visser and Wijnen [18-21], the population expected to awake due to a single event night-time noise (awakenings) is estimated as a function of SEL only (Figure 2-6). However, Quehl and Basner [22], in their work developed in order to establish dose-response curves regarding the annoying impact of nocturnal aircraft noise, concluded that not only the energy equivalent noise level (calculated by integrating the sound energy from all noise events over a given time period) commonly used in noise abatement rules, but also the number of aircraft events are a major source of nocturnal aircraft noise induced annoyance (see Figure 2-8). They also concluded that the noise exposure in the last two decades has changed in qualitative terms. There has been a strong increase in air traffic with a simultaneous reduction of the emission levels of a single aircraft. According to them, this fact explains why airport residents claim today that the noise has increased during the past few years.

Clarke [3] highlights that the primary obstacle to the implementation of advanced noise abatement procedures, such as CDAs, is the inability of air traffic controllers to maintain manually the precise sequencing and spacing required for maximum take off and landing rates in heavy traffic. Thus, he concludes that the introduction of automation that not only predicts the performance and noise impact of aircraft, but also assist the controller in determining and maintaining appropriate sequencing and spacing is critical to the successful utilisation of these procedures. In reference [23], in turn, the development of an aircraft noise pollution model for trajectory optimisation based on simulation data of a Boeing 737-200 is described. The model developed is used to obtain the footprint on the ground that is exposed to noise levels at or above 70 dB given a particular aircraft orientation, altitude, and thrust setting. This footprint is determined by the intersection with the ground of the surface (ellipsoid) around the aircraft inside of which the noise is at or above 70 dB. It is concluded that although the model was developed for a specific aircraft, the methodology would be applicable to other different ones.

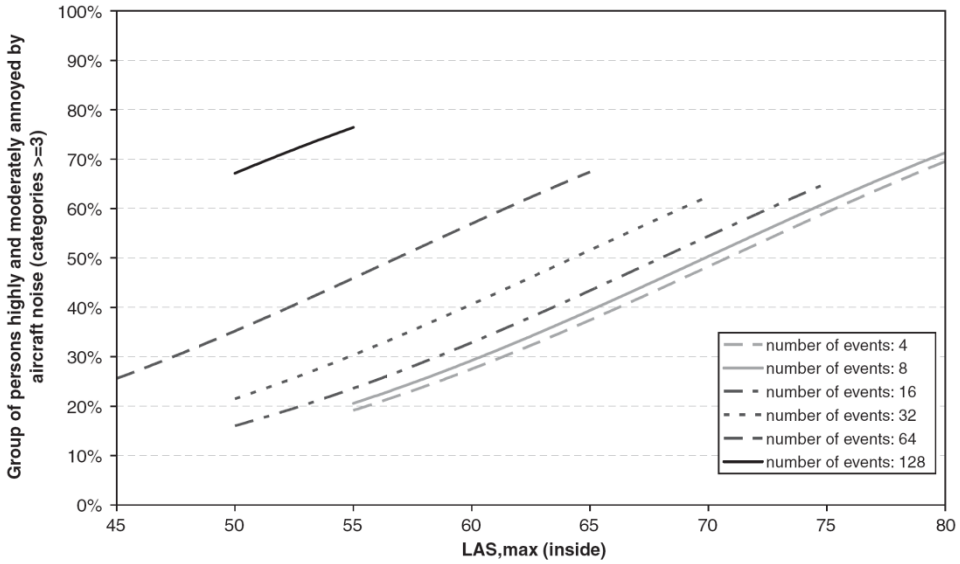


Figure 2-8. Aircraft noise annoyance as a function of $L_{AS,max}$ and number of noise events [22]

Norgia [24] describes a numerical approach utilised for the computation of noise contours (footprint) generated during aircraft take off and landing operations. In the model, for the generation of a single noise contour, the trajectory followed by the aircraft is divided into several straight-line segments. Along any segment, a constant noise-level surface (circular cylinder) is determined. The intersection of this surface with the ground plane originates an elliptic curve, part of which represents the contribution of this particular segment to the total contour. The total contour is obtained from the summation of the contributions of all segments of the trajectory. The model developed was subsequently utilised to define a new noise abatement procedure during aircraft take off at an Italian airport. The results of the simulations indicated that through the use of this model noise contours can be obtained quickly and efficiently.

En route Descent Advisor (EDA), details of which can be found in references [25-27], is a decision support computer tool that is being developed at the National Aeronautics and Space Administration (NASA) Ames Research Center for managing complex en route traffic subject to metering restrictions. The ultimate goal of EDA is to allow future use of controller procedures based on trajectory management instead of the existing ones based on sector management. Among the multiple capabilities of EDA, those related to arrival trajectory optimisation seem to bring multiple benefits as claimed by its authors. They indicate that EDA allows both horizontal and vertical trajectory optimisation of arrival flight trajectories, which in turn result in more fuel-

efficient arrivals. Some of the EDA benefits mechanisms are graphically illustrated in Figure 2-9.

In general, EDA proposes several concepts for trajectory optimisation including (i) top of descent (TOD) optimisation, which improves the flight's vertical descent profile by moving its TOD location further downstream, minimising flight time at less efficient, lower altitudes (bottom of descent – BOD – fixed); (ii) user preferred routing, which facilitates flow-rate conformance, independent of path; and (iii) relaxed static metering fix restrictions: (a) vertical anchor point (improvement of flight's vertical descent profile by moving the bottom of descent downstream of the current metering fix location), and (b) horizontal anchor point (improvement of the horizontal arrival trajectory by moving the current metering fix, enabling in this way a more direct route to the runway).

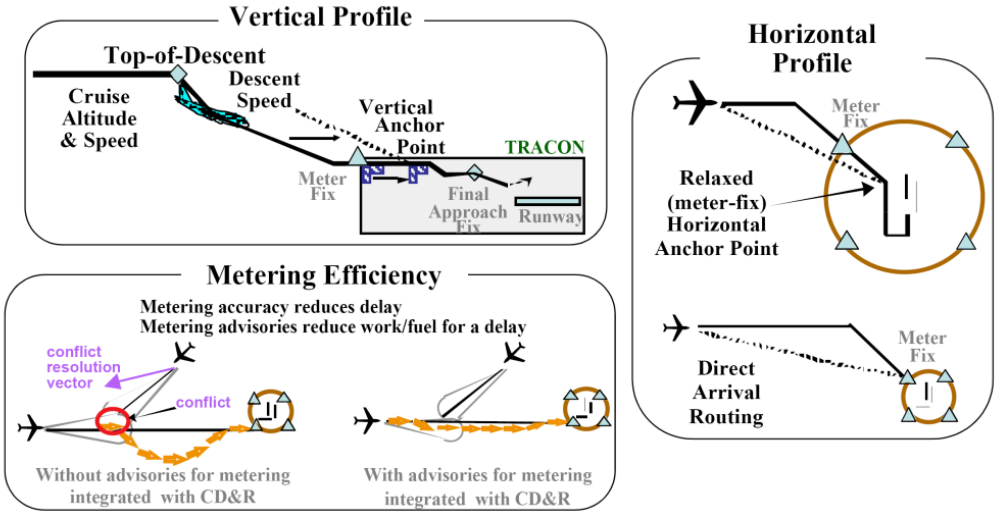


Figure 2-9. EDA benefit mechanisms [25]

A methodology to generate optimal 4D-trajectories subject to multiple time constraints is presented by Hagelauer and Mora-Camino [28]. The work was developed based on the fact that in future precise time control of aircraft flight trajectories is expected to allow a significant increase in capacity, while keeping the present level of safety. The 4D-trajectory optimisation problem was formulated as an optimal control problem, and neural networks were used to reduce the computational time related to the calculation of the costs associated with each decision step in the search process. The Direct Operating Cost (DOC) – fuel plus flight time costs – was considered as the cost function in the optimisation process. Results obtained from a 4D-cruise optimisation

process with multiple time constraints showed that a considerable amount of fuel can be saved (when compared to fixed altitude profile solutions). Thus, the authors concluded that the approach described seems to provide a solution for on-line 4D-trajectory optimisation for the next generation of Flight Management Systems (FMS).

Different issues related to the minimisation of the noise impact of aircraft are addressed in some detail in reference [29]. In particular, the development and use of analytical and semi-empirical aircraft trajectory and noise models in order to define low-noise flight procedures are described. Particular consideration is given to both the mathematical aspects involved in the aircraft trajectory model and its associated constraints, as well as the aircraft noise control criteria used to define the cost function to be utilised in the optimisation processes. The main results related to a set of operational measures to be implemented in order to reduce the aircraft noise levels in the vicinity of airports.

In order to reduce the noise level around airports, most of the noise abatement procedures involve measures in which both elapsed flight time, and thrust level are reduced. This results in turn in a decrease in the level of aircraft gaseous emissions. Even so it is important to highlight some of the technologies that are currently under development in order to mitigate the negative effects of these gaseous emissions. As emphasised in reference [2], these technologies, which mainly seek to adaptively modify aircraft engine performance, eventually could lead to improved engine component efficiency and/or reduced weight, reducing overall fuel burn and consequently $CO_2$ emissions. Among others, these technologies include inlet, fan, and compressor flow control; compressor stall, blade clearance, and combustion control; active bearings; as well as active materials and wireless sensors.

An alternative for reducing aircraft gaseous emissions is switching from kerosene supported aviation to liquid hydrogen supported aviation as highlighted in reference [30]. It is indicated in that work that cryoplane technology would not only eliminate particle and $CO_2$ emissions (if hydrogen is not produced from fossil energy sources), but also reduce oxides of nitrogen ($NO_x$) emissions. However, hydrogen engines would emit more water vapour ($H_2O$), which in turn would contribute to contrail formation. Different scenarios for a respective gradual technology transition between 2015 and 2050 from a global point of view are evaluated and analysed in reference [30]. Analyses

are mainly based on the level of $CO_2$, $H_2O$, and $NO_x$ emitted, as well as on contrails, radiative forcing, and global surface temperature changes. The results associated with all cryoplane transition scenarios suggest, in general, smaller increases in $CO_2$ concentrations, higher $H_2O$ emission indices, lower $NO_x$ emission indices, less but larger ice crystals in contrails, and a lower total aviation impact on earth surface temperature (Figure 2-10), when compared to those values corresponding to the kerosene scenario.

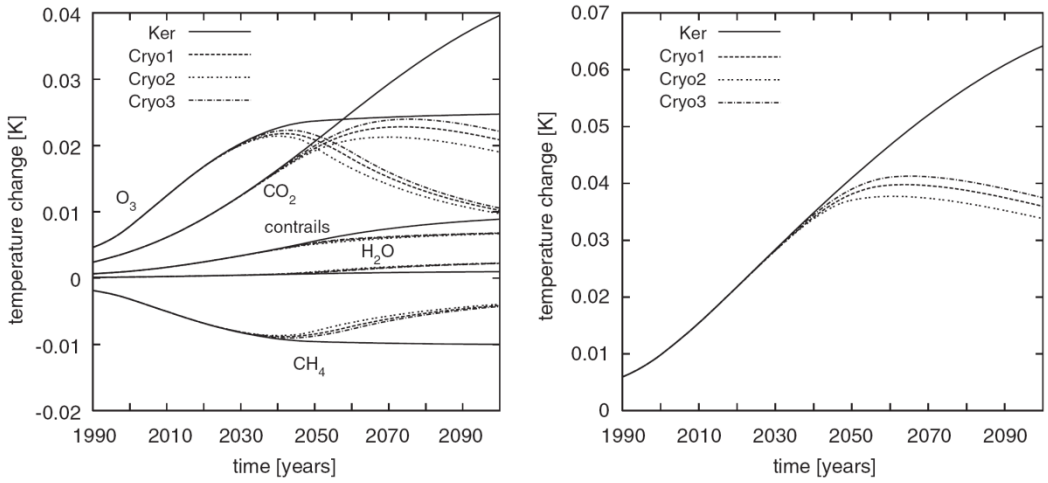


Figure 2-10. Global mean surface temperature change for cryoplane transition scenarios [30]

## 2.3 Further References

As already indicated, a key aspect, when addressing the problem of the impact of aircraft operations on the environment, is the inclusion of environmental considerations at the early stage of the aircraft/engine design process. This aspect is emphasised by Antoine *et al.* in references [31,32]. In their work, a design tool that includes different design modules that address key aspects of aircraft such as aerodynamics, performance, stability/control, structures, and economics, was developed. This tool was subsequently utilised for carrying out optimisation processes of a 280-passenger, twin-engine airliner (6,000 nm range). For these optimisation processes, different design variables (i.e., aircraft geometry, engine parameters, and performance), as well as different constraints (i.e., engine-out climb gradient, drag-to-thrust ratio, stability margins, etc.), were utilised. Pareto set of solutions (e.g., Figure 2-11) obtained from the minimisation of the aircraft operating cost, fuel consumption, $NO_x$ emissions, and noise, are summarised in

these studies. The main results indicated that significant reductions in emissions and perceived noise are possible to achieve, if aircraft are optimised based on these objective functions. Thus, for an increase in operating cost of 9%, $NO_x$ emissions could be reduced by as much as 54%, whereas cumulative certification noise could be lowered by 15 EPNdB for a cost increase of 25%. The authors concluded that the trend emerging from the analyses of the seemingly conflicting objectives of noise, fuel consumption, and $NO_x$ emissions (Figure 2-11), is the opportunity for significant reductions in aircraft environmental impact by designing the aircraft to fly slower and at lower altitude, i.e., 'slower, lower, greener'.

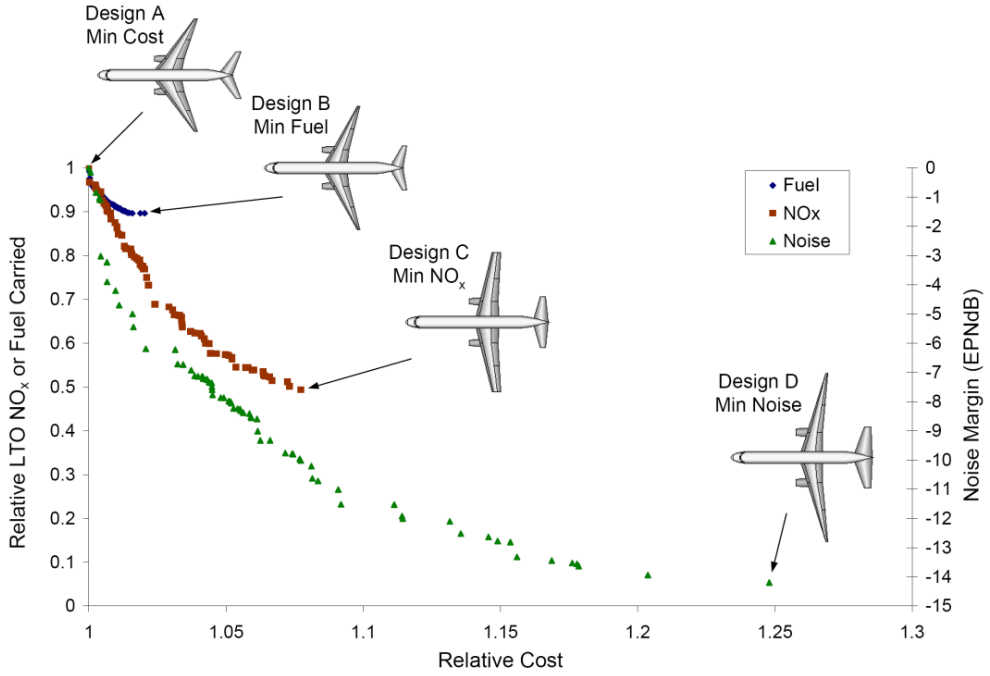


Figure 2-11. Pareto fronts of fuel carried, $NO_x$ emissions, and noise margin vs. cost [32]

Le Dilosquer [33] studied the influence of civil subsonic aero engine design and flight operations on atmospheric pollution, particularly, gaseous emissions. The pollutants considered in the analyses included $NO_x$, $H_2O$, and $CO_2$. Other pollutants such as carbon monoxide (CO), unburned hydrocarbon (UHC), soot, smoke, and sulphur dioxide ($SO_2$), were not considered. This was due to fact that the relative importance of these pollutants on earth's atmosphere pollution is smaller when compared to the corresponding one associated with those pollutants considered in Le Dilosquer's work. Since aircraft $NO_x$ contribute to both the increase of the tropospheric ozone, and to the destruction of the stratospheric ozone, the study was focused on

medium and long range aircraft. This was done with the purpose of evaluating the consequences of releasing significant amounts of $NO_x$ at high altitudes on earth's atmosphere, and eventually on global warming. For the analyses, a computer simulation system was developed. This computer program consisted of three main modules developed and integrated in order to simulate the aircraft flight route, the performance of the aircraft engines, and the formation of pollutants in the engine combustors.

Simulations of a long range widebody passenger aircraft (Boeing 747-400) were then carried out using the system developed. The objective of these simulations was to evaluate mainly the influence on net trust (FN) and specific fuel consumption (SFC) of designing the aero engine for both low landing and take off (LTO) cycle emissions, and low mission emissions. The main conclusions indicates that mission $NO_x$ reductions of up to 10% over designs optimised for LTO $NO_x$ are possible, suggesting that current International Civil Aviation Organization (ICAO) regulations are not an adequate criterion for controlling mission $NO_x$. It was also concluded that other operational measures (e.g. cruise speed reductions) could bring further reductions, but some of these improvements would be made at the expense of fuel burn, $CO_2$ and $H_2O$, payload-range capability, and direct operating costs. It was concluded, in addition, that the benefits from engine cycle and flight profile optimisations are not negligible, but smaller when compared not only to the potential gains associated with the introduction of low-$NO_x$ technology (30-80%), but also to the cumulative improvements (next 20 years) in airframe weight and aerodynamics, and the use of more efficient navigation processes (30%).

The potential benefits of adopting 'all' or 'more' electric aircraft concepts for secondary power systems of high capacity long range aircraft are assessed by Laskaridis [34]. In his work Laskaridis analyses qualitatively and quantitatively different issues associated to the implementation of these concepts in practice. Initially, in order to determine how these concepts fit with the overall design approach, future trends in aircraft and engine design are reviewed. The effects of off-takes (namely, bleed air and shaft power) on the performance of the engine, as well as the limitations of secondary power systems are then studied. An aircraft performance model was subsequently developed in reference [35] and utilised for the assessment of the impact of the 'all' or 'more' electric technologies on long range aircraft. Finally, conceptual design and

electric systems architectures suitable for the all or more electric technologies are developed and presented.

The main conclusions of Laskaridis' work indicate that engine parameters such as overall pressure ratio (OPR) and turbine entry temperature (TET) have an important effect on engine performance when bleed air or power extraction is utilised for the operation of aircraft secondary power systems. On the other hand, when a constant percentage of off-take is utilised, its associated penalties on engine performance do not depend on engine bypass ratio. It is also concluded that the power extracted in the form of bleed air for the operation of the aircraft environmental control system is about twice as much the actual power required. This is clearly a limitation of current secondary power systems. In addition, aircraft mass changes eventually would depend on the configuration of the electric system utilised and the extent of adopting all electric technologies. Finally, it is concluded that the adoption of 'all' or 'more' electric technologies could enable the design of more efficient aircraft, i.e., aerodynamic efficiency improvement and reduction in overall fuel consumption (about 4% for the long range aircraft studied); and that the impact of this type of technologies depends on the configuration of the specific aircraft being analysed.

Three main factors that characterise the environmental impact of aircraft operations: noise, air pollution around airports, and climate change, are discussed by Green in reference [36]. From these factors, because of its long term importance, the impact on climate change is extensively discussed in Green's work. Green argues that from the three main contributors to climate change from aircraft, $CO_2$, $NO_x$, and contrails, the last two ones (i.e., $NO_x$ and contrails) are the most promising targets. However, he adds, because of the long life of $CO_2$ in the atmosphere, it is vital that a significant reduction in $CO_2$ emissions is achieved in the long term. He suggests that, based on previous works, the introduction of technology related to contrail avoidance would be cost effective, and probably the single most powerful way of the reducing the environmental impact of aircraft operations, even though it would increase the level of $CO_2$ emitted. Regarding $NO_x$ emissions, Green recognises the conflict between reducing $CO_2$ and $NO_x$ simultaneously. He indicates that increasing OPR and TET in order to increase engine thermal efficiency will increase $NO_x$ emissions, and, consequently, it does not seem the best way forward. The main conclusions of Green's work mainly

indicate that measures (regulatory, economic, etc.) to be implemented in future should promote reduction in the impact on climate change rather than reduction in $CO_2$ emissions, since that measures based solely on $CO_2$ emissions are likely to do more harm than good.

Several questions oriented to the identification of civil aircraft design priorities are addressed by Brooker [5]. The design priorities discussed include air quality, climate change, and noise. In Brooker's work, these environmental concerns are classified as 'externalities', i.e., things arising from the production or consumption of goods that affect third parties. Thus, in order to estimate their associated external costs, ways of weighting these externalities, which allow the establishment of the type of policy (taxes, emissions, charges, marketable permits, etc.) that can be considered, are discussed. He concludes that future aircraft designs should focus on reducing significantly climate change impact; and that it is vital to avoid design compromises that prejudice this primary goal. Regarding the reduction in both gaseous emissions (in order to improve air quality) and noise, he concludes that the targets related to these issues should be pursued only to the extent that they do not affect both improved fuel efficiency, and reduced climate change emissions.

Filipone [37] addresses the benefits of operating subsonic commercial aircraft at speeds below the long-range cruise speed. Thus, he looks critically at the consequences of flying a subsonic commercial airliner slower on fuel savings, exhaust gas emissions, and overall costs. The case study considered involves the analysis of a subsonic jet airline operating over short to medium distances: flight segments up to 1,000nm. The limit of nominal 1,000nm was dictated by the possible delay at arrival. Particular emphasis is placed on the benefits of operating the aircraft at Mach numbers ($M \approx 0.77$ to 0.78) slightly lower than the corresponding cruise Mach number ($M = 0.80$). Some of the main results obtained by Filipone are illustrated in Figure 2-12. This figure corresponds to a general representation of the fuel versus time performance, which gives percentage values of fuel saving over percentage values of time saving. In Filipone's study, it is concluded that a cruise M reasonably lower that the nominal one helps to conserve a considerable amount of fuel. Estimated savings are about 1.8% of the total mission fuel for a 1,000nm flight segment (≈ 150,000kg per year). These fuel

savings are achieved at a cost of a delay of less than three minutes on each flight segment.

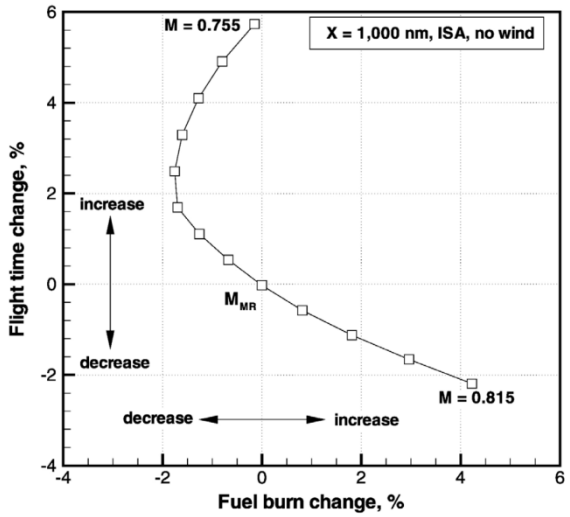


Figure 2-12. General representation of fuel vs. time performance [37]

It is worth highlighting that other alternatives for reducing the environmental impact of aircraft operations, different to those ones described through the studies summarised in this chapter, have been also considered in the past. Some of these alternatives are more unconventional than others. One particular example of these alternatives involves the use of air-to-air refuelling [38,39]. It is claimed that use of this type of technology would produce overall savings of the order of 30-40% fuel and 35-40% financial [38]. Even though these savings are very significant in terms of the impact on aviation's contribution to reducing atmospheric pollution, there are still some safety issues that need to be addressed carefully, and which, probably, will prevent the use of this type of technology for civil applications in the short term.

Finally, it is important to emphasise that the authors of all studies described briefly in this chapter and of many others available in literature have something in common that is very important for the aviation industry as a whole. They believe that environmental issues associated with commercial aircraft operations constitute a critical aspect currently. They also believe that there are different alternatives that could reduce the impact of commercial aviation on the environment. However, if not analysed carefully, some of these routes or alternatives are likely to do more harm than good. This is because, even though they can reduce some of the factors that exacerbate the aircraft environmental problem, they also can increase other ones that make this

problem worse. Therefore, a primary goal (impact on climate change, for instance) needs to be firstly identified, and compromises that prejudice this primary goal should be avoided. Based on the different efforts being made worldwide, which are reflected in the large amount of studies available in open literature, it seems likely that the main pollutants originated from aircraft operations will be reduced in future. It is expected of course that this enables the aviation industry to grow in a continuous and sustainable manner.

# 3
# Emissions Prediction Model

The development and implementation of a gaseous emissions prediction model which allows the reliable calculation of emissions trends from current and potential future aircraft gas turbine combustors is summarised in this chapter. Initially the model requirements are established, and the main strategies that can be adopted for combustor emissions prediction are then described. The methodology followed for simulating combustion chambers and the algorithms utilised for estimating the level of the main pollutants of interest formed inside the same are next summarised. The emissions prediction model developed has been verified through simulations of an actual combustor. The main results obtained from these simulations using the model developed are also shown and discussed in this chapter.

## 3.1
## Model Requirements

In general the establishment of the main requirements of any computational model in development is directly related to its ultimate goal. In this particular case, the ultimate goal of the emissions prediction model developed is to allow the reliable calculation of emissions trends from current and potential future aircraft gas turbine combustors. More specifically, its use in efficient evaluation and optimisation processes performed for design space explorations and trade-off studies constitutes one of the main objectives of the model developed. Particular examples of these evaluation and optimisation processes constitute those ones carried out in this work involving both aircraft trajectories, and aircraft engine cycles, which are described in the following chapters. The results obtained from the utilisation of this model are expected to be used eventually for analysing aircraft/engine design trade-offs and interdependencies, and helping policy-makers in decision-making processes.

Based on both its ultimate goal and its intended usage, the main requirements of the emissions prediction model described in this thesis were established as follows:

- Suitability of the model for predicting emissions from potential future aircraft gas turbine combustors. In other words, the approach to be utilised for the emissions prediction and the algorithms involved should allow both the modelling of novel concepts of aircraft gas turbine combustors, and the estimation of the level of pollutants emitted.
- Suitability of the model for carrying out reliable calculations of emissions trends. This means that emissions trends are good enough for what is expected from the model. If, in addition, absolute values of emissions are predicted properly, this would constitute an additional advantage of the emissions model. However, in the context in which this model was developed, this does not represent an initial requirement.
- Use of aircraft/engine-level design parameters (e.g., combustor inlet pressures, temperatures, etc.) instead of combustor-level design ones (e.g., parameters associated with fuel injector designs, recirculation zone patterns, etc.). There are two main reasons that support this requirement. The first one relates to the sensitivity of the information. Information about engines in general and combustors in particular is considered sensitive and can be hardly obtained. The second reason relates to the generality of the model. If combustor-level design parameters were utilised in the model, it would loose generality, and it might be applicable only to particular types of combustors.
- Generality and simplicity are important. The model should be as general (see previous requirement) and simple as possible. However, simplicity should not represent a detriment of the reliability of the results to be obtained. Thus, a compromise between the reliability of the results and the complexity of the model has to be achieved at some stage. This compromise can be achieved through the identification of those phenomena (physical, chemical, etc.) occurring inside aircraft gas turbine combustors that should be simulated, and those ones that should not. Phenomena that should be modelled include those ones that allow the reliable calculation of emissions

trends. In turn, phenomena that might increase the level of complexity of the model only without producing appreciable benefits should not be included in the model.

- Minimum computational time. Since one of the main uses of the model will involve its utilisation in aircraft/engine optimisation processes, the computational time involved in the emissions prediction is a critical parameter. The emissions prediction should be then carried out in a practical (shortest possible) time. Otherwise, this might prevent its use in optimisation processes.
- Modularity and extensibility features are welcomed. As indicated above, the model should be able to predict emissions from potential future aircraft gas turbine combustors. This means that novel concepts of aircraft gas turbine combustors will need to be accommodated in the future. Obviously good features of model modularity and extensibility will make much easier this process. These modularity and extensibility features could also help greatly in the adaptation of the model to other types of engines, for instance, industrial gas turbines.

According to these requirements, the emissions prediction model was developed and implemented, and the main stages of this development and implementation are described in detail in the following sections.

## 3.2 Emissions Prediction Modelling

In general, as pointed out in [40], three broad strategies can be adopted for combustor emissions prediction: empirical correlations, stirred reactor models (or physics-based models as they are sometimes described), and comprehensive numerical simulations involving detailed Computational Fluid Dynamics (CFD) calculations. On one hand, empirical correlations, in which fine details of the combustion chemistry and internal flow are completely subsumed into global expressions (largely established from measurements), present some basic limitations. This is because the complex processes occurring inside the combustor are only coarsely represented. This shortcoming is

compounded by the observation that different combustion concepts require the creation of new experimental databases. However, in a more rapidly evolving design phase it is unlikely that such data will become available; and therefore, a purely correlation-based approach to emissions prediction can provide little guidance [40], and at the same time prevents its use for potential future combustors designs. Even though detailed data on combustor performance can be incorporated in empirical correlations that map the variation around the flight envelope, such data is proprietary and not generally accessible. Furthermore, such correlations can only satisfactorily be applied to specific engine architectures and accommodate only minor design changes.

Detailed numerical simulations of the turbulent reacting flow inside the combustor involving CFD computations, on the other hand, represent the other extreme of the approaches to gas turbine emissions prediction. However, this approach is both time consuming and requires a detailed definition of the combustor geometry, which again would not be available for assessing technology trade-offs for potential future combustor designs, and may be difficult to obtain for even current designs [41]. The lack of robustness/reliability made evident through the continuous need for validating data obtained empirically constitutes another drawback of this approach. The computational time involved in each combustor CFD simulation would also inhibit their use in models developed to optimise aircraft trajectories and/or aircraft engine cycles. Stirred reactor models, in which the turbulent flow is sufficiently idealised and the time-dependent chemistry of pollutant formation may be computed exactly, therefore represent a robust compromise between the empirical and CFD-based options.

The concept of stirred reactors was widely studied during the early 1970s and 1980s mainly with the objective of establishing a better understanding of the process of formation of the different pollutants emitted from gas turbine combustors. During the last decade, stirred reactors models [41-44] have been mainly utilised in the development of computational models to predict trends in the level of emissions produced by gas turbine combustors currently in service. The model proposed by Visser and Kluiters [42] was set up by defining a series of perfectly-stirred reactors (PSR), which modelled combustion, mixing, steam/water injection, and their effects on emission formation using semi-empirical models for the reaction kinetics. Subsequently, Shakariyants *et al*. [43] extended this combustor model through the inclusion of other

physical phenomena such as fuel evaporation, and the consideration of local combustion efficiencies in each reactor.

A comparison of two emissions modelling methods, an empirical and a physics-based approach, is presented by Allaire *et al*. [41]. The predictive capability of each method is assessed by comparing model estimates of oxides of nitrogen ($NO_x$) and carbon monoxide (CO) emissions to combustor proprietary and certification data. For the case of the physics-based approach, a set of parallel PSRs was used for the modelling of the combustor primary zone. This representation recognises that a single PSR, which assumes perfectly mixing, would not be an adequate model for this combustor region, once most of the pollutants of interest are sensitive to local variations in fuel-air-ratio (FAR) in the combustor.

## 3.3 Combustor Modelling

The approach adopted in the present work utilises a number of stirred reactors for the modelling of a given combustion chamber and the estimation of the level of $NO_x$, CO, unburned hydrocarbons (UHC), and soot/smoke emissions. Three generic reactor models were developed: a perfectly-stirred reactor (PSR) model, a reactor model consisting of a series of perfectly-stirred reactors (PSRS), and a partially-stirred reactor (PaSR) model. A typical reactor configuration illustrating the use of the three generic reactor models developed for the simulation of a conventional combustor (Figure 3-1) is shown in Figure 3-2. Additional details about this reactor configuration are provided in the section corresponding to the case study analysed in this work.

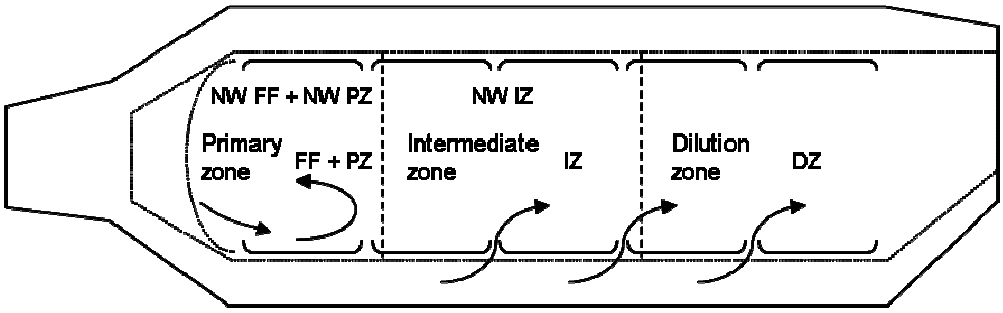


Figure 3-1. Conventional combustor schematic representation

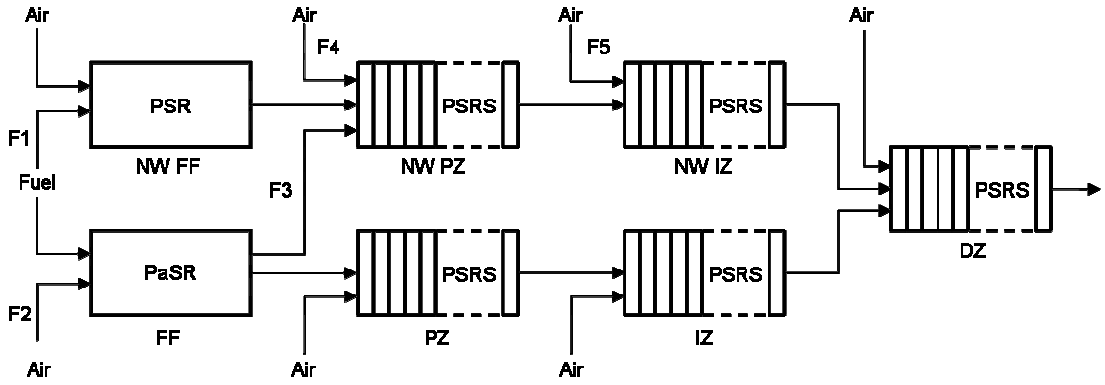


Figure 3-2. Conventional combustor – Multi-reactor model

### 3.3.1 Perfectly-Stirred Reactor (PSR) Model

The chemical reactor theory focuses mainly on the influence of the different levels of turbulent mixing on the chemical reactions within prescribed volumes rather than on the details of spatially-varying velocities and turbulence fields within a combustor [45]. In order to clarify the interaction between chemistry and fluid mechanics in continuous combustion, two modes of continuous flow mixing can be defined: (i) 'stream mixing', which occurs between fuel and air streams, and which is required to achieve locally flammable mixture proportions; and (ii) 'backmixing', in which recirculating partially or wholly burned gases are mixed with fresh reactants in order to achieve sustained self-ignition without the aid of external energy sources [45]. Stream mixing is represented by plug flow reactors (PFR), and backmixing by stirred reactors. The PSR is one in which backmixing is assumed to be infinitely fast so that the exit stream is representative of the homogeneous reactor contents. For gas turbine combustors, as highlighted in [45], the PSR approach on its own is not an appropriate model because it does not represent even macro-level inhomogeneities inside the combustor. This aspect has prompted the development of the concept of partially stirred reactors which will be discussed later.

Two streams enter the PSR model developed: a gas stream (air or combustion products) and a fuel/air stream. In the PSR model, mixing of these two streams is assumed to occur instantaneously, followed by an instantaneous process of attainment of chemical equilibrium. These equilibrium conditions are assumed to remain constant along all the PSR length. The equilibrium calculations are performed using the NASA CEA program [46,47], which is based on the minimisation of Gibbs free energy at

constant pressure and temperature subject to the constraint of conservation of elements. The combustion heat release is obtained from the equilibrium calculations. This assumption is supported by previous research work [48], in which good agreement was found between the temperature and completeness of combustion profiles obtained from both kinetic schemes and equilibrium models.

Most exhaust pollutants of interest – in particular those emitted from gas turbines, where the residence times are relatively short, and which are being studied in this work – are not in local chemical equilibrium. In making quantitative estimates of exhaust pollutant levels it is therefore necessary to include more detailed representations of finite rate chemistry. Thus the PSR model includes kinetics calculations of $NO_x$, CO, UHC, and soot/smoke. All the other species are assumed to be in chemical equilibrium. Similarly, the kinetics of radical formation is neglected and equilibrium radical concentrations prevail. Once the gas conditions, flow rates at the inlet and exit of the PSR, and its length are known, the PSR residence time is calculated and utilised for the integration of the reaction rates of the pollutants being analysed. Since the concentrations of these pollutants are very low, when compared to those corresponding to the combustion products in chemical equilibrium, it is assumed that the heat release is not affected by their formation. Finally, the exhaust pollutant levels together with the combustion products in equilibrium at the exit of a given PSR are supplied as inputs to the downstream reactors utilised in a multi-reactor arrangement.

### 3.3.2 Series of Perfectly-Stirred Reactors (PSRS) Model

Models of this type were first developed by Hammond and Mellor [48-50] during the early 1970s. In order to obtain a variation in the residence time distribution, plug flow reactors used normally to model the combustor secondary and dilution zones were replaced by a sequence of perfectly-stirred reactors (PSRS) of finite and equal volume. The semi-continuous air addition permits closer approximations of the airflow distribution computed using turbulent jet mixing phenomena. Thus, the PSRS reactor model developed consists of a series of perfectly-stirred reactors in which each individual PSR has its own discrete amount of air and fuel addition; that is, its own equivalence ratio or mixture fraction. The number of reactors that can be incorporated

into a PSRS reactor is user-specified, and it depends on the level of discretisation required in the volume of any particular combustor region. In practice, when these reactors are utilised, the number of perfectly-stirred reactors in each PSRS is increased until an independence of the results to this parameter is achieved.

### 3.3.3 Partially-Stirred Reactor (PaSR) Model

It was already indicated that for the modelling of gas turbine combustors, the PSR approach on its own is not an appropriate model because it does not represent even macro-level inhomogeneities inside the combustor. Consequently, a partially-stirred reactor (PaSR) model was developed in such a way that variations in gas composition, temperature and residence time, which influence directly the rates of pollutant formation, in particular $NO_x$ formation, are described statistically; however, only gross flow features at the reactor exit are predicted. Following [45,51], in the PaSR model it is assumed that mixing is complete to a scale which is small compared with the combustor dimensions, but not on a molecular scale. Hence, within the zone there exists a number of well stirred eddies or fluid elements which have different residence times. Then, considering that the eddy size is small compared with the combustor dimensions, the distribution of fuel among the eddies can be approximated by a Gaussian (normal) distribution about the overall mean value, whose (standard) deviation represents how completely the flow inside the reactor is mixed [51].

Following this approach, the mixture fraction, *f*,

$$f = \frac{\dot{m}_f}{\dot{m}_f + \dot{m}_a} = \left(1 + \frac{1}{\phi . FAR_s}\right)^{-1} \qquad (3\text{-}1)$$

is assumed to be normally distributed about the mean value and with a given (standard) deviation. The nature of the Gaussian distribution is such that its probability density function (PDF) only tends to zero as *f* tends to ±∞; however, in practice the mixture fraction only varies from 0 to 1. In this work a 'Clipped Gaussian' distribution (Figure 3-3) has been adopted.

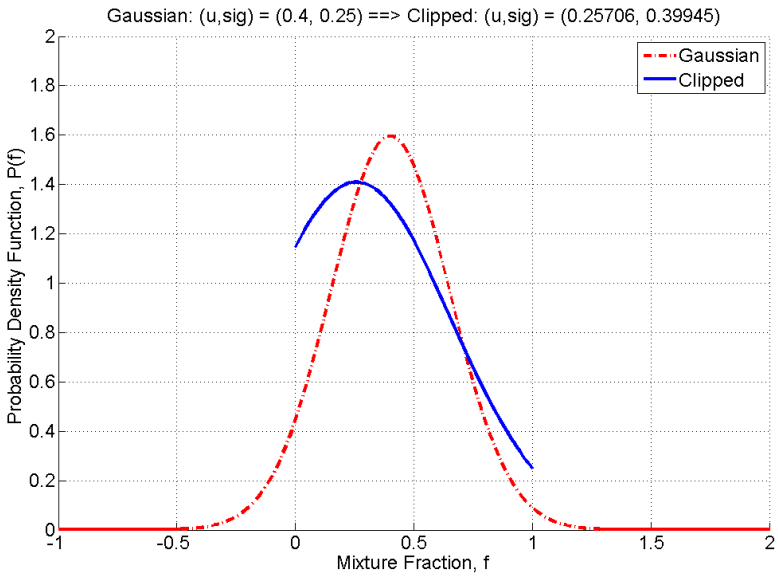


Figure 3-3. Gaussian vs. Clipped Gaussian distribution

As illustrated in Figure 3-3, a Clipped Gaussian function is basically a renormalised, truncated Gaussian function. The characteristic parameters of the Clipped Gaussian distribution, i.e., mean value and deviation (variance), are determined iteratively from those ones corresponding to the Gaussian (normal) distribution. The main advantage of using a Clipped Gaussian function is that the mixture fraction PDF integral from 0 to 1 (Clipped Gaussian distribution) is equal to the corresponding integral over the range $\pm\infty$ (Gaussian distribution). Additional details about Clipped Gaussian functions can be found in [52].

Before using the PaSR as described so far, it is necessary to know the value of the (standard) deviation corresponding to the Gaussian distribution of the mixture fraction, so that it is possible to calculate the mean value and deviation (variance) of the Clipped Gaussian distribution. In this sense, Fletcher and Heywood [51] introduced a parameter called 'mixing' (or 'unmixedness' as it is sometimes referred to) parameter (S), defined as the (standard) deviation of the mixture fraction divided by its mean value, Eq. (3-2), which is a measure of the uniformity of turbulent mixing within the reactor, with $S = 0$ corresponding to the completely mixed case.

$$S = \frac{\sigma}{f_m} \tag{3-2}$$

Sturgess [53,54] indicates that the mixing parameter can be established empirically by matching modelling predictions to measured emissions data, and that its values would be expected to differ from combustor to combustor, depending on combustor primary zone details, that is where this type of reactors are intended to be used. However, he argues that since the functions of the primary zone are the same in any combustor, it could be anticipated that combustors belonging to same class (swirl-stabilised annular combustors for instance) might have similar values of *S*. From the results of a sensitivity study carried out, Allaire *et al*. [41] concluded that the emissions of $NO_x$ and CO are strong functions of *S*, particularly idle CO. Thus, in their study [41] they varied the mixing parameter at each power setting in the engine certification data in such a way to minimise an objective function, which measured the difference between the emission indices of $NO_x$ and CO predicted and those corresponding to the engine certification data.

As pointed out by other authors [41], unmixedness is difficult to estimate because there are a number of issues (fuel physical state, instantaneous mixing of gases and air, incomplete kinetic modelling, unmixedness itself, etc.) that are not accounted for following this approach, but which can be compensated by this parameter. In this work it is not intended to use the mixing parameter as a correction factor for everything the model does not capture properly. Thus, as illustrated in Figure 3-4, some sort of generic correlation between the mixing parameter and the reactor equivalence ratio has been utilised. For comparison purposes, this figure also shows values of the mixing parameter obtained by Sturgess [53] for the case of swirl-stabilised annular combustors, and those used by Allaire *et al*. [41] in their analysis of a single-annular combustor. However, the reader must bear in mind that there is no such a generic correlation between the mixing parameter and the equivalence ratio, as highlighted in [53]. This correlation should be therefore verified each time that a particular engine/combustor configuration is being modelled.

Finally, it is important to emphasise that in order to both keep the model developed as simple as possible, and avoid an increase in the level of uncertainties in the results obtained (originated from assumed values for certain parameters that are not available in open literature), some phenomena that occur inside the combustor such as

fuel evaporation, combustion unsteadiness, and flow recirculation, among others, have not been included in the emissions model described in the present work.

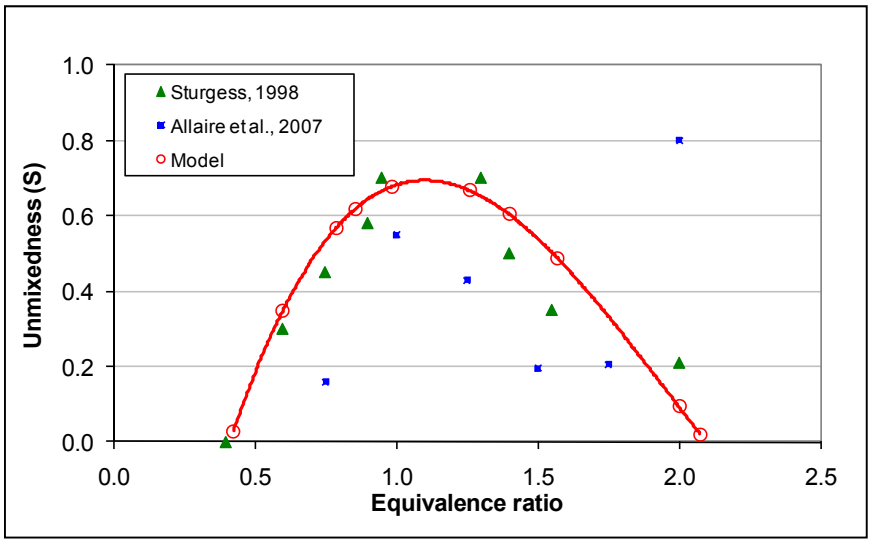


Figure 3-4. Unmixedness vs. Equivalence ratio (Sturgues, 1998 [53]; Allaire et al. [41])

## 3.4 Pollutant Formation Modelling

In this section, the algorithms utilised for modelling the formation of the four pollutants of interest, namely $NO_x$, CO, UHC, and soot/smoke, in each of the three types of generic reactors described previously are summarised.

### 3.4.1 Oxides of Nitrogen ($NO_x$)

The oxides of nitrogen – nitric oxide (NO) and nitrogen dioxide ($NO_2$), collectively referred to as $NO_x$ – are one of the pollutants that have generated most concern during the last years. This is mainly due to fact that, even though $NO_x$ emissions from aircraft engines reach their maximum value during take-off and climb-out, a large part of the total amount of $NO_x$ emitted by a long range aircraft – up to 80% as indicated in previous works [55] – is released at high altitudes, where aircraft are the main if not the only ones responsible for the emission of this type of pollutant. Most of the NO formed in combustion subsequently oxidises to $NO_2$ [56]. But at elevated temperatures, $NO_2$ removal is rapid, due to the presence of high radical concentrations, and $NO_2$ will be converted back to NO [57]. Consequently in most flames, formation of

$NO_x$ is based on NO formation. $NO_x$ can be produced by four mechanisms [56]: (i) thermal NO, (ii) nitrous oxide ($N_2O$) mechanism, (iii) prompt NO, and (iv) fuel NO.

#### 3.4.1.1 Thermal NO and $N_2O$ Mechanism

Thermal NO is produced by the oxidation of atmospheric (molecular) nitrogen in high temperature regions of the flame and in the post-flame gases [56]. In this work, the thermal NO formation rate is predicted according to the extended Zeldovich mechanism [51, 56-58]:

$$N_2 + O \leftrightarrow NO + N \quad \text{R1} \quad (3\text{-}3)$$

$$N + O_2 \leftrightarrow NO + O \quad \text{R2} \quad (3\text{-}4)$$

$$N + OH \leftrightarrow NO + H \quad \text{R3} \quad (3\text{-}5)$$

and the $N_2O$ contribution to the formation of NO according to [51,59]:

$$H + N_2O \leftrightarrow N_2 + OH \quad \text{R4} \quad (3\text{-}6)$$

$$O + N_2O \leftrightarrow N_2 + O_2 \quad \text{R5} \quad (3\text{-}7)$$

$$O + N_2O \leftrightarrow NO + NO \quad \text{R6} \quad (3\text{-}8)$$

Then in order to calculate the thermal NO formation rate from the mechanisms described above, it is necessary to determine the concentrations of molecular oxygen ($O_2$), molecular nitrogen ($N_2$), oxygen (O), hydroxyl radical (OH), hydrogen (H), nitrogen (N), and $N_2O$. Thus, in accordance with previous works [45,51,59], assuming that (i) the concentrations of $O_2$, $N_2$, O, OH, and H are given by their equilibrium values at the local temperature, pressure, and mixture fraction (NO formation reactions slower than energy-releasing reactions), and (ii) the concentrations of N and $N_2O$ are in steady state (N and $N_2O$ formation rates faster than NO formation rate), a rate equation that computes the changes in NO mass fraction ($Y_{NO}$) can be written as (see details in Appendix B):

$$\frac{dY_{NO}}{dt} = \frac{2\bar{M}_{NO}}{\rho}(1-\alpha^2)\left\{\frac{R_1}{1+\alpha K_1} + \frac{R_6}{1+K_2}\right\} \quad (3\text{-}9)$$

In Eq. (3-9), $\alpha$ is defined as $\alpha = [NO]/[NO]_e$. In this work, $\alpha$ is calculated using actual values of NO concentration from a previous calculation step (i.e., upstream reactors). $R_i$ denotes in turn a 'one way equilibrium' reaction rate. For instance, from Eq. (3-3), R1 = $k_{1f}[NO]/[NO]_e$, where $k_{1f}$ is the forward reaction rate coefficient. In this study, the rate coefficients have been taken from Miller and Bowman [58]. Additionally $K_1$ and $K_2$ are defined as $K_1 = R_1/(R_2 + R_3)$ and $K_2 = R_6/(R_4 + R_5)$. The last term on the right hand side of Eq. (3-9) represents the $N_2O$ contribution to the NO rate formation. For typical gas turbine operating conditions, this term is generally negligible [45]. Eq. (3-9) as shown is directly utilised in the reactor models described above.

#### 3.4.1.2 Prompt NO

What characterises prompt NO formation is the fact that it is formed at a rate faster than that calculated from the thermal NO mechanism described before. Three sources of prompt NO in hydrocarbon fuel combustion can be then identified [57]: (i) non-equilibrium O and OH concentrations, which accelerate the rate of formation of $NO_x$ through the thermal NO mechanism; (ii) the Fenimore prompt NO mechanism (reaction of hydrocarbon radicals with molecular nitrogen); and (iii) reaction of O atoms with $N_2$ to form $N_2O$, and subsequently NO. In this study, the rate of NO formation through this mechanism (prompt NO) is estimated according to a modified version of the global kinetic parameter derived by De Soete [60], and following the approach utilised in [61] (considering Jet-A as the fuel in this particular case, which can be represented by $C_{12}H_{23}$):

$$\frac{dY_{NO}}{dt} = \left(\frac{\bar{M}_{NO}}{\rho}\right) f_{pr} k'_{pr} ([O_2]_e)^a [N_2]_e [C_{12}H_{23}] exp\left(\frac{-36499.507}{T}\right) \qquad (3\text{-}10)$$

where,

$$f_{pr} = 4.75 + 0.0819x - 23.2\phi + 32\phi^2 - 12.2\phi^3$$

$$k'_{pr} = 6.4 \times 10^6 \left(\frac{0.0820575T}{P}\right)^{a+1} \qquad (3\text{-}11)$$

$$a = \begin{cases} 1.0, & X_{O_2} \leq 4.1 \times 10^{-3} \\ -3.95 - 0.9 \ln X_{O_2}, & 4.1 \times 10^{-3} < X_{O_2} \leq 1.11 \times 10^{-2} \\ -0.35 - 0.1 \ln X_{O_2}, & 1.11 \times 10^{-2} < X_{O_2} < 0.03 \\ 0.0, & X_{O_2} \geq 0.03 \end{cases}$$

In equations (3-10) and (3-11) $f_{pr}$ is a correction factor that incorporates the effect of fuel type, and $a$ is the oxygen reaction order which is calculated as a function of the oxygen mole fraction ($X_{O_2}$). Additional details of these equations can be found in [61]. Since aviation fuels (kerosenes and other light distillate fuels) do not contain significant levels of fuel-bounded nitrogen, the contribution of Fuel NO to the NO rate formation will be insignificant. Thus, the $NO_x$ formed by the Fuel NO mechanism has not been included in this work.

### 3.4.2 Carbon Monoxide (CO)

As highlighted in [54,56], much of the CO arises from incomplete combustion of the fuel. When temperatures are very high, CO emissions will be high due to dissociation of carbon dioxide ($CO_2$). For short-residence times and/or low reactant temperatures, they will also be high due to incomplete combustion. The modelling of CO emissions in this work is carried out assuming that during combustion all fuel first reacts instantaneously to CO and water ($H_2O$), and then the CO conversion (oxidation) proceeds through [62,63]:

$$CO + OH \leftrightarrow CO_2 + H \qquad \text{R7} \qquad (3\text{-}12)$$

From Eq. (3-12), assuming equilibrium conditions for OH and H, and taking into account carbon atoms conservation, similarly to what was considered in [62], the rate of CO oxidation can be written as (for more details, see Appendix C):

$$\frac{dY_{CO}}{dt} = -k_{7f}\left(\frac{\overline{M}_{CO}}{\rho}\right)[OH]_e\left\{1 + \frac{[CO]_e}{[CO_2]_e}\right\}([CO] - [CO]_e) \qquad (3\text{-}13)$$

where $k_{7f}$ represents the forward reaction rate constant of Eq. (3-12) – reaction R7. Equation (3-13) is integrated along all the reactors used to model a particular combustion chamber, in a similar way to the case of $NO_x$ emissions.

### 3.4.3 Unburned Hydrocarbons (UHC)

The reaction kinetics of UHC and soot/smoke, and consequently their modelling, are much more complex than for CO and $NO_x$ formation. Thus, in this work only simplified expressions for the formation rate of these pollutants will be used to predict their emission levels. The modelling of the UHC is performed following the methodology described in [64]. It is assumed that the fuel initially reacts according to:

$$C_{12}H_{23} + 6O_2 \leftrightarrow 12CO + 11.5H_2 \qquad \text{R8} \qquad (3\text{-}14)$$

The quasi-global reaction rate for Eq. (3-14) – reaction R8,

$$\frac{dY_{C_{12}H_{23}}}{dt} = -2 \times 10^5 \left[\frac{\left(\bar{M}_{C_{12}H_{23}}\right)^{0.5}}{\bar{M}_{O_2}}\right] \times \left(\frac{9T}{1000} - \frac{1}{2}\right) P^{0.3} Y_{O_2} exp\left(\frac{-6914.947}{T}\right) \left(Y_{C_{12}H_{23}}\right)^{0.5} \qquad (3\text{-}15)$$

is then integrated along all the reactors used to simulate a given combustor chamber, starting at an initial concentration corresponding with the fuel entering to the first reactor(s). Additional details about the UHC kinetic model can be found in Appendix D.

### 3.4.4 Soot/smoke

The production of soot, which if it is not subsequently oxidised will be emitted through the combustor exhaust as smoke, is mainly the result of incomplete conversion of carbon elements in the fuel to CO and $CO_2$ [45]. In gas turbine combustors it is produced in the richest parts of the combustion zone, and it is undesirable not only from an environmental point of view, but also because it is the principal source of thermal radiation to the combustor liner. Although the details of the mechanism remain poorly understood [40,45], the main processes involved in soot formation and oxidation can be characterised by four steps: particle nucleation, surface growth, coagulation, and oxidation. The two first stages constitute the soot formation processes, which are followed by the soot oxidation process in which the soot is burned to form gaseous products such as CO and $CO_2$. Soot consists mostly of carbon (about 96%), and a mixture of hydrogen, oxygen, and other elements [56]. Thus the soot density is

generally accepted between 1800-2000 kg/m$^3$ which is close to graphite density. In this study, the soot formation process is modelled according to an empirical expression suggested by Rizk and Mongia [65]. Thus the rate of soot formation ($S_f$), in m$^3$ soot/s, is expressed as (omitting the term for soot oxidation):

$$S_f = 1.4887 \times 10^{-4} \left(\frac{\phi . FAR_s}{\dot{m}_a T}\right) P^2 (18 - H_{cont})^{1.5} \left(\frac{\dot{m}_{g_t}}{\rho_{soot}}\right) \tag{3-16}$$

In the soot oxidation process, the major oxidation species are considered to be oxygen molecules ($O_2$) and hydroxyl radical (OH). The rate of soot oxidation ($W'_{O_2}$), in kg soot/m$^2$.s, due to $O_2$ is determined from the Nagle and Strickland-Constable formula [66]:

$$W'_{O_2} = 12 \left\{ \left[ x_s \left( \frac{k_A p_{O_2}}{1 + k_Z p_{O_2}} \right) \right] + \left[ k_B p_{O_2} (1 - x_s) \right] \right\} \tag{3-17}$$

where,

$$x_s = \left( \frac{1}{1 + \frac{k_T}{k_B p_{O_2}}} \right) \tag{3-18}$$

The temperature dependence in Eq. (3-17) occurs via the reaction rate constants $k_A$, $k_B$, $k_Z$, and $k_T$, which in this study they are taken from [67]. Expressing Eq. (3-17) as a function of the surface area of the aerosol it becomes [68] (see details in Appendix E),

$$W_{O_2} = \pi^{1/3} . 6^{2/3} . {f_v}^{2/3} . N^{1/3} . W'_{O_2} / \rho_{soot} \tag{3-19}$$

Following the same approach used in [68], the role of OH radical attack is evaluated from the kinetic theory of collision rate. Then the OH oxidation of soot is expressed as [68],

$$W_{OH} = 10.14 . \theta . {f_v}^{2/3} . N^{1/3} . X_{OH} . T^{-1/2} \tag{3-20}$$

where $\theta$ is the collision efficiency which has been chosen to be 0.2 in this study. The overall rate of soot oxidation is the sum of the terms given by equations (3-19) and (3-20), in m$^3$ soot/m$^3$.s.

In order to predict the level of soot produced during combustion according to the methodology described, it is necessary to determine first two parameters: the particle

number density ($N$) and the soot volume fraction ($f_v$). As pointed out in [68], it is possible to neglect the variations in number densities, $N$, and to adopt a suitable average number density (of the order of $10^{18}$ $m^{-3}$). This parameter is user-specified in this work. The soot volume fraction ($f_v$) required during the combustor simulations is computed as the difference between the amount of soot formed and oxidised in the previous calculation step. Finally, the soot volume fraction at the end of the combustor chamber is utilised to calculate the particulate mass loading ($PML$), which is converted subsequently into Smoke Number (SN) using the correlation presented in [69], and reproduced in Appendix E for the sake of completeness.

## 3.5 Model Overview

Before describing the application of the emissions prediction model developed to general case study, it is worth highlighting the main characteristics of the model, in terms of model architecture, programming language, etc. A schematic representation of the emissions model and its main modules is shown in Figure 3-5. In this figure only the main interactions (represented by arrows) among the modules are illustrated. The model has been coded using *Fortran 90* as the main programming language. Even though a procedural language (Fortran 90) was utilised, modularity and extensibility features were considered as the main factors determining the general architecture of the model. This was motivated by the fact that, in future, novel concepts of aircraft gas turbine combustors will need to be accommodated.

As illustrated in Figure 3-5, the emissions model comprises five main modules (bigger rectangles in Figure 3-5). The main module is the 'Emissions_Index' module. This module drives the computation process and, among other things, it reads data from the input file and writes results to the different output files. The 'Emissions_Index' module uses (i.e., makes calls to) subroutines from the 'Chamber' module, in which the different combustion chamber configurations (currently, only conventional combustor configurations are available) has been coded. The 'Region' module contains several subroutines that model the different regions of combustion chambers, such as primary, intermediate, and dilution zone. These subroutines are used by the 'Chamber' module. The 'Reactor' module contains, in turn, the subroutines developed for modelling the

generic chemical reactors described in Section 3.3. The subroutines in the 'Region' module use one or more of these subroutines present in the 'Reactor' module. Finally, the 'Chemistry' module is composed of several subroutines that contain the algorithms utilised for simulating the formation of the main pollutants of interest. These subroutines are mainly used inside the 'Reactor' module.

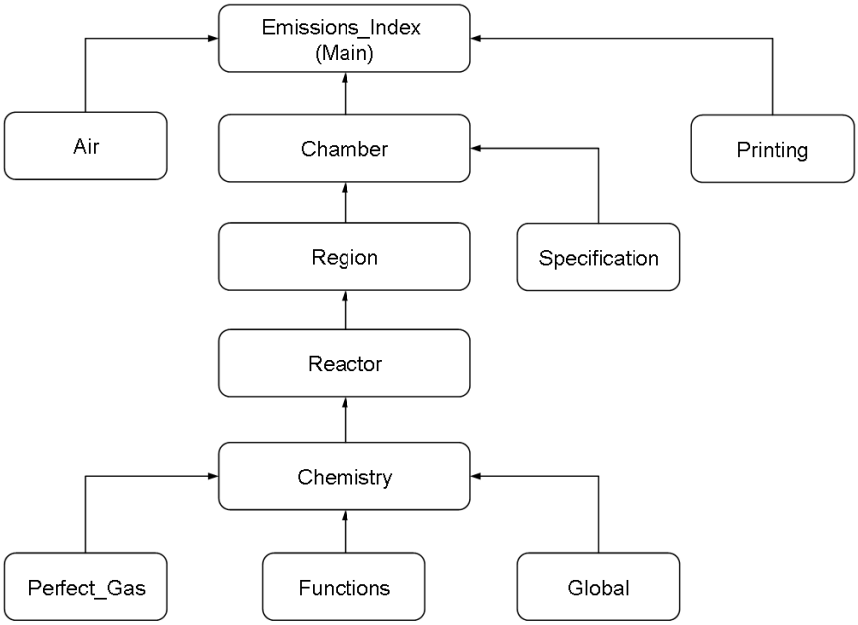


Figure 3-5. Emission prediction model – Schematic representation

The emissions prediction model developed also comprises other secondary modules. These secondary modules include the following ones: 'Air' (subroutines for computing air composition), 'Printing' (subroutines for printing results), 'Specification' (contains parameters considered constant during the calculations), 'Perfect_Gas' (subroutines for calculating thermodynamic properties of ideal gases), 'Functions' (contains several functions, including those ones for computing reaction rate coefficients), and 'Global' (contains parameters considered common to all modules). Since a fully objected-oriented programming language such as C++ has not been used in the development of the model, an attempt to represent its architecture (Figure 3-5) using a standardised modelling language such as UML (Unified Modelling Language) has not been performed. Thus the arrows in Figure 3-5 simply point to the module inside which the subroutines or parameters (from the modules in which the arrows start) are utilised.

## 3.6
## Case Study

### 3.6.1
### General Description

It is clear that, in order to demonstrate that the methodology developed for gas turbine emissions prediction is robust, an extensive validation process of the algorithms implemented should be carried out using detailed gas turbine data. Unfortunately, such data is considered sensitive information by industry and can not be found in the public domain. In order to provide insight into the results that can be obtained using this methodology, a general case study involving the simulation of a typical two-spool high bypass ratio turbofan (with separate exhausts) using a (Rich-burn Quick-mix Lean-burn, RQL) conventional combustor was analysed (GE CF6-80E1 engine data available in the public domain was used for the simulations). This particular aircraft engine was selected for the present analysis because other researchers [42,43] in the past have utilised engines belonging to the same family.

All the engine simulations were performed using TurboMatch [70], and incorporated data from the open literature [71,72]. Thus, Figure 3-6 shows the predicted engine power at static sea-level conditions as a function of the fuel flow supplied. The respective values associated with the engine certification data [73] are also included in this figure for comparison purposes. The conventional combustor used in the particular engine simulated in this case study is modelled following a similar approach to that utilised by Rizk and Mongia [74] for simulating conventional combustors.

Accordingly, Figure 3-2 illustrates the reactors arrangement utilised in this particular case. Note that, unlike the Rizk and Mongia's work, in this work the first part of the combustor primary zone, which simulates the initial mixing and reaction of the fuel with the nozzle and swirler air – called flame front (FF), is modelled using a partially-stirred reactor (PaSR), which takes into account inhomogeneities in this combustor region. In turn, the second part of the combustor primary zone, called primary zone (PZ), the combustor intermediate (or secondary) zone (IZ), and the combustor dilution zone (DZ) are modelled by a sequence of perfectly-stirred reactors (PSRS).

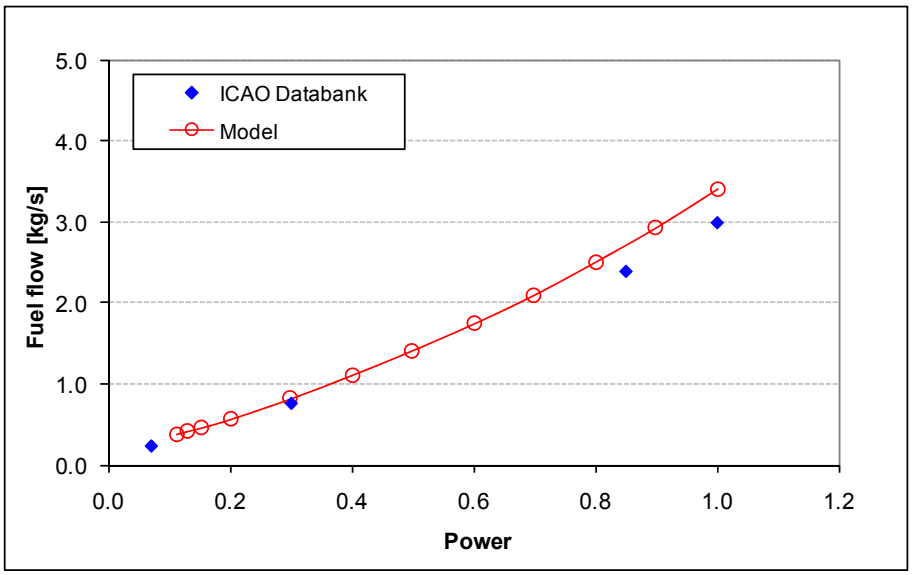


Figure 3-6. Fuel flow vs. Power setting (ICAO Databank [73])

Other details involved in the combustor modelling are similar to those considered in reference [74]. Thus, each of the combustor regions upstream the DZ (FF, PZ, and IZ) is simulated by two generic reactor models in parallel that occupy the core and near-wall (NW) regions of each of these zones. At the end, the outcomes of both core and near-wall reactors mix together to form a single PSRS, which models the combustor DZ. Since it was not possible to obtain detailed engine/combustor data for carrying out these case study simulations, estimates of the same were performed based on information publicly available. Table 3-1 summarises the combustor data utilised in the combustor simulations carried out in this general case study.

Table 3-1. GE CF6-80E1 combustor data

| Zone | FF | PZ | IZ | DZ |
|---|---|---|---|---|
| Flow Area [$m^2$] | 0.21 | 0.21 | 0.21 | 0.21 |
| Length [m] | 0.031 | 0.031 | 0.094 | 0.094 |
| Air inflow fraction | 0.20 | 0.20 | 0.20 | 0.40 |

When simulating a conventional combustor using the reactors arrangement shown in Figure 3-2, in reference [74] three arbitrary model parameters were defined: F1 (fraction of fuel reaching the near-wall mixing zone), F2 (proportion of the swirler and dome air that goes into the PaSR reactor - lean blowout reactor in the original work), and F3 (fraction of the burning gases admitted into the second near wall reactor). In addition to these three parameters, in this work two new ones, F4 and F5, were defined.

F4 and F5 represent the fraction of air initially assigned to the PZ and IZ that goes into their near-wall reactors, respectively.

A sensitivity analysis of the influence of these arbitrary parameters on the level of emissions produced by this particular combustor was carried out. Details of the results obtained from this sensitivity analysis can be found in Appendix F. Table 3-2 shows the values of the model parameters utilised for producing the emission results presented in this work. These values were selected in such a way to minimise the difference between the level of emissions predicted using the model developed and the corresponding one associated with the engine certification data [73]. A summary of the results obtained taking into account the considerations described above is presented in the following section.

Table 3-2. Model parameters – Combustor configuration

| F1 | F2 | F3 | F4 | F5 |
|---|---|---|---|---|
| 0.15 | 0.60 | 0.15 | 0.20 | 0.20 |

### 3.6.2 Results and Discussion

The main results obtained in this case study, which basically involves a verification exercise of the emissions prediction model developed, are summarised in this section. Firstly the evolution of some characteristic parameters including equivalence ratio, temperature, and residence time along the combustor axial direction is presented. Then predicted levels of the combustor exhaust emissions in terms of emissions indices (EI) are shown.

#### 3.6.2.1 Axial Position

All results shown in this section relate to the variation of the main characteristic parameters of the combustor along its axial direction (Figure 3-7 to Figure 3-9), and correspond to the case in which the engine is operating at full power conditions. Thus, in Figure 3-7 variations in equivalence ratio and mixture fraction along of the combustor axial direction can be observed. As a consequence of the combustor airflow partition, and the assumed values for the model parameters (F1 – F5), it can be observed

from this figure that the core equivalence ratio in the PZ is relatively high, which creates a relatively low core temperature, as can be observed in Figure 3-8. One of the consequences of this relatively low core temperature might be the underestimation of the level of $NO_x$ produced, due to the direct dependence of this pollutant to high temperatures. However, according to the model requirements, this should not really represent a problem as long as the emissions trends are representative.

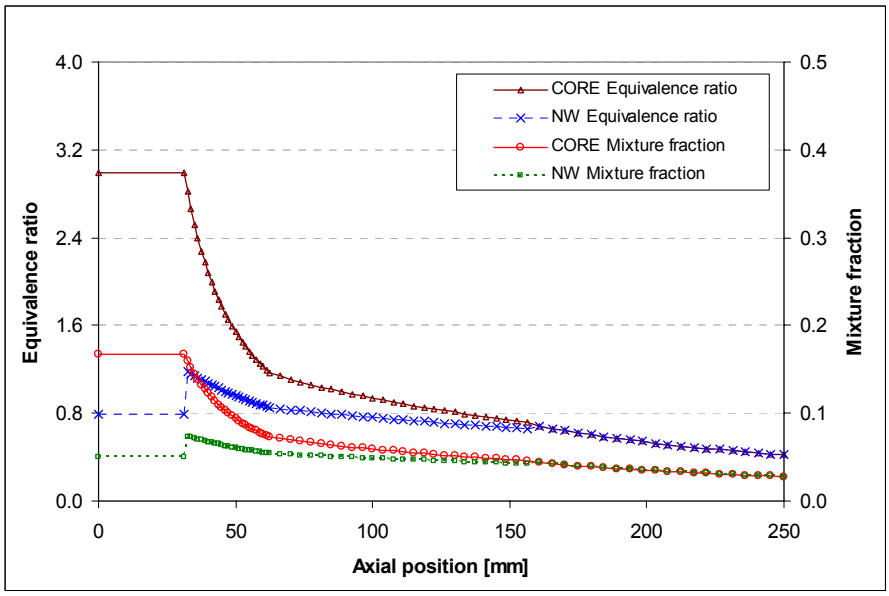


Figure 3-7. Equivalence ratio and Mixture fraction vs. Axial position

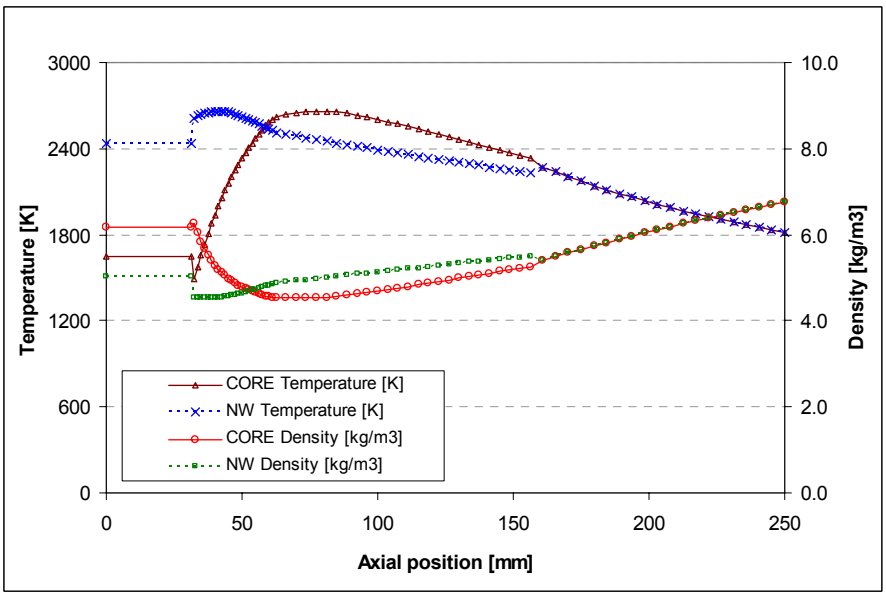


Figure 3-8. Temperature and Density vs. Axial position

In Figure 3-8 it is also possible to see the inverse relationship between temperature and density, the higher the temperature, the lower the density. Certainly, density is very important because it is directly related to the combustor residence time and, consequently, to the level of the pollutants formed inside gas turbine combustors. It is important to emphasise that, in order to calculate the weighted average of the parameters that characterise the inlet conditions to the combustor DZ, the mass flow rate of the combustion gases has been utilised. This last aspect is clearly observed in Figure 3-9, which shows the evolution of the combustor residence time along the combustor axial direction.

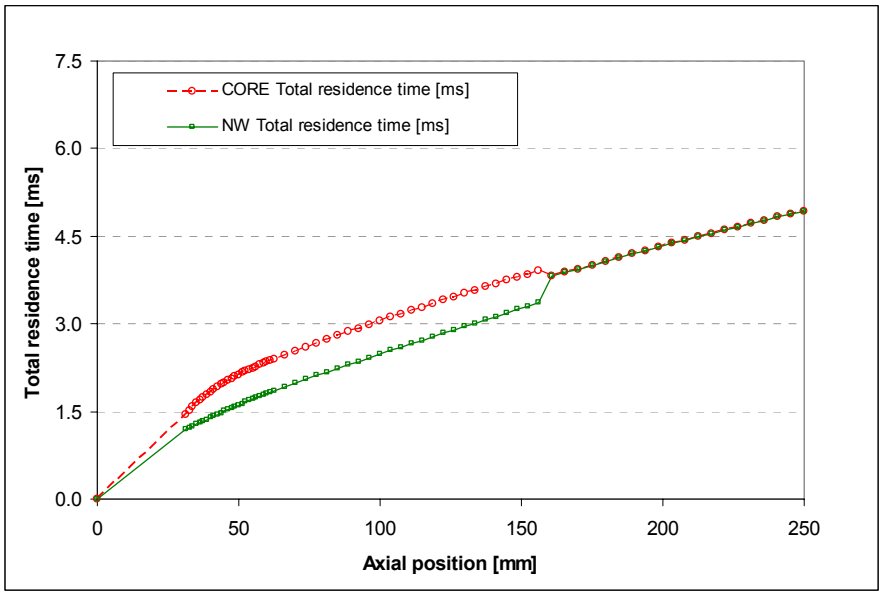


Figure 3-9. Total residence time vs. Axial position

### 3.6.2.2 Emission Indices

The predictive capability of the emissions model developed is illustrated in Figure 3-10 to Figure 3-13, which show the levels of $NO_x$, CO, UHC, and soot/smoke produced by the engine as a function of its power setting. From these figures it is possible to conclude that in general the trends observed in practice are well reproduced for the four pollutants being modelled. However, as already mentioned, due to all the complexity involved in modelling the kinetics of UHC and soot/smoke, considerable uncertainty surrounds the prediction of these two pollutants. By contrast, the modelling of $NO_x$ and CO formation is more secure and the emissions trends predicted are considered reliable.

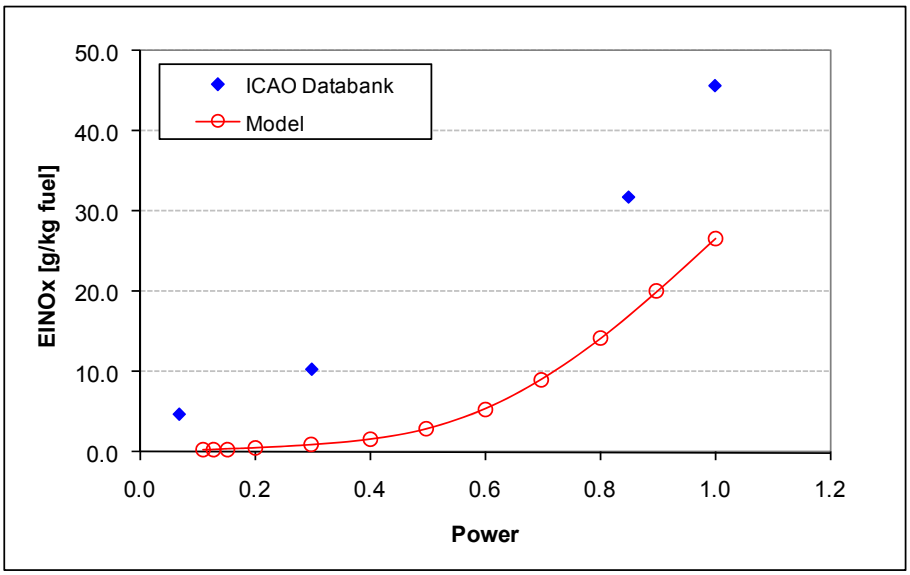


Figure 3-10. $NO_x$ emissions vs. Power setting (ICAO Databank [73])

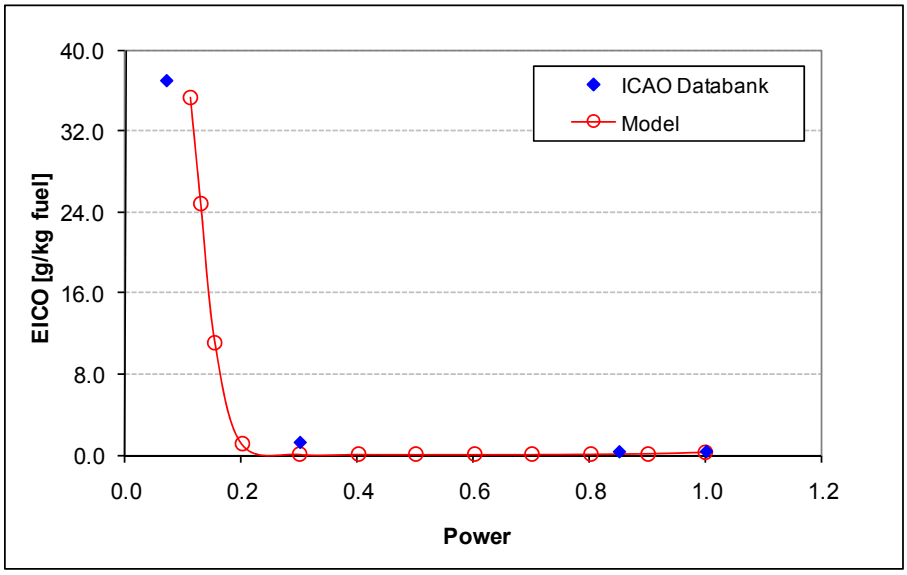


Figure 3-11. CO emissions vs. Power setting (ICAO Databank [73])

As can be observed in Figure 3-10, for the conventional combustor simulated in this case study, the $NO_x$ emissions are underestimated. It is believed that one of the main reasons relates to the introduction of a mean residence time based entirely on bulk flow properties. In the absence of recirculation (c.f., [48]) or a residence time distribution, the calculated residence time (computed as being directly proportional to both density and volume of the reactor and inversely proportional to the mass flow rate) is relatively short, as illustrated in Figure 3-14, which shows variations in the combustor

outlet temperature (COT) and residence time ($t_{res}$) as a function of the engine power setting.

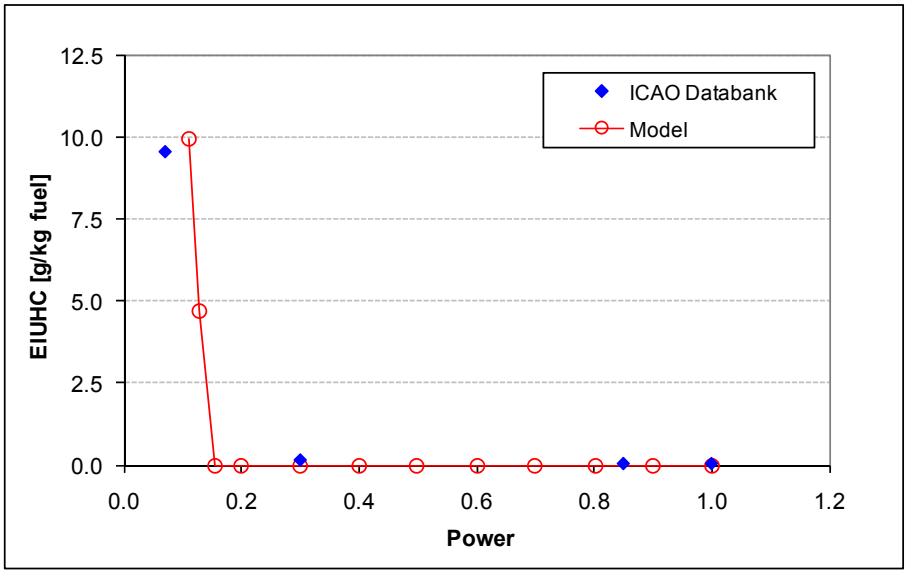


Figure 3-12. UHC emissions vs. Power setting (ICAO Databank [73])

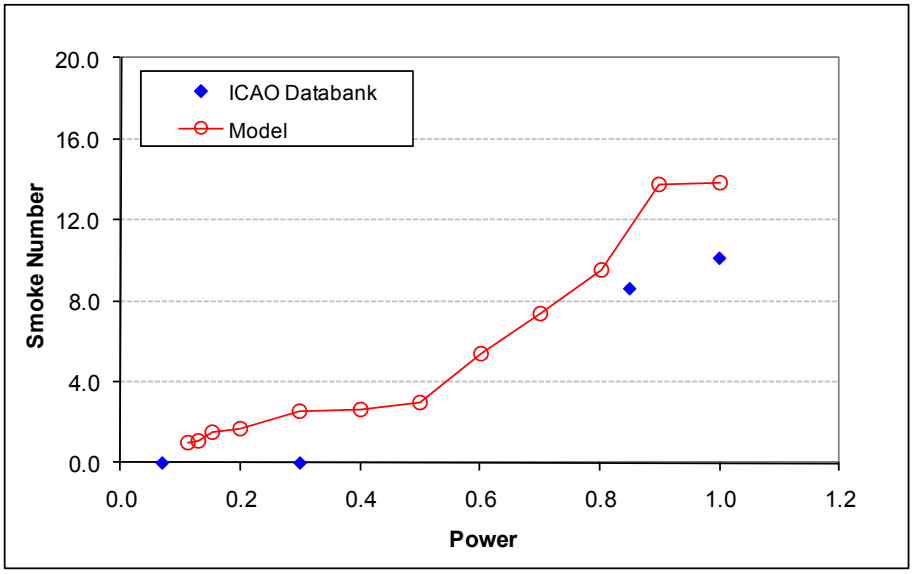


Figure 3-13. Soot/smoke emissions vs. Power setting (ICAO Databank [73])

Thus, if the residence time in the combustor PZ and IZ is doubled, which roughly represents the recirculation process of half the flow passing through these regions, the increased $NO_x$ emissions would be approximately twofold too, which would be in a closer correspondence with the engine certification data [73]. However, since the model developed in this work will be used mainly as a sensitivity analysis tool, in which the predicted emissions trends are more important than the absolute levels, no attempts to

include recirculation zone patterns have been made. Arbitrary factoring of residence time in the absence of more detailed flow field information from measurement or CFD computations would appear inappropriate. Extension of the models to potential future aircraft gas turbine combustors, based on novel concepts such as those of Lean Direct Injection (LDI) and Lean Pre-vaporised Premixed combustion (LPP), will involve the introduction of further generic reactor models incorporating, for example, fuel droplet evaporation and flame stability considerations.

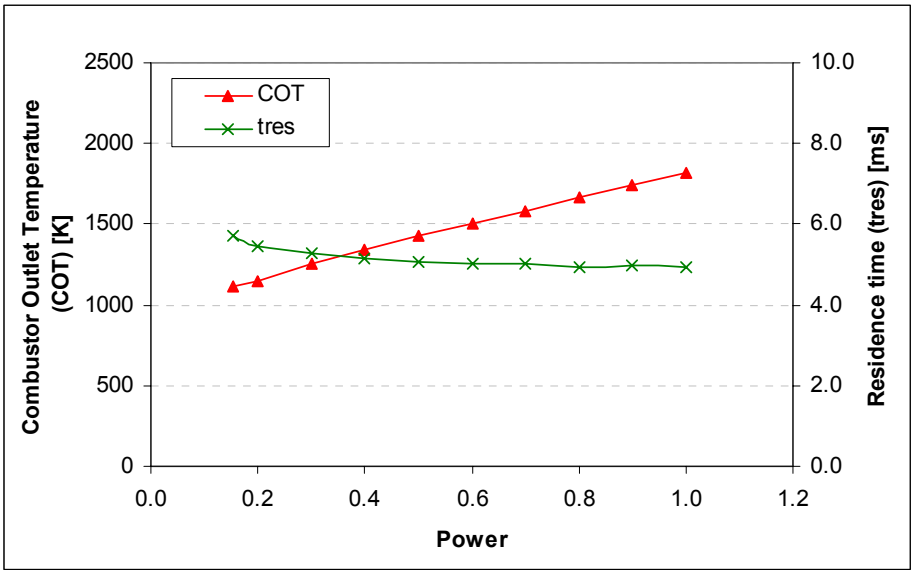


Figure 3-14. Combustor outlet temperature (COT) and Residence time ($t_{res}$) vs. Power setting

As mentioned previously, the ultimate goal of the emissions prediction model described in this chapter involves its use in efficient optimisation processes. These processes will be carried out with the objective of evaluating and optimising both aircraft flight trajectories and aircraft engine cycles. It is expected that these optimisation processes eventually allow the determination of 'greener' aircraft trajectories and engine cycles, which help to minimise the impact of commercial aircraft operations on the environment. The following chapters describe the application of the emissions prediction model described for these purposes.

# 4
# Trajectory Optimisation

This chapter is focused on optimisation problems and, in particular, on those main aspects that characterise trajectory optimisation problems. The first sections discuss general aspects of optimisation, as well as a general classification of the different optimisation problems that can be found in practical applications. Aircraft trajectory optimisation problems are then classified according to their main features. This is followed by a description of the main numerical techniques that can be utilised for solving this particular type of optimisation problems. The description presented is only a summary of the main features that characterise these techniques. For further information about them the reader may refer to the books by Walsh [75], Schwefel [76], Bunday [77], Fletcher [78], Everit [79], Krotov [80], and Rao [81]. Finally, the last section briefly describes part of the past experience on optimisation problems through the presentation of a summary of some of the research work developed about this subject at both Cranfield University, and other research organisations.

## 4.1
## General Aspects of Optimisation

Optimisation can be seen as the process of obtaining the best result or the best possible solution under any given set of circumstances. Thus optimisation can be defined as the science of determining the best solutions to certain mathematically defined problems, which are often representations of physical reality [78]. Alternatively, it can be defined as the process of finding the conditions that yield the maximum or minimum value of a given function [81]. From a mathematical point of view there is no reason in considering both maximisation and minimisation, since the maximisation process of a given function is equivalent to the minimisation process of the negative of the same function. Thus only one the two processes, maximisation or minimisation, could be used to describe a general optimisation process.

As expected, there is no a single method available for efficiently solving all optimisation problems. Thus a number of optimisation methods have been developed in the past, many of which are customised for a specific problem. One particular group of optimisation methods is the optimum seeking methods, also known as mathematical programming techniques, which are generally studied as a part of operations research. Operations research is the branch of mathematics concerned with both the application of scientific methods and techniques to decision making problems, and the establishment of the best or optimal solutions [81]. Table 4-1 shows a particular classification of the methods of operations research according to Rao [81], in which it is possible to observe the most important mathematical programming techniques developed so far. Mathematical programming techniques are particularly important because they determine the minimum of a function of several variables under a prescribed set of constraints. Stochastic process techniques and statistical methods, in turn, are used to analyse, respectively, problems described by a set of random variables and experimental data [81]. In this chapter, a particular emphasis is placed on some of the main mathematical programming techniques and their suitability to aircraft trajectory optimisation problems.

Table 4-1. Methods of operations research [81]

| Mathematical Programming Techniques | Stochastic Process Techniques | Statistical Methods |
|---|---|---|
| Calculus methods | Statistical decision theory | Regression analysis |
| Calculus of variations | Markov processes | Cluster analysis, pattern recognition |
| Nonlinear programming | Queuing theory | Design of experiments |
| Geometric programming | Renewal theory | Discriminate analysis (factor analysis) |
| Quadratic programming | Simulation methods | |
| Linear programming | Reliability theory | |
| Dynamic programming | | |
| Integer programming | | |
| Stochastic programming | | |
| Separable programming | | |
| Multiobjective programming | | |
| Network methods: CPM and PERT | | |
| Game theory | | |
| Simulated annealing | | |
| Genetic algorithms | | |
| Neural networks | | |

### 4.1.1 Optimisation Problem Statement

There are different ways of stating an optimisation problem which mainly depend on its type and method utilised to obtain its solution. Thus, from a generic point of view,

an optimisation or a mathematical programming problem – constrained problem – can be stated as follows [81]:

Find

$$X = \begin{Bmatrix} x_1 \\ x_2 \\ x_3 \\ \vdots \\ x_k \end{Bmatrix} \tag{4-1}$$

which minimises *f(X)*, subject to '*c*' constraints

$$\begin{aligned} g_j(X) &\leq 0, \qquad j = 1,2,3,\dots,m \\ h_l(X) &= 0, \qquad l = m+1, m+2, \dots, c \end{aligned} \tag{4-2}$$

where *X* is an *k*-dimensional vector called the design vector, *f(X)* is called the objective function, and $g_j(X)$ and $h_l(X)$ are known as inequality and equality constraints, respectively. Additionally, the number of variables *k* and the number of constraints *m* and/or *c* do not need to be related in any way.

During the design process any engineering system or component is defined by a set of quantities which can be viewed as either fixed or variable. All quantities that are treated as variables in the design process are called design or decision variables and collectively represent the design vector *X*. In practice, the design variables cannot be chosen arbitrarily; rather, they have to satisfy certain specified requirements. The restrictions that must be satisfied to produce an acceptable design are collectively called design constraints. Thus the design constraints are intended to limit the range of the design variables within values, which are meaningful for the problem being analysed.

As highlighted in [81], conventional design procedures aim at finding an acceptable design which merely satisfies the requirements of the problem. However, in general, there will be more than one acceptable design, and the purpose of optimisation is to choose the best one of the many acceptable designs available. Thus a criterion has to be chosen for comparing acceptable designs and for selecting the best one. The criterion, with respect to which the design is optimised, when expressed as a function of the design variables, is known as the criterion or merit or objective function [81]. The choice of the objective function is governed by the nature of problem, and it is straightforward in most design problems. However, there may be cases where the optimisation with respect to a particular criterion may lead to results that may not be

satisfactory with respect to another criterion. Therefore the selection of the objective function can be one of the most important decisions in the whole optimum design process [81].

### 4.1.2 Classification of Optimisation Problems

There are several criteria and methodologies for classifying and solving optimisation problems, respectively [75-81]. Here, in order to identify the main features of trajectory optimisation problems, the different classifications of optimisation problems will be briefly reviewed. Thus, optimisation problems can be classified according to the following criteria [81]:

- Existence of constraints: (i) constrained or (ii) unconstrained, depending on whether or not constraints exist in the problem.
- Nature of the design variables: (i) parameter or static optimisation problems, where the objective is to find values to a set of design parameters that minimises some prescribed function of these parameters subject to certain constraints; and (ii) trajectory or dynamic optimisation problems, where the objective is to find a set of design parameters, which are all continuous functions of some other parameter, that minimises an objective function subject to a set of constraints.
- Physical structure of the problem: (i) optimal control and (ii) non-optimal control problems. This is further discussed at the end of this section.
- Nature of the equations involved (objective function and constraints): (i) linear, (ii) nonlinear, (iii) geometric, and (iv) quadratic programming problems. In particular, if any of the functions among the objective and constraint functions is nonlinear, the problem is called nonlinear programming (NLP) problem.
- Permissible values of the design variables: (i) integer programming problems, where some or all of the design variables are restricted to take on only integer values; and (ii) real-valued programming problems, where all the design variables are permitted to take any real value.

- Deterministic nature of the variables: (i) deterministic programming problems, in which all of the parameters involved are deterministic; and (ii) stochastic programming problems, in which some or all of the parameters involved are probabilistic (nondeterministic or stochastic).
- Separability of functions: (i) separable or (ii) non-separable programming problems, depending on whether or not the objective function and the constraints are separable. And,
- Number of objective functions: (i) single or (ii) multi-objective programming problems, depending on the number of objective functions utilised.

Since trajectory optimisation problems are usually treated as optimal control problems [82], it is important to highlight how an optimisation problem is stated from the point of view of the optimal control theory. An optimal control problem is a mathematical programming problem which can be formulated as a collection of stages, where each stage evolves from the preceding stage in a prescribed manner [81]. It is usually described by the control (design) variables, which define the system and govern the evolution of the system from one stage to the next; and by the state variables, which describe the behaviour or status of the system in any stage. Thus, the problem involves determining a set of control variables such that the total objective function (performance index, PI) over all the stages is minimised subject to a set of constraints on the control and state variables. An optimal control problem can be stated as follows [81]:

Find

$$X = \begin{Bmatrix} x_1 \\ x_2 \\ x_3 \\ \vdots \\ x_k \end{Bmatrix} \tag{4-3}$$

which minimises

$$f(X) = \sum_{i=1}^{s} f_i(x_i, y_i) \tag{4-4}$$

subject to the constraints:

$$\begin{aligned} q_i(x_i, y_i) + y_i &= y_{i+1}, \quad && i = 1,2,\dots,s \\ g_j(x_j) &\le 0, && j = 1,2,\dots,s \\ h_l(y_l) &\le 0, && l = 1,2,\dots,s \end{aligned} \tag{4-5}$$

where $x_i$ is the $i^{th}$ control variable, $y_i$ the $i^{th}$ state variable, and $f_i$ the contribution of the $i^{th}$ stage to the total objective function; $g_j$, $h_l$, and $q_i$ are functions of $x_j$, $y_l$ and $x_i$ and $y_i$, respectively, and $s$ is the total number of stages.

## 4.2 Trajectory Optimisation Problem

According to the classification of optimisation problems given in the previous section, an aircraft trajectory optimisation problem can be classified as:

- Constrained – design constraints will be used to limit the range of the design variables,
- Dynamic – each design variable will be a function of one or more parameters (e.g., time),
- Optimal control – a number of stages, where each stage evolves from the preceding one in a prescribed manner, will be involved,
- Nonlinear – the function (s) relating inputs (design variables) and outputs (objective function) is (are) unknown and it (they) is (are) presumed to be nonlinear, non-smooth, and non-differentiable,
- Real-valued – most of the design variables will be permitted to take any real value,
- Deterministic – most of the parameters involved are deterministic,
- Non-separable – objective functions and constraints are non-separable, and
- Multi-objective – more than one criterion (objective function) will need to be satisfied simultaneously.

In addition, the problem can also be classified as multi-modal, as the space is unknown, but it is assumed that there are several local minima (or maxima). It can also be classified as multi-dimensional since a number of parameters will be involved during the optimisation process.

## 4.3
## Numerical Methods for Trajectory Optimisation

The most important mathematical programming techniques that can be used for finding the minimum of a function of several variables under a prescribed set of constraints are indicated in Table 4-1. The classical methods of differential calculus when used in conjunction with Lagrange multipliers and Kuhn-Tucker conditions can be used to identify the constrained optimum point of a function of several variables. However, these methods lead to a set of nonlinear simultaneous equations that may be difficult to solve [81]. In turn, the techniques of nonlinear, linear, geometric, quadratic, or integer programming, which most of them are numerical techniques involving iterative processes, can be used for the solution of the particular class of problems indicated by the name of the technique.

The last group of techniques shown in Table 4-1 (simulated annealing, genetic algorithms, and neural network methods) is a relatively new class of mathematical programming techniques, which have come into prominence during the last two decades. These techniques are inspired by nature and mimic aspects and/or processes that can be observed in natural environments, such as annealing, evolution, adaptation, and learning. Since it is not the objective of this work to describe in detail all methods that could be used for solving aircraft trajectory optimisation problems, only the main features of the most important ones, grouped according to Schwefel [76] – hill climbing methods, random search methods, and evolutionary methods, will be presented here.

### 4.3.1
### Hill Climbing Methods

These methods are most frequently applied in engineering design, and they are characterised by their manner of searching for a maximum (optimum), which corresponds closely to the intuitive way a sightless climber might feel his way from a valley up to the highest peak of a mountain [76]. These methods can be applied in one-dimensional and multi-dimensional problems. The methods used for solving one-dimensional problems can be classified as simultaneous and sequential methods. Simultaneous methods carry out a number of simultaneous trials in order to determine the value of the objective function at those points, and they declare then the point with

the smallest (largest) value the minimum (maximum). In sequential methods, in turn, the trials for determining a minimum are made sequentially, and intermediate results are retained, which are used to locate the next trial more favourably. Techniques used for solving one-dimensional problems are important because they constitute the basis of many of the multi-dimensional strategies currently available. In a general sense, multi-dimensional methods extend the basic ideas used in one-dimensional optimisation techniques to several dimensions. These methods can be classified as [76]: direct search methods (coordinate method, pattern search, Rosenbrock method, simplex, and complex method, among others), gradient methods, and Newton methods.

Direct search methods only use the values of the objective function during the optimisation process, i.e., they do not construct a model of the objective function; instead, the directions and to some extent the step lengths are fixed heuristically, or by other means, rather than in an optimal way [76]. The attraction of these techniques, which sometimes are called trial-and-error methods, lies in their simplicity and the fact that they have proved successful in practical applications. Examples of these methods, which are useful when the path followed to determine an optimum value is irrelevant, include those methods known as ‘hill climbing search’ and ‘simulated annealing search’, which are described by Russell and Norvig in reference [83].

The hill-climbing search algorithm is simply a loop that continually moves in the direction of increasing value, i.e., uphill, which terminates when it reaches a "peak" where no neighbour has a higher value [83]. Unfortunately, the hill climbing search method often gets stuck when it finds local maxima, because it does not have anywhere else to go. This problem appears due to fact that the hill-climbing algorithm never makes "downhill" movements towards states with lower values. In the simulated annealing search method, this problem of getting stuck on local maxima is corrected to some extent. This is done through the introduction of random walks that allows transitions out of local maxima and makes the algorithm more efficient and complete. The name of this method is derived from the simulation of thermal annealing of critically heated solids, where a slow and controlled cooling of a heated solid ensures proper solidification with a highly ordered, crystalline state that corresponds to the lowest internal energy [81].

During the optimisation process, gradient methods such as the steepest descent and conjugate gradient use not only the value of the objective function, but also its first partial derivative. They assume that the objective function is continuously differentiable. Thus all hill climbing techniques which use search directions based on the first partial derivatives of the objective function are called gradient methods [76]. Due to fact that the gradient represents a local property of a function, to follow its path exactly would mean determining a curved trajectory in the n-dimensional space. However, this problem which is more complicated than the original optimisation one is only approximately soluble numerically [76]. In practice, a number of gradient methods exist which differ in the level of discretisation utilised, and thereby with respect to how exactly they follow the gradient trajectory.

Newton methods, in addition, make use of the second partial derivatives of the objective function. These strategies exploit the fact that, if a function can be differentiated any number of times, its value at a given point can be represented by a Taylor series constructed at another point. The optimisation process is carried out in several steps involving the calculation of the objective function's first and second derivatives, and the inversion of the Hessian matrix. Thus if the objective function is quadratic, then the optimisation process can be carried out in a single step involving the calculation of its first and second derivatives, and the inversion of the Hessian matrix. If this is not the case, the optimisation process will become an iterative one. Newton methods can present convergence problems, as in the case in which the Hessian matrix is singular (non invertible). The success (or failure) of finding the optimum value depends on the starting point, which in turn requires a good knowledge of the objective function and the search space. All variants of Newton methods focus on increasing the reliability of the Newton iteration without sacrificing the high convergence rate. Exceptions to this rule constitute the quasi-Newton methods, which do not evaluate the Hessian matrix explicitly, and the modified Newton methods for which first and second derivatives must be provided at each point [76].

### 4.3.2 Random Search Methods

According to Schwefel [76], random search methods are those methods in which the parameters vary according to probabilistic, instead of deterministic, rules. Since these methods search for the optimum along random directions, which are not oriented with respect to the structure of the objective function, their use implies, in general, a higher cost because they do not take optimal single steps. However, the advantage is that these methods can be applied in every case [76]. These methods are utilised in situations in which many deterministic optimisation algorithms do not have the desired success. These situations include those ones in which (i) the partial derivatives of the objective function are discontinuous, (ii) the finite step lengths are greater than a narrow valley (the geometric picture of a minimisation problem), and (iii) the calculated or measured values are subject to stochastic perturbation (e.g., rounding errors in computational optimisation). Many of the deterministic optimisation methods described in the previous section, such as the hill climbing search and simulated annealing search methods, use random decisions at some stage to avoid premature termination of the search for an optimum. Consequently, a detailed description of the main random search methods currently available will not be presented here. For further information about these (random search) methods the reader may refer to the books by Schwefel [76] and Russell and Norvig [83].

### 4.3.3 Evolutionary Methods

Evolutionary techniques are inspired by nature and mimic biological structures and processes that can be observed in natural environments with the object of solving technical problems. They are based on Darwin's principles of species evolution: the reproduction cycle, the natural selection, and the diversity by variation [84]. The most important evolutionary methods are: evolutionary programming, evolution strategies, genetic programming, and genetic algorithms. Since, by definition, different species do not exchange genetic material, evolutionary programming methods explicitly try to model organic evolution at the level of evolving species without making use of any kind of recombination [84]. Evolution strategies, on the other hand, contain an element of

recombination between solutions, in a similar manner to real numbered genetic algorithms. Genetic algorithms will be discussed later in this chapter. In genetic programming, in turn, the Darwinian principle of reproduction and survival of the fittest, and the genetic operation of sexual recombination are utilised to create a new offspring population of individual computer programs from the current population of programs [85].

Similarly to the other evolutionary techniques, genetic algorithms (GAs) are based on the principles of natural genetics and natural selection. Thus, the basic elements of natural genetics – reproduction, crossover, and mutation – are used in the genetic search procedure. Among all evolutionary techniques, GAs are probably the methods with the most widespread use, and they have had a significant impact on optimisation [83]. Ways in which GAs differ from traditional methods of optimisation include [81]: (i) a population of points is utilised for starting the procedure instead of a single design point, (ii) GAs use only the values of the objective function, i.e., the derivatives are not used in the search procedure, (iii) in GAs the design variables are represented as strings of binary (or real) variables that correspond to the chromosomes in natural genetics, (iv) the objective function value corresponding to a design vector plays the role of fitness in natural genetics, and (v) in every new generation, a new set of strings is produced by using randomised parents selection and crossover from the old generation. In general, the evolutionary methods described, in particular GAs, are extremely robust which make them well suitable for problems in which the functions relating inputs to outputs are unknown and may have an unexpected behaviour; and where standard nonlinear programming techniques would be inefficient, computationally expensive, and in most cases, find a relative optimum that is the closest to the starting point [81].

## 4.4 Selection of the Trajectory Optimisation Technique

Betts [82] considers evolutionary methods – including GAs and other techniques involving some sort of stochastic process during the optimisation process – as not being appropriate for trajectory optimisation problems and as being computationally inferior when compared to methods using gradient information. Even so, it appears that evolutionary techniques, in particular GAs, may indeed prove very suitable candidates

for solving the aircraft trajectory optimisation problem. A number of reasons to support this point of view are presented below:

- GAs do not use specific knowledge of the optimisation problem domain. Instead of using previously known domain-specific information to guide each step, they make random changes to their candidate solutions and then use the fitness function to determine whether those changes produce an improvement. This is an important aspect because, with multi-model integration, for aircraft trajectory optimisation, the functions relating inputs to outputs are unknown. Since GAs optimisation routines are both model and problem independent, and they allow the users to run different models (simultaneously if required) for simulating different disciplines (such as aircraft and engine performance, emissions formation, etc.), they appear to be the ideal candidate.
- GAs perform well in problems for which the fitness landscape is complex (discontinuous and multi-modal, i.e., many local optima), and in which a number of constraints and objectives (multi-objective) are involved.
- GAs are well suited to solving problems where the space of all potential solutions is large (which is a particular characteristic of nonlinear problems).
- GAs use a parallel process of search for the optimum, which means that they can explore the solution space in multiple directions at once. Thus, if one path turns out to be a dead end, they can easily eliminate it and progress in more promising directions, thereby increasing the chance of finding the optimal solution.

From the four main evolutionary algorithms briefly described, GAs have been chosen because of their large number of previous successful applications worldwide, including those ones described in the works developed by Gulati [86], Rogero [87], Sampath [88], and Whellens [89]. However, it is important to highlight that the hybridisation of GAs with other optimisation techniques has not been discarded. This is due to fact that although GAs are an extremely efficient optimisation technique, they are not the most efficient for the entire search phases [87]. Thus, in future, hybrid optimisation methods will be considered as they have the potential to improve the

performance in a given search phase. Examples of these techniques constitute those ones associated with the use of both a random search phase during the beginning of the optimisation process – to increase the quality of the initial population, and a hill climbing phase at the end of the optimisation – to refine the quality of the optimum point once the global optimum region has been found.

## 4.5 Past Experience on Optimisation Problems

In this section a review of the main studies carried out at Cranfield University and by other research organisations about optimisation problems using GAs and other techniques is presented and described in some detail. These studies constitute the basis of the algorithm for aircraft trajectory optimisation utilised in this work, and whose results will be detailed in the following chapters.

A GAs-based optimisation technique for fault diagnostics of engines that are relatively poorly instrumented, i.e., having fewer measurements than performance parameters being determined, is presented by Gulati [86 ]. The lack of information due to the fewer measurements resulted in the need of using engine multiple operating points for carrying out the fault diagnostics processes. Thus, in the fault diagnostics processes carried out by Gulati, each engine operating point involved the use of one objective function (to be minimised) relating actual and simulated engine measurements. The use of multiple operating points implied therefore solving a multi-objective optimisation problem.

Consequently, the main issues addressed during Gulati's work were related to the choice of the engine operating points, as well as the type of multi-objective optimisation technique to be used by the GAs-based optimiser. After implementing and testing other techniques, one based on the concept of Pareto optimality was selected and utilised for solving the multi-objective optimisation problem as it produced the best results. When tested on a number of engine types, the methodology and tool developed during this work demonstrated its ability to accurately identify faulty components and quantify the fault, as well as to carry out sensor fault detection, isolation, and accommodation processes.

Rogero [87] describes the development and application of a novel combustor preliminary design methodology which provides a partial automation of the combustor design process. The methodology is presented in the form of a design optimisation tool which was developed based on GAs. The problem posed by the optimisation of the combustor preliminary design was considered as being mainly constrained, multi-objective, multi-modal, nonlinear, and non-differentiable. Taking into account these problem characteristics, GAs were selected as the technique for solving the optimisation problem due to their robustness and suitability for this type of problems. The capability of the optimisation tool developed was validated against different optimisation problems with known solutions, and the results demonstrated excellent optimisation performance especially for high-dimensional problems. The optimisation tool was then applied to several combustor design test cases, where it demonstrated its capability to successfully achieve the required performance targets and to optimise some key combustor parameters such as liner wall cooling flows and $NO_x$ emissions. Since it proved its usefulness in other applications, including wing profiles optimisation and combined cycle power plants performance optimisation, Rogero concluded that the methodology (and tool) developed could be applied for a wide range of engineering domains.

The development and implementation of an integrated faults diagnostics model based on GAs is described by Sampath [88]. (i) The use of response surfaces for computing objective functions and increasing the search space exploration while easing the computation burden, (ii) the heuristic modification of GAs parameters through the use of master-slave configurations, and (iii) the use of elitist model concepts to preserve the accuracy of the solution, constitute the three main aspects that characterise Sampath's model. Initially, a faults diagnostics system using basic GAs approaches was developed, and although the system detected component and instrumentation faults with a reasonable accuracy, it took a relatively long time for obtaining the solutions. Thus enhancements on the original system were introduced in three areas: search accuracy, convergence speed, and search space (hybrid model).

The model accuracy was improved through the use of the concept of elitism (preservation of best solutions from the earlier generations), and the introduction of a master-slave configuration (continuing monitoring of the performance of a slave GAs model). Convergence speed was increased by using embedded expert systems, which

were implemented to guide genetic operators more directly towards better strings; and response surfaces, which through the construction of approximate models of the objective function reduced the number of full-cost functions evaluations. Finally, the optimisation of the search space was carried out through a hybridisation of the GAs model. Thus a problem specific search technique (nested neural network) was utilised to act as a pre-processor of the GAs model and to determine a sub-region in the search space where the optimum solution is likely to be found. From the simulations carried out, it was concluded that the hybrid model developed improved the accuracy, reliability, and consistency of the results obtained. Additionally, it also resulted in a significant reduction in the computational time.

Whellens [89] investigated the feasibility, applicability, and value of a novel methodology for the preliminary design of aero engines, which involved the consideration of a number of disciplines including performance, gaseous emissions, noise, weight, and operating costs, among others. The investigation of this novel methodology was carried out through the development of a "pilot" MDO tool and its subsequent use in three case studies: (i) turbofan optimisation for minimum global warming potential (GWP), (ii) intercooled recuperated turbofan optimisation for minimum mission fuel burn, and (iii) environmental trade-offs for turbofans. In that work, a detailed description of the analysis tools developed for the modelling of the disciplines indicated above is presented, together with the GAs-based optimisation technique developed for performing the different MDO processes.

The main results of the work developed by Whellens [89] indicated that a turbofan optimised for minimum cruise GWP has a lower OPR and TET than one optimised for minimum cruise SFC, subsequently resulting in a fuel-inefficient engine. Also, the results showed that the advantage of intercooled recuperated turbofans when compared to conventional ones is dependent on the thrust range of the engine. More specifically, the advantages of using intercooled recuperated systems are larger for smaller engine sizes. According to Whellens, the reason behind this finding is that the smaller the engine size, the lower the engine OPR, and the higher the effectiveness of the recuperator. Regarding the optimisation processes performed in order to analyze the environmental trade-offs for turbofans, the results indicated that, in general, increasing bypass ratio (BPR) and decreasing OPR is the best way of complying with the

regulations, while maintaining acceptable levels of fuel burn or stage cost performance. From the results, the author concluded that the positive experience with the pilot MDO suggests that an automated methodology for preliminary design of aero engines is feasible, applicable, and valuable; and that the next step would constitute the development of a full-scale MDO tool for similar purposes.

An algorithm for trajectory optimisation based on direct methods is described by Hargraves and Paris [90]. Trajectory optimisation problems considered in that work involved those ones described by a sequence of vehicle/flight stages. In their approach, which in a fundamental sense involved the reduction of the optimal control problem to a NLP problem, they used linear interpolation for the control variables, a third-order Hermite interpolation for the state vector, and employed a collocation scheme to satisfy the differential equations involved. Several test cases were solved using the authors' optimisation package NPDOT (Nonlinear Programming for Direct Optimisation of Trajectories). NPDOT was validated against CTOP (Chebyshev Trajectory Optimisation Program), and provided comparable performance with respect to computational time. The authors concluded that the method developed was found to be superior to other procedures in terms of cost and robustness.

Schultz [91] describes a method for computing optimal three-dimensional aircraft trajectories based on Euler-Lagrange optimisation theory and energy state approximations. The optimum controls were found by either maximising or minimising a modified Hamiltonian containing two adjoint variables. The solution was then computed by iteration of these two variables. Since the convergence of the solution was sensitive to the values of these parameters, an iteration method was utilised to reduce this sensitivity. Schultz's work concludes by showing results of the application of the methodology proposed to a number of cases studies involving the computation of optimal three-dimensional trajectories, minimum time to a given fixed position.

The application of a direct transcription method, which combines a nonlinear programming algorithm with a discretisation of the trajectory dynamics, to the optimal design of a commercial aircraft trajectory, subject to realistic constraints on the aircraft flight path, is described by Betts and Cramer [92]. The applications were characterised by a relatively large number of trajectory phases involving nonlinear path constraints. The systems of differential algebraic equations, formed when the path constraints were

adjoined to the state equations, were solved using the transcription method. The tabular data utilised in the optimisation processes describing aircraft aerodynamics and propulsion was treated using tensor product B-spline approximations of order 3. In order to illustrate the usefulness of the methodology proposed, several optimisation processes involving a number of typical mission profiles, including minimum fuel, maximum range, and minimum take-off weight, were analysed and their results presented. From the results obtained, the authors concluded that the methodology presented is efficient and robust; and that, at the same time, it permits flexibility in the specification of both the problem constraints and the mission profile.

A survey of numerical methods to solve trajectory optimisation problems is presented by Betts [82]. The optimisation problem is there formulated as an optimal control problem involving a number of phases or stages. All methods described exploit gradient information and involve application of Newton's methods in order to determine the optimum value. They are classified as either indirect or direct methods. Indirect methods solve an optimal control problem by applying explicitly the optimality conditions stated in terms of the adjoint differential equations, the maximum principle, and the associated boundary conditions. Thus they require the analytical computation of the gradient and then the location of a set of variables such that the gradient is zero. In contrast, direct methods convert the original optimal control problem into a NLP problem which is solved directly using mathematical programming techniques. Thus they do not require an analytic expression for the necessary conditions and typically do not require initial guesses for the adjoint variables. One of the last paragraphs of Betts' work deals with trajectory optimisation methods based on GAs. Interestingly, Betts classifies evolutionary methods, including GAs, simulated annealing, and other techniques involving some sort of stochastic process during the optimisation process, as not being appropriate for trajectory optimisation problems and as being computationally inferior when compared to methods using gradient information.

Finally, a general method for the evaluation of theoretical optimal laps for a transient vehicle model is presented by Casanova [93], and applied to finding the minimum lap time for a Formula One racing car. The minimum time vehicle manoeuvring problem is formulated as an optimal control problem, and it is solved using mathematical programming techniques. It is indicated in Casanova's work that

novel techniques were used to solve the resulting nonlinear programming problem, which enabled to achieve an effective optimisation with satisfactory accuracy, robustness, and computational efficiency. Car and circuit models were set up, and optimisation processes were carried out to analyse the sensitivity of the vehicle performance and configuration to the vehicle design parameters. The author of that work concluded that the methodology developed accurately quantifies the vehicle performance in terms of manoeuvring time; and that the optimal solution was in excellent agreement with the dynamics properties of the model of the vehicle.

## 4.6 Commercially Available Tools for Trajectory Optimisation

In order to evaluate its mathematical performance, it is expected that the results obtained using the optimisation algorithms developed and/or adapted in this work are compared, at some stage, against other optimisation algorithms results. In this work, these other optimisation algorithms have been taken from commercially available software packages. There are a number of optimisation algorithms (i.e., optimisers) suitable for carrying out aircraft trajectory optimisation processes. A detailed description of all these optimisers and/or tools is beyond the scope of this work. Thus, in the last section of this chapter, only the main features of two of the most 'important' ones, Matlab [94] and Isight [95], will be described. From these two optimisers and/or tools, only one of them, Matlab [94], has been utilised in this work for verification and/or validation purposes of the optimisation algorithms developed and/or adapted. The other one, Isight [95], is expected to be used in future for verifying and/or validating further developments of these optimisation algorithms.

As already mentioned, the commercial software Matlab [94] (and its associated optimisation algorithms) has been utilised for verifying and/or validating the optimisation algorithms developed and/or adapted in this work. This commercially available tool has been chosen because it is probably one of the most popular computational programs worldwide. Matlab optimisation toolboxes include several algorithms for solving a wide range of constrained and unconstrained continuous and discrete problems [94]. In addition to the traditional optimisation techniques, Matlab also includes optimisation algorithms based on GAs, direct search, and simulated

annealing. These algorithms can be used for problems that are difficult to solve with other techniques, such as those characterised for having objective functions that are discontinuous, highly nonlinear, stochastic, or having unreliable or undefined derivatives [94]. Its relative ease of use made it the ideal candidate for the initial comparisons with the optimisation algorithms utilised in this work.

Isight is also a commercial optimiser used by academia and industry. Isight has also been integrated as part of the TERA [96,97] concept conceived by Cranfield University. TERA is a multi-disciplinary optimisation tool which increases the visibility of the risks and enables the user to compare and rank competing power-plant schemes on a formal and consistent basis. The TERA has been and is currently being deployed successfully on several European Union collaborative projects to assess the potential of geared turbofan concepts, intercooled and recuperated concepts, and open rotor concepts, among others. Isight provides users with a wide range of flexible tools for creating simulation process flows, involving not only other commercial packages but also internally developed programs, in order to automate the exploration of design alternatives and identification of optimal performance parameters [95]. In addition, in order to enable an effective and thorough exploration of the design space, Isight also allows the user to perform design of experiments, optimisation, and approximations [95]. Finally, it is important to emphasise that, for verifying and/or validating further developments of the optimisation algorithms developed and/or adapted in this work, other well known optimisers such as Isight [95] are expected to be used in future.

# 5
# Genetic Algorithms-based Optimiser

Since the optimisation algorithms utilised in the present research project are based on genetic algorithms (GAs), basic concepts associated with this optimisation technique are initially presented in this chapter. The only objective of reviewing these GAs concepts is to establish the necessary basis for understanding the main characteristics of the GAs-based optimiser utilised in this work. Thus only the main features that characterise this optimisation technique are presented in this chapter. For further information about GAs in general the reader may refer to the books by Quagliarella [84], Goldberg and Sastry [98], Luger [99], Haupt and Haupt [100], Callan [101], Goldberg [102], Gen and Cheng [103], and Goldberg [104]. The last part of this chapter provides a short description of the main characteristics of the GAs-based optimiser utilised in the present research project. The description presented highlights the main modifications introduced in the past in a general-purpose GAs library in order to adapt it to engineering design optimisation problems thereby maximising its performance.

## 5.1
## Genetic Algorithms

Genetic algorithms (GAs) are a stochastic approach utilised for optimisation and search processes based on the mechanisms of natural selection and Darwin's main principle: survival of the fittest [84]. Among all evolutionary techniques, GAs are probably the most widely known methods currently. They also have perhaps the most widespread use. Their applications include, among others, game playing, classification tasks, engineering design, and computer programming [101]. This section is focused on GAs and their utilisation for finding (optimum) solutions to optimisation problems from the point of view of engineering design. Thus, the main mechanisms involved during an optimisation process using GAs are first summarised, and the main features characterising these mechanisms are then described in detail.

### 5.1.1 Genetic Algorithms Mechanisms

The mechanics of finding solutions to optimisation problems using GAs can be summarised as follows [102]. Let's suppose that one wants to find a 'solution' to a given 'problem'. In order to apply a genetic algorithm to that problem, the first step is to 'encode' the problem as an artificial 'chromosome' (or chromosomes). There are different encoding methods available, for instance, binary encoding, integer encoding, real-number encoding, etc. Another step in solving the problem is to establish a way of differentiating good solutions from bad solutions. This typically involves the use of mathematical models that help to determine what good a solution is (standard notion of 'objective' function [102]). Independently of the way in which good solutions are identified, it is necessary to have something that determines a solution's relative 'fitness to purpose', and whatever it is will be used by the genetic algorithm to guide the evolution process of future generations.

Having done that, the next step involves the evolution process of the solutions. This process starts by creating an initial 'population' of encoded solutions. There are two common ways of creating the initial population, randomly or by using good potential solutions previously determined. Regardless of the initialisation process, the idea is that the genetic algorithm searches from a population of solutions, not a single one. Once the initial population is created, 'selection' and 'genetic operators' will process the population iteratively until a given 'stopping criterion' is (or given 'stopping criteria' are) satisfied. At the end, the final population will contain, hopefully, better solutions than those present in the initial population.

There are a variety of operators utilised in optimisation processes involving GAs, but the common ones are (i) selection, (ii) recombination (crossover), and (iii) mutation. Selection allocates more offspring to better individuals (principle of survival of the fittest imposed). There are different ways of carrying out the selection process; but, regardless of selection method utilised, the whole idea is to prefer better solutions to worse ones. However, simply selecting the best solutions from a previous generation is not enough, thus some means (e.g., recombination and mutation) of creating new and probably better individuals (potential solutions) need to be utilised.

Recombination (or 'crossover' as it is also commonly referred to) combines parts of parental solutions to form new and possibly better offspring. In other words, it recombines traits of two or more parents in order to create new individuals. As explained in the following sections, there are many ways of performing a recombination process; but, regardless of the methodology, the main idea is to create offspring that are not identical to any particular parent. A similar situation occurs in the mutation process. However, what differentiates mutation from recombination is the fact that mutation acts by modifying a single individual.

Let *P(t)* define a population of candidate solutions, $X_i^t$, at generation t:

$$P(t) = \{X_1^t, X_2^t, \dots, X_n^t\} \tag{5-1}$$

A general structure of GAs-based optimisation processes, which summarises the GAs mechanics described previously, is as follows [102,103]:

```
begin
    set generation t = 0;
    initialise the population P(t);
    evaluate fitness of each member (1 → n) of the population P(t);
    while (not termination condition) do
        select members from population P(t) based on fitness;
        produce offspring from selected members using genetic operators;
        evaluate fitness of offspring;
        replace, based on fitness, candidates of P(t) with offspring;
        set generation t = t + 1
    end
end
```

(5-2)

Finally, it is important to highlight that there are two important issues associated with search strategies, in particular with GAs [103]: exploiting the best solution and exploring the search space. In GAs, the genetic operators essentially carry out a blind search, while selection operators hopefully direct the genetic search toward the desirable area of the search space. When developing GAs-based optimisation tools for real applications, a general principle is to have a good balance between exploitation and

exploration of the search space. This idea of exploitation versus exploration is directly related in literature [105] to other two factors used in genetic search: population diversity and selection pressure (selection pressure or selective pressure is defined as the ratio of the probability that the most fit chromosome – chromosome with maximum fitness – is selected as a parent to the probability that the average chromosome is selected [100]).

Whitley [105] argues that the only two primary factors in genetic search are population diversity and selection pressure, which are inversely related. Increasing selective pressure results in a faster loss of population diversity, and maintaining population diversity offsets the effect of increasing selective pressure. Since it has a strong influence on GAs performance, the selection pressure needs to be controlled as directly as possible. A selection pressure which is too high might result in a premature convergence of the optimisation process; and, conversely, a selection pressure which is too low will not direct the optimisation strongly enough and genetic drift (changes in gene frequencies in a population resulting from chance rather than selection – it can lead to extinction of genes and reduction of genetic variability in the population [100]) might appear in the population [104]. In practice, different techniques are utilised to keep the selection pressure relatively constant during the whole optimisation process. The following sections describe in more detail particular aspects that characterise GAs-based optimisation processes.

### 5.1.2 Problem Encoding

As indicated in the previous section, one of the first things to do in order to apply a genetic algorithm to a given problem is to encode it as an artificial chromosome or chromosomes. Over the last decades, different encoding methods have been created in order to allow an effective implementation of GAs for particular problems. One way of classifying the encoding methods is according to the type of symbol used as the alleles (values) of a gene. According to this, encoding methods can be classified as [103]: binary encoding, real-number encoding, integer encoding, and general data structure encoding.

Binary encoding is the typical encoding method utilised with GAs. In this type of encoding, binary strings composed of 0s and 1s are used to represent the genes of a chromosome. Binary encoding for engineering optimisation problems is known to have severe drawbacks due to the existence of Hamming cliffs [103]. The problem of Hamming cliffs is associated with the fact that under certain conditions the distance between two values in the phenotype space (solution space) may be completely different to the corresponding one in the genotype space (coding space). Thus two neighbouring values in the phenotype space may be completely distant in the genotype space. In these particular situations, in order to cross the Hamming cliff, it would be necessary to change simultaneously a large number of bits. As a consequence of this the probability that crossover and mutation occurs is considerably reduced.

Real-number encoding is more appropriate for engineering optimisation problems, since the parameters involved are usually expressed as real numbers. This type of encoding avoids all difficulties associated with the use of a binary (discrete) encoding when optimising 'continuous' search spaces. The fact that the topological structures of the phenotype and the genotype space are identical for real-number encoding allows easy formation of the genetic operators utilised in the process. Currently it is widely accepted that real-number encoding performs much better than binary encoding for function optimisation and constrained optimisation problems [103]. Integer or literal permutation encoding, in turn, is best used for combinatorial optimisation problems; while that data structure encoding is suggested for more complex real-world problems, where it is necessary to capture the nature of the problem [103].

### 5.1.3 Problem Initialisation

A GAs-based optimisation process is in essence an evolutionary process which starts with an initial population of encoded solutions and searches for better ones. This implies that an initial population of solutions need to be created at the beginning of the process. The initial population of solutions (chromosomes) can be created by randomly choosing values for the genes from the search space, or by using good potential solutions that have been previously determined. The origin of these good potential solutions can be diverse. They could be obtained from a previous optimisation process

carried out using GAs or other optimisation techniques, an identification process performed based on prior knowledge about how the optimum solutions might look like, or any other process using defined criteria for identifying good potential solutions. Regardless of the methodology utilised for determining the initial population of solutions, what is really important is the fact that the optimisation process starts from a population of solutions and not from a single one.

### 5.1.4 Selection and Genetic Operators

The operator selection and the two genetic operators, crossover (recombination) and mutation, constitute the main operators utilised in GAs. These operators process the population of solutions iteratively until a termination condition is satisfied. At the end of the process, it is expected that the final population contain better solutions than those ones present in the initial population. These three main GAs operators are briefly described next.

#### 5.1.4.1 Selection

The principle of survival of the fittest imposed in GAs implies discarding the chromosomes with the lowest fitness at each generation. This process is carried out through the selection operator which allocates more offspring to better individuals. Selection provides the driving force in GAs: with too much force, the genetic search will converge prematurely; and with too little force, the evolutionary process will take longer than necessary [103]. Selection operators are used for two different purposes, for selecting parent chromosomes (which will be used as parents to create offspring through the use of genetic operators), and for inserting new offspring into the population. There are different ways of carrying out the selection process. Gen and Cheng [103] describe several selection methods developed over the past two decades. Two common selection methods utilised to select parent chromosomes are ‘roulette wheel selection’ and ‘stochastic universal sampling’ (SUS).

Roulette wheel selection is the best known selection method. In this method, an area proportional to its fitness is allocated to each chromosome on a virtual roulette wheel. The selection process is carried out by spinning the wheel a number of times

equal to the number of chromosomes to be selected (each time a single chromosome is selected). One drawback associated with this selection method is related to the fact that it has a tendency to select a large number of copies of the best chromosome, which can lead to loss of diversity. This problem of selecting a large number of copies of the best chromosome is corrected to some extent when using the SUS selection method. In the SUS method, like in the roulette wheel selection, a chromosome occupies an area on the wheel proportional to its fitness. However, instead of spinning the wheel several times for selecting chromosomes, a single spin of the wheel identifies all parent selections simultaneously. This is possible because there is another wheel on the outside of the roulette wheel containing a number of equally spaced pointers equal to the number of chromosomes to be selected [101].

There are also different methods or strategies for inserting offspring into the population. Two common methods are the 'tournament selection' and the 'ranked selection' methods (more appropriate names for these methods in the particular case of inserting offspring into the population would be 'tournament replacement' and 'ranked replacement'). The tournament selection method randomly chooses a set of chromosomes and selects the best chromosome from that set [103]. In other words, it promotes a tournament among a given number of chromosomes randomly chosen (usually two or three), and the winner of the tournament (chromosome with the highest fitness) is selected for further processing. In this way, the pool of selected chromosomes which comprises tournament winners has a higher average fitness than the average population fitness. Ranked (or ranking) selection, on the other hand, uses only a ranking of chromosomes to determine survival probability (chromosomes fitness values are not utilised) [103]. Thus, in order to carry out the selection process using this method, the population is first sorted according to their fitness values (from the best to the worst chromosome), and a probability of selection is then assigned to each chromosome according to its ranking, but not according to its fitness.

#### 5.1.4.2 Crossover (Recombination)

As implied previously, the selection mechanism exploits accumulated information to guide the search process towards optimum solutions by allocating more offspring to the fittest chromosomes; whereas, genetic operators explore new regions of the search

space. It is important that the disturbance produced by the genetic operators on the search is minimum; but, at the same time, it is also important that the genetic operators are able to efficiently sample other regions of the search space [101]. Crossover or recombination is a genetic operator that combines traits of two or more parental solutions to form new and possibly better offspring. Depending on the type of encoding used in the process, different methods of performing a recombination process can be utilised.

For search processes involving binary encoding, there are four recombination methods commonly utilised: 'single-point crossover', 'double point crossover', 'multi-point crossover', and 'uniform crossover'. In the single-point crossover only one crossover position is randomly selected, and the binary strings are exchanged between the parental chromosomes about this point, thereby producing two new offspring. Similarly, in the double point crossover and the multi-point crossover two crossover positions or multiple crossover positions are randomly selected and binary strings are exchanged between the parental chromosomes about these crossover points. The uniform crossover is, in turn, a generalisation of the multi-point crossover. In this method every locus of the parental chromosomes is a potential crossover point. The recombination process is carried out creating randomly a crossover mask containing the information about which parent will provide the offspring with the required bits.

Alternative crossover techniques are used in optimisation processes involving real-number encoding. These techniques include, among others, 'weighted averaging crossover', 'blend crossover' (BLX), and 'simulated binary crossover' (SBX). Of course, the simplest way of producing an offspring from two parental chromosomes is by averaging or blending them. This is the principle behind the weighted averaging crossover. It is clear that in real coded chromosomes, each chromosome is represented as a vector of real numbers. Then, for a problem with 'k' design variables (or genes), the real-number vector (chromosome) will be given by:

$$X = \{x_1, x_2, \dots, x_k\} \tag{5-3}$$

Gen and Cheng [103] defines an 'arithmetic crossover' as the combination of two vectors, $X_1$ and $X_2$, as follows:

$$X_1' = \lambda_1 X_1 + \lambda_2 X_2 \tag{5-4}$$

$$X_2' = \lambda_1 X_2 + \lambda_2 X_1$$

where the multipliers $\lambda_1$ and $\lambda_2$ (subject to the condition $\lambda_1 + \lambda_2 = 1$) represent the weights randomly selected during the crossover process. Depending on the permissible values of the multipliers $\lambda_1$ and $\lambda_2$, different sub-types of crossover methods can be derived. The (weighted) averaging crossover, as defined by Davis in reference [106], corresponds to the special case in which $\lambda_1 = \lambda_2 = 0.5$. The averaging crossover suffers from contraction effects due to the fact that it allows the creation of offspring only along the line generated between the two parental chromosomes. This problem is solved to some extent by utilising a blend crossover (BLX), which uses exploration factors (α) that increase the exploration capability of the crossover operator.

The BLX crossover, which was introduced by Eshelman and Schaffer [107], randomly creates offspring within a hyper-rectangular region defined by the parental points [103]. Assume a one-dimensional case (one variable) with two parental points $p_1$ and $p_2$ ($p_1 < p_2$), and exploration factors $0 < \alpha_1, \alpha_2 < 1$. For this case, the BLX randomly chooses a point in the range $[p_1 - \alpha_1(p_2 - p_1), p_2 + \alpha_2(p_2 - p_1)]$ in order to generate a given offspring [103]. A special situation is that of $\alpha_1 = \alpha_2$. In this case, the BLX crossover operator is called BLX-α. It has been reported [107] that BLX-0.5 ($\alpha = 0.5$) performs better than other BLX operators with other different α values.

The simulated binary crossover (SBX) was developed by Deb and Agrawal [108]. This crossover operator utilises a probability of creating an arbitrary child solution from a given pair of parental solutions similar to that used in binary crossover operators. This crossover operator is mainly characterised by the use of both (i) a spread factor (β) (defined as the ratio of the absolute differences of the children points to that of the parental points [108]) that controls the spread of the children with respect to that of their parents, and (ii) a distribution function to perform the crossover processes of the parental solutions. When compared to other real-coded crossover operators such as BLX-0.5, the SBX operator has demonstrated a better performance [108].

#### 5.1.4.3 Mutation

Mutation is the second genetic operator used by GAs to explore the search space. What differentiates mutation from recombination or crossover is the fact that mutation

acts by modifying only a single chromosome. In a fundamental sense, a mutation process allows the whole search space to be sampled before the process converges (prematurely). This is done by forcing the algorithm to explore other areas of the search space by randomly introducing changes, or mutations, in some of the variables comprising a given chromosome [100]. For binary coded problems, this process is carried out by simply changing bits from 0 to 1, and vice versa. However, for continuous GAs the mutation process is a little bit more complicated than that. Typical mutation operators for real-number encoding include the following: 'uniform mutation', 'creep mutation with and without decay', 'non-uniform mutation', and 'dynamic vectored mutation' (DVM).

For a given parent $X$, Eq. (5-3), if the element (gene) $x_i$ of it is selected for mutation, a random change of the value of this selected gene within its domain, given by a lower $LB_i$ and upper $UB_i$ bound, will result in the following transformation:

$$\{x_1, x_2, \dots, x_i, \dots, x_k\} \rightarrow \{x_1, x_2, \dots, x_i', \dots, x_k\}, \;\; x_i, x_i' \in [LB_i, UB_i] \qquad (5\text{-}5)$$

This process is referred to by some authors [109] as a random mutation method. Uniform mutation involves, in turn, a process in which the values of $x_i'$ are drawn uniformly randomly from [$LB_i$, $UB_i$] [110]. A position wise mutation probability is usually utilised with this mutation method.

Non-uniform mutation was introduced by Michalewicz [109]. In this method, the value of $x_i'$ is randomly selected from the following two options:

$$\begin{aligned} x_i' &= x_i + \Delta(t, UB_i - x_i) \\ x_i' &= x_i - \Delta(t, x_i - LB_i) \end{aligned} \qquad (5\text{-}6)$$

The function $\Delta(t, y)$ returns a value in the range [0,$y$], which approaches to 0 as t increases ($t$ represents the generation number). This property causes the mutation operator to search the space uniformly initially (when $t$ is small), and very locally at later stages [109]. The function $\Delta(t, y)$ is defined as:

$$\Delta(t, y) = y.\left(1 - r^{\left(1 - \frac{t}{t_{max}}\right)^b}\right) \qquad (5\text{-}7)$$

where $r$ is a random number from [0,1], $t_{max}$ the maximum generation number, and $b$ a parameter determining the degree of non-uniformity.

Creep mutation basically operates by adding or subtracting a random number to a gene of the chromosome selected for mutation. In the way that it is described in reference [106], the mutation of a given gene, $x_i$, is limited to a creep range centred on its original value. Thus, a mutated gene, $x_i'$, is computed according to:

$$x_i' = x_i + (2r - 1)\Delta_{max} \tag{5-8}$$

where,

$$\Delta_{max} = \delta.(UB_i - LB_i) \tag{5-9}$$

In Equations (5-8) and (5-9), $\Delta_{max}$ is the maximum size used for the creep mutation, $\delta$ the range ratio, and $r$ a random number from [0,1]. The level of disruption produced by the mutation process is controlled by the creep size $\delta$.

In the creep mutation with decay method, the creep size is altered as a function of the stage of the search process, according to [87]:

$$\delta_{t+1} = \delta_t.(1 - \gamma) \tag{5-10}$$

where $\gamma$ represents the creep decay rate ($t$ is the generation number). This type of implementation allows the use of large values of $\delta$ in the beginning of the search process and small ones at the end; balancing in this way the exploration and exploitation capabilities required during the process.

Dynamic vectored mutation (DVM) is a method proposed by Rogero in reference [87]. This mutation operator was developed in an attempt to solve some limitations present in other operators. It allows mutation in all directions of a multi-dimensional search space and not only along a single dimension axis. This method can be summarised as follows.

Consider the chromosome $X$ given by Eq. (5-3) as a k-dimensional vector. From this vector (chromosome), a displacement vector $V_d$ of magnitude $m$ and random direction is created, whose end point determines the mutated chromosome. The next step involves the computation of the maximum magnitude of $V_d$, $\Delta_{max}$, that would result in a solution within the boundaries of the genes. The magnitude $m$ of $V_d$ is then allocated with a probability inversely proportional to its value $m$ and bounded by $\Delta_{max}$.

Thus, the magnitude $m$ is calculated as:

$$m = a.\bar{\beta}(\eta) \tag{5-11}$$

where $a$ is constant factor, and $\overline{\beta}$ defined according to (similarly to the polynomial probability distribution used by Deb and Agrawal [108]):

$$\bar{\beta}(\eta) = \left(\frac{1}{1-\alpha r}\right)^{(1-\eta)^{\gamma}} \tag{5-12}$$

In Eq. (5-12), $\eta$ is the search (optimisation) process completion ratio, $\gamma$ the iteration dependency factor that controls the function curvature (depending of the value of $\eta$), and $\alpha$ calculated as follows:

$$\alpha = 1 - \left((1 + a.\Delta_{max})^{-\left(\frac{1}{1-\eta}\right)\gamma}\right) \tag{5-13}$$

According to the way in which the DVM operator was derived, the probability of creating a mutated chromosome is reduced as the distance from the original point (parental chromosome) increases; and the line of iso-probability approximates to a hyper-sphere in k dimensions. Its capability of reaching the whole search space constitutes the main characteristic of the DVM operator.

### 5.1.5 Constraints Handling

As highlighted in the literature [87], many engineering optimisation problems are controlled by three main factors: explicit constraints, implicit constraints, and performance parameters. Explicit constraints are constraints imposed on the input parameters. In order to take into account these constraints, therefore, it is not necessary to evaluate the chromosome (s). It implies that a good representation of the optimisation problem (e.g., appropriate selection of the design variables) could eliminate the need of this type of constraints. Implicit constraints, which are constraints imposed on the problem performance parameters, require on the other hand the evaluation of the chromosome in order to determine the value of the parameters they constrain. This type of constraints will be addressed in some detail in this section. Performance parameters, which will need to be optimised in a given problem, are addressed in turn in Section 5.1.6.

As implied above, implicit constraints (which will be hereafter simply referred to as ‘constraints’) can not be directly computed from the input variables. Thus it is necessary to evaluate the chromosome in order to determine the value of the parameter being constrained by a given constraint. Over the past few decades, different techniques have been developed in order to deal with this type of constraints, and, in this section, the most important ones are briefly reviewed.

Since GAs basically find the optimum of an unconstrained problem, modifications to the approach utilised when dealing with this type of problems need to be introduced when analysing constrained ones. However, some difficulties appear when GAs are applied to constrained problems, because the genetic operators used in the search process often produce unfeasible offspring. At this point, it is important to highlight that, in general, a search space ($\mathcal{S}$) contains two subspaces: feasible ($\mathcal{F}$) and unfeasible ($\mathcal{U}$). These subspaces do not need to have any type of association each other. When dealing with search or optimisation problems, one looks for feasible optimum solutions. However, during the process one has to deal with several feasible and unfeasible solutions at the same time; and, as emphasised in the literature [103,111], handling unfeasible solutions is far from trivial.

Gen and Cheng [103] indicate that the existing constraint handling techniques used in constrained problems can be roughly classified as: rejecting methods, repairing methods, and penalty methods. Rejecting methods simply discard the unfeasible chromosomes created throughout the evolutionary process. Since these methods just eliminate the unfeasible solutions without giving any indication of the search space feasible regions, the performance of the search process is poor. Thus, these methods use the simplest but also the least effective way of dealing with the problem. Repairing methods, in turn, involve the use of repair procedures which are utilised for creating feasible chromosomes from unfeasible ones.

The penalty approach, which involves the application of a penalty to the objective function for any violation of the constraints, is perhaps the most common technique used for constrained optimisation problems [103]. This method transforms the original constrained problem into an unconstrained one by penalising unfeasible solutions. However, the big issue with this technique is how to determine the penalty term or

penalty function, which effectively allows the search process to be guided towards more promising areas of the search space.

In general, there are two ways of constructing an evaluation function, $eval(X)$, with a penalty term [103]:

$$eval(X) = f(X) + p(X) \tag{5-14}$$

or,

$$eval(X) = f(X).p(X) \tag{5-15}$$

In Equations (5-14) and (5-15), $X$ represents a given chromosome, $f(X)$ the objective function, and $p(X)$ the penalty term. The permissible values of $p(X)$ depend on both the type of problem (maximisation or minimisation), and the form in which the evaluation function is expressed (addition Eq. (5-14) or multiplication Eq. (5-15)).

Penalty functions can be of two types: constant penalty and variable penalty. In the constant or fixed penalty approach, the same penalty is imposed to each member of the population failing to satisfy the constraints [87]. This approach is known to be less effective for complex problems, and therefore the tendency is to use variable penalty techniques. The variable penalty technique contains, in general, two parts [103]: (i) a variable penalty ratio, which can be adjusted according to both the degree of violation of the constraints, and the stage (iteration number) of the search process; and (ii) a penalty amount for the violation of the constraints.

As highlighted in the literature [103], there are no general guidelines for designing and constructing an efficient penalty function. This process is usually quite problem dependent. Thus, as described in reference [111], over the years several and sophisticated penalty functions, specific to the problem and the optimisation algorithms utilised, have been developed. However, the most difficult part when following this approach is usually determining suitable penalty parameters needed to guide the search process towards the constrained optimum [112]. The need of these penalty parameters arises from the fact that it is necessary to have objective function and constraint violation values of the same order of magnitude.

One particular implementation of the penalty approach is the constraint handling method developed by Deb [112]. Deb's approach is based on three criteria: (i) any feasible solution is preferred to any unfeasible solution, (ii) among two feasible

solutions, the one having better objective function value is preferred, and (iii) among two unfeasible solutions, the one having smaller constraint violation is preferred. Thus, because solutions are never compared in terms of both the objective function value and the level of constraint violation, penalty parameters are not needed in this method. Unfeasible solutions are compared only in terms of their constraint violation and the population of solutions in a given generation. On a number of test problems, Deb's method [112] has shown better efficiency and robustness than other methods developed previously.

### 5.1.6 Objective Handling

As highlighted in Chapter 4, optimisation can be seen as the process of finding the conditions that yield the optimum value of a given function under any set of circumstances. In other words, it can be seen as the process of finding solutions over a set of possible choices which allow the optimisation of certain criteria. When there is only one criterion to consider, the process is known as single-objective optimisation process; and, when there is more that one criterion that must be treated simultaneously, as multi-objective optimisation process [103]. In many real applications, multiple and conflicting objectives need to be tackled simultaneously, while satisfying several constraints.

The optimisation of an aircraft trajectory for both minimum environmental impact and minimum fuel burned constitutes a typical example of a multi-objective optimisation problem. Consider that the release of certain pollutants, such as $NO_x$, affects the environment more drastically as the aircraft flight altitude increases. Then, when optimising for minimum environmental impact, the optimisation process will result in a solution in which the aircraft will fly as low as possible. In order to minimise the fuel burned, in turn, the optimisation process will result in a solution in which the aircraft will fly as high as possible. As it can be realised in this example, the two objectives considered create a conflict in the aircraft operation (flight altitude). Thus, multi-objective optimisation problems usually receive a different treatment to that received by single-objective ones.

In order to have a better idea of how multi-objective optimisation problems are dealt with in practice, it is necessary first to understand what 'nondominated' solutions mean. When dealing with single-objective optimisation problems, an attempt to obtain the best solution is carried out. However, in multi-objective optimisation problems, there is not necessarily a single 'best' solution with respect to all objectives [103]. Thus, a solution can be the best according to a given objective; but, at the same time, it could be the worst according to the other ones considered in the analysis. Therefore, for this type of problems, there usually exist a set of solutions which cannot be simply compared with each other, because it would require additional information regarding the priority of the objectives. For these solutions, called 'nondominated' solutions or 'Pareto optimal' solutions, no improvement in any objective function is possible without penalising at least one of the objective functions involved [103].

In order to select a nondominated solution as the solution for a given multi-objective optimisation problem, additional information related to the priority or preference of the several objectives needs to be provided. In general, these preferences represent an emphasis on particular objectives according to their relative importance determined either arbitrarily or based on prior knowledge of the problem being analysed. Once the preferences have been established, it is possible to order the solutions present in a given nondominated set, and then obtain from that set the final solution to the problem. This final solution is usually called the 'best-compromised' solution. There are basically two methodologies that can be followed when dealing with multi-objective optimisation problems [103]: (i) generating approaches, and (ii) preference-based approaches.

Generating approaches, which are used when no prior knowledge about the objectives preference structure is available, identify an entire set of Pareto solutions or an approximation of the same. Preference-based approaches, in turn, attempt to obtain a compromised or preferred solution. These approaches are used when the relative importance of the objectives is known and quantifiable. Traditionally, the methods utilised for solving multi-objective optimisation problems involve the reduction of the multiple objectives to a single one, and the use of conventional techniques to solve the single-objective optimisation problems generated from this process. Typical examples

of these techniques include the weighted-sum approach, the compromise approach, and the goal attained or target vector optimisation method.

The weighted-sum approach basically assigns weights to each objective function in order to combine them into a single-objective function. The weights utilised can be seen as representations of the relative importance of the objectives involved in the problem. If all the weights used for creating the single-objective function are positive, the optimum solution to the problem is a nondominated one [103]. In the compromise approach, in turn, solutions closest to the 'ideal point' (point composed by the optimum value of each objective function determined independently) are identified [103]. Since the ideal point is usually not attainable, a compromise among the objectives must be achieved in order to determine an alternative solution. The fact that an alternative solution is used instead of the ideal one results in a 'regret', which is quantified in terms of the distance of the alternative solution to the ideal one. Thus, in this method, a regret function is minimised in order to obtain a compromised solution. During the process, the regret function tries to impose the same level of importance to each objective function. However, different degrees of importance can be also utilised by using a vector of weights, as used in the weighted-sum approach. The target vector optimisation method will be separately dealt with in Section 5.1.6.1.

A typical example of the generating approaches is the Pareto approach. In this method, it is assumed that no information about the preference among objectives is available; and that for each objective function, the greater the value, the better. One particular GAs-based implementation of the Pareto approach for solving multi-objective optimisation problems is the Pareto ranking [103]. This method involves sorting the population based on Pareto ranking, and assigning selection probabilities to individuals according to this ranking. The ranking procedure is as follows: (i) assign rank 1 to all nondominated individuals and remove them from contention; (ii) find the nondominated individuals from the remaining ones, assign rank 2 to them, and remove them from contention; and (iii) follow the same process until the entire population is ranked. Following this procedure, all nondominated solutions are assigned an identical fitness value, which provides them an equal reproduction probability.

Finally, it is important to highlight that there are some problems associated with generating techniques that are not observed with most preference-based approaches.

One of these problems is the judgment that a decision-maker has to make in order to select a solution from an entire set of Pareto solutions. With a small number of criteria, two or three, this (solution) selection process can be carried out relatively easily. However, for more than three criteria, this process becomes both complicated (increasing in difficulty almost exponentially with the number of objectives), and also computationally expensive and very difficult to visualise graphically [103].

#### 5.1.6.1 Target Optimisation

The target vector optimisation method (or 'optative' [113] or 'goal attained' method as it is also sometimes referred to) essentially involves the minimisation of the difference between the values of the performance parameters controlling a given optimisation problem and their corresponding target values. In order to clarify how this method works, it is first necessary to state a multi-objective optimisation problem as follows (similarly to the problem statement used in Chapter 4):

Find

$$X = \begin{Bmatrix} x_1 \\ x_2 \\ x_3 \\ \vdots \\ x_k \end{Bmatrix} \tag{5-16}$$

which optimise $F$, given by,

$$F = \{f_1(X), f_2(X), \dots, f_p(X)\} \tag{5-17}$$

and subject to '$c$' constraints

$$\begin{aligned} g_j(X) &\leq 0, \qquad j = 1,2,3, \dots, m \\ h_l(X) &= 0, \qquad l = m+1, m+2, \dots, c \end{aligned} \tag{5-18}$$

In equations (5-16) - (5-18), $X$ is a $k$-dimensional vector called the design vector, $F$ the multi-objective function ($p$ objectives or criteria), and $g_j(X)$ and $h_l(X)$ the inequality and equality constraints, respectively.

Thus, the target optimisation method, initially presented by Wienke [113] and extended by Rogero [87] for the case of engineering optimisation problems, can be regarded as the process of optimising a set of $k$ design variables $X$, such that the set of $p$ performance parameters $F$ approaches a set of $p$ targets $F^*$ ($F^* = \{f_1^*, f_2^*, \dots, f_p^*\}$),

while satisfying the following lower and upper performance parameters boundaries: $LB \leq F \leq UB$. In this way, the optimisation of each performance parameter $f_i$ corresponds to achieving a target $f_i$*. The set of targets $F$* comprises the finite targets $T$* and the optimisation (minimisation or maximisation – non-finite) targets $O$* ($F$* = $T$* + $O$*). Following this approach, the quality of a given design is defined by three factors [87]: range error factor, target achievement factor, and optimisation factor.

The range error factor, $R_e(X)$, measures the level of satisfaction of the range constraints, and it is defined as a function of the normalised distance between $F$ and the nearest point from [$LB$, $UB$]:

$$R_e(X) = \left(\frac{\sum_{i=1}^{k} \lambda_i^2}{k}\right)^{0.5}, where \tag{5-19}$$

$$\lambda_i = \begin{cases} 1, & LB_i \leq f_i \leq UB_i \\ 1 - max\left(\frac{f_i - UB_i}{f_i}, \frac{LB_i - f_i}{LB_i}\right), & Otherwise \end{cases} \tag{5-20}$$

According to this definition, the range error factor varies between 0 and 1. It is equal to 1 when all range constraints are satisfied ($X \in \mathcal{F}$), and it tends to 0 when the performance parameters correspond to design variables belonging to the extreme of the unfeasible search space ($X \in \mathcal{U}$). Here, again, $\mathcal{S}$ represent the whole search space, $\mathcal{F}$ the feasible search space, and $\mathcal{U}$ the unfeasible one ($\mathcal{S} = \mathcal{F} + \mathcal{U}$).

The target achievement factor, $T_a(X)$, measures, in turn, the degree of achievement of the targets. It is defined as a function of the normalised distance between $F$ and $T$*. Thus, for finites targets ($f_i$ and $f_i$* $\in$ $T$*), $T_a$ is determined as:

$$T_a(X) = \left(\frac{\sum_{i=1}^{k} \lambda_i^2}{k}\right)^{0.5}, where \tag{5-21}$$

$$\lambda_i = \begin{cases} \frac{f_i - f_i^*}{f_i}, & f_i > f_i^* \\ \frac{f_i^* - f_i}{f_i^*}, & Otherwise \end{cases} \tag{5-22}$$

Based on this definition, the target achievement factor is equal to 0 if all targets are achieved exactly, and it tends to 1 when the values of the performance parameters are well out of range.

The optimisation factor, *O(X)*, provides an indication of the direction to be followed by the optimisation process: maximisation or minimisation. This factor is selected in such a way that a poor performance towards the minimisation or maximisation of the performance parameters results in values of *O(X)* that tend to 1, and a good performance results in values that tend to $+\infty$.

For a given optimisation problem when both finite and non-finite targets (performance parameters involving maximisation and/or minimisation) are present, the optimisation objectives (non-finite targets) have the priority over the targets (finite targets). In these cases, the target optimisation is just utilised to push (using a small pressure) the unaffected performance parameters towards their target values [87]. Thus, for a general multi-objective case, the fitness function is defined as:

$$Fitness(X) = \begin{cases} O(X) - T_a(X), & X \in Feasible \\ R_e(X), & X \in Unfeasible \end{cases} \quad (5\text{-}23)$$

Further details about this particular implementation of the target vector optimisation method are described in reference [87].

### 5.1.7 Stopping Criteria

As any other evolutionary algorithm, a GAs-based search algorithm (or a GAs-based optimisation one) evolves solutions from generation to generation selecting and reproducing parents until a stopping criterion is (or stopping criteria are) met. Three termination criteria are most frequently utilised: maximum number of generations, maximum number of evaluations (i.e., maximum number of chromosomes or potential solutions to be evaluated during a given search or optimisation process), and maximum fitness value. Alternative stopping strategies involve concepts such as population convergence criteria (e.g., sum of deviations among individuals smaller than a specified threshold), and lack of improvement in the best solution over a given number of generations [103]. Several of these strategies are not exclusive and can be used in conjunction with each other.

### 5.1.8 Other Concepts in Genetic Algorithms

In this section, several other concepts that are usually utilised to improve the performance of GAs are briefly described.

#### 5.1.8.1 Elitism

Elitism simply means that one or more of the best individuals (i.e., most fitted chromosomes) generated within a given generation are propagated into subsequent generations. In general, this technique guarantees the genetic material present in the best individuals is not lost in between the generations. However, the elitism concept must be utilised carefully, because, as pointed out by Goldberg [102], its overall effect is difficult to quantify. On one hand, it can help the mixing process by ensuring that the best individuals are available to create better ones. However, it can also negatively affect the selection process by favouring the selection of elite individuals, thereby reducing diversity and increasing the tendency of premature convergence. Results suggest that elitism improves local search at the expense of global perspective [104].

#### 5.1.8.2 Adaptive Genetic Algorithms

As mentioned in Section 5.1.1, the success of a GAs-based search process is characterised by a good balance between exploitation and exploration in the search space. This balance is strongly dependent on key GAs factors such as population size, crossover ratio, and mutation ratio, among others. Thus, an adaptive GAs-based search process is one where these key GAs factors are dynamically varied according to the progress of the search or optimisation process. Since the use of GAs for searching optimum solutions involves an intrinsically dynamic and adaptive process, the use of fixed parameters (which occurs in most standard applications involving GAs) is in contrast to the evolutionary nature of the algorithm. Thus, it is natural to try to modify or adapt key GAs parameters as the search process progresses. The adaptation of the GAs parameters can be mainly carried out in three ways [103]: (i) deterministic, by using a determinist rule to modify a given parameter (e.g., by using a rule that gradually decreases the mutation rate as the generation number increases); (ii) adaptive, by taking

feedback information from the current state of the search; and (iii) self-adaptive, by using a self-adaptive mechanism which enables GAs parameters to evolve within the evolutionary process.

A particular implementation of adaptive GAs is described by Sampath in reference [88]. According to Sampath's implementation, the process starts in a similar fashion as a standard GAs-based search process, but after a few generations, some GAs key parameters are controlled based on other statistical ones. The process is characterised by the use of a 'master-slave' configuration, which consists of a 'master' GAs-based controller that monitors the functioning of a 'slave' GAs-based model. The master evaluates the performance of the slave GAs at each generation. This evaluation is carried out based on the monitoring of several statistical parameters, including (i) the population diversity factor, which measures the population diversity during a given generation; (ii) population size factor, which controls the size of the population at each generation; (iii) population mean fitness factor, which measures the mean fitness of the population; and (iv) fitness improvement factor, which measures the performance of the GAs-based search process.

#### 5.1.8.3 Genetic Algorithms Hybridisation

Hybrid GAs are GAs combined with other search or optimisation techniques. As they incorporate what is best in its competitors, they are expected to perform better than traditional GAs for particular applications. Hybridisation of GAs is carried out because, as highlighted by Davis [106], traditional GAs, although robust, are generally not the most successful search or optimisation algorithms for any particular domain. This reflects a natural phenomenon, which relates to the fact that individuals that do well across a variety of environments are never the best in any particular environment. One of the most common ways of hybridising GAs is by incorporating local search techniques to the main GAs search or optimisation process. Following this approach, GAs are utilised to perform global exploration among populations, while local search methods are used to perform local exploitation around chromosomes [103]. In other words, GAs find the region where the optimum is located, and then the local optimisation techniques take over to find the optimum value.

GAs hybridisation can be carried out in a variety of ways, including the following [100,103]: (i) incorporating heuristics into the initialisation in order to generate a well-adapted initial population; (ii) running GAs until it slows down, letting then a local search technique continue the process; (ii) after every certain number of generations, running a local search method on the best solution or solutions and adding the resulting chromosomes to the population; and (iv) adding a local search heuristic to the GAs basic loop, which working together with crossover and mutation operators carries out quick and localised search processes thereby improving offspring before returning them for evaluation. The complementary properties of GAs and local search techniques allow hybrid GAs to usually perform better than either method in isolation.

It is worth emphasising that GAs can be hybridised with several other techniques, including expert systems (which guide genetic operators more directly towards better strings), response surfaces (which construct objective function's approximate models to reduce full-cost functions evaluations), and neural networks (which act as pre-processors of GAs determining sub-regions in the search space where the optimum is likely to be found). However, for the sake of brevity, these other types of GAs hybridisation will not be discussed in this work.

## 5.2 Optimiser Development

In order to carry out the processes of evaluation and optimisation of environmentally friendly aircraft propulsion systems, it was decided to either develop and implement an optimisation tool, or modify and adapt an existing one capable of performing these tasks. Thus, different numerical methods that could be used for this purpose were firstly reviewed, and a suitable optimisation technique was initially selected (see further details in Chapter 4). A familiarisation process with several programming languages, including FORTRAN, C/C++, and Java, was also carried out.

The next step in the development of the optimisation algorithms (optimiser) involved reviewing the track record of optimisers developed by Cranfield University for a range of applications, and identifying a candidate which could be used as a suitable 'starting point'. This led to the decision to use the GAs-based optimisation routines developed by Rogero [87,114] as the basis for the development of the optimiser utilised

in this work. Rogero's optimiser, which was developed for carrying out optimisation processes of combustor preliminary designs, already includes several algorithms for each of the main phases (selection, crossover, and mutation) involved in the optimisation process using this technique. However, there are additional enhancements that can be introduced in future to further improve the quality of the optimiser. These improvements include the use of adaptive GAs (e.g., 'master-slave' configurations), which would allow the use of optimum GAs parameters (e.g., population size, crossover ratio, and mutation ratio, etc.) during the optimisation processes; and also the inclusion of the concept of Pareto optimality (Pareto fronts), which would improve its capabilities when performing multi-objective optimisation processes. These improvements can be introduced based on successful past experiences of these concepts as part of previous optimisers [86,88] developed by Cranfield University.

The optimisation algorithms are constantly evolving and additional capabilities and/or refinements will be implemented in the future. Consequently, only a brief description of the main aspects characterising the current status of these optimisation algorithms is presented here. The optimiser used in this study has been implemented with a high degree of modularity, intended to support large changes and extensibility features. The code has been developed using Java as the main programming language. The fact that Java is platform independent brings a significant advantage when working on a heterogeneous set of computers, especially the advanced support for networking and graphics [114]. Even though Java is considered as being slower than fully compiled languages such as C/C++, this is not considered to be a major drawback, since distributed processing can counter the slower execution time of Java programmes.

The core of the optimiser has been developed following the basic structure of 'SGA Java V1.03' from Hartley [115], a Java implementation of the 'simple GA' (SGA) from Goldberg [104]. However, the original model has been recoded and extensively modified to both adapt it to engineering design optimisation problems and maximise its performance. The main modifications performed are related to the improvement of the optimisation performance, through an adaptation of the application domain, and improvements in both the technique and the genetic operators utilised during the optimisation process.

Since the application domain considered during the optimiser development was engineering design, the chromosome modules have been developed in such a way to support real-number parameter encoding in conjunction with a definition of the allowable range for the parameters (genes). In addition, algorithms for keeping a historical record of all created chromosomes and for preventing the creation of duplicate ones have been implemented. Regarding the improvement of the GAs technique, concepts such as elitism (preservation of the genetic material of the best members through generations), steady state replacement (partial replacement of the newly generated chromosomes to avoid the loss of potentially good genetic material), and fitness scaling (use of techniques to maintain the selection pressure relatively constant along the whole optimisation process – trade-off between premature convergence and genetic drift), have been introduced.

Another phase of the optimisation performance improvement involved the implementation of more advanced and efficient GAs operators (mutation, crossover, and selection) [87]. Accordingly, in addition to the standard random mutation operator, other mutation operators such as creep mutation with and without decay, and dynamic vectored mutation (DVM) have been implemented in the optimiser. When utilised, the decay rate reduces the mutation range as the GAs population ages, resulting in a broad capability to explore during the optimisation initial stages and to carry out fine local searches in later stages. DVM allows in turn mutation in all directions and not only along a dimension axis. Additionally, this operator is able to reach the whole search space and is not biased [87].

Since real-number encoding was selected as the default encoding for the optimisation processes, several crossover techniques (suitable for this type of encoding) have been implemented in the optimiser, including the weighting averaging crossover method (children are a weighted average of two parent points), the blend crossover BLX-$\alpha$ method (weighting averaging with exploration capabilities), and the simulated binary crossover SBX method (creation of solutions within the whole search space). All crossover operators implemented include features for consanguinity prevention (i.e., duplicate chromosomes are not allowed). Selection operators implemented in the optimiser include, among others, a modified roulette wheel selection operator (with limitations on the number of instances of a chromosome), and the stochastic universal

sampling SUS technique (which minimises the bias and drift connected with the repeated spinning of the wheel). The tournament replacement and the ranked replacement have been improved and implemented in the optimiser as replacement operators.

One aspect that characterises the optimisation process of practical engineering problems is the large number of parameters that must be accommodated. This is particularly true when optimising aircraft propulsion systems, especially, when aircraft trajectory optimisation problems are dealt with. For these particular problems, in order to describe properly a given flight path, a number of flight segments, each involving several design variables and constraints (e.g., altitude, speed, etc.), need to be utilised. Thus, the optimiser (as highlighted by Rogero in reference [114] when describing the optimisation routines utilised as the basis for the optimiser described here) uses a unique optimisation method based on Wienke's idea of target vector optimisation [113] (more details about this method can be found in section 5.1). In this method, designers can define, for each parameter, a target to be attained, a range within which this parameter should remain, and the requirement to maximise or minimise the given parameter. Consequently, the quality of the design is determined by the achievement of the targets, the possibility of the violation of ranges, and the optimisation of the selected parameters. This approach enables designers to have total control over the optimisation process with neither having to know very much about the optimisation algorithms nor having to devise a fitness function [114]. Finally, it is important to emphasise once again that the optimisation algorithms utilised in this research project are currently in development, and they may be changed in future. Thus, the optimisation results presented in the following chapters were obtained using the current version of the optimiser, whose main characteristics are summarised above.

# 6
# Evaluation and Optimisation of Propulsion Systems Part A: Aircraft Trajectory Optimisation

This chapter describes the first part of the main results obtained from the processes of evaluation and optimisation of environmentally friendly aircraft propulsion systems. Initially, general aspects about atmospheric parameters, aircraft speeds, and computational models utilised, among others, are highlighted. Aircraft propulsion systems are then optimised from the point of view of the operation of the propulsion system. More specifically, aircraft flight trajectories are optimised considering that the aircraft/engine configuration is unchanged, i.e., aircraft/engine configuration already designed and in operation. The main results of these optimisation processes are finally presented and discussed.

## 6.1
## General Considerations

This section describes general concepts about atmospheric parameters and aircraft speeds. It also briefly summarises the methodology adopted for the optimisation of aircraft trajectories and the computational models involved.

### 6.1.1
### Atmospheric Parameters

The performance of aircraft is directly related to the conditions of the medium (i.e., atmosphere) in which aircraft fly. The earth's atmosphere is a sequence of thick layers that have almost the same chemical composition, but their own approximately constant temperature gradient (negative of their lapse rate) [116]. Commercial aircraft operations usually take place in the lowest layer, called 'troposphere', which extends up to an altitude of approximately 11,000m. The second layer, called 'stratosphere', which has essentially the same chemical composition as the troposphere, extends from

11,000m to approximately 20,000m, and it is currently being routinely accessed by passenger jet aircraft [116].

There are three main parameters that characterise the atmosphere: temperature ($T$), pressure ($P$), and density ($\rho$). Air can be largely considered as an ideal gas, and as such it obeys the ideal gas low,

$$P = \rho RT \tag{6-1}$$

or, in terms of ρ,

$$\rho = \frac{P}{RT} \tag{6-2}$$

In equations (6-1) and (6-2), $R$ represents the specific gas constant. Atmospheric density plays an important role due to fact that several parameters characterising the performance of an aircraft, such as lift, drag, thrust, etc., directly depend on it.

Consider for simplicity that the atmosphere is in equilibrium, that is, the pressure is the same in all directions. Then, the pressure on the bottom of an imaginary circular cylinder composed of air (height $dh$ and vertical axis) is given by [116]:

$$P = -\rho g dh \tag{6-3}$$

where $g$ is the acceleration of gravity. This hydrostatic relation, together with the ideal gas law, Eq. (6-1) or (6-2), allow the calculation of the vertical distribution of two of the three main atmospheric parameters ($T$, $P$, and $\rho$) given the corresponding (vertical) distribution (actual or assumed) of the third one. The International Standard Atmosphere (ISA) model [117] is one of several atmospheric models available in the public domain that provides the vertical distribution of this third parameter, which in turn allows the computation of the corresponding vertical distributions of the other two ones. Table 6-1 gives the ISA model defining parameters corresponding to the troposphere. There, α represents the standard constant temperature lapse rate, and the subscript '0' indicates sea level conditions (0.0m).

Table 6-1. Defining parameters for ISA troposphere (adapted from [116])

| $T_0$ [°C] | $P_0$ [N/m$^2$] | $\rho_0$ [kg/m$^3$] | α [°C/m] | g [m/s$^2$] |
|---|---|---|---|---|
| 15.0 | 101,325.0 | 0.21 | 0.00650 | 9.80665 |

Thus, using the ISA model in conjunction with both the ideal gas law and the hydrostatic relation presented in Eq. (6-3), it is possible to compute the vertical distribution of the three main parameters that characterise the atmosphere, as illustrated in Figure 6-1. In this figure, it is possible to observe the progressive drop in (relative) temperature from sea level up to the tropopause (atmospheric boundary between the troposphere and the stratosphere), as well as the reduction of relative density and relative pressure from sea level up to 15,000m. The ratios of $T$, $P$, and $\rho$ to their corresponding sea level standard values are known as θ (theta), δ (delta) and σ (sigma), and they are defined as:

$$\theta = \frac{T}{T_0} \tag{6-4}$$

$$\delta = \frac{P}{P_0} \tag{6-5}$$

$$\sigma = \frac{\rho}{\rho_0} \tag{6-6}$$

The values of these ratios are shown in Figure 6-1 as a function of the geopotential altitude (acceleration of gravity constant).

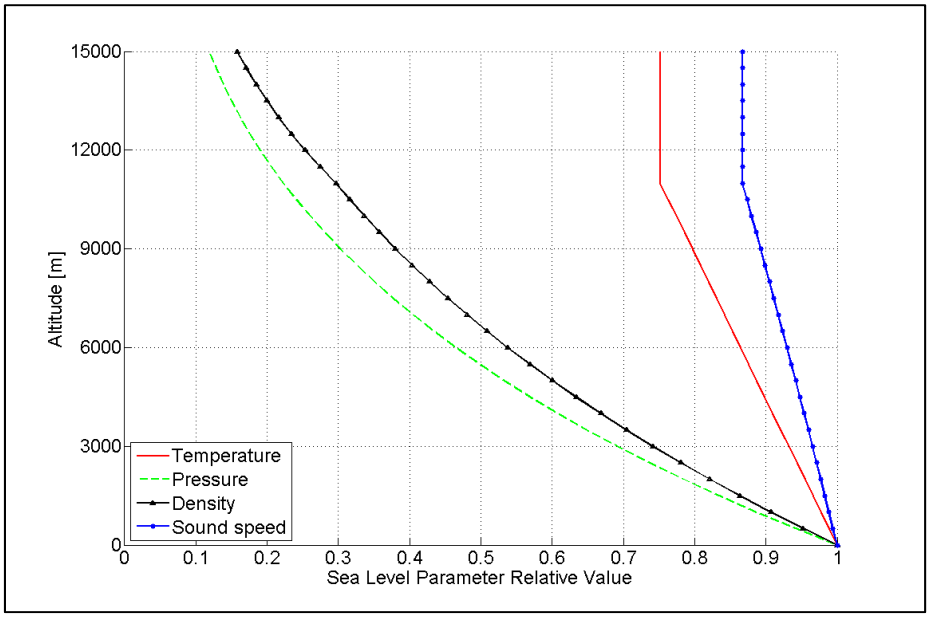


Figure 6-1. Standard atmospheric parameters vs. Altitude

As observed in Figure 6-1, the atmospheric temperature decreases as the altitude increases. In other words, it generally gets colder at higher altitudes. There is no simple explanation about this fact. One idea about this issue takes into consideration the presence of $CO_2$ and $H_2O$ (vapour) in the atmosphere [116]. It is believed that lower level $CO_2$ and $H_2O$ heat up, from the earth, the gases present at the lowest part of the atmosphere. As altitude increases, this radiation diminishes as the lower gases have absorbed much of it. Moreover, as the amount of these gases decreases with the increase in altitude, the higher level $CO_2$ and $H_2O$ gases radiate into space. This means that radiation is lost and the higher gases cool. All these phenomena result in what is well known and accepted, that is, as altitude increases temperature generally decreases. For completeness, Figure 6-1 also includes the variation of the relative speed of sound as a function of altitude. Due to the direct relationship between speed of sound, $a$, and atmospheric temperature (for a gas with a given composition, $a$ depends only on temperature),

$$a = \sqrt{\gamma RT} \tag{6-7}$$

the speed of sound (relative or absolute) behaves, as expected, similarly to the temperature as altitude changes. In Eq. (6-7), $\gamma$ is the ratio of specific heats of the gas.

### 6.1.2 Aircraft Speeds

Another reason why the main characteristics of the atmosphere have been emphasised in the previous section is because several aircraft cockpit instruments, such as airspeed indicators, have atmospheric parameters as inputs. Since the speed of the aircraft has been used as one of the main design variables for optimising aircraft trajectories, a particular emphasis will be placed on airspeed indicators and the airspeeds (aircraft speeds measured in relation to the air mass it flies in) that they indicate.

Figure 6-2 shows a schematic representation of an airspeed indicator (based on a Pitot-static tube), which illustrates the main input and output of the indicator. In Figure 6-2, $P_T$ represents the total or stagnation pressure (i.e., pressure of air at rest), $P$ the static pressure, $q$ the dynamic pressure, and IAS the Indicated Airspeed. In

incompressible flow, the dynamic pressure represents the pressure developed by the forward motion of a body and it is given by [116,118-120]:

$$q = \frac{1}{2}\rho V^2 \tag{6-8}$$

where $V$ is the True Airspeed (TAS) of the body relative to the air.

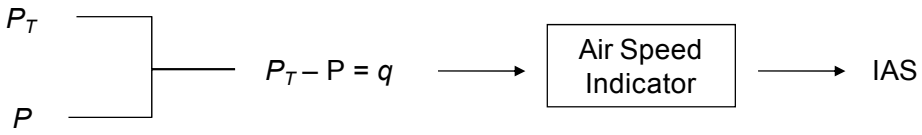


Figure 6-2. Schematic representation of an airspeed indicator [116]

As illustrated in Figure 6-2, the IAS is the airspeed read directly from the airspeed indicator on an aircraft at any given flight condition and altitude. There are a number of factors that contribute to the difference between the value of IAS read from the indicator and the actual speed of the aircraft relative to the air, TAS. These factors include, among others, instrument error, position error, compressibility effects, and density effects [119]. According to the level of correction applied to the IAS, other different airspeed terms can be obtained, as shown in Figure 6-3.

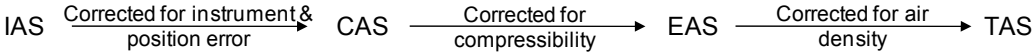


Figure 6-3. Airspeed indicator corrections [116]

In Figure 6-3, CAS is the Calibrated Airspeed, which means IAS corrected for position, installation, and instrument error; and EAS is the Equivalent Airspeed, which in turn means CAS corrected for compressibility effects. By definition, at standard sea level conditions both EAS and CAS are equal to the TAS [118]. The EAS establishes equivalence of the dynamic pressure at sea level and at altitude [119], that is, it represents the speed of an aircraft flying at a given altitude such that its dynamic pressure is equivalent to the corresponding pressure at sea level. Thus, from Eq. (6-8),

$$q = \frac{1}{2}\rho V^2 = \frac{1}{2}\rho_0 EAS^2 \tag{6-9}$$

the TAS can be related to the EAS by,

$$V = TAS = \frac{EAS}{\sqrt{\frac{\rho}{\rho_0}}} = \frac{EAS}{\sqrt{\sigma}} \tag{6-10}$$

There are other aircraft speeds such as Ground Speed (GS), which is the speed of the aircraft over the ground, and flight Mach number ($M$). The flight Mach number is the ratio of the aircraft TAS to the ambient speed of sound, $a$,

$$M = \frac{TAS}{a} = \frac{TAS}{\sqrt{\gamma RT}} \tag{6-11}$$

Utilising equations (6-10) and (6-11) the flight Mach number can be correlated to the EAS as follows:

$$M = \frac{TAS}{a} = \frac{TAS}{\sqrt{\gamma RT}} = \frac{EAS}{\sqrt{\gamma RT\sigma}} \tag{6-12}$$

In the trajectory optimisation processes carried out in this work, the aircraft trajectories have been defined as a function of the aircraft flight altitude and one or more of the following airspeed parameters: TAS, Mach number, and EAS. Due to the direct relation among these airspeed parameters (e.g., Eq. (6-12)), a brief discussion about them is presented next. As illustrated in Figure 6-4, keeping the TAS constant results in a non-linear decrease in EAS as altitude increases as a consequence of the non-linear decrease in density observed (Figure 6-1). Since Mach number is inversely proportional to temperature, as altitude increases it also increases up to the Tropopause where it remains constant with respect to altitude. This reflects an opposite behaviour to that shown by the temperature (Figure 6-1).

Variations (increases) in altitude whilst holding EAS constant result in non-linear increases in both TAS and Mach number as shown in Figure 6-5. The main driving factors in this case are the temperature and density (both in the troposphere and only density in the stratosphere), which decrease as altitude increases. In turn, a constant Mach number results in decreases in both TAS (due to the decrease in temperature) and EAS (due to the decrease in temperature and density) as altitude increases (Figure 6-6). The invariance of the temperature with altitude in the stratosphere (Figure 6-1) results in the discontinuous variation in Mach number (Figure 6-4) and TAS (Figure 6-6) observed.

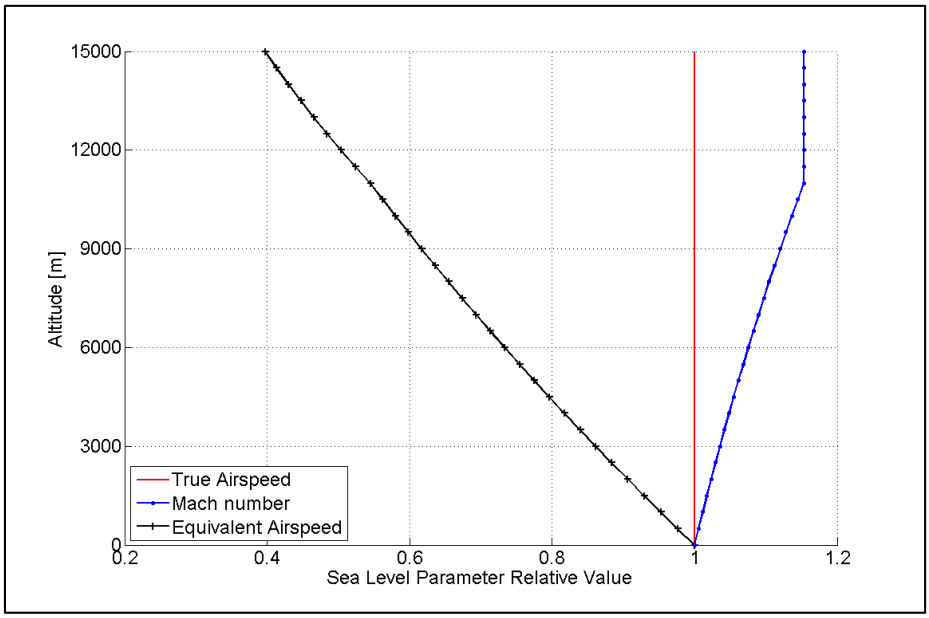


Figure 6-4. Airspeed variations for constant True Airspeed (TAS)

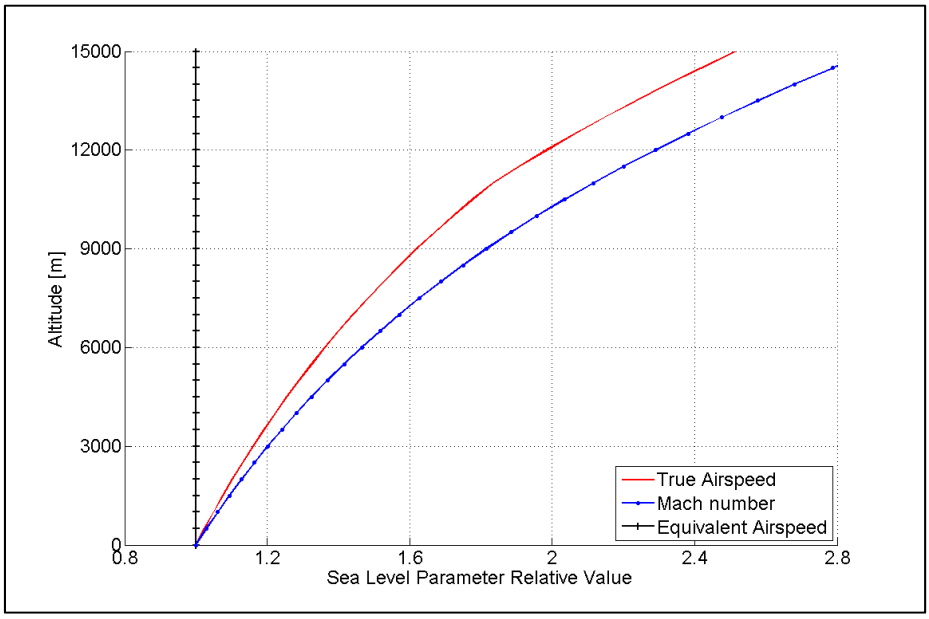


Figure 6-5. Airspeed variations for constant Equivalent Airspeed (EAS)

Finalising this section, Figure 6-7 exemplifies the constriction of the speed range with altitude for a given civil aircraft. In this figure, $V_{stall}$ represents the stall speed, $V_{crit}$ the critical speed, and $V_{NE}$ the never-exceed speed (as before, V is the aircraft true airspeed, TAS). The stall speed is the minimum flight velocity at which steady sustained flight is possible, and it depends mainly on the altitude and the maximum lift coefficient [119]. The critical speed is directly related to the critical Mach number, which is the Mach number at which the flow somewhere on the aircraft surface first reaches the

sonic speed [120]. The never-exceed speed is the maximum speed at which an aircraft can operate. This speed is determined by the structural limits of the aircraft, and it depends for a given aircraft and gross weight on the flight altitude [121].

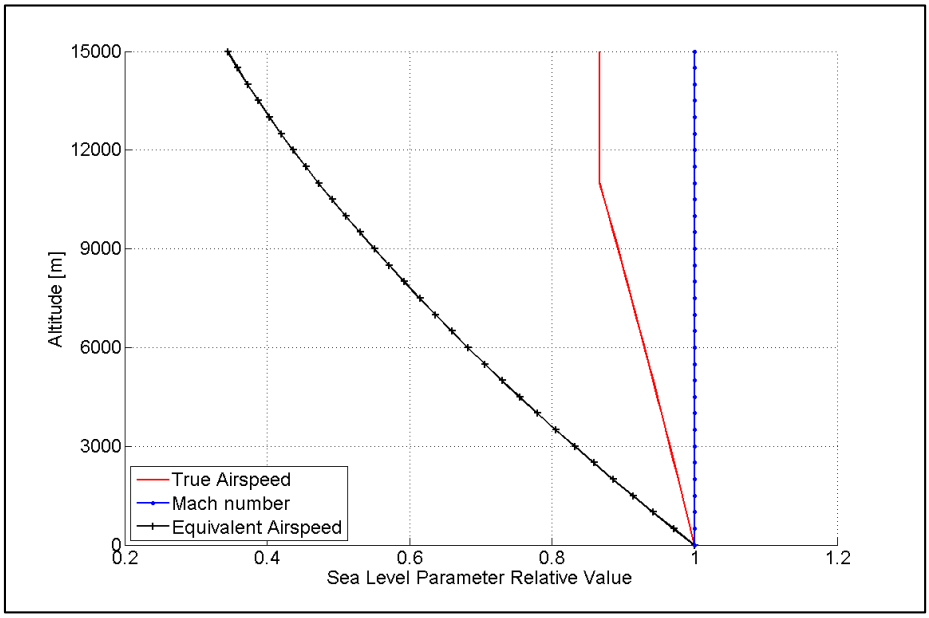


Figure 6-6. Airspeed variations for constant Mach number (M)

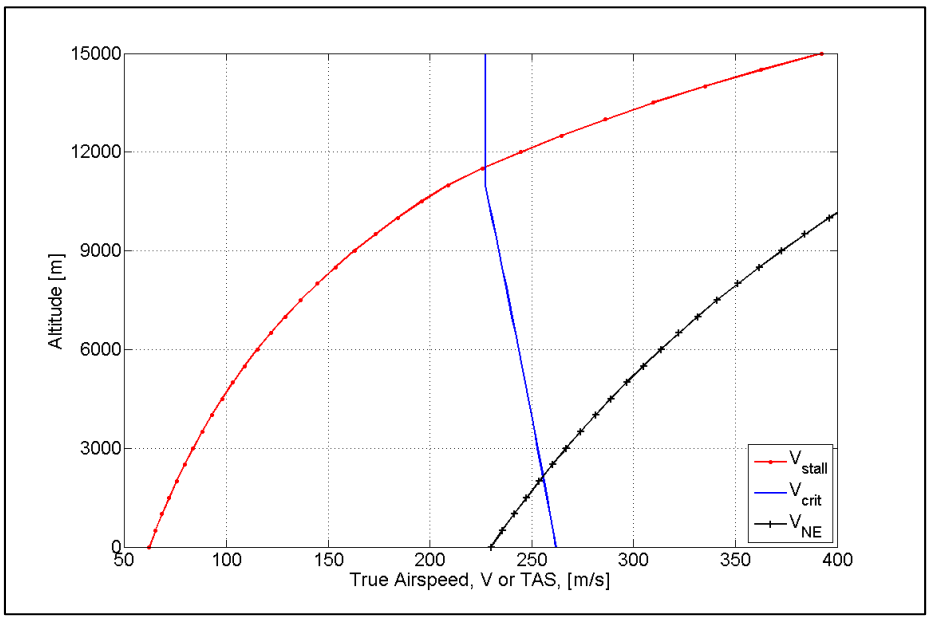


Figure 6-7. Civil aircraft speed range

In Figure 6-7 it is possible to observe that the curves corresponding to the stall speed and critical speed intersect at about 12,000m. At this altitude the aircraft could no longer fly, because if the speed is reduced it would stall, and if the speed increases it

would become uncontrollable. This limiting altitude can be lifted by increasing the critical Mach number, through better aerodynamics; and/or by reducing the stalling speed, by either increasing the lift coefficient or reducing the wing loading. In this work, when optimising aircraft trajectories, only the stall speed has been considered.

### 6.1.3 Computational Models

For performing the aircraft trajectory optimisation processes in this work, three computational models, i.e., the aircraft performance simulation model (APM), the engine performance simulation model (TurboMatch), and the emissions prediction model (Hephaestus), have been utilised. Figure 6-8 illustrates the general arrangement of these models, as well as the different parameters exchanged among them.

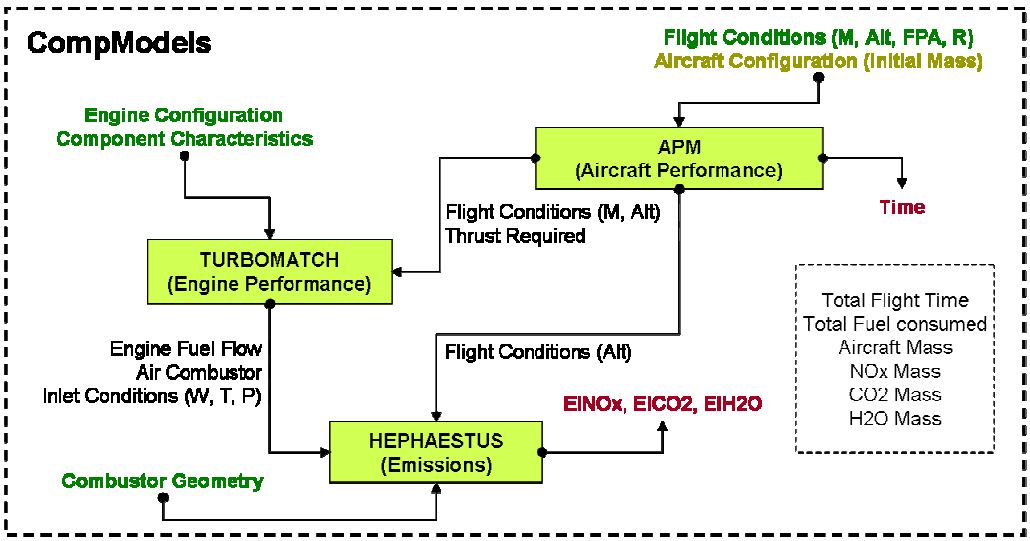


Figure 6-8. Aircraft trajectory optimisation – Models configuration

The aircraft performance model (APM) [122] utilised in this work is a generic tool which is able to determine flight path performance for a given aircraft design. The APM uses steady state performance equations to resolve aerodynamic lift and drag, and determines the thrust required for a given kinematic flight state. In order to easily identify the behaviour of the optimisation algorithms across a homogeneous search space, simplifications to the model have been imposed. Airspeed limitations, such as critical Mach number, never-exceed speed, as well as wave drag at transonic Mach number, have not been implemented. The model is suitable in the limit:

$$\lim_{dx \to 0} FN_{req}\,(h) \tag{6-13}$$

whereby variations in atmospheric parameters with altitude (h) are accurately, and smoothly, represented. Large ground range step sizes, *dx*, result in finite and discrete altitude steps and affect the accurate representation of an actual optimal trajectory (Figure 6-9). In general, APM uses end-points to compute performance. The user must declare a trajectory segment in terms of ground range and altitude intervals whereby a constant flight path angle is then defined. Flight conditions are then assumed to be constant over that segment. Aircraft weight and segment speeds are also necessary inputs. The aircraft modelled in this research project corresponds to a typical mid-sized, single-aisle, twin turbofan airliner with a maximum take off weight (MTOW) of about 72,000kg and a seating capacity of approximately 150 passengers.

The performance of the engines was simulated using TurboMatch [70], the in-house Cranfield University gas turbine performance code that has been refined and developed over a number of decades. TurboMatch can be used to simulate the performance of an extensive range of both Aero and Industrial engines cycles ranging from a simple single shaft turbojet to complex multi-spool turbofans with mixed exhausts and complex secondary air systems. It can also be utilised to simulate the performance of novel and conceptual cycles including wave rotors, pulse detonators, constant volume combustion systems, distributed propulsion systems and intercooled and recuperated cycles. Performance simulations range from simple steady state (design and off-design point) to complex transient performance computations.

According to the methodology developed in this work for optimising aircraft trajectories, the engine operating conditions are determined based on net thrust required for flying a given trajectory segment ($FN_{req}$), which is computed a priori by the APM. However, due to the fact that the engine performance model used here (TurboMatch) currently does not take thrust as an input, an iterative process has been designed and implemented with TurboMatch in order to carry out the optimisation processes. As illustrated in Figure 6-10, this iterative process basically involves three steps: (i) an initial guess of the turbine entry temperature (TET), based on the flight conditions, thrust required, and nozzle area ($A_{noz}$); (ii) execution of TurboMatch for this guessed TET; and (iii) comparison of the calculated thrust with the required one. At the end of

the iterative process, the main parameters characterising the operation of the engine, including fuel mass flow rate and combustor inlet conditions, are known. Appendix G provides additional details about how to estimate the initial TET guess necessary to start the iterative process described above.

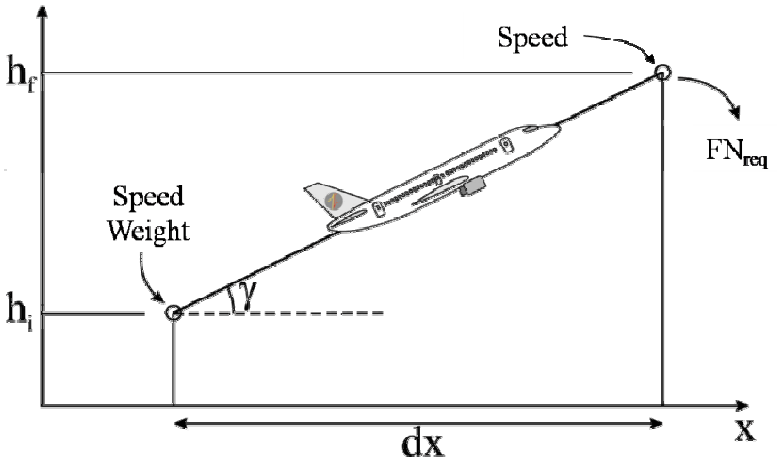


Figure 6-9. APM – Trajectory segment definition (adapted from [122])

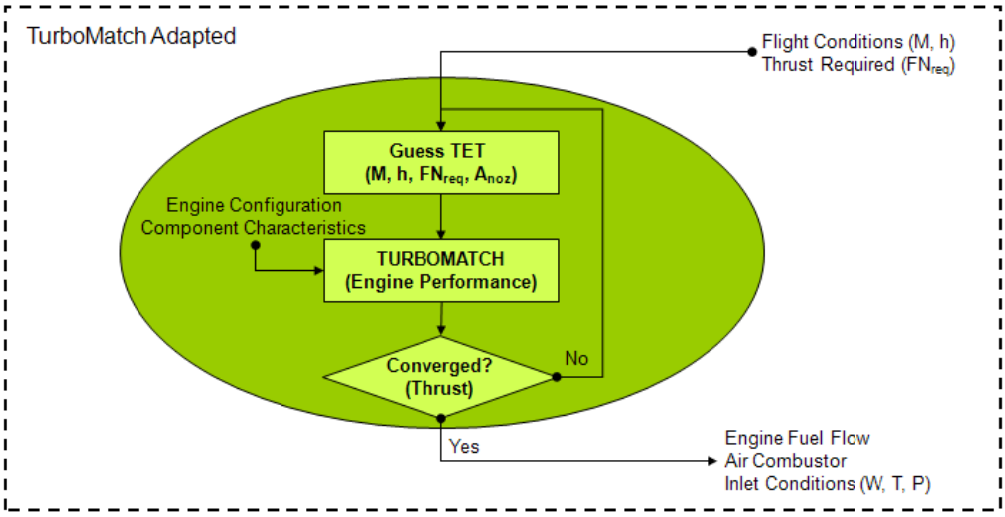


Figure 6-10. TurboMatch iterative process

The gaseous emission predictions were performed using the Cranfield University emissions prediction software Hephaestus. An integral part of Hephaestus constitutes the emissions prediction model described in Chapter 3 and in reference [123], which follows an approach based on the use of a number of stirred reactors for both the modelling of a given combustion chamber, and the estimation of the level of the main pollutants produced from gas turbine combustors. Following this particular approach, critical zones within the combustor are represented by individual stirred reactors,

incorporating the processes of mixing, combustion heat release, and pollutant formation. To take into account inhomogeneities in gas composition and temperature which influence directly the rates of pollutant formation, a stochastic representation of turbulent mixing in the combustor primary zone is utilised. In the following sections the results of the trajectory optimisation processes performed using the three models described previously will be summarised.

### 6.1.4 Aircraft Trajectory Definition

When optimising aircraft trajectories in this work, the first step involved the definition of the aircraft trajectory to be optimised. In other words, the definition of the problem that represent to optimise a given aircraft trajectory. Since all the optimisation processes carried out involved only vertical profiles, only three parameters were used to define a given aircraft trajectory: flight altitude (h), aircraft speed (TAS, EAS, or M), and range (R) – the horizontal distance flown by the aircraft. Figure 6-11 shows a schematic representation of a generic aircraft trajectory, which was divided in four segments. The intention in this work was to optimise aircraft trajectories between city pairs; therefore, the range was generally kept constant during the optimisations. Thus, in general, only altitude and aircraft speed were varied (i.e., used as design variables) when computing optimum aircraft trajectories according to a given optimisation criterion or optimisation criteria.

There are two important aspects to emphasise when describing the way in which aircraft trajectories were defined in this work. (i) Each trajectory segment was defined by both its initial and final states (in terms of altitude and speed), and its corresponding horizontal distance flown, range (which was usually kept constant during the optimisation process). (ii) It was possible to use different aircraft speeds (TAS, EAS, or M) to define different trajectory segments along the same aircraft trajectory. This means that, for instance, the first three segments of the aircraft trajectory illustrated in Figure 6-11 could have been flown at constant or variable EAS, and the last segment at constant Mach number.

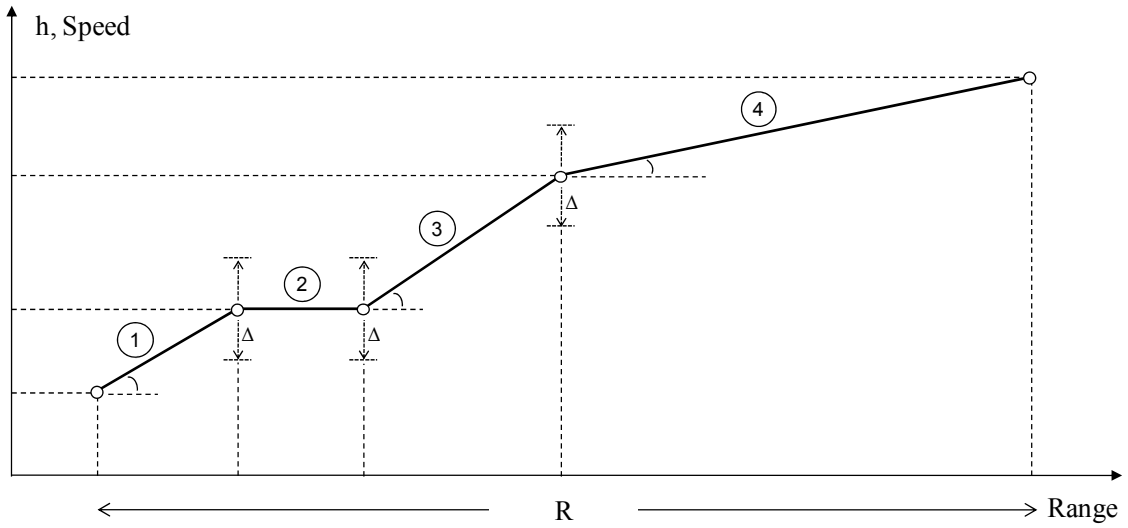


Figure 6-11. Generic definition of aircraft trajectories

This flexibility in the definition of the aircraft trajectory problem allowed the realistic representation of flight procedures utilised currently in practice. An example of these procedures constitutes the typical climb profile of commercial aircraft. The referred climb is divided in four segments: (i) climb from 1,500ft to 10,000ft at constant EAS and restricted to 250kts EAS; (ii) acceleration at 10,000ft (level flight) to 320kts EAS; (iii) climb from 10,000ft at constant EAS (320kts) up to the height at which the cruise Mach number is achieved; and (iv) climb from this altitude at constant Mach number (cruise M) up to the top of climb (TOC) altitude. All these details involved in the modelling of aircraft trajectories were taken into account in this work through the particular trajectory definition utilised. Of course, during the evaluation and optimisation of the aircraft trajectories, continuity in altitude and aircraft speeds between segments was guaranteed when required.

### 6.1.5
### Optimisation process

The methodology followed for optimising a given trajectory in terms of sequence of computations is described in this section. The optimiser (optimisation algorithms) developed and/or adapted in this work, which was (were) used for carrying out the optimisation processes in this research, will be called hereafter 'Polyphemus'[†] (oPtimisatiOn aLgorithms librarY for PHysical complEx MUlti-objective problemS). In the case studies described in the following sections, Polyphemus first randomly changes the values of the design variables (altitude and/or aircraft speed in one or more trajectory segments) in order to create a group of potential solutions. For a given potential solution, making use of the initial aircraft weight the APM carries out the computations related to the first segment of the aircraft trajectory, determining in this way the thrust required, flight time, etc. TurboMatch subsequently uses the flight conditions and the thrust required to determine the engine operating point, thereby establishing the engine fuel flow and other engine parameters related to the combustor (air) inlet conditions. Hephaestus then makes use of the combustor inlet conditions and combustor geometric details (such as length and area) to calculate the emission indices corresponding to the main pollutants of interest. Based on the fuel flow and flight time, the fuel burned during the first trajectory segment, and the new aircraft weight (that is, the initial weight less fuel burned), are calculated. The computations then continue in a similar fashion for all the remaining trajectory segments. When all the segments are computed, among other calculations, the total flight time, fuel burned, and gaseous emissions produced during the whole aircraft trajectory are computed. This process is

[†] Polyphemus is a Greek mythological figure, whose name means 'famous'. Polyphemus was a member of a race of (one-eyed) giants called 'cyclopes'. In the optimisation context, POLY (phemus) means that the optimiser is applicable to MANY types of optimisation problems. Additionally, the fact that Polyphemus was a giant implies that the optimiser can be used to solve large and complex optimisation problems.

repeated for all the potential solutions, and for the all the generations of potential solutions that Polyphemus utilises in order to determine an optimum trajectory according to criteria initially specified by the designer. The results which follow were obtained following this procedure.

## 6.2
## Aircraft Trajectory Optimisation Case Studies

In this section the main results of the different aircraft trajectory optimisation case studies obtained using Polyphemus are described. In all these case studies aircraft flight trajectories have been optimised considering that the aircraft/engine configurations are unchanged, i.e., aircraft/engine configurations already designed and in operation. The main design variables utilised involved parameters associated with flight altitude and aircraft speed. The minimisation of the total flight time, fuel burned, and $NO_x$ emitted have been considered as the main objective functions.

### 6.2.1
### Summary of Case Studies

Several aircraft flight profiles have been optimised mainly to assess the mathematical performance of Polyphemus. Accordingly, several cases studies, each of them involving the optimisation of a given aircraft flight profile, have been separately analysed. A brief description of these case studies is presented below:

- *Case Study 1: Simple Climb Profile Optimisation.* This case involved the optimisation of the climb phase of a typical aircraft flight profile. Only explicit constraints were utilised. Additionally, it was assumed that each climb segment is flown at constant Mach number (step M changes between segments).
- *Case Study 2: Climb Profile with Speed Continuity Optimisation.* In this second case, step changes in aircraft speed were avoided through the specification of speeds at the beginning and end of each climb segment. Consequently, continuity in aircraft speed was guaranteed. The climb profile optimised corresponded to that one used in the first case study.

- *Case Study 3: Implicitly Constrained Climb Profile Optimisation.* In the two first case studies, only explicit constraints were utilised. In this third case study, an implicit constraint was included. The climb profile optimised was the same as in the second case study.
- *Case Study 4: Full Flight Profile Optimisation.* In this fourth case study, a flight profile involving climb, cruise, and descent was optimised. Explicit and implicit constraints were utilised. The optimisation approach utilised in this case was similar to that one used in the third case study.
- *Case Study 5: Full Flight Profile Multi-objective Optimisation.* Multi-objective optimisation processes were performed in this fifth case study. The flight profile optimised was the same as in the fourth case study, but this time the optimisation involved more that one objective function.
- *Case Study 6: Full Flight Profile Range Optimisation.* This last case study was analysed in order to illustrate other uses of Polyphemus. Given an aircraft flying directly from city A to city B, it involved the determination of the location of an intermediate stop (to be used for refuelling purposes, for instance), which is optimum according to given criteria.

### 6.2.2 Case Study 1: Simple Climb Profile Optimisation

#### 6.2.2.1 General Description

It is clear that in order to demonstrate the suitability of an optimiser for optimising aircraft trajectories, an extensive validation process of the algorithms implemented need to be carried out using as test cases different analytical problems with known optimal values. In the case of Polyphemus, this part of the validation process has already been performed (see reference [87]) and is therefore not repeated here. In this work, the mathematical performance of Polyphemus is analysed when possible through comparisons of the results obtained using this optimiser and other commercially available optimisation algorithms [94]. Thus, in order to provide some insight into the results that can be expected using Polyphemus, this optimiser was firstly deployed on a single flight phase of a typical aircraft flight profile (climb). The same flight constraints

defining the flight path were then used with other optimisation algorithms from a commercially available software package [94]. This provided a means of quantitative comparison of the performance of the different algorithms and techniques, which was the main scope of this first case study.

In general, in the case studies analysed in this work (including this first case), the aircraft flight profile has been divided into only a small number of segments. This afforded greater visibility on the characteristics of the performance of Polyphemus when assessing results. This would have proved more difficult if the trajectory had been divided into a greater number of segments. These hypotheses are a simplification of real cases but provide numerical solutions that are used to commission the methodology. In order to obtain meaningful results in terms of actual optimal trajectories, the flight path needs to be divided into a much larger number of segments, each small enough so that the errors associated with the assumptions made within each segment will be cumulatively insignificant.

Consequently, in this first case study, the flight profile in question was divided into only four segments; similar to the generic flight profile exemplified in Figure 6-11. The four climb segments were defined by arbitrarily defining segment lengths (range, R), with the overall climb being defined by the cumulative range, start and end altitudes, and Mach numbers (ISA, international standard atmosphere, assumed). During the optimisation processes, the intermediate Mach numbers (initial Mach number in segments 2 and 3) and altitudes (initial altitude in segments 2, 3 and 4) were allowed to vary in such a way as to minimise the total flight time, fuel burned, and $NO_x$ emissions. This, of course, resulted in step Mach number changes between segments, which, in effect, represent an effective average value over the relevant segment.

It is relevant to note that, since the main objective of this first case study was the evaluation of the mathematical performance of Polyphemus rather than the generation of realistic trajectories, only a minimum number of (explicit) constraints were introduced. These were related to the range of permissible values of the design variables (h and M). The lower and upper bounds for these permissible ranges were set at 457m (1,500ft) and 10,668m (35,000ft) respectively for h (which correspond to the start and end altitudes) and 0.38 and 0.80 respectively for Mach number.

In this work, the flight path angle (FPA) was not used as a design variable or performance parameter in any of the optimisation processes performed. Consequently, this parameter was not used in the optimisation processes as either an explicit or implicit constraint. However, in order to compute only trajectories that closely represent actual ones, its permissible values were limited to a range previously defined. The FPA limitation was carried out inside the framework illustrated in Figure 6-8. However, the modelling of this limitation was not part of any of the three computational models used in this work and also schematically represented in this figure. In future, it is expected that this FPA constraint and other operational and physical ones constitute a different model which is used to compute accurate and realistic trajectories. Thus, in this work when dealing with trajectory segments belonging to climb (e.g., this first case study) and cruise phases, the lower and upper bounds of the FPA permissible range were specified as being equal to 0 and 7.5deg, respectively. In turn, for the case of trajectory segments belonging to descent phases, the corresponding range was set up as -7.5 and 0deg.

Table 6-2 defines, in terms of altitude (h), Mach number (M), and ground range (R) covered, the start and end points of the four segments of an arbitrary climb profile used as the reference (baseline) trajectory in this case study. In this table it is possible to observe that Segment 2 depicts a section at constant altitude, which is often encountered in situations such as in ATC (air traffic control) restrictions. For completeness, Table 6-2 also summarises the design variables utilised in this first case study, as well as the ranges of permissible values considered.

Table 6-2. Case Study 1 – Baseline trajectory and design variables

| Seg. No. | $h_i$ [m] | $h_f$ [m] | M [--] | R [km] | Design Variables |
|---|---|---|---|---|---|
| 1 | 457 | 3048 | 0.38 | 20 | -- |
| 2 | 3048 | 3048 | 0.46 | 10 | $0.38 \leq M \leq 0.80$, $457 \leq h_i \leq 10668$ |
| 3 | 3048 | 7000 | 0.58 | 60 | $0.38 \leq M \leq 0.80$, $457 \leq h_i \leq 10668$ |
| 4 | 7000 | 10668 | 0.80 | 100 | $457 \leq h_i \leq 10668$ |

The other two optimisation algorithms against which the current algorithm was compared in this case study were taken from a commercial software package [94]. One of these two algorithms corresponded to a direct search method and, more specifically, to a pattern search algorithm called mesh adaptive search (MADS). Following this

approach, at each step, the algorithm searches a set of points looking for one where the value of the objective function is lower than the value at the current point. If it finds a point that improves the current objective function, the new point becomes the current point at the next step of the algorithm [94]. The second optimisation algorithm used from the referred commercial software was one that follows the same optimisation approach as Polyphemus, i.e., GAs

#### 6.2.2.2 Results

The baseline climb profile for this case study as well as the optimal trajectories computed using Polyphemus and the commercial optimisers [94] are illustrated in Figure 6-12 for comparison purposes. Both Polyphemus and the optimisation algorithms from the commercial package yielded very similar results, as can be observed in Figure 6-12 and detailed quantitatively in Table 6-3, which shows the gains in terms of reduction of climb flight time (~ -16%) and fuel burn (~ -6%). Even though this first optimisation case study (climb profile) corresponded to a hypothetical one, the reasonable agreement among the optimisers (average discrepancies ~2%) confirmed the validity of the approach and provided the necessary motivation for continuing with the development of Polyphemus and carrying out the other optimisation case studies described in the following sections.

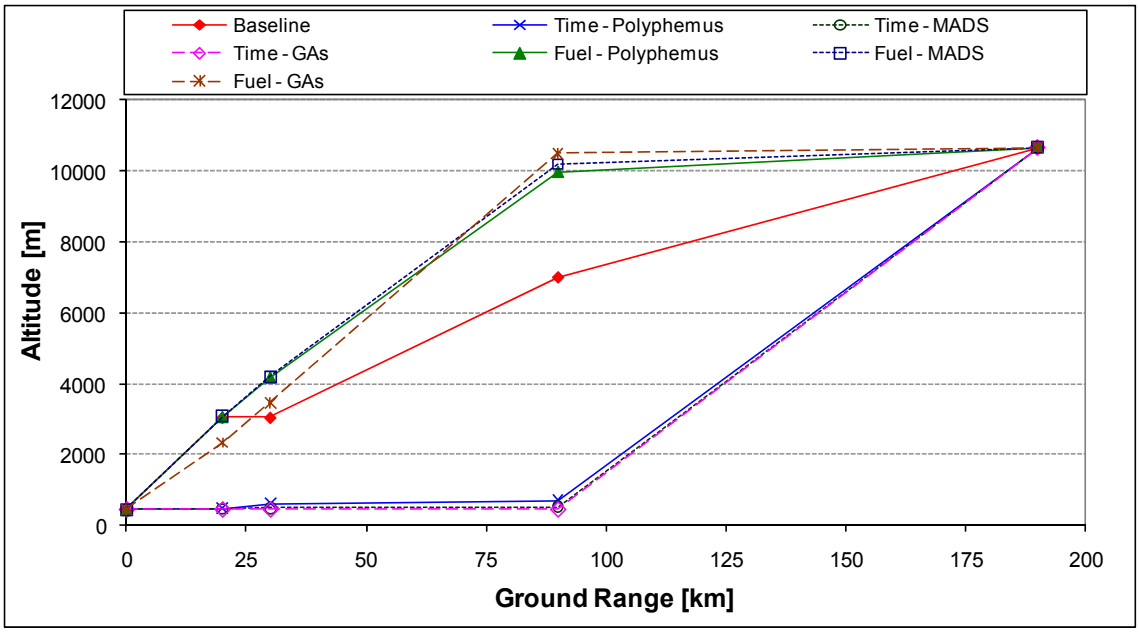


Figure 6-12. Case Study 1 – Comparison of optimisation algorithms

Figure 6-13 shows in turn the reference climb profile used in this case study and the optimum trajectories obtained using Polyphemus from the minimisation of the total flight time, fuel burned, and $NO_x$ emissions produced during the whole climb profile. The results associated with these optimum trajectories when translated into quantitative terms (Table 6-4) show significant reductions (relative to the baseline trajectory) in the total climb flight time (~ -16%), fuel burn (~ -6%), and $NO_x$ emissions produced (~ -43%). The nature of these results is briefly discussed next.

Table 6-3. Case Study 1 – Optimisation algorithms results (relative to baseline)

| Objective Function/ Optimiser | Flight Time [%] | Fuel Burned [%] |
|---|---|---|
| Time – Polyphemus | -16.2 | 50.5 |
| Time – MADS [94] | -16.3 | 52.6 |
| Time – GAs [94] | -16.3 | 53.0 |
| Fuel – Polyphemus | 3.7 | -6.7 |
| Fuel – MADS [94] | 3.1 | -6.7 |
| Fuel - GAs [94] | 4.7 | -6.0 |

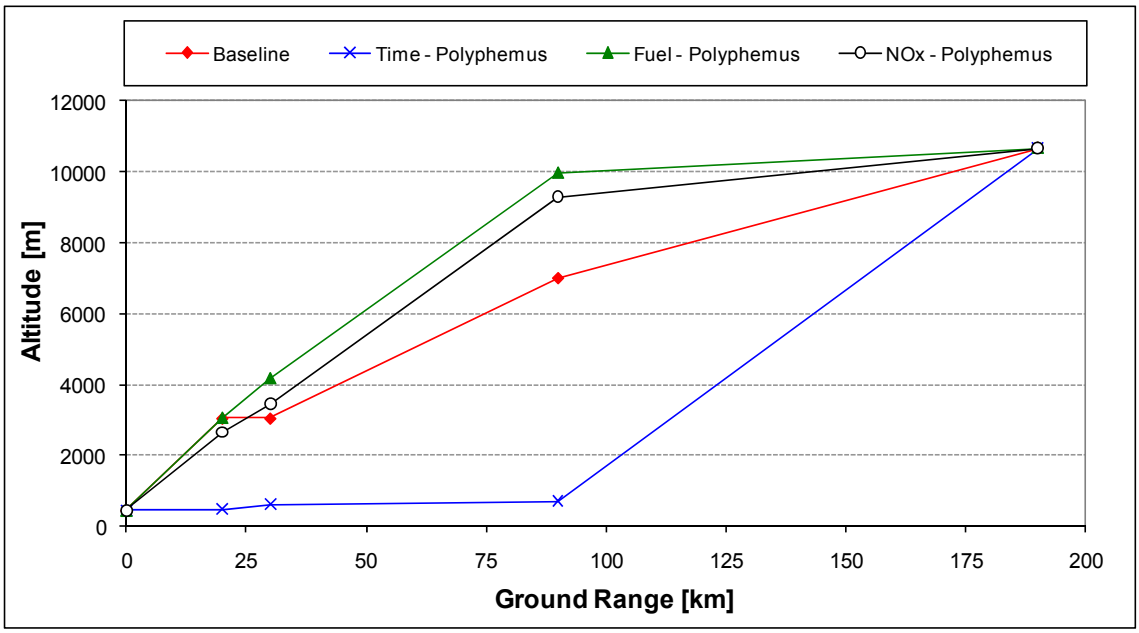


Figure 6-13. Case Study 1 – Baseline vs. Optimum trajectories

Figure 6-14 shows the flight Mach number for each segment of the climb phase for the baseline trajectory and the three optimised trajectories. From this figure it is possible to see that in order to minimise the time spent during climb, Polyphemus suggests a solution where the aircraft flies at the highest Mach number permissible,

which was fixed at 0.38 and 0.80 in the first and four segment, respectively, and free to rise to 0.8 in the remaining middle two. Polyphemus also suggests that the aircraft should fly at low altitudes for as long as possible before climbing rapidly to the target end altitude (Figure 6-13).

This is mathematically correct, since the speed of sound is the highest at sea levels (see Figure 6-1), thus enabling the aircraft to fly faster (maximisation of TAS) if it could actually achieve M 0.8 at this level. In practice, however, this solution is not realistic, not least because the never exceed speed ($V_{NE}$) is much lower than Mach 0.8 at sea level, thus restricting large transport category aircraft from approaching such high Mach numbers. Nevertheless, it is an interesting solution, confirming that the optimiser is working correctly in the absence of M (or TAS) constraints.

Table 6-4. Case Study 1 – Optimum trajectories results (relative to baseline)

| Objective Function/ Optimiser | Flight Time [%] | Fuel Burned [%] | $NO_x$ Emitted [%] |
|---|---|---|---|
| Time – Polyphemus | -16.2 | 50.5 | 694.2 |
| Fuel – Polyphemus | 3.7 | -6.7 | -19.3 |
| $NO_x$ – Polyphemus | 17.1 | -1.1 | -43.6 |

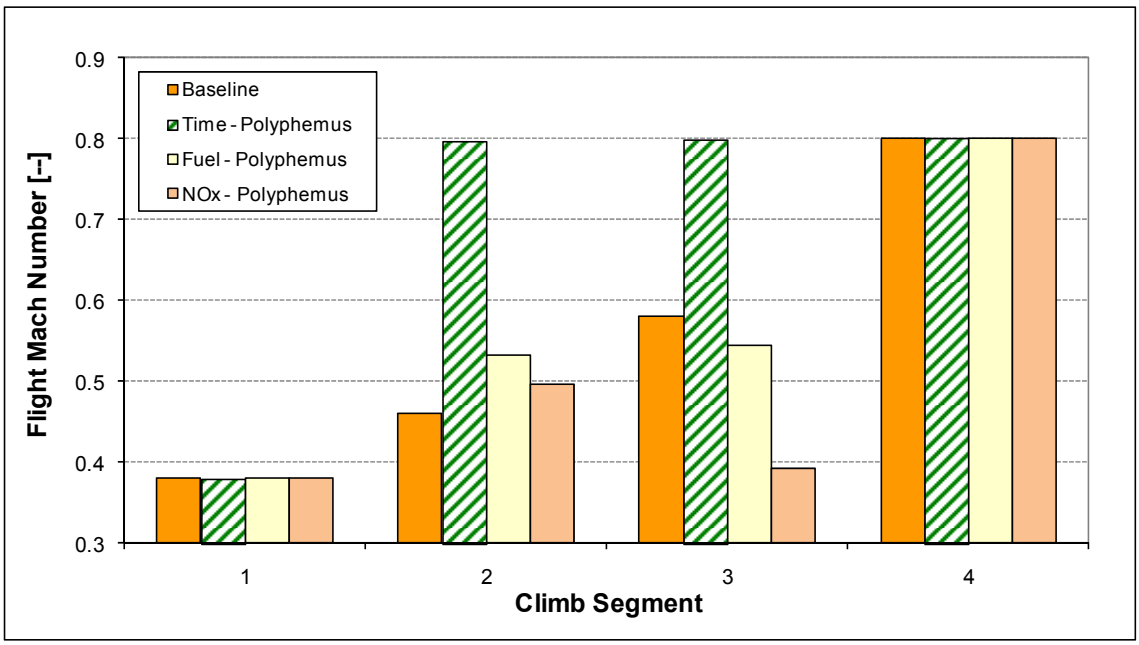


Figure 6-14. Case Study 1 – Mean Mach number at each climb segment

Figure 6-13 and Figure 6-14 show that, in order to reduce fuel burn, the optimiser suggests flying slower and higher than the reference trajectory (segment 3). This, again,

is conceptually correct (given the design of the reference trajectory). It is interesting to note that the fuel optimised trajectory proposes second and third segments affording a greater fuel burn (relative to the baseline – Figure 6-15) in order to gain height which, then, subsequently yields a lower fuel burn in the last segment and an overall lower fuel burn for the climb profile as a whole.

Initially from what can be observed in Figure 6-13 in terms of flight profile, one could conclude that the trajectories optimised for minimum fuel burned and $NO_x$ emissions are similar. However, there are significant differences between these two trajectories. The main one is related to the fact that the $NO_x$ emissions optimised trajectory is flown at relatively lower Mach numbers than the fuel burned optimised one (see Figure 6-14). These lower Mach numbers result in lower engine thrust settings, i.e., the thrust required to fly a given segment is lower, which in turn result in lower engine TET values. This effect is shown in Figure 6-16.

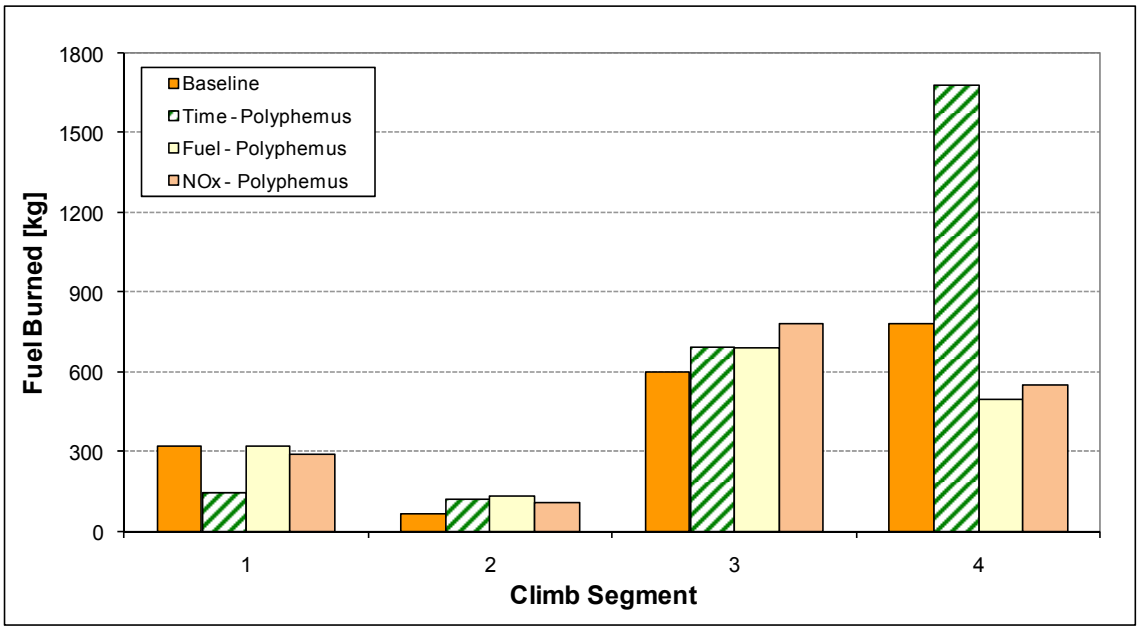


Figure 6-15. Case Study 1 – Fuel burned at each climb segment

Consequently, due to fact that one of the main factors determining the level of $NO_x$ emissions produced (besides the fuel burned) is TET, the trajectory optimised for minimum $NO_x$ emissions produces a significant reduction in the amount of $NO_x$ emitted (when compared to the baseline trajectory, Table 6-4). Interestingly, Figure 6-16 also shows that, in order to minimise $NO_x$ emissions, the optimiser proposes a trajectory in which the engine TET remains almost constant (~1,400-1,500K) for the entire climb

profile. It is relevant to note in this discussion that the level of $NO_x$ formed at temperatures near to and above 1,700-1,800K increases exponentially with temperature.

Figure 6-17 summarises (graphically) the main results obtained when computing the three optimum trajectories analysed above. One aspect to highlight in Figure 6-17 is the level of gaseous emissions, in terms of $NO_x$, $CO_2$, and $H_2O$, of the optimum trajectories relative to the reference climb trajectory. As expected, the variations in $CO_2$ and $H_2O$ are directly proportional to the variations in the amount of fuel burned (species in chemical equilibrium). However, as observed in Figure 6-17, the aircraft trajectory optimised for flight time significantly increases the amount of $NO_x$ emissions. One of the main factors responsible for this significant increase in $NO_x$, besides the increase in fuel burn, is the increase in TET (Figure 6-16) resulting from the higher thrust settings. Another interesting observation in Figure 6-17 is the increase in total flight time obtained for the trajectory optimised for minimum $NO_x$ emissions. Although this parameter increases, the total fuel burned slightly decreases as a consequence of the lower thrust settings (i.e., lower engine fuel flow relative to the baseline trajectory). Additional details about the results analysed in this first case study can be found in references [124,125].

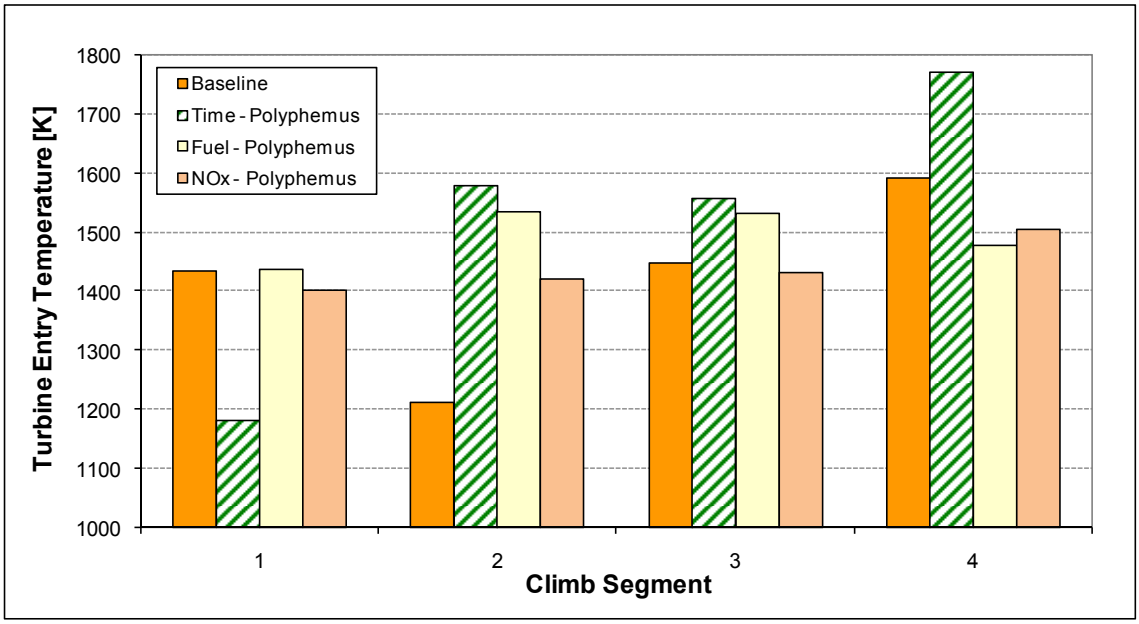


Figure 6-16. Case Study 1 – TET at each climb segment

To finalise this first case study it is important to highlight that in the other trajectory optimisation processes carried out in this work, whose main results are

summarised in the cases studies described in the following sections, complexities (in terms of operational constraints, number of segments, number of trajectory flight phases, etc.) were included gradually. This gradual addition of complexities to the case studies analysed afforded again greater visibility of the mathematical performance of Polyphemus when assessing results. This would have proved more difficult if the analysis had been initiated with very complex trajectories. Accordingly, several trajectory optimisation processes were performed, and their main results are summarised in the following case studies.

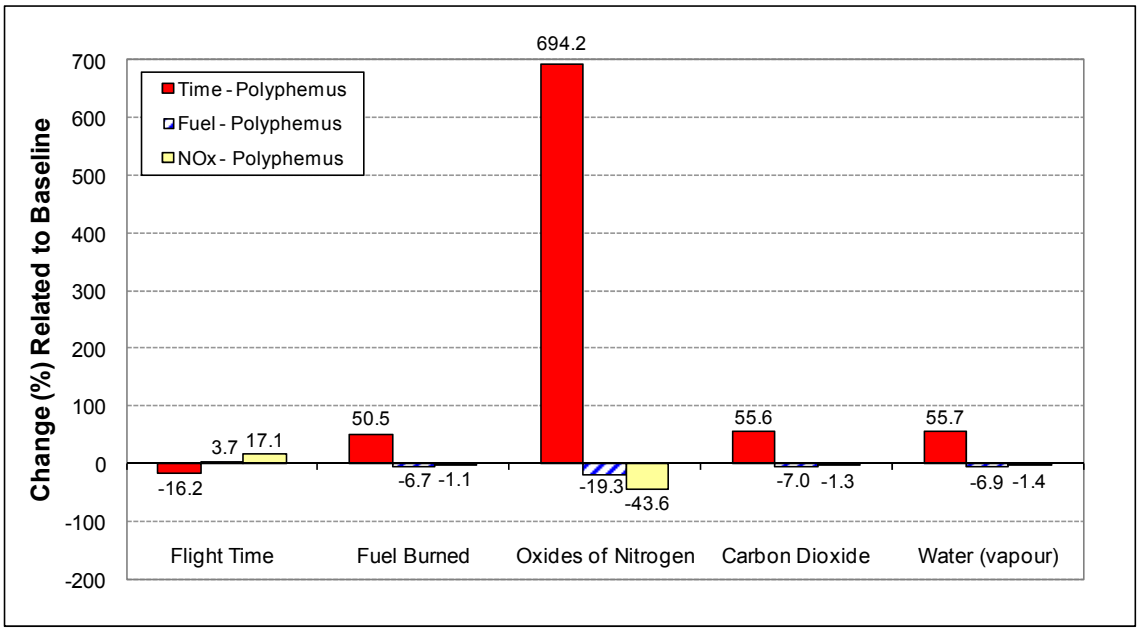


Figure 6-17. Case Study 1 – Optimum trajectories results (relative to baseline)

## 6.2.3 Case Study 2: Climb Profile with Speed Continuity Optimisation

### 6.2.3.1 General Description

As highlighted before, in the first case study the flight Mach number was kept constant along each climb segment, which, of course, resulted in step Mach number changes between segments. However, these step changes in Mach number yield discontinuities in the aircraft speed. Therefore, for this second case study, step changes in the aircraft speed were avoided by specifying speeds at the beginning and end of each climb segment. Consequently, continuity in the aircraft speed was guaranteed. In addition, some operational ATC constraints were also considered. All the modifications

introduced in this case enabled to represent more realistically climb profiles described by commercial aircraft.

In terms of number of segments, segment lengths, and initial and final climb altitudes, the climb profile optimised in this second case study is identical to the one used in the first case study, whose generic representation is illustrated in Figure 6-11. As in the first case, ISA conditions were assumed and the FPA was limited to values between 0 and 7.5deg. During the optimisation processes, only the initial aircraft speed (EAS) in segment 1 and the initial altitude in segment 3 were varied in such a way so as to minimise the total flight time, fuel burned, and $NO_x$ emissions produced. The arbitrary climb profile used as the reference trajectory in this second case study can be described as follows:

- 1st segment: Climb at constant EAS, 250kts EAS or 128.6m/s, from 1,500ft (457m) up to 10,000 ft (3,048m)
- 2nd segment: Acceleration at 10,000ft (level flight) to 320kt EAS (164.6m/s)
- 3rd segment: Climb at constant EAS (320kts) up to 25,341ft (7,724m), where (cruise) Mach number is equal to 0.8
- 4th segment: Climb at constant M (0.80) up to 35,000ft (10,668m)

Table 6-5 defines, in terms of altitude (h), aircraft speed (M or EAS), and ground range (R) covered, the start and end points of the four segments of the climb profile used as the baseline trajectory. In this table it is interesting to note the way in which the aircraft speeds are defined, i.e., different trajectory segments have (when required) different speed regimes (segments 1 and 3 are flown at constant EAS, segment 2 at variable EAS, and segment 4 at constant M). This is a typical example of the flexibility in the definition of the trajectory optimisation problem as discussed in the beginning of this chapter. Due to the direct relationship between Mach number and EAS (Eq. (6-12)), for a given M the EAS is only a function of altitude. Then, defining M and EAS in the start of segment 4 (or at the end of segment 3) as being equal to 0.8 and 320kts (164.6m/s), respectively, the corresponding altitude was determined (7,724m in this particular case). This altitude (also shown in Table 6-5) was kept constant during the optimisation processes.

The design variables utilised in this second case study are also indicated in Table 6-5 for completeness. The lower and upper bounds of the range of permissible values of

the initial EAS in segment 1 correspond to, respectively, the aircraft stall speed (89.0m/s EAS for the particular aircraft being simulated), and the maximum EAS permissible below 10,000ft (according to ATC restrictions), i.e., 250kts EAS or 128.6m/s. In turn, the range of values in which the initial altitude in segment 3 can be varied when optimising the trajectories was established in such a way to avoid the aircraft losing altitude during the climb process.

Table 6-5. Case Study 2 – Baseline trajectory and design variables

| Seg. No. | $h_i$ [m] | $h_f$ [m] | $M_i$ [--] | $M_f$ [--] | $EAS_i$ [m/s] | $EAS_f$ [m/s] | R [km] | Design Variables |
|---|---|---|---|---|---|---|---|---|
| 1 | 457 | 3048 | -- | -- | 128.6 | 128.6 | 20 | $89.0 \leq EAS_i \leq 128.6$ |
| 2 | 3048 | 3048 | -- | -- | 128.6 | 164.6 | 10 | -- |
| 3 | 3048 | 7724 | -- | -- | 164.6 | 164.6 | 60 | $3048 \leq h_i \leq 7724$ |
| 4 | 7724 | 10668 | 0.80 | 0.80 | -- | -- | 100 | -- |

The trajectories optimised in this case study essentially followed the climb schedule described previously for the baseline trajectory. However, in the optimisation process the initial EAS (and consequently the final one) in segment 1 and the initial altitude in segment 3 were varied within the ranges of their permissible values indicated in Table 6-5, in such a way so as to determine optimum trajectories which minimise the total flight time, fuel burned, and $NO_x$ emissions produced. The following section summarises the main results obtained.

#### 6.2.3.2 Results

Similarly to the first case study, the numerical performance of Polyphemus was also analysed in this case through comparisons of the results obtained using this optimiser with those obtained using the MADS algorithm [94]. The climb profile utilised as baseline in this case study as well as the optimum trajectories computed using Polyphemus and the commercial optimiser [94] are shown in Figure 6-18. Figure 6-19 illustrates, in turn, a magnification of the second and third segments shown in Figure 6-18, which allows a clearer visualisation of the nature of the optimum trajectories determined.

As can be observed in Figure 6-19, both Polyphemus and MADS [94] yielded again very similar results (average discrepancies less than 3%). Table 6-6 summarises

these results in quantitative terms. From this table it is possible to see that all optimum trajectories computed originated reductions in the total climb time (~ -2.2%), fuel burned (~ -0.3%), and the level of gaseous emissions produced, in terms of $NO_x$ emissions (~ -3.5%).

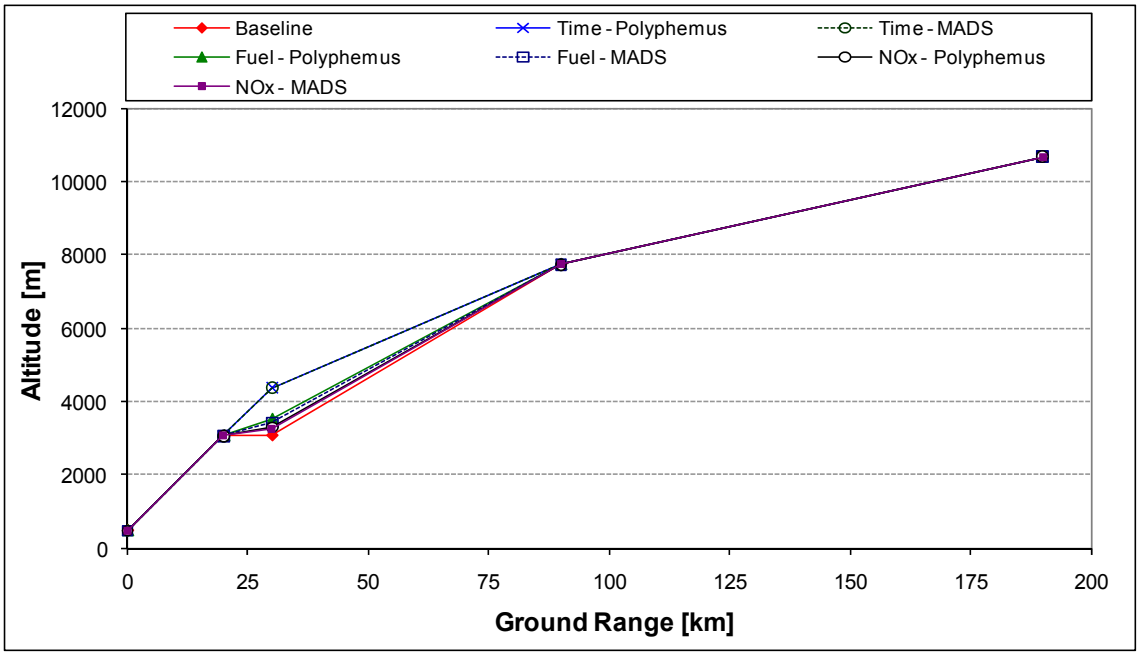


Figure 6-18. Case Study 2 – Comparison of optimisation algorithms

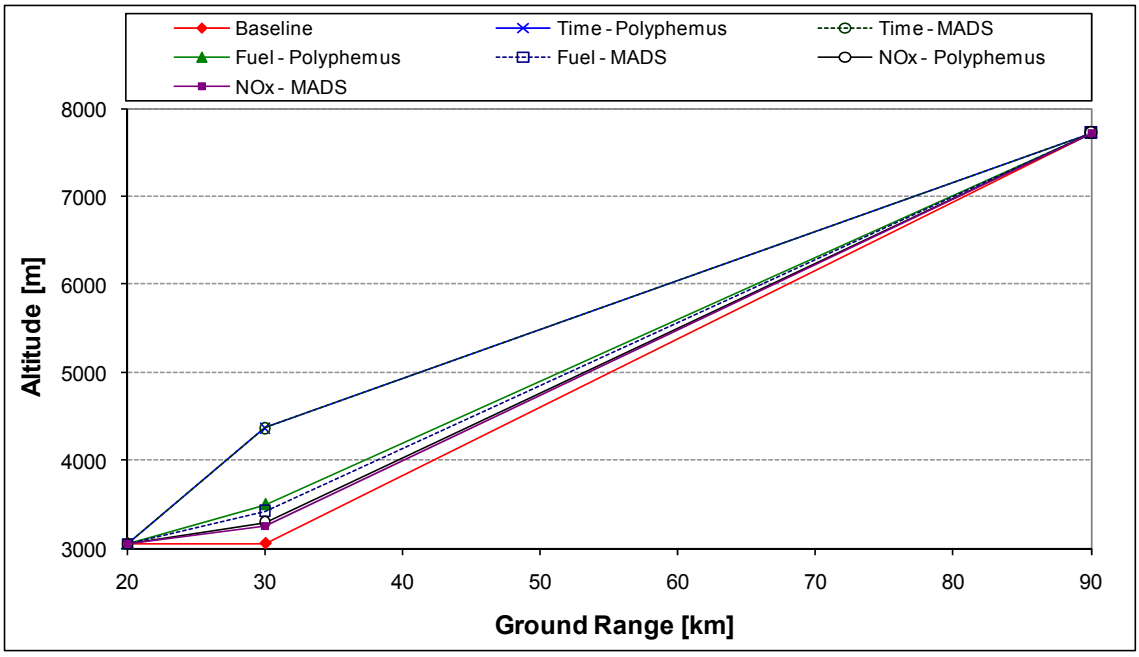


Figure 6-19. Case Study 2 – Comparison of optimisation algorithms magnified

In order to have a clear view of the results obtained using Polyphemus, Figure 6-20 shows the detail of segments 2 and 3 of the reference climb profile used in this case study as well as of the optimum trajectories computed with this optimiser. Interestingly, in Figure 6-20 it is possible to see that in order to minimise the total flight time Polyphemus suggests that the aircraft should fly segments 2 and 3 at higher altitudes than the baseline trajectory. At first sight, it would appear contradictory to what it is expected according to the results obtained in the first case study. This and other aspects will be further analysed next.

Table 6-6. Case Study 2 – Optimisation algorithms results (relative to baseline)

| Objective Function/ Optimiser | Flight Time [%] | Fuel Burned [%] | $NO_x$ Emitted [%] |
|---|---|---|---|
| Time – Polyphemus | -2.2 | 0.8 | 40.0 |
| Time – MADS [94] | -2.2 | 0.8 | 40.2 |
| Fuel – Polyphemus | -0.8 | -0.3 | -1.0 |
| Fuel – MADS [94] | -0.6 | -0.3 | -1.3 |
| $NO_x$ – Polyphemus | 6.2 | 3.7 | -3.6 |
| $NO_x$ – MADS [94] | 6.2 | 3.6 | -3.5 |

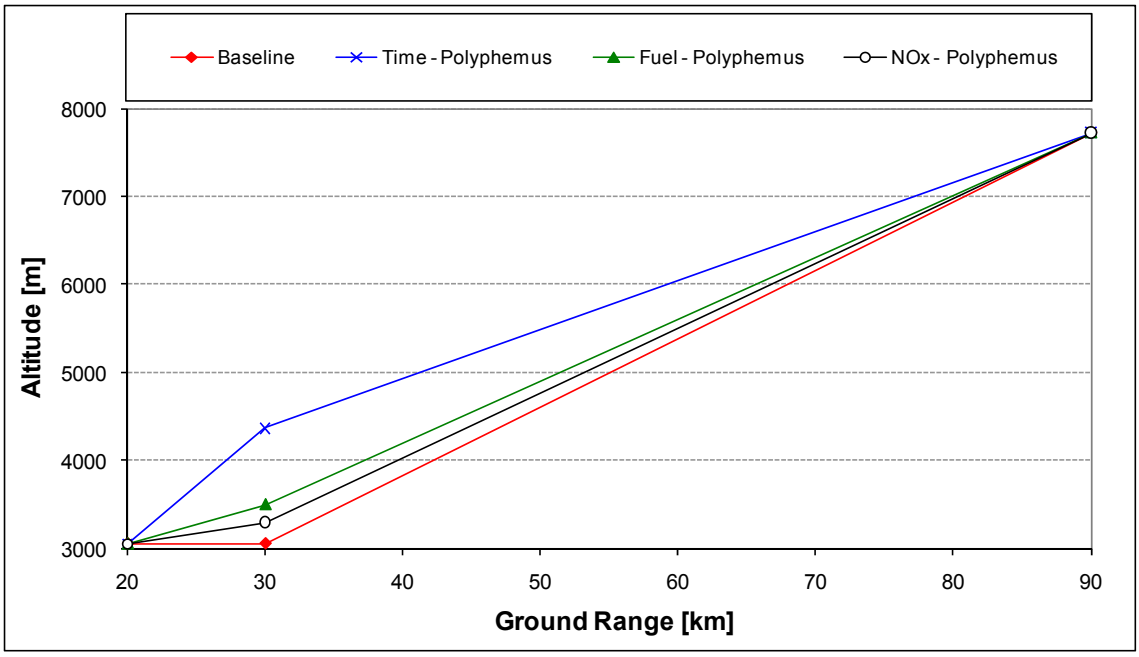


Figure 6-20. Case Study 2 – Baseline vs. Optimum trajectories (magnified)

As implied before, minimisation of flight time means maximisation of TAS, as it also can be verified in Figure 6-21. Thus in order to minimise the time spent during climb, in this case Polyphemus suggests a solution where the aircraft flies the first

segment at the highest EAS permissible (Figure 6-22), which was fixed at 128.6m/s; and starts the third segment at the highest altitude permissible (4,365m), which corresponds to the highest FPA permissible (7.5deg). This is conceptually correct because (i) in the first segment, for a given altitude, TAS increases with the increase in EAS (Eq. (6-10)); and (ii) in the beginning of third segment, for a given EAS, TAS increases as altitude increases (Figure 6-5). For completeness, Figure 6-23 shows the flight Mach number variation along the whole climb profile. As can be confirmed from this figure, Mach number step changes are not present anymore in this second case study.

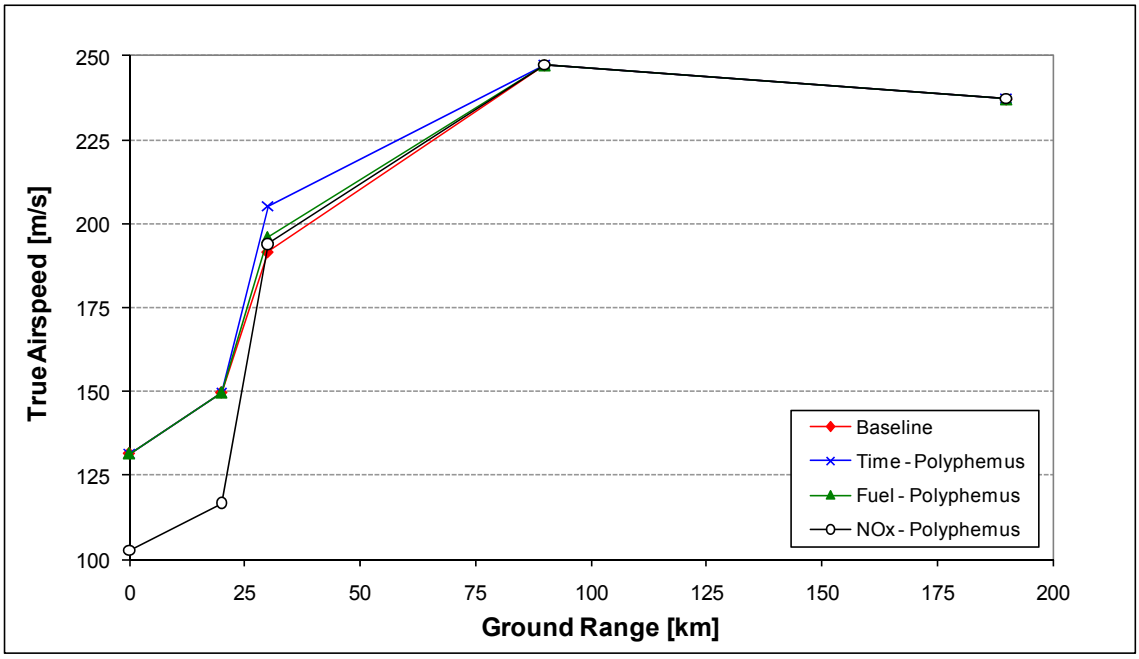


Figure 6-21. Case Study 2 – True airspeed (TAS)

Figure 6-20 and Figure 6-21 show that, in order to reduce fuel burned, the optimiser suggests a solution where the aircraft flies faster and higher than the reference trajectory (segments 2 and 3). In particular, as illustrated in Figure 6-22, it suggests flying the first segment at the highest EAS permissible (fixed at 128.6m/s). It is clear that in order to minimise the total amount of fuel burned, the total energy required by an aircraft to describe a given flight profile must be minimised. Thus, in the particular situation being analysed, the total energy required to climb must be minimised as well.

The total energy required by an aircraft to make a given manoeuvre (i.e., to fly a given flight profile) from the initial to final state is the sum of the aircraft energy change

($\Delta E_{ac}$) required plus the path dependent energy ($E_{path}$) required to impart that change, as follows:

$$E_{req} = \Delta E_{ac} + E_{path} \tag{6-14}$$

In the particular case in which the aircraft energy end states (initial and final kinetic and potential energies) is constrained, neglecting for a moment the aircraft mass changes, the total aircraft kinematic energy change ($\Delta E_{ac}$) is fixed. For example, a climb from 10,000ft to 25,000ft with initial and final speeds 250kts and 300kts, respectively, requires a fixed kinematic energy change. The climb is performed however against dissipative forces, such as aerodynamic drag, which have a path-dependence when determining the energy dissipated. An aircraft climbing over a long path length at high drag dissipates more energy than another one flying a shorter path at lower drag. In this example, the minimisation of the path dependent energy is then responsible for the minimisation of the total energy required by the aircraft to fly the referred climb profile.

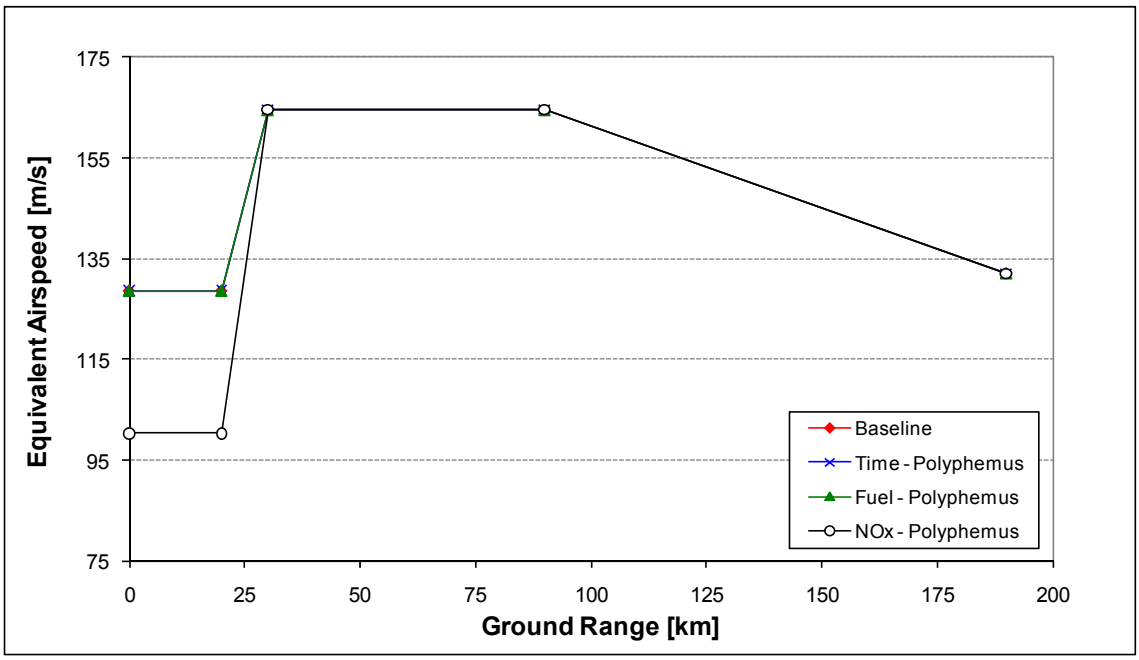


Figure 6-22. Case Study 2 – Equivalent airspeed (EAS)

According to Eq. (6-14), the total energy required ($\Delta E_{req}$) is minimised when both $\Delta E_{ac}$ and $E_{path}$ are minimised. Assuming that $\Delta E_{ac}$ and $E_{path}$ are independent, i.e., that the path taken is independent of the initial and final states, $\Delta E_{req}$ is minimised when $\Delta E_{ac}$ is minimised as well. Therefore, in the climb example mentioned above, if the

initial speed constraint is eliminated, $\Delta E_{ac}$ is minimised when the initial kinetic energy is maximised. This particular situation has a close relationship with the flight profile optimised in this second case study, i.e., the initial and final altitudes of the climb profile and the final aircraft speed are fixed. Consequently, in order to minimise the total energy required to climb, the initial kinetic energy needs to be maximised. It implies in turn the maximisation of the initial aircraft speed, i.e., TAS. This TAS maximisation leads to a situation in which the aircraft flies the first segment at the highest EAS permissible as observed in Figure 6-22.

According to the analysis carried out above, for the specific climb profile optimised in this case study, one would therefore expect the minimum fuel burn to occur when the aircraft begins the climb at the highest permissible speed and climbs with minimum drag along the shortest path. This is not realistic however, as these flight conditions (altitude and speed) will generally not correspond to those conditions leading to the minimisation of the total energy required to climb (minimum drag path, minimum SFC engine operating point, etc.). A trade-off must therefore be established at some stage. The fuel optimised trajectory computed in this case study is a typical example of the referred trade-off. Figure 6-24 illustrates then the fuel burned associated with the baseline trajectory as well as the three optimum trajectories computed in this case study.

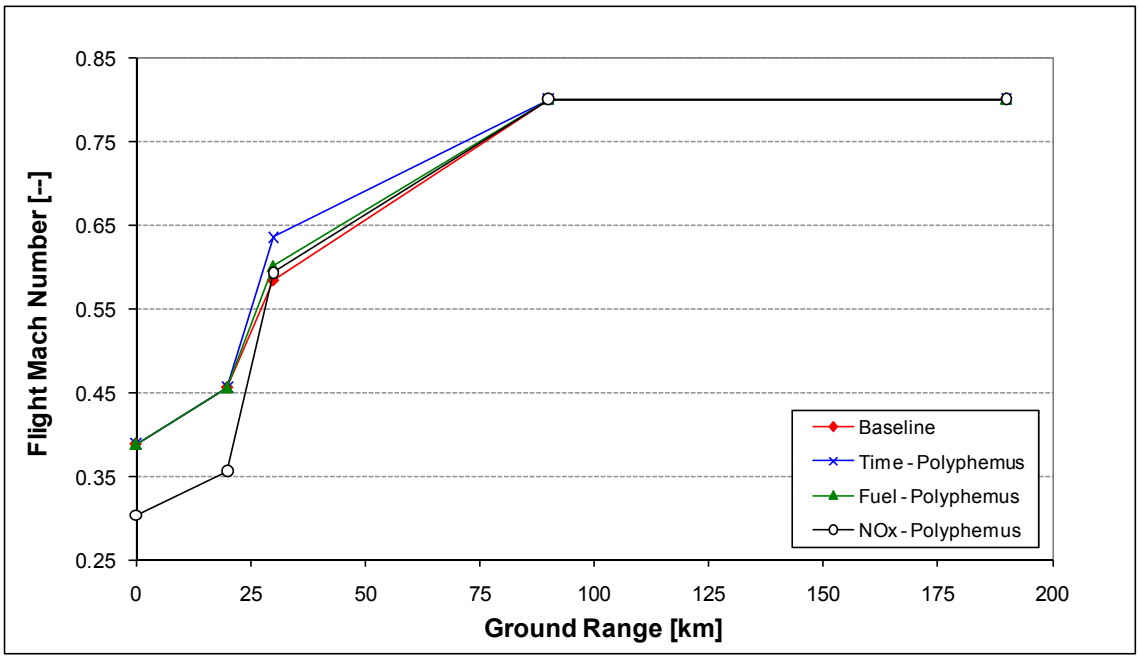


Figure 6-23. Case Study 2 – Flight Mach number

The original assumption was that the aircraft mass (including fuel on-board) remains constant throughout each segment, and therefore the whole climb profile. This has a direct impact upon the aircraft drag, thrust required and the total kinematic energy. In reality, as the aircraft climbs and fuel is burned, the mass reduces. The effect of assuming a constant mass is to over-estimate the drag, thrust required and total energy as the time variable evolves. One of the main factors driving the minimisation of the fuel burned during a given flight profile is the aircraft mass changes. Therefore, by accounting for the change in aircraft mass as a function of fuel burn a more accurate model of the climb may be established.

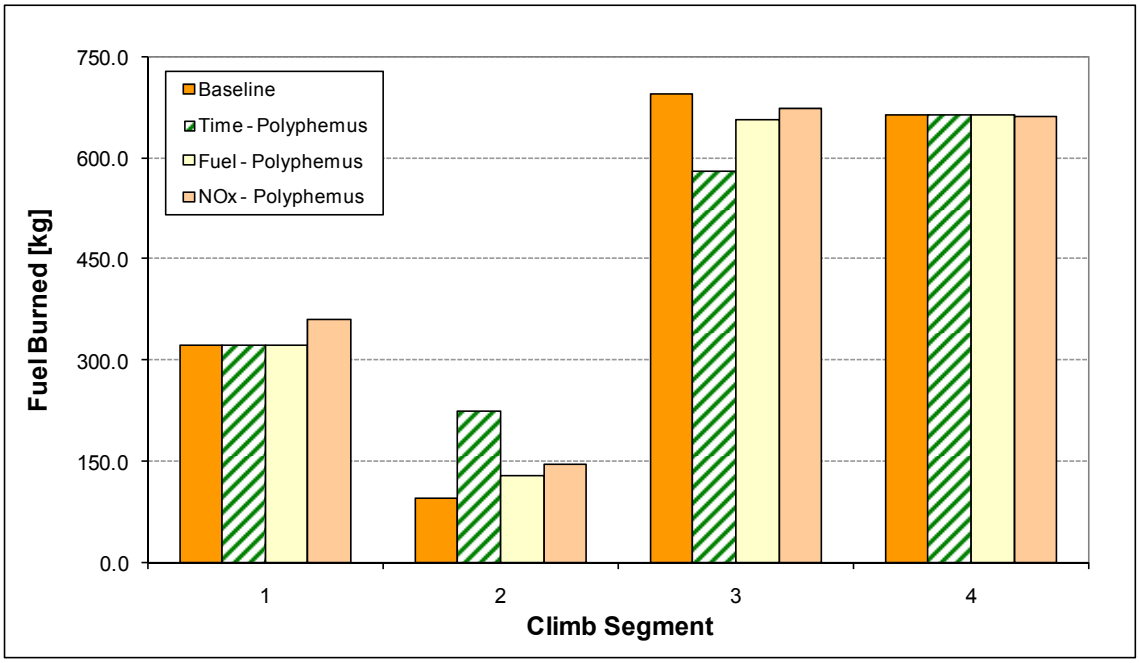


Figure 6-24. Case Study 2 – Fuel burned at each climb segment

As can be observed in Figure 6-20 and Figure 6-21, the trajectory optimised for minimum $NO_x$ emissions is flown higher and mostly slower than the baseline trajectory. Once again, when minimising the $NO_x$ emissions produced the main driver is the engine thrust setting. As highlighted before, in general lower speeds mean lower engine thrust settings, which are in turn translated in lower engine TET values, Figure 6-25. Similar to the first case study, Figure 6-25 also shows that in order to minimise $NO_x$ emissions the aircraft describes a trajectory in such a way that the engine TET remains almost constant (~ 1,400-1,500K) along the whole climb profile. Thus, as a rule of thumb it is possible to say that $NO_x$ emissions optimised trajectories utilise relatively low and

almost constant engine TET values, as a result of the relatively low engine thrust settings used to fly a given trajectory. These low thrust settings are usually obtained by reducing the aircraft speed which result in increases in the total flight time. Even though the increase in the flight time has a direct influence on the total amount of fuel burned and, consequently, on the level of gaseous emissions produced, during the optimisation process there is a tendency to reduce the aircraft speed because the fuel burned is a secondary factor when computing $NO_x$ emissions. In other words, when determining $NO_x$ emissions optimised trajectories is more important to reduce TET than fuel burned. Consequently, as illustrated in Figure 6-17 and Figure 6-26, respectively, trajectories optimised for minimum $NO_x$ emissions can decrease or increase the total fuel burned along a given trajectory.

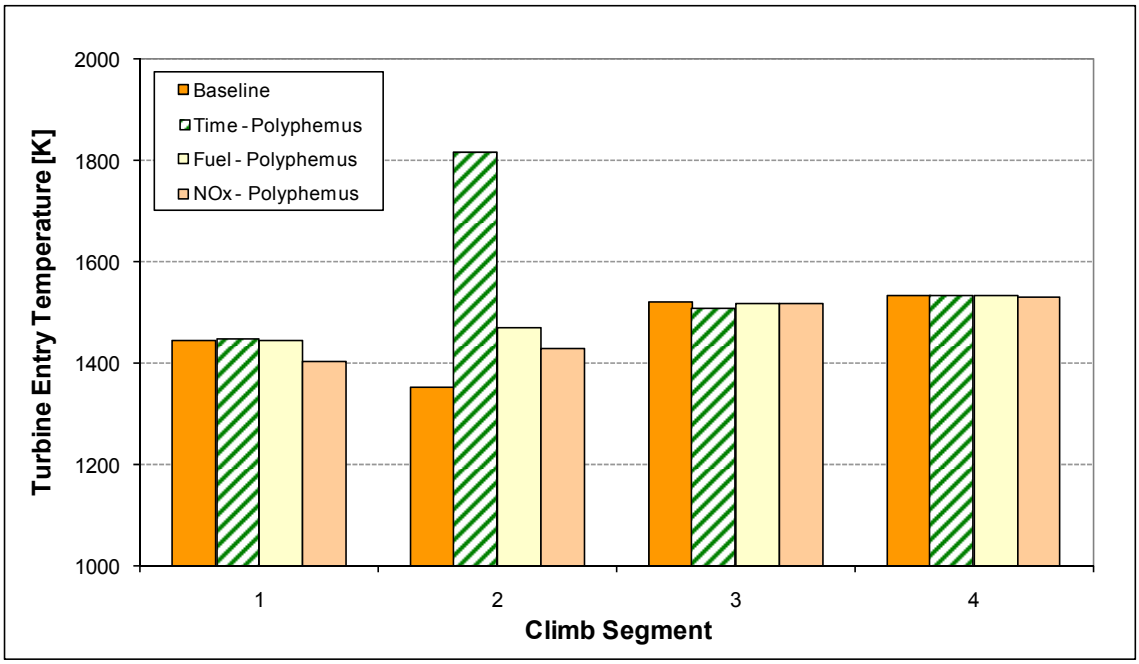


Figure 6-25. Case Study 2 – TET at each climb segment

Finally, Figure 6-26 summarises the main results obtained when computing the three optimum trajectories analysed in this case study. As expected, in this figure one can see that the variations in $CO_2$ and $H_2O$ are directly proportional to the variations in the amount of fuel burned (species in chemical equilibrium). In Figure 6-26 it is also possible to see the increase in flight time as well as in fuel burned associated with the trajectory optimised for minimum $NO_x$ emissions. Another interesting aspect to highlight in this figure relates to the fact that the aircraft trajectory optimised for

minimum flight time significantly increases the amount of $NO_x$ emissions. This result is directly related to the large amount of thrust being required to fly the second climb segment, where the aircraft climb and accelerates at the same time. Of course, this large requirement in engine thrust translated into high TET values (Figure 6-25), and, consequently, into significant increases in the level of $NO_x$ emissions produced (Figure 6-26).

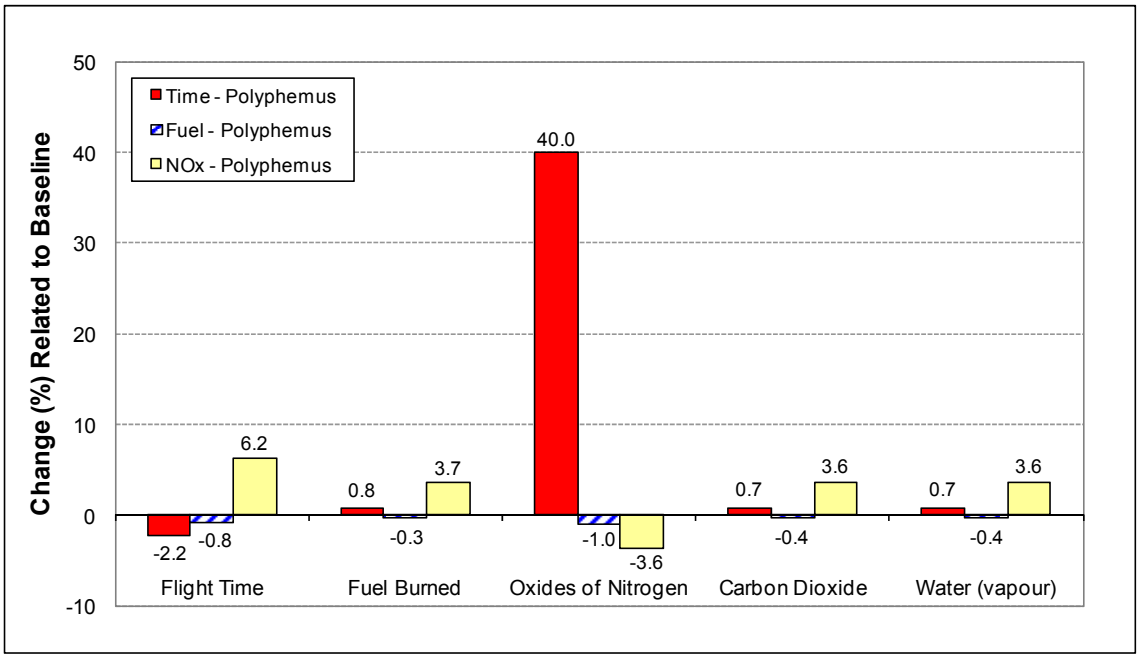


Figure 6-26. Case Study 2 – Optimum trajectories results (relative to baseline)

## 6.2.4 Case Study 3: Implicitly Constrained Climb Profile Optimisation

### 6.2.4.1 General Description

In Chapter 5 it was indicated that for engineering optimisation problems, essentially, two types of constraints can be encountered, explicit constraints and implicit constraints. The former are constraints imposed on the problem input parameters, and the latter are constraints imposed on the problem performance parameters – implicit constraints require in general the evaluation of the mathematical model representing the optimisation problem (or the evaluation of the chromosome in a GAs-based optimisation) in order to determine the value of the parameters they constrain. A complete optimisation problem includes both explicit and implicit constraints. For the

two past case studies, only explicit constraints were utilised through restrictions explicitly imposed on the design variables (input parameters). However, real engineering optimisation problems always include implicit constraints. Therefore, in this third case study constraints of this type have been included.

The climb profile optimised in this third case study, including its baseline, is exactly the same as in the second case study (see Table 6-7). However, this time two new design variables and an implicit constraint were added, and optimum trajectories (which minimise total flight time, fuel burned, and $NO_x$ emissions produced) were determined. All design variables utilised in this third case study are indicated in Table 6-5. As observed in this table, two of them, the initial EAS in segment 1 and the initial altitude in segment 3, are the same as in the previous case study. However, the upper limit of the range of permissible values of the initial altitude in segment 3 was reduced to 4,400m (which corresponds approximately to the highest FPA permissible, 7.5deg) to decrease the computational time involved when computing the optimum trajectories.

The other two design variables used in this third case study related to the final EAS in segment 2 and initial altitude in segment 4 (Table 6-7). In other words, during the optimisation, after flying the first trajectory segment the aircraft was allowed to accelerate to a given EAS (segment 2), to climb at constant EAS (using the previous segment final EAS) up to an altitude where (cruise) Mach number is about 0.8 (segment 3), and finally to climb at constant M from this altitude to 35,000ft (segment 4). The lower and upper bounds of the range of permissible values of the final EAS in segment 2 corresponded to the equivalent airspeeds that yield Mach numbers of about 0.8 at the lowest and highest permissible altitudes associated with the beginning of segment 4. In turn, the range of values in which the initial altitude in segment 4 can be varied when optimising the trajectories was established in such a way to avoid the aircraft losing altitude during the climb process.

Table 6-7. Case Study 3 – Baseline trajectory and design variables

| Seg. No. | $h_i$ [m] | $h_f$ [m] | $M_i$ [--] | $M_f$ [--] | $EAS_i$ [m/s] | $EAS_f$ [m/s] | R [km] | Design Variables |
|---|---|---|---|---|---|---|---|---|
| 1 | 457 | 3048 | -- | -- | 128.6 | 128.6 | 20 | $89.0 \leq EAS_i \leq 128.6$ |
| 2 | 3048 | 3048 | -- | -- | 128.6 | 164.6 | 10 | $133.8 \leq EAS_f \leq 221.2$ |
| 3 | 3048 | 7724 | -- | -- | 164.6 | 164.6 | 60 | $3048 \leq h_i \leq 4400$ |
| 4 | 7724 | 10668 | 0.80 | 0.80 | -- | -- | 100 | $3048 \leq h_i \leq 10668$ |

As mentioned before, in addition to these design variables, an implicit constraint was utilised in this case study. This implicit constraint was related to the flight Mach number in segment 4. Accordingly, the allowable range of this parameter was established as being ± 0.5% of its nominal value, 0.8 in this case. Obviously, it was not possible to use this parameter as an explicit constraint because Mach numbers were not used as design variables in this case study. There are different ways of handling implicit constraints as explained in Chapter 5. However, most of the constraint handling techniques currently utilised involve some sort of penalisation to the unfeasible solutions, which varies mainly according to level of violation of the constraints. In this way, the probability of generating solutions that do not respect the constraints of the problem is greatly reduced. Consequently, well designed optimisation algorithms in general produce only optimum solutions that fulfil the constraint requirements of the optimisation problem. The following section summarises the main results obtained as part of this third case study.

#### 6.2.4.2 Results

In a similar fashion to the first two case studies presented before, the numerical performance of Polyphemus is also analysed through comparisons of the results obtained using this optimiser and one of the other two commercially available optimisation algorithms (GAs [94]) utilised before. This commercial algorithm was selected because of the inability of the one used in the previous case study (MADS algorithm [94]) to optimise complex problems involving several design variables and implicit constraints. The climb profile taken as baseline in this case study as well as the optimum trajectories computed using Polyphemus and the commercial optimiser [94] are shown in Figure 6-27.

As can be observed in Figure 6-27 and quantitatively in Table 6-8, both Polyphemus and the GAs-based optimisation algorithm from the commercial package yielded similar results (average discrepancies ~ 3%). Even so, in terms of flight altitude, the third segment of the minimum flight time optimum trajectories present a discrepancy of about 800m (Figure 6-27). One of the sources of this discrepancy may be associated with the fact that the commercial optimiser was not fully converged when these results were taken. However, no attempts to identify the exact sources of this

discrepancy have been made. From Table 6-8 it is possible to see that the three optimum trajectories computed originated significant reductions in the total climb time (~ -11%), fuel burned (~ -5%), and level of $NO_x$ emitted (~ -12%). In order to highlight the results obtained using Polyphemus, Figure 6-28 illustrates the reference climb profile used in this case study and only the optimum trajectories computed with this optimiser.

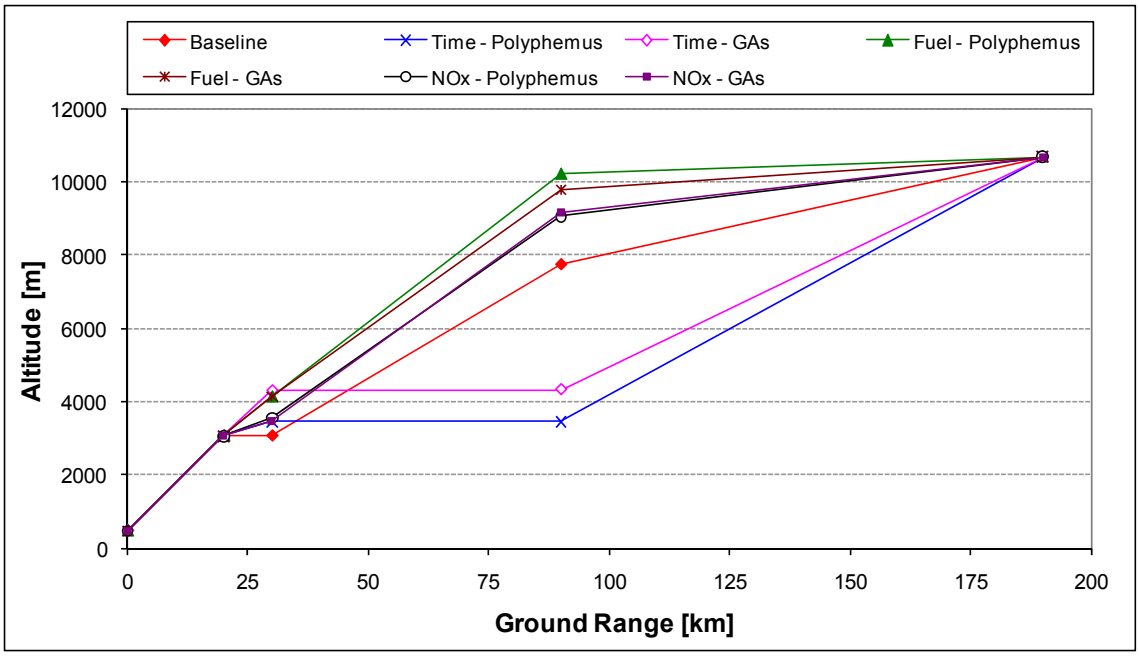


Figure 6-27. Case Study 3 – Comparison of optimisation algorithms

Table 6-8. Case Study 3 – Optimisation algorithms results (relative to baseline)

| Objective Function/ Optimiser | Flight Time [%] | Fuel Burned [%] | $NO_x$ Emitted [%] |
|---|---|---|---|
| Time – Polyphemus | -11.6 | 26.1 | 245.3 |
| Time – GAs [94] | -10.8 | 21.9 | 249.6 |
| Fuel – Polyphemus | 6.6 | -5.0 | 0.4 |
| Fuel – GAs [94] | 5.1 | -4.7 | -2.2 |
| $NO_x$ – Polyphemus | 9.6 | -0.3 | -12.8 |
| $NO_x$ – GAs [94] | 9.9 | -0.4 | -11.9 |

The results obtained in this third case study are similar to those obtained in the first case study analysed in this chapter. Thus, when minimising the time spent during climb, i.e., maximising TAS (Figure 6-29), Polyphemus suggests a solution where the aircraft flies the first segment at the highest EAS permissible (Figure 6-30), which was fixed at 128.6m/s. This is conceptually correct because in the first segment, due to the flight altitude is fixed, TAS increases with the increase in EAS (Eq. (6-10)). The

optimiser also suggests that the aircraft should accelerate in the second segment to the highest EAS permissible, fixed at 221.2m/s; and fly the following segments at low levels as long as possible before climbing rapidly to the target end altitude (Figure 6-28). This is again mathematically correct because, firstly, as previously indicated, once established the flight altitude the TAS increases with the increase in EAS; and, secondly, for a given Mach number the TAS increases with the decrease in altitude (speed of sound is the highest at sea levels – Figure 6-1). Clearly, the influence of the third and fourth segments on the total climb time is more important than that one associated with the second segment. Otherwise, the initial altitude in segment 3 would be the highest permissible. Obviously, this does not happen in this case as it can be observed in Figure 6-28. For completeness, Figure 6-31 shows the flight Mach number variation along the whole climb profile.

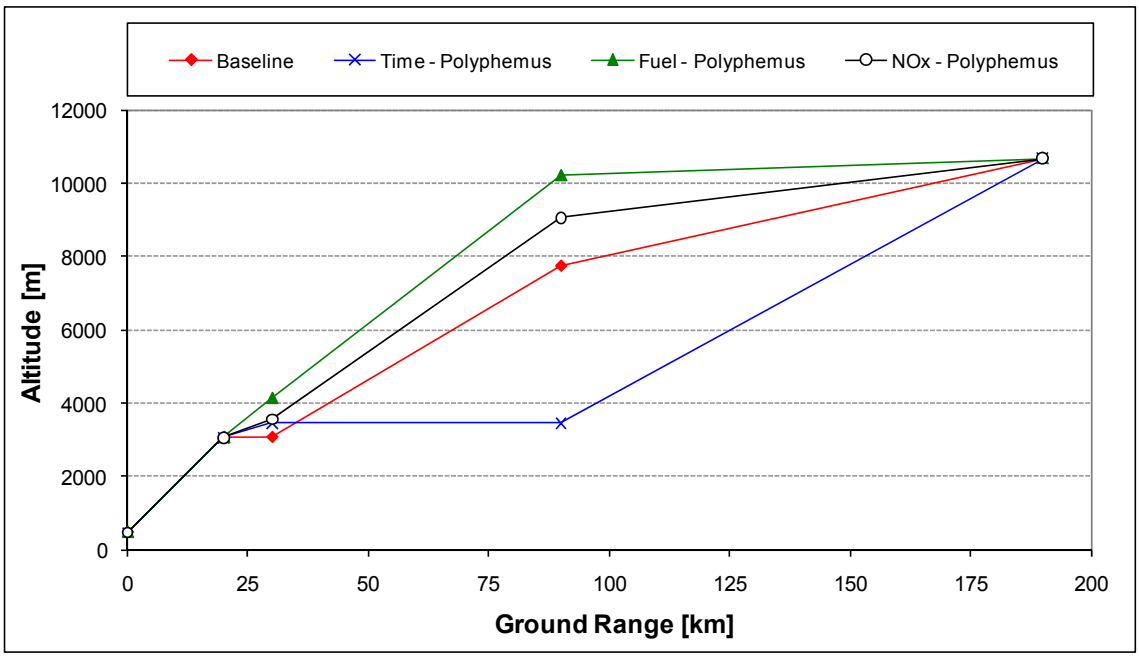


Figure 6-28. Case Study 3 – Baseline vs. Optimum trajectories

In general, Figure 6-28 and Figure 6-29 show that, in order to reduce the climb fuel burned, Polyphemus suggests flying mostly slower and higher than the reference trajectory. In particular, as illustrated in Figure 6-30, it suggests flying the first segment at the highest EAS permissible (fixed at 128.6m/s). This is exactly the same situation encountered in the second case study. Thus, in order to minimise the total energy required to climb, the total aircraft kinematic energy change needs to be minimised. Since the aircraft kinematic energy change is minimised when the initial kinetic energy

is maximised, it implies in turn the maximisation of the initial aircraft speed, i.e., TAS. This TAS maximisation leads to a situation in which the aircraft flies the first segment at the highest EAS permissible (Figure 6-30). Figure 6-32 illustrates the fuel burned associated with the baseline trajectory as well as the three optimum trajectories computed in this case study.

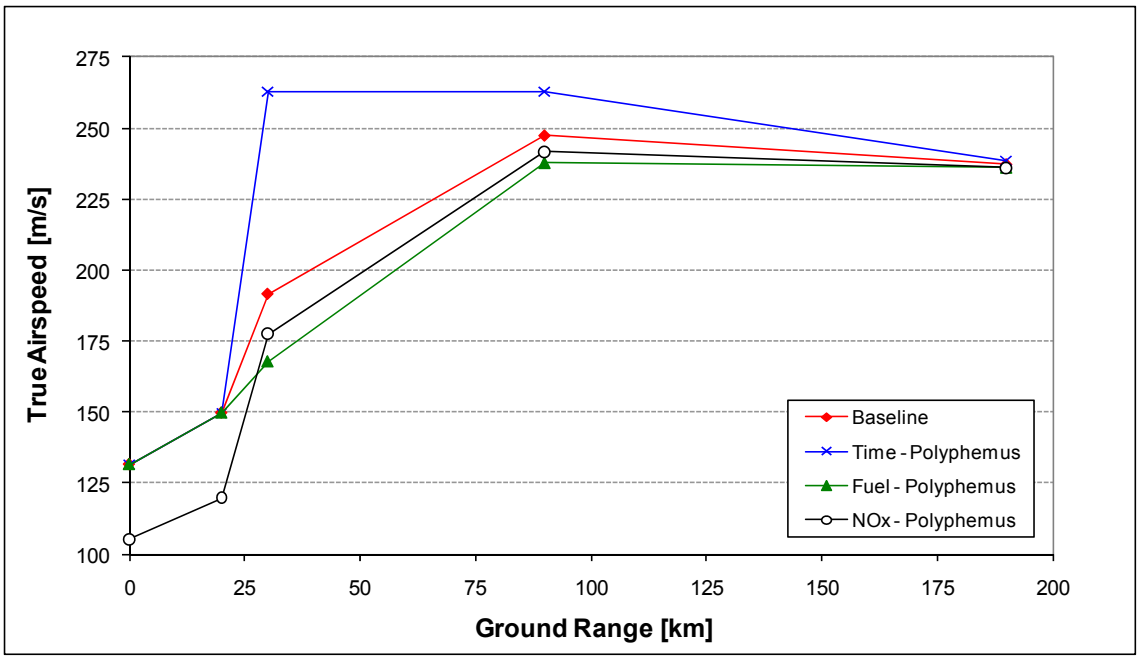


Figure 6-29. Case Study 3 – True airspeed (TAS)

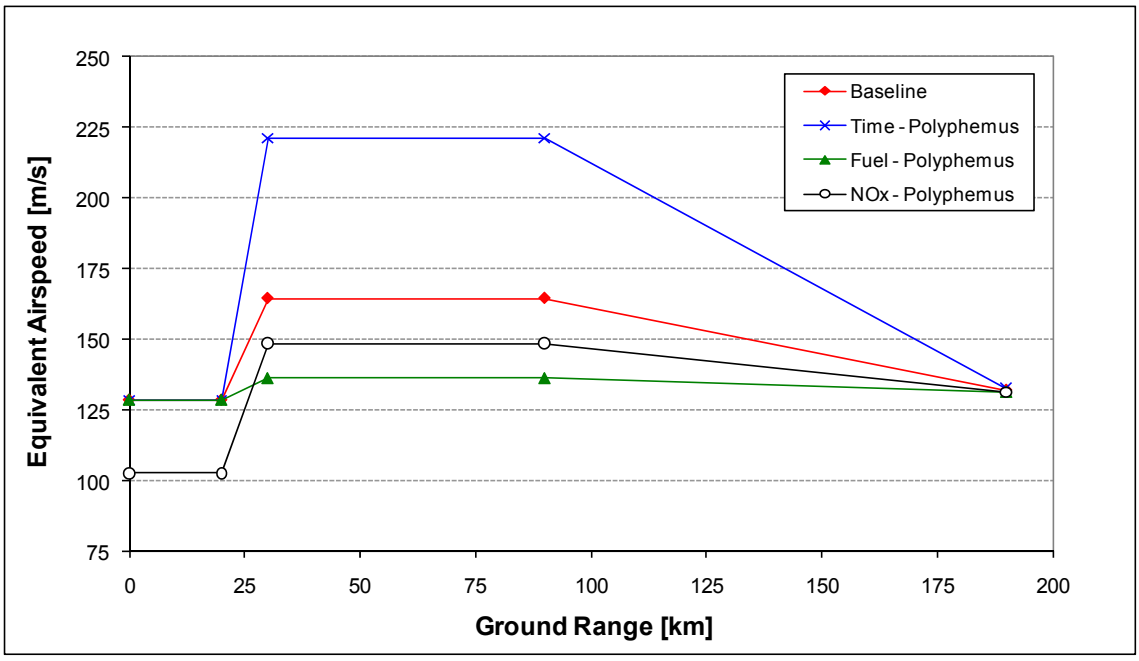


Figure 6-30. Case Study 3 – Equivalent airspeed (EAS)

As highlighted in the previous case study, one of the main factors driving the minimisation of the fuel burned during a given flight profile is the aircraft mass changes. There are different factors that affect the fuel burned and, consequently, the changes in the aircraft mass. The aircraft speed and the flight altitude constitute two of these main factors. Reducing the speed and increasing the altitude reduce drag and, consequently, the thrust required to fly a given segment. This lower thrust requirement translates into a lower engine thrust setting, and, consequently, a lower fuel burn. However, neither altitude nor speed can be increased or decreased arbitrarily. A speed reduction implies in general an increase in flight time, which can negatively affect the total fuel burned. In addition, in order to achieve quickly higher altitudes, higher engine thrusts, meaning higher thrust settings, will be also required. These higher thrust settings will require higher fuel flows, which negatively affect the fuel being burned during the process.

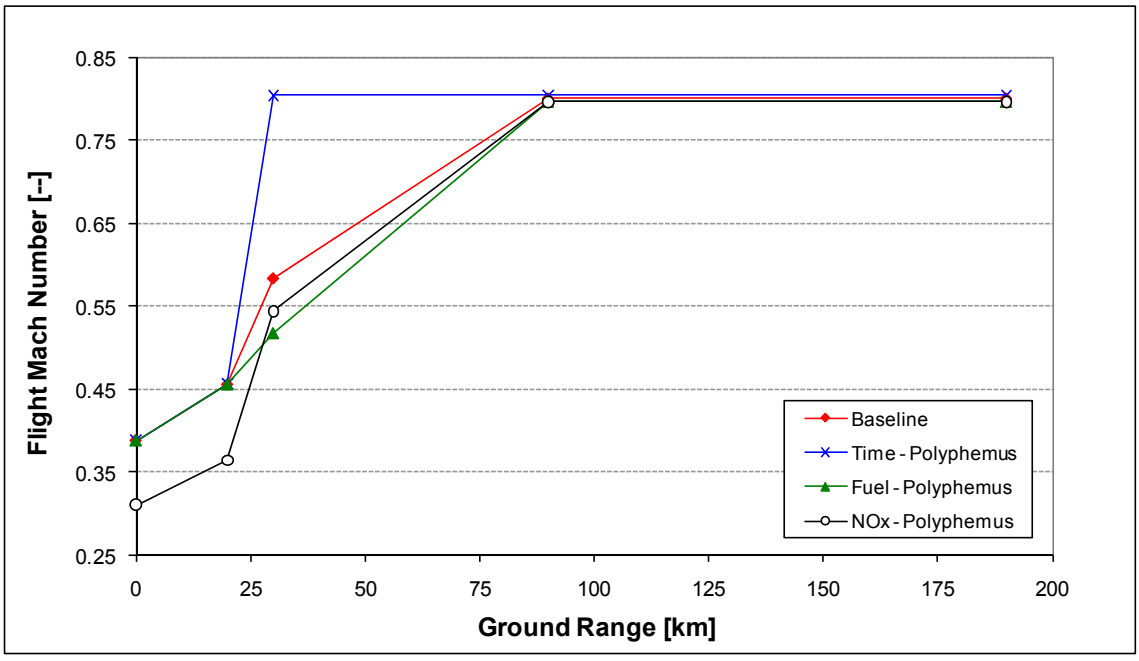


Figure 6-31. Case Study 3 – Flight Mach number

Therefore, a compromise between aircraft flight altitude and speed, which directly affect the changes in the aircraft mass, needs to be achieved at some stage. The fuel optimised trajectory computed in this case is a typical example of the referred compromise. It is interesting to note in Figure 6-32 that this fuel optimised trajectory proposes second and third segments affording a greater fuel burn (relative to the

baseline) in order to gain height which, then, is translated into a lower fuel burn in the last segment and an overall lower fuel burn for the whole climb profile. In Figure 6-30 it is possible to see that, as expected, the (third segment) EAS associated with the baseline trajectory is in between those equivalent airspeeds corresponding to the minimum flight time and fuel burned optimised trajectories. This is an expected result because commercial aircraft usually fly (segment 3) at this speed, which is determined mainly from the optimisation (minimisation) of the aircraft direct operating cost (DOC) that involves both fuel burn and flight time.

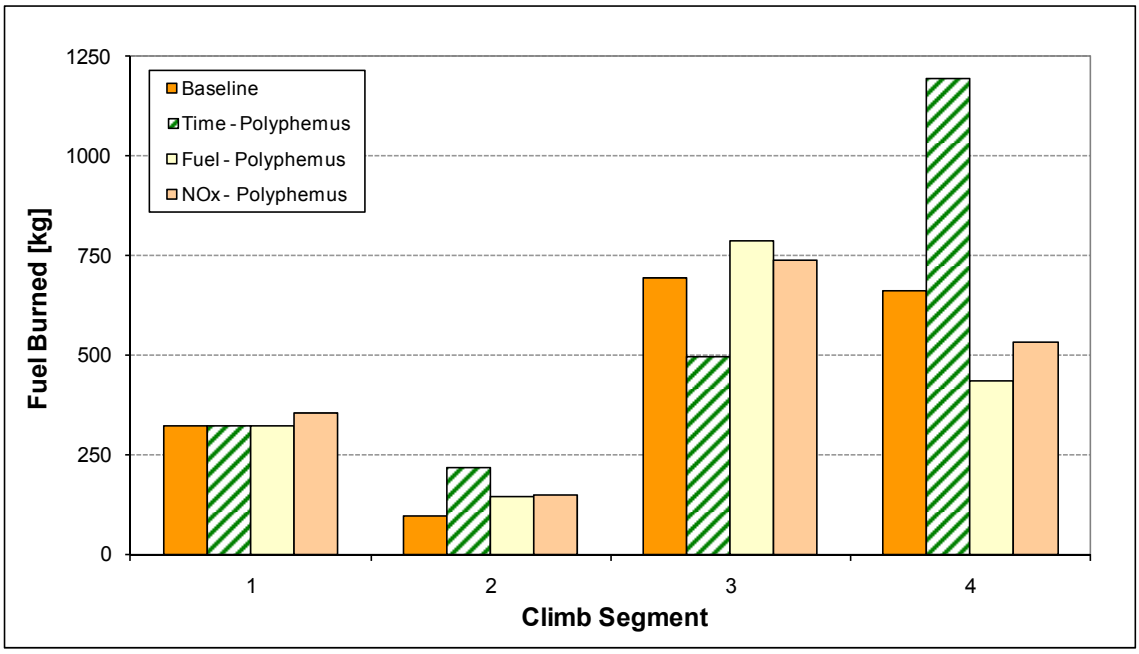


Figure 6-32. Case Study 3 – Fuel burned at each climb segment

Regarding the trajectory optimised for minimum $NO_x$ emissions, from Figure 6-28 and Figure 6-29 one can see that this trajectory is also flown mostly slower and higher than the baseline trajectory utilised. In principle, this trajectory looks very similar to the fuel optimised one. Thus, in general, this lower speed and higher altitude lead to reductions in the thrust required to fly the climb segments. These lower thrust requirements are in turn translated into lower engine TET values (Figure 6-33), which in turn result in reductions in the level of $NO_x$ emissions. Similar to the first two case studies analysed, Figure 6-33 also shows that in order to minimise $NO_x$ emissions the aircraft describes a trajectory in such a way that the engine TET remains almost constant (~ 1,400-1,500K) along the whole climb profile. This fact confirms the rule of thumb mentioned in the previous case study, in which it was indicated that $NO_x$

emissions optimised trajectories utilise relatively low and almost constant engine TET values, as a result of the relatively low engine thrust settings utilised.

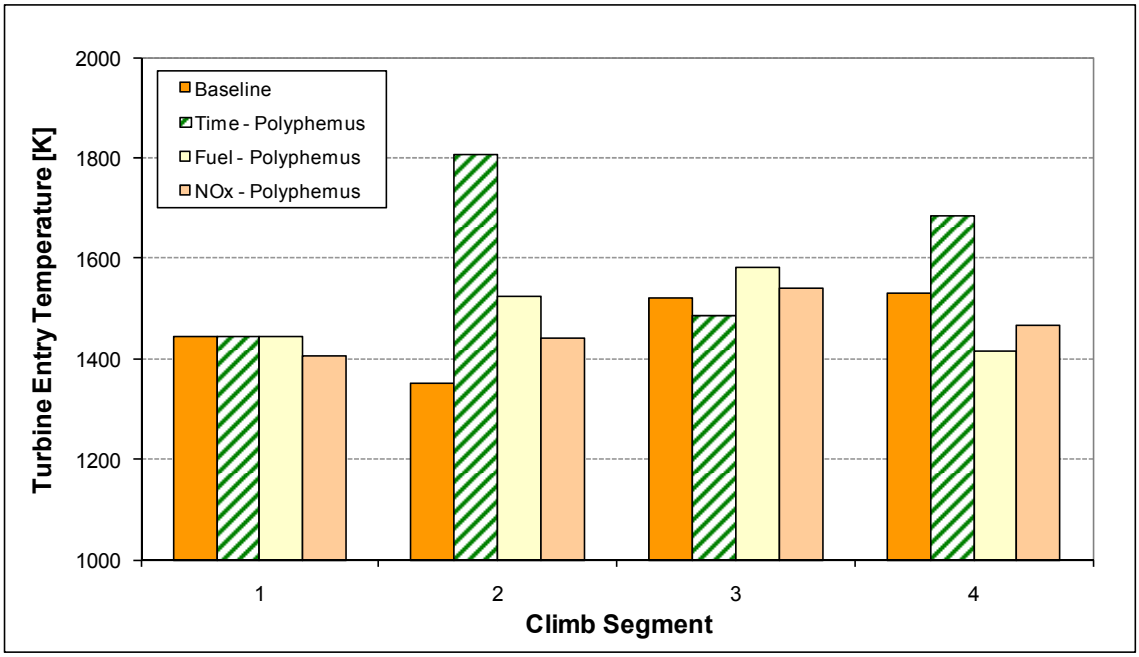


Figure 6-33. Case Study 3 – TET at each climb segment

Finally, Figure 6-34 summarises the main results obtained when computing the three optimum trajectories analysed in this third case study. As before, in this figure it is possible to see that the variations in $CO_2$ and $H_2O$ (species in chemical equilibrium) are directly proportional to the variations in the amount of fuel burned. Figure 6-34 also illustrates that even though the $NO_x$ emissions optimised trajectory increases total flight time the total amount of fuel burned is slightly reduced. As indicated before, this is a direct consequence of the lower engine thrust settings utilised. In Figure 6-34 it is also worth noticing that the aircraft trajectory optimised for minimum flight time significantly increases the amount of $NO_x$ emissions. This result is partially due to the large amount of thrust required to increase both the aircraft kinetic energy in segment 2 and the potential energy in segment 4. This higher requirement in engine thrust translated into higher TET values (Figure 6-33), and, consequently, into significant increases in the level of $NO_x$ emissions (Figure 6-34). To conclude it is important to highlight that the three case studies analysed until now provide the required basis for analysing more complex trajectories. Thus, the following cases studies will involve the optimisation of whole aircraft trajectories, and their results will enable a better

understanding of the capabilities of Polyphemus for carrying out aircraft trajectory optimisation processes.

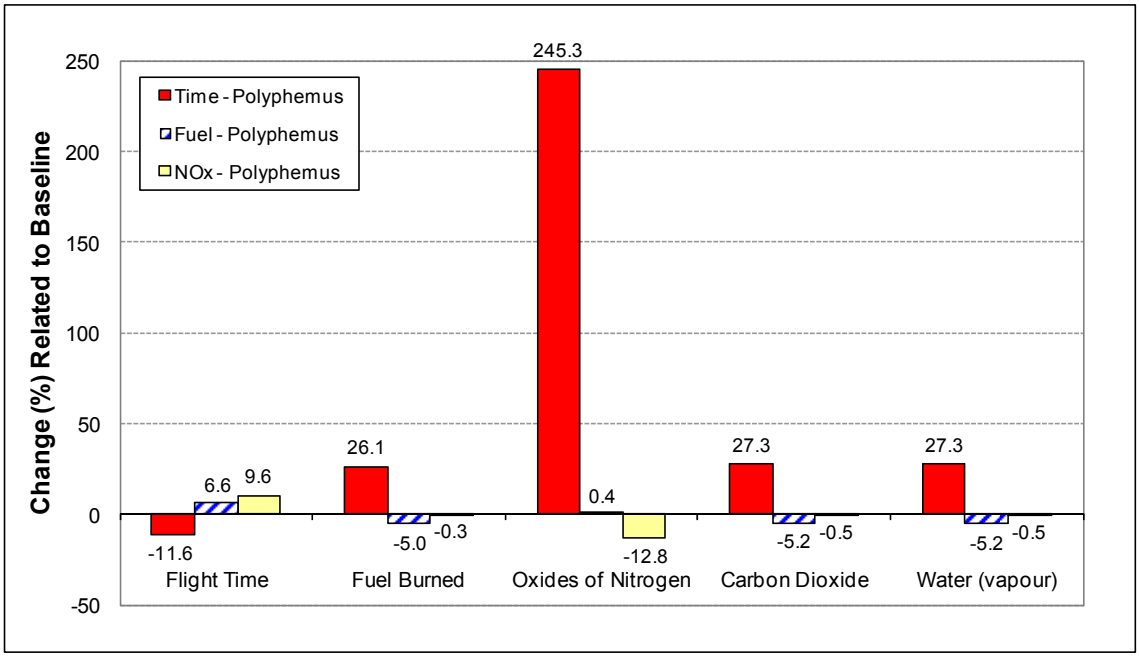


Figure 6-34. Case Study 3 – Optimum trajectories results (relative to baseline)

## 6.2.5 Case Study 4: Full Flight Profile Optimisation

### 6.2.5.1 General Description

After dealing with climb profiles involving complexities gradually introduced, the next step involved naturally the optimisation of whole aircraft trajectories. Thus, this fourth case study summarises the main results obtained from the optimisation of whole flight profiles. Similar to the previous case studies, in order to afford greater visibility on the characteristics of the performance of Polyphemus when assessing results, the whole flight profile was divided into only a small number of segments, and involved only three of the main flight phases encountered in aircraft trajectories: climb, cruise, and descent. Consequently, as schematically represented in Figure 6-35, in this fourth case study, the flight profile was divided into only eight segments. Climb: segments 1 to 3; cruise: segments 4 and 5; and descent: segments 6 to 8.

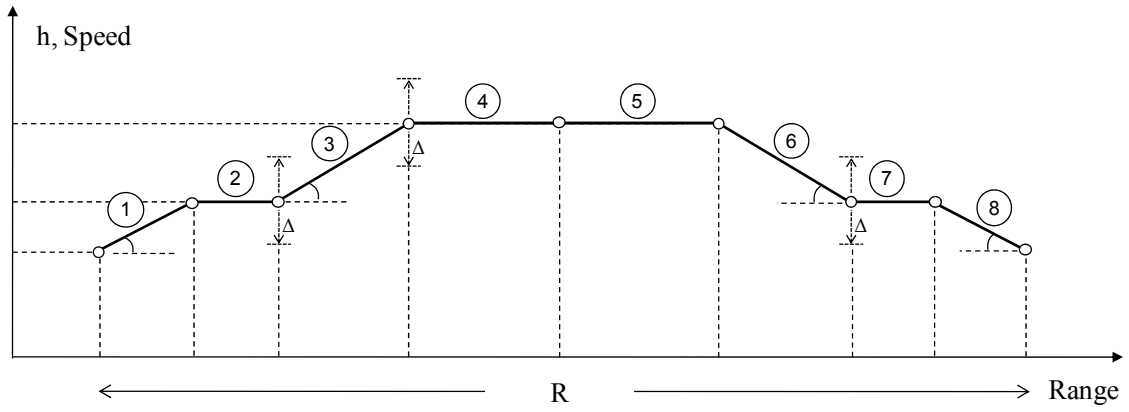


Figure 6-35. Schematic representation of full flight profile

As implied above, for the sake of clarity and simplicity, the aircraft trajectory flight phases involving take-off and approach/landing have been not included in the analyses carried out in this case study. In a similar fashion to previous analyses, ISA conditions were assumed and the FPA was limited to values between 0 and 7.5deg during climb and cruise, and -7.5 and 0deg during descent. Accordingly, optimum trajectories which minimise the total flight time, fuel burned, and $NO_x$ emissions produced were computed.

The arbitrary full flight profile used as the reference or baseline trajectory in this fourth case study can be described as follows:

- 1st segment: Climb at constant EAS, 250kts EAS or 128.6m/s, from 1,500ft (457m) up to 10,000 ft (3,048m)
- 2nd segment: Acceleration at 10,000ft (level flight) to 320kt EAS (164.6m/s)
- 3rd segment: Climb at constant EAS (320kts) up to 25,341ft (7,724m), where (cruise) Mach number is equal to 0.8
- 4th segment: Cruise at 25,341ft (level flight) at constant M (0.80)
- 5th segment: Cruise at 25,341ft (level flight) at constant M (0.80)
- 6th segment: Descent at constant EAS (320kts) from 25,341ft (7,724m) to 10,000 ft (3,048m)
- 7th segment: Deceleration at 10,000ft (level flight) to 250kt EAS (128.6m/s)
- 8th segment: Descent at constant EAS, 250kts EAS or 128.6m/s, from 10,000 ft (3,048m) to 1,500ft (457m)

Table 6-9 summarises the values of the main parameters (altitude, aircraft speed, and ground range covered) that characterise the eight-segment trajectory described above, which was utilised as the baseline trajectory in this fourth case study. All design variables used in this case study are also indicated in Table 6-9. As observed in this table, the first three design variables (initial EAS in segment 1, final EAS in segment 2, and initial altitude in segment 3) correspond to the same variables used in the previous (third) case study. However, the lower and upper bounds of the range of permissible values of the final EAS in segment 2 have been slightly modified. In this case, they correspond to the equivalent airspeeds that yield Mach numbers of about 0.8 at the lowest and highest permissible altitudes associated with the beginning of segment 4. In turn, the range of values in which the initial altitude in segment 4 can be varied when optimising the trajectories was established in such a way so as to allow the aircraft cruising at altitudes between 20,000ft (6,096m) and 40,000ft (12,192m).

The last two design variables and their associated ranges of permissible values were established similarly to the corresponding ones used during the climb phase. Thus, the upper limit of the range of permissible values of the initial altitude in segment 7 was established as being equal to 4,400m (which corresponds approximately to the highest FPA permissible, -7.5deg). In turn, the lower and upper bounds of the range of permissible values of the initial EAS in segment 8 corresponded to the aircraft stall speed (89.0m/s EAS), and the maximum EAS permissible below 10,000ft (250kts EAS or 128.6m/s according to ATC restrictions), respectively.

Table 6-9. Case Study 4 – Baseline trajectory and design variables

| Seg. No. | $h_i$ [m] | $h_f$ [m] | $M_i$ [--] | $M_f$ [--] | $EAS_i$ [m/s] | $EAS_f$ [m/s] | R [km] | Design Variables |
|---|---|---|---|---|---|---|---|---|
| 1 | 457 | 3048 | -- | -- | 128.6 | 128.6 | 20 | $89.0 \leq EAS_i \leq 128.6$ |
| 2 | 3048 | 3048 | -- | -- | 128.6 | 164.6 | 10 | $117.1 \leq EAS_f \leq 184.6$ |
| 3 | 3048 | 7724 | -- | -- | 164.6 | 164.6 | 160 | $3048 \leq h_i \leq 4400$ |
| 4 | 7724 | 7724 | 0.80 | 0.80 | -- | -- | 230 | $6096 \leq h_i \leq 12192$ |
| 5 | 7724 | 7724 | 0.80 | 0.80 | -- | -- | 230 | -- |
| 6 | 7724 | 3048 | -- | -- | 164.6 | 164.6 | 140 | -- |
| 7 | 3048 | 3048 | -- | -- | 164.6 | 128.6 | 20 | $3048 \leq h_i \leq 4400$ |
| 8 | 3048 | 457 | -- | -- | 128.6 | 128.6 | 70 | $89.0 \leq EAS_i \leq 128.6$ |

Similar to the implicitly constrained climb profile optimised in the previous case study, in addition to these design variables, an implicit constraint was also utilised in

this fourth case study. This implicit constraint was related to the flight Mach number in segment 4, whose value was also used in segment 5. Accordingly, the allowable range of this parameter was established as being ± 0.5% of its nominal value, 0.8 in this case. As emphasised before, it is not possible to use this parameter as an explicit constraint when the same is not utilised as a design variable. Based on these considerations, optimum whole flight profiles minimising the total flight time, fuel burned, and $NO_x$ emissions produced have been computed in this fourth case study, and the following section summarises the main results obtained.

#### 6.2.5.2 Results

In a similar manner to the climb profiles studied before, the numerical performance of Polyphemus is again analysed through comparisons of the results obtained using this optimiser and one of the other two commercially available optimisation algorithms (GAs [94]) utilised previously. The whole flight profile used as baseline in this case study as well as the optimum trajectories computed using both Polyphemus and the commercial one [94] are shown in Figure 6-36.

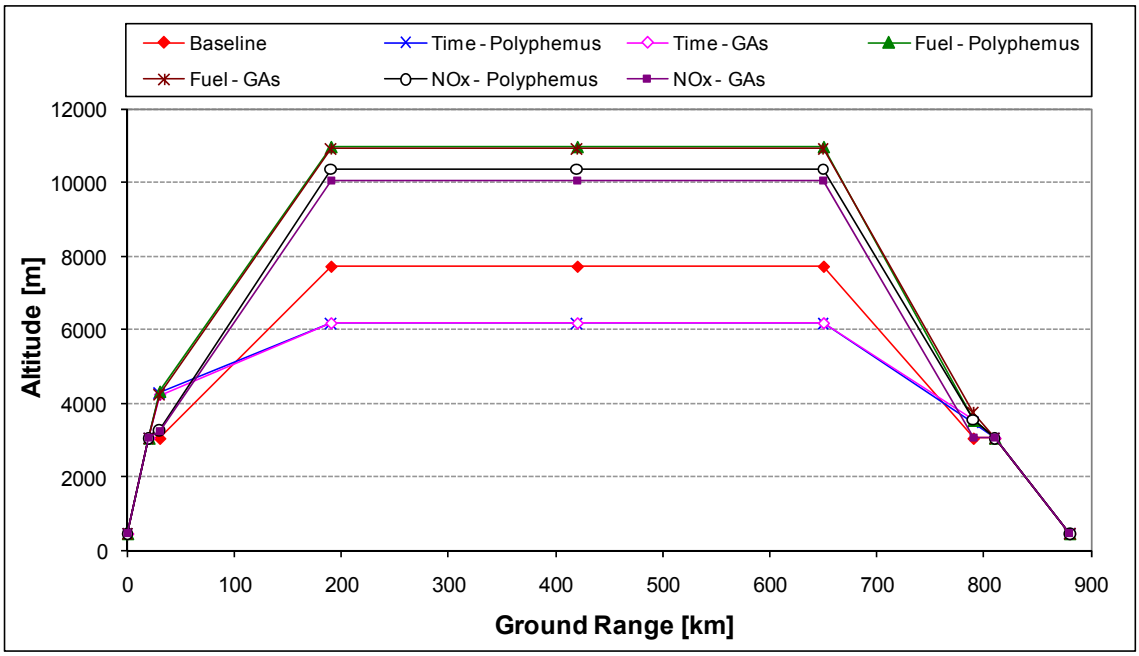


Figure 6-36. Case Study 4 – Comparison of optimisation algorithms

As can be graphically observed in Figure 6-36 and quantitatively in Table 6-10, both Polyphemus and the GAs-based (commercial) optimisation algorithm yielded very

similar results (average discrepancies ~ 1%). Similar to other cases studies analysed previously, from Table 6-10 it can be seen that the three optimum trajectories computed originated significant reductions in the total climb time (~ -5%), fuel burned (~ -17%), and level of $NO_x$ emitted (~ -34%). In order to highlight the particular results obtained using Polyphemus, Figure 6-37 shows the reference trajectory used in this case study and only the optimum trajectories computed with this optimiser.

Table 6-10. Case Study 4 – Optimisation algorithms results (relative to baseline)

| Objective Function/ Optimiser | Flight Time [%] | Fuel Burned [%] | $NO_x$ Emitted [%] |
|---|---|---|---|
| Time – Polyphemus | -5.2 | 14.5 | 126.7 |
| Time – GAs [94] | -5.2 | 14.0 | 123.4 |
| Fuel – Polyphemus | 8.8 | -17.2 | -24.7 |
| Fuel – GAs [94] | 8.3 | -17.3 | -26.3 |
| $NO_x$ – Polyphemus | 9.8 | -13.3 | -35.1 |
| $NO_x$ – GAs [94] | 9.9 | -13.0 | -33.4 |

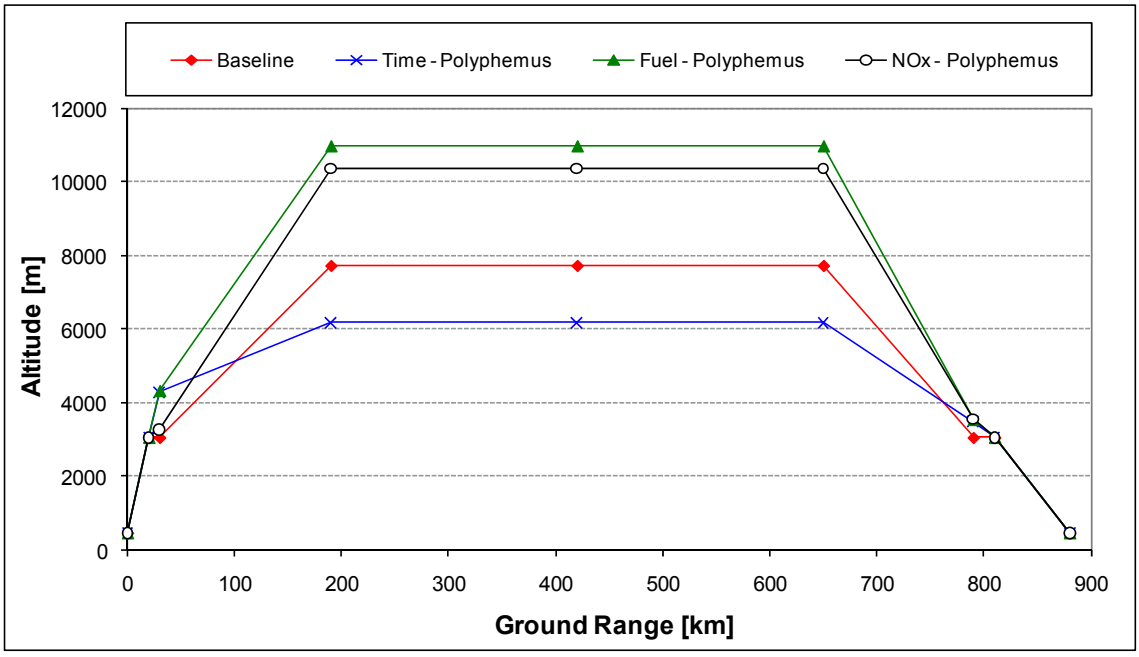


Figure 6-37. Case Study 4 – Baseline vs. Optimum trajectories

In order to have a better understanding of the nature of the optimum trajectories computed in this case study, each of them will be analysed briefly and separately. Firstly, minimisation of total flight time implies, as highlighted before and illustrated in Figure 6-38, maximisation of TAS. Thus, when determining the minimum flight time optimised trajectory, Polyphemus suggests a solution where the aircraft flies the first

and the last segments at the highest EAS permissible (Figure 6-39), which was fixed at 128.6m/s due to ATC restrictions. This is conceptually correct because the first and last segments are flown at fixed altitudes, where TAS increases with the increase in EAS, Eq. (6-10).

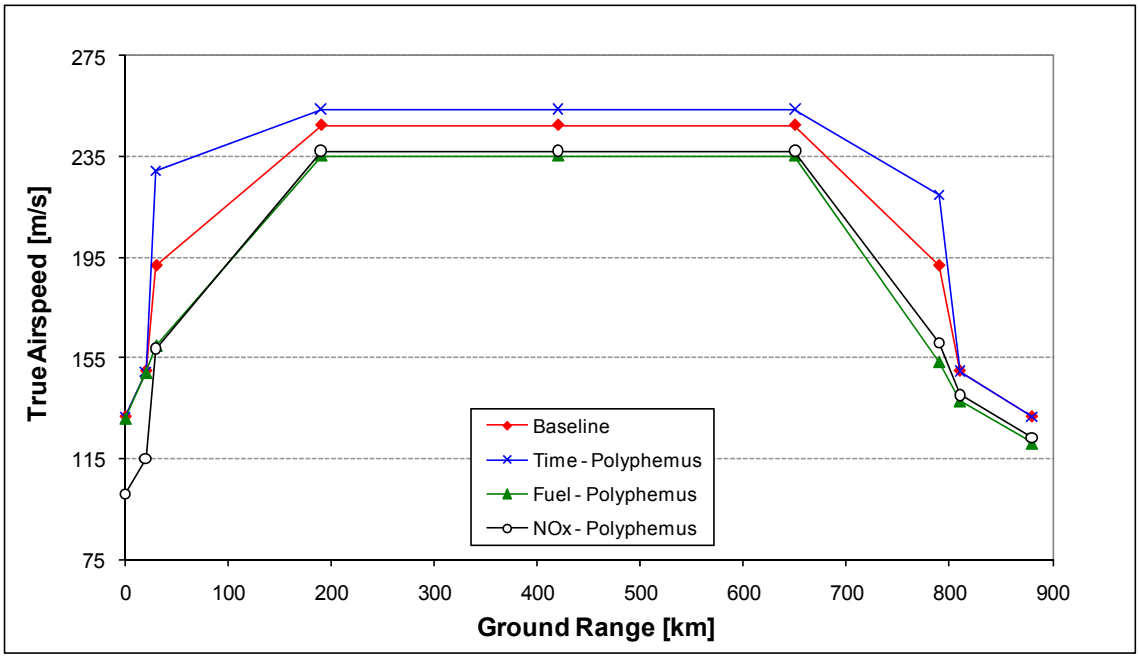


Figure 6-38. Case Study 4 – True airspeed (TAS)

Polyphemus also suggests that the aircraft should accelerate in the second segment to the highest EAS permissible (fixed at 184.6m/s), and start the third segment as high as possible and as low as possible the fourth one (Figure 6-37). This is again mathematically correct because, firstly, TAS increases with the increase in both flight altitude and EAS (segments 2 and 3); and, secondly, for a given Mach number the TAS increases with the decrease in altitude (speed of sound is the highest at sea level – Figure 6-1) – segments 4 and 5. As a consequence of the larger distance covered by the cruise segments 4 and 5, their influence on the total flight time is more important than that associated with the third and sixth segments. This is reflected by the fact that the aircraft has a tendency to cruise at low altitude levels as observed in Figure 6-37. For completeness, Figure 6-40 shows the flight Mach number variation along the whole flight profile. As can be verified in this figure, all trajectories computed fulfilled the requirement of the implicit constraint imposed (flight Mach number at cruise ~ 0.8).

Regarding the fuel optimised trajectory, Figure 6-37 and Figure 6-38 show that in order to reduce the total fuel burned the optimiser suggests flying mostly slower and higher than the reference trajectory. In particular, as illustrated in Figure 6-39, it suggests flying the first segment at the highest EAS permissible (fixed at 128.6m/s). This situation is similar to those ones encountered in the last two case studies. As already mentioned, in order to minimise the total fuel burned during the flight profile, the total energy required during the process must be minimised. It implies in turn the minimisation of aircraft kinematic energy change. Since in this fourth case study the initial and final altitudes are the same, it means that the overall change in kinetic energy must be minimised (neglecting for simplicity the aircraft mass changes). It implies, consequently, the maximisation of the initial aircraft speed and the minimisation of the final one (in terms of TAS).

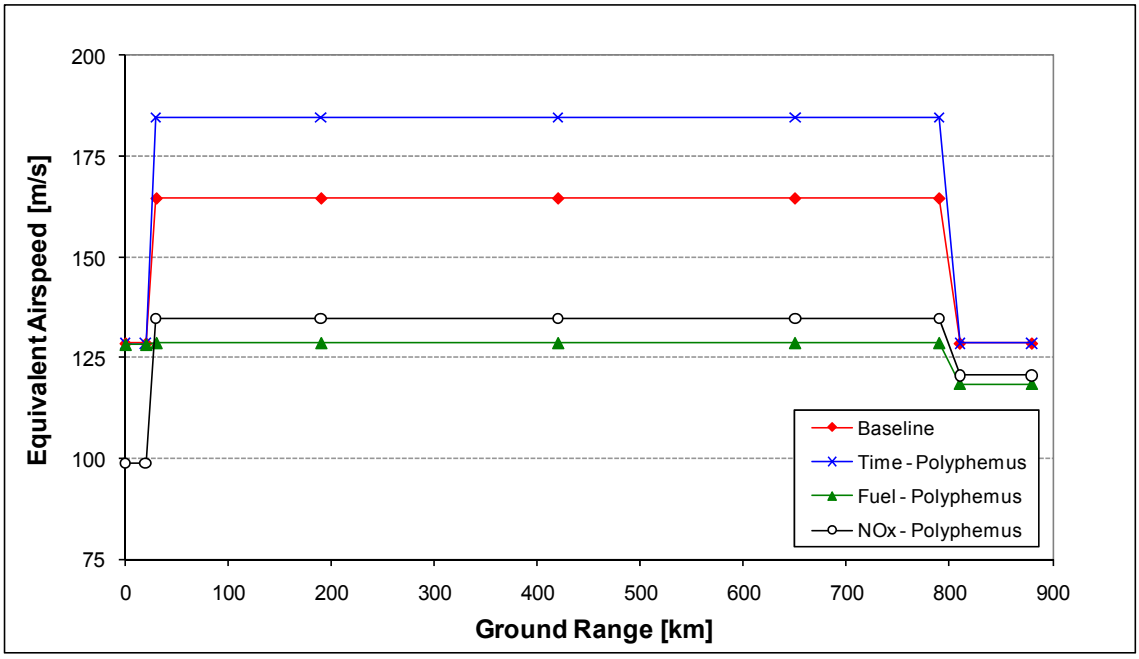


Figure 6-39. Case Study 4 – Equivalent airspeed (EAS)

Accordingly, the TAS maximisation makes that the aircraft flies the first segment at the highest EAS permissible as shown in Figure 6-39 (for a given altitude, TAS increases with the increase in EAS). Additionally, Figure 6-39 also shows that even though the aircraft arrives to the end point at a low speed, this does not correspond to the lowest EAS permissible (fixed at 89.0m/s). It is believed that the one reason behind this is related to the fact that in general reducing speed means increasing flight time,

which also negatively affects the fuel burn. Consequently, it seems that this result is a compromise between two factors, one that has a tendency to reduce the aircraft speed, minimisation of the overall change in kinetic energy; and the other to increase this speed, in order to reduce the flight time, and consequently the fuel burn. Another aspect that may be influencing this particular result (EAS in segment 8) is the path dependent energy, which has a direct relationship with the aircraft speed and which also needs to be minimum.

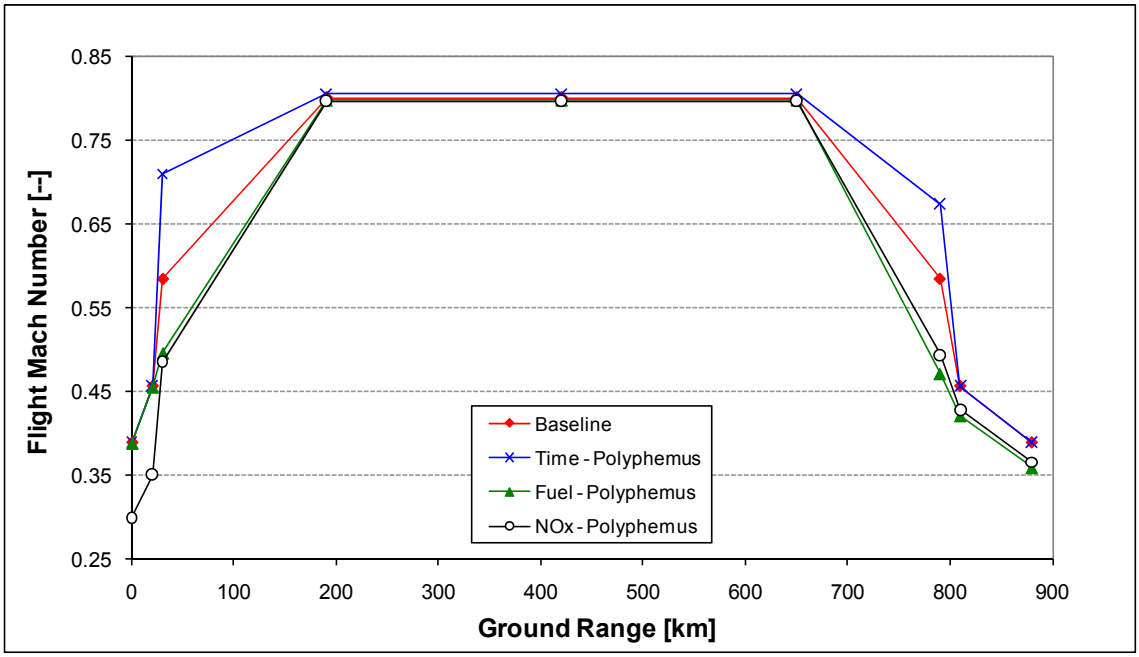


Figure 6-40. Case Study 4 – Flight Mach number

In the foregoing analysis, the aircraft mass changes were neglected as indicated. However, in order to understand the nature of fuel optimised trajectories, these aircraft mass changes can not be ignored. This is because aircraft mass changes are one of the main factors driving the minimisation of the fuel burned during a given flight profile optimisation process. In the analysis presented in the previous case study, it was pointed out that there are two main parameters that affect the fuel burned and, consequently, the changes in the aircraft mass: the aircraft speed and the aircraft flight altitude. These two parameters directly or indirectly affect, in turn, other parameters such as drag, thrust required (to fly a given segment), flight time, and engine thrust setting (consequently, fuel flow, TET, etc.), among others. It implies that a fuel optimised trajectory represents in fact a trade-off among all these parameters, some of which conflict with each other.

Therefore, during the optimisation process, a compromise between aircraft flight altitude and speed, which directly affect the changes in the aircraft mass, is achieved at some stage, and the result of this compromise is characterised by the fuel optimised trajectory determined. Figure 6-41 illustrates the fuel burned associated with the baseline trajectory as well as the three optimum trajectories computed in this fourth case study. In this figure it is interesting to note that the fuel optimised trajectory proposes a second segment affording a greater fuel burn (relative to the baseline) in order to gain height which, then, in conjunction with the lower aircraft speeds is translated into a lower fuel burn in the subsequent segments and an overall lower fuel burn.

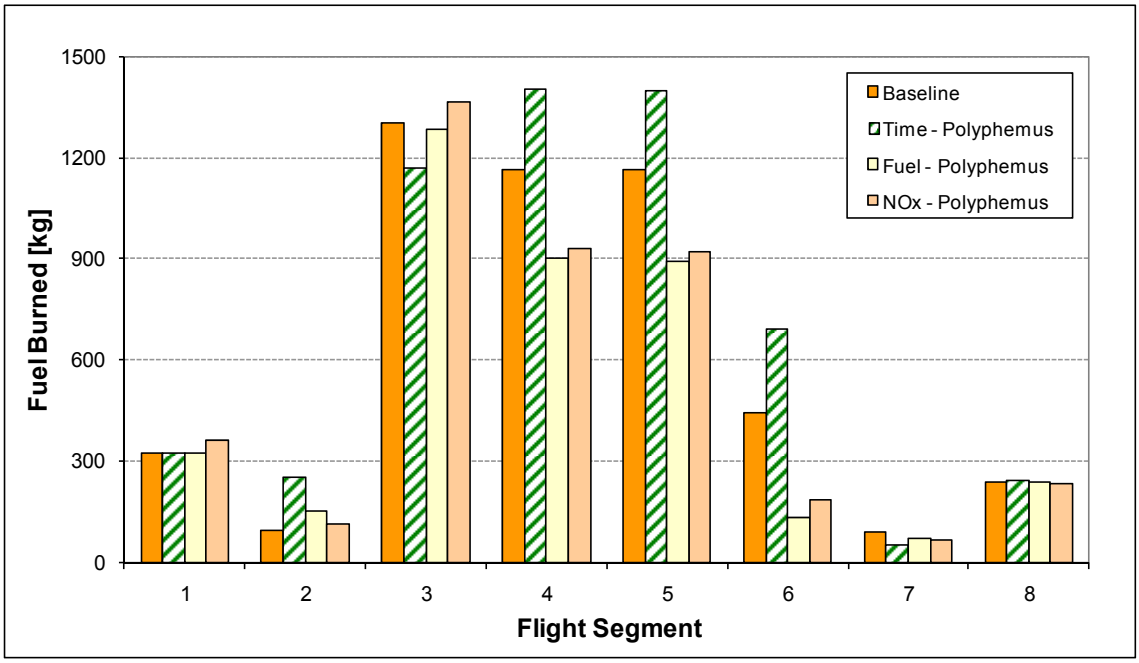


Figure 6-41. Case Study 4 – Fuel burned at each flight segment (segments – climb: 1-3; cruise: 4-5; descent: 6-8)

For the flight profile optimised for minimum $NO_x$ emissions, from Figure 6-37 and Figure 6-38 it is possible to see that this trajectory is flown similarly to the fuel optimised one, i.e., mostly slower and higher than the baseline trajectory utilised. The relative lower speed and higher altitude utilised to fly this trajectory originate in general reductions in the thrust required to fly the trajectory segments. These lower thrust requirements are in turn translated into lower engine TET values (Figure 6-42), which ultimately result in reductions in the level of $NO_x$ emissions produced. Figure 6-42 also illustrates that from all TET values associated with the three optimum trajectories determined and the reference trajectory, the TET values corresponding to the $NO_x$

emissions optimised trajectory are the lowest ones. This is expected, of course, because this parameter has a direct influence on the level of $NO_x$ emissions produced by gas turbine combustors.

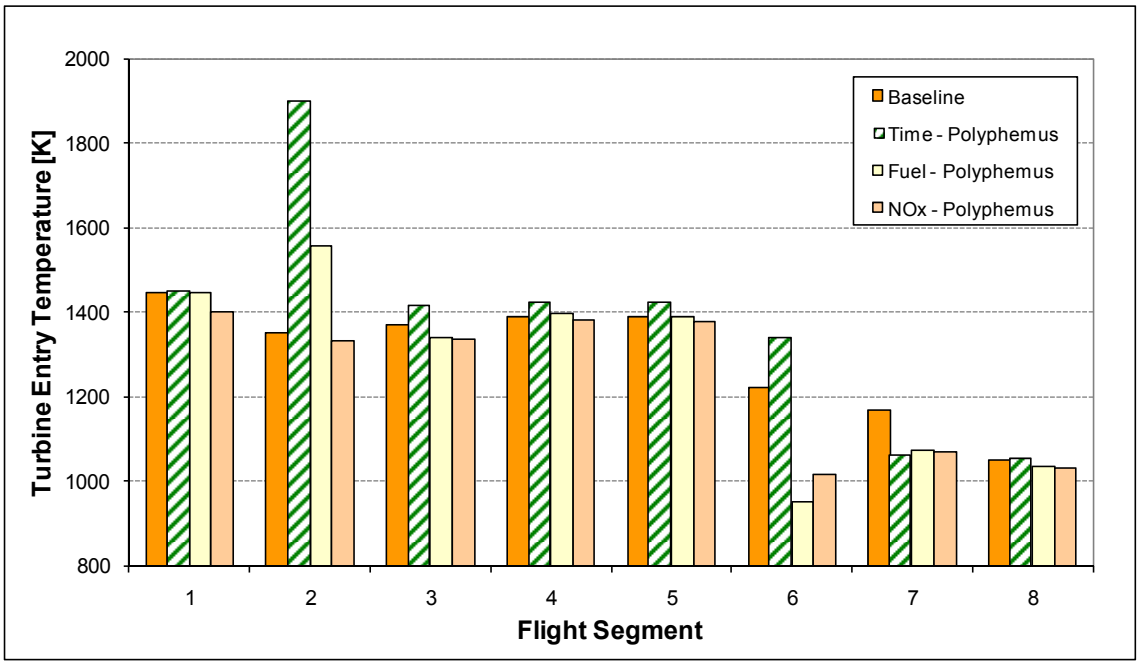


Figure 6-42. Case Study 4 – TET at each flight segment (segments – climb: 1-3; cruise: 4-5; descent: 6-8)

As customary in the case studies analysed, closing this section Figure 6-43 shows a comparison of the main results obtained when computing the three optimum trajectories determined in this fourth case study. As expected, this figure illustrates that the variations in $CO_2$ and $H_2O$ (species in chemical equilibrium) are directly proportional to the variations in the amount of fuel burned. Figure 6-43 also shows that even though the $NO_x$ emissions optimised trajectory increases total flight time the total amount of fuel burned is largely reduced. As pointed out before, this is a consequence of the lower engine thrust settings utilised to fly this trajectory. Similar to the first three case studies, Figure 6-43 shows that the aircraft trajectory optimised for minimum flight time significantly increases the amount of $NO_x$ emissions. This result is partially due to the large amount of thrust required to increase the aircraft kinetic and potential energy in segment 2. The relatively high engine thrust required in this second segment resulted in a high engine TET value (~ 1,900K), as observed in Figure 6-42. Due to $NO_x$ emissions increases exponentially with temperature at such high TET values, this fact led to the significant increases in the level of $NO_x$ emitted observed in Figure 6-43.

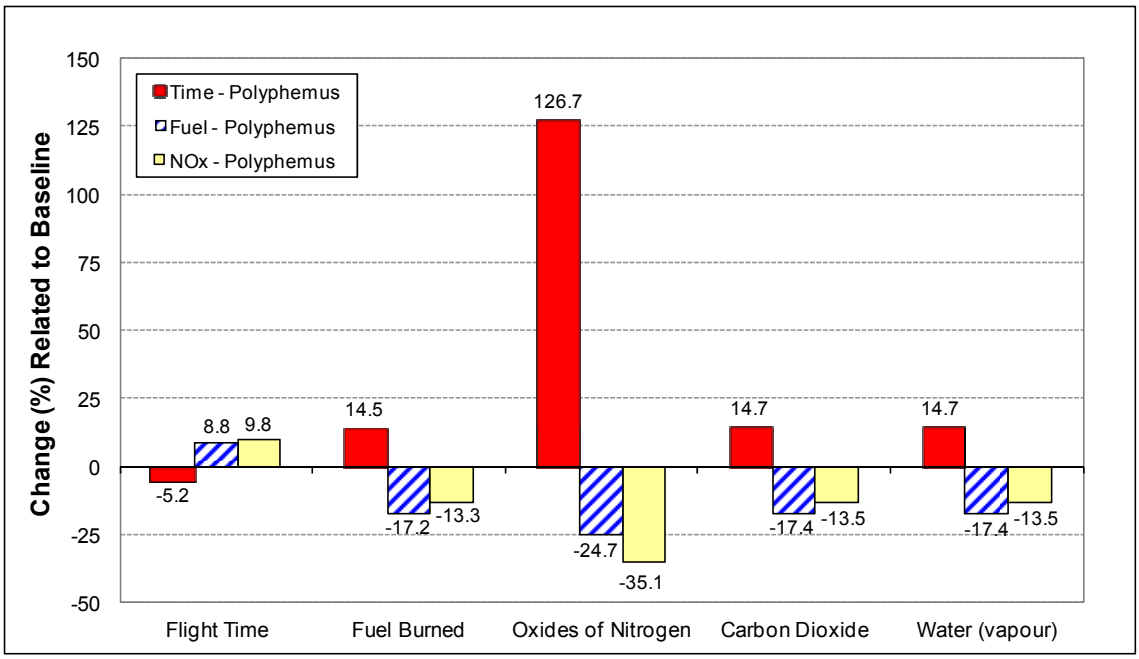


Figure 6-43. Case Study 4 – Optimum trajectories results (relative to baseline)

Finally, it is important to emphasise that this fourth case study completes the set of main case studies analysed in this work in order to both assess the suitability of Polyphemus for carrying out this type of tasks, and comply with one of the objectives of this research project, which relates to the optimisation of aircraft propulsion systems from the point of view of their operation. Thus, the last two cases studies analysed in this chapter are only a complementary part to what was described before. These cases are presented as an attempt to illustrate other uses of Polyphemus, as well as to facilitate the setting of the optimisation processes described in the following chapter.

### 6.2.6
### Case Study 5: Full Flight Profile Multi-objective Optimisation

#### 6.2.6.1
#### General Description

It was indicated before that the evaluation and optimisation of propulsion systems are carried out in this work from two different perspectives, operation and preliminary design. As part of the optimisation based on the operation of the aircraft propulsion systems, aircraft flight trajectories have been optimised as described in this chapter. From the propulsion system design point of view, engine cycle optimisation-type processes have been performed, and their main results will be presented in the following

chapter. However, in order to perform this last task, i.e., to optimise the preliminary design of aircraft propulsion systems, it was necessary to define a reference aircraft trajectory to be used during the optimisation processes. Three different options for this reference trajectory were initially considered: (i) an arbitrary trajectory; (ii) one of the optimum trajectories computed in the fourth case study described above; and (iii) an optimum trajectory determined from a multi-objective optimisation process involving the objectives utilised in the previous case studies. From these three options, the first two were discarded mainly because of the lack of criteria or basis for selecting, first, an arbitrary trajectory, and, second, one of the optimum trajectories computed in the last case study. Thus, it was decided to carry out multi-objective optimisation processes in order to determine a suitable multi-objective optimum reference trajectory for the engine design optimisation assessments. The main outcomes from these processes are summarised in this fifth case study.

As highlighted in Chapter 5, two broad strategies can be adopted when dealing with multi-objective optimisation problems, generating approaches and preference-based approaches. Generating approaches such as the Pareto method, on one hand, are used when no prior knowledge about the objectives preference structure is available, and they allow the identification of an entire set of Pareto solutions or an approximation of the same. Preference-based approaches such as the weighted-sum approach and the target vector optimisation method, on other hand, attempt to obtain a compromised or preferred solution, utilising in the process a known and quantifiable relative importance of the objectives involved.

Polyphemus utilises an approach for the handling of optimisation objectives based on the target vector optimisation method. Thus, when dealing with multi-objective optimisation problems using Polyphemus, target values (previously determined) for each of the objectives involved need to be specified in order to carry out the optimisation process. The differences between the values of the objective functions at a given stage and their target values are used during the optimisation process to internally compute the objectives preference structure, which ultimately determines the optimum solution to be obtained. This means that the values indicated as targets of the objectives are the main drivers of the optimisation process, and they ultimately determine the direction in which the optimisation process has to proceed. It implies that, in turn,

different target values of the objective functions can yield different optimum results. Even though these different optimum solutions are still valid results, sometimes this is not the best way forward when optimising multi-objective problems, because these different solutions represent only a single point in the solutions Pareto front. However, no attempts to introduce more complex multi-objective handling capabilities to Polyphemus have been performed in this research project, because it constitutes part of future developments.

Accordingly, in this case study multi-objective optimisation processes involving the determination of optimum full flight profiles which minimise, first, flight time and fuel burned; and second, flight time, fuel burned, and $NO_x$ emissions, have been carried out using Polyphemus. The full flight profile optimised in this case is identical to that one used in the previous case study, in terms of reference trajectory, number of segments, design variables, explicit and implicit constraints, etc., and its details will not be described again. The only difference was related to the optimisation objectives utilised. As indicated above, two multi-objective optimisation processes were performed, one involving the simultaneous minimisation of flight time and fuel burned, and the other included in addition the level of $NO_x$ emitted. The values of minimum flight time, fuel burned, and $NO_x$ emitted computed during the single-objective optimisation processes carried out in the previous case study were utilised in this case as the target values of the objectives required. The following section summarises the main results obtained from the referred multi-objective optimisation processes.

#### 6.2.6.2 Results

The flight profile used as baseline in this case study (which is equal to that one used in the previous case study), as well as the optimum trajectories computed from the multi-objective optimisation processes carried out using the current optimiser are shown in Figure 6-44. For comparison purposes this figure also shows the results obtained from the single-objective optimisation processes performed in the last case study, i.e. Case Study 4 (dashed lines). From Figure 6-44 it is possible to observe that the multi-objective results show an expected behaviour, in terms of flight altitude. When optimising for flight time and fuel burned, the optimum trajectory determined is flown at an altitude that is in between those altitudes corresponding to the minimum flight

time and minimum fuel burned computed separately in the previous case study. Similarly, the flight time, fuel burned, and $NO_x$ emitted optimised trajectory is flown at high altitudes because the minimisation of $NO_x$ emissions requires such high altitudes (see Figure 6-37 and Figure 6-44). This last trajectory is flown slightly higher than the previous one because in this case there are two objectives (fuel and $NO_x$) pushing the solution to high altitude regions, whereas the time and fuel optimised trajectory has only one objective (fuel) producing the same effect.

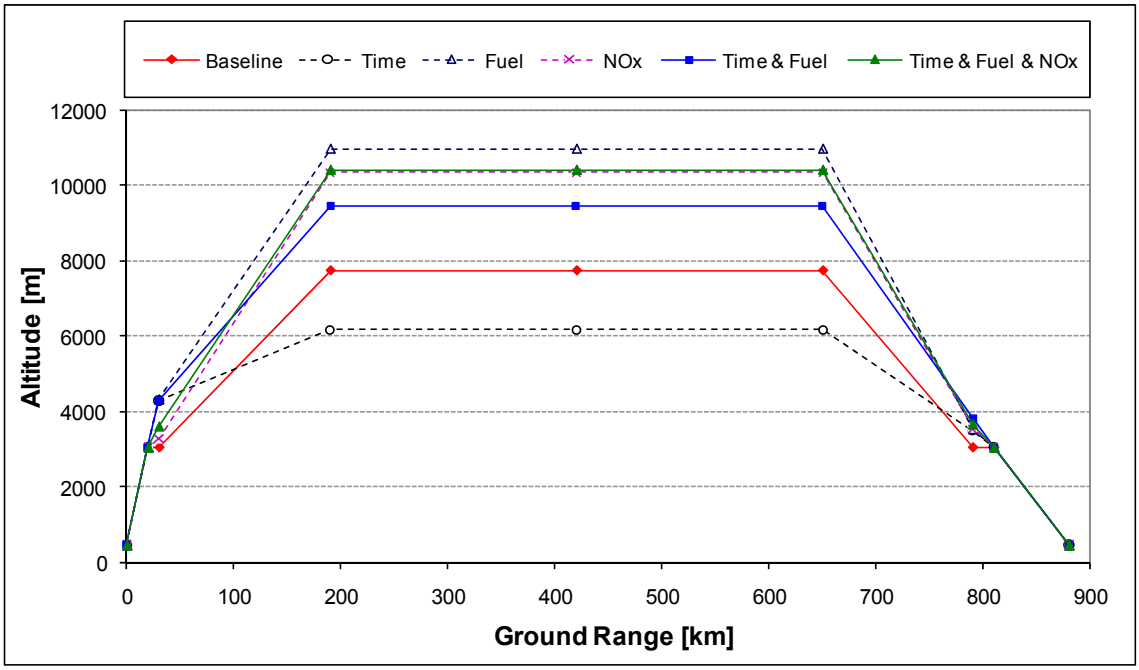


Figure 6-44. Case Study 5 – Single-objective (dashed lines) vs. Multi-objective optimisation (continuous lines)

Highlighting the particular multi-objective optimisation results obtained using Polyphemus, Figure 6-45 shows the reference trajectory used in this case study and only the multi-objective optimum trajectories determined. Table 6-11 summarises, in turn, the results associated with these optimum trajectories when translated into quantitative terms. Since, in general, minimum flight time is synonymous with low flight altitudes (Figure 6-37 and Figure 6-44), the optimum results determined in this case study resulted in an increase in flight time, instead of a decrease in it, as can be verified in Table 6-11. This is mainly due to the fact that the optimum trajectories computed are flown at relatively high altitudes (Figure 6-45) and low aircraft speeds (Figure 6-46) when compared to the reference trajectory utilised. These relative low aircraft speeds

are also reflected, naturally, in the relative low equivalent airspeeds and Mach numbers observed in Figure 6-47 and Figure 6-48, respectively.

The total fuel burned and $NO_x$ emissions produced were favoured, of course, with the relative high altitudes and low aircraft speeds associated with the two optimum trajectories computed in this case study. Thus, as shown in Table 6-11, these parameters show large reductions when compared to the baseline trajectory. As emphasised before, these high altitudes and low speeds lead to a reduction in drag, which is translated into lower thrust requirements, and, consequently, into lower fuel flows and turbine entry temperatures. As shown in this case, these lower fuel flows result in general in lower fuel burns. Similarly, because of the direct relationship between TET and $NO_x$ emitted, these low TET values yield significant reductions in the level of $NO_x$ emissions. Figure 6-49 illustrates the fuel burned for both the baseline trajectory and the two multi-objective optimum trajectories computed in this case study. It is important to note in this figure that the optimised trajectories propose a second segment (or second and third segments) affording a greater fuel burn (or greater fuel burns) relative to the baseline, in order to gain height (and reduce drag) which, then, in conjunction with the lower aircraft speeds is translated into lower fuel burns in the subsequent segments and overall lower fuel burns.

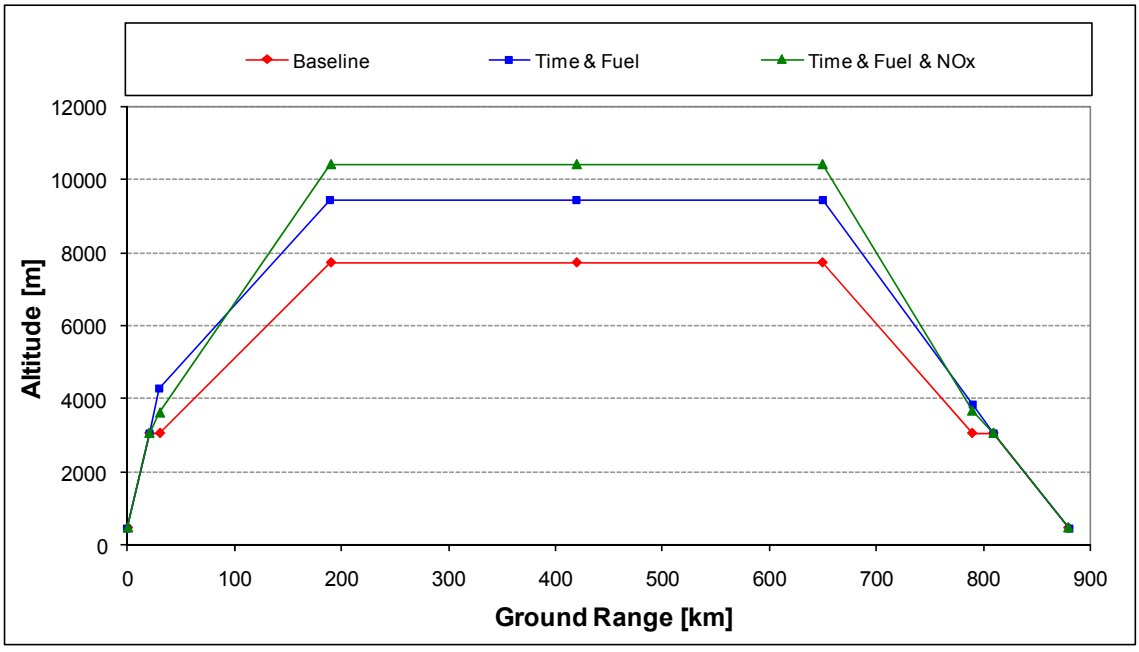


Figure 6-45. Case Study 5 – Baseline vs. Optimum trajectories

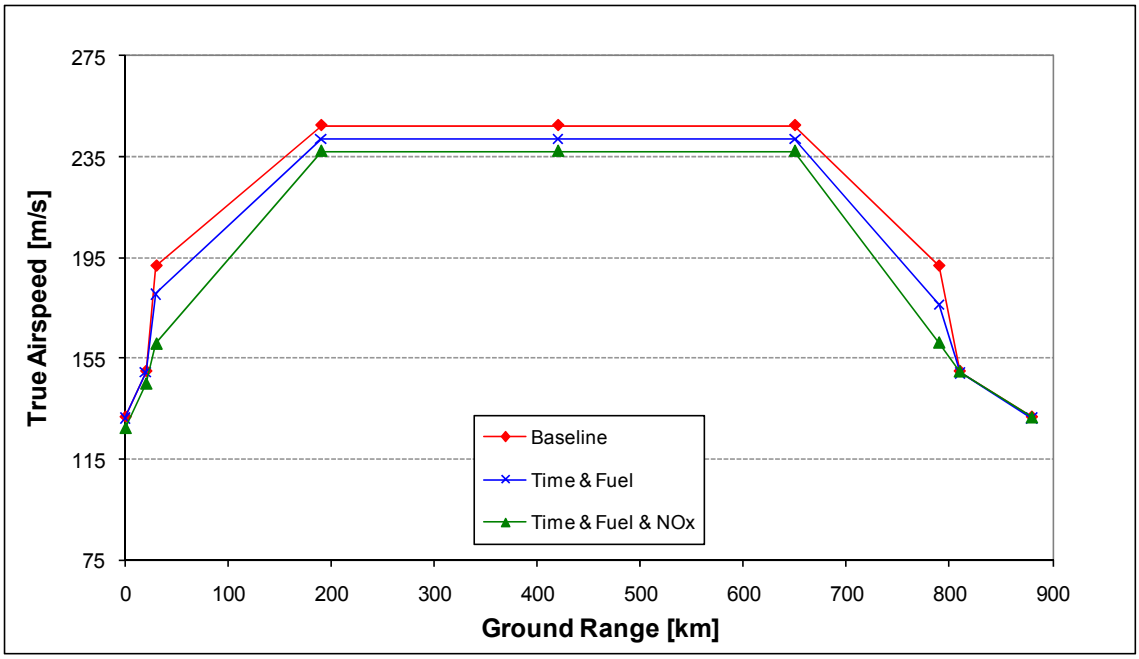


Figure 6-46. Case Study 5 – True airspeed (TAS)

Table 6-11. Case Study 5 – Optimum trajectories results (relative to baseline)

| Objective Function/ Optimiser | Flight Time [%] | Fuel Burned [%] | $NO_x$ Emitted [%] |
|---|---|---|---|
| Time & Fuel | 2.8 | -11.9 | -5.6 |
| Time & Fuel & $NO_x$ | 7.2 | -15.0 | -33.2 |

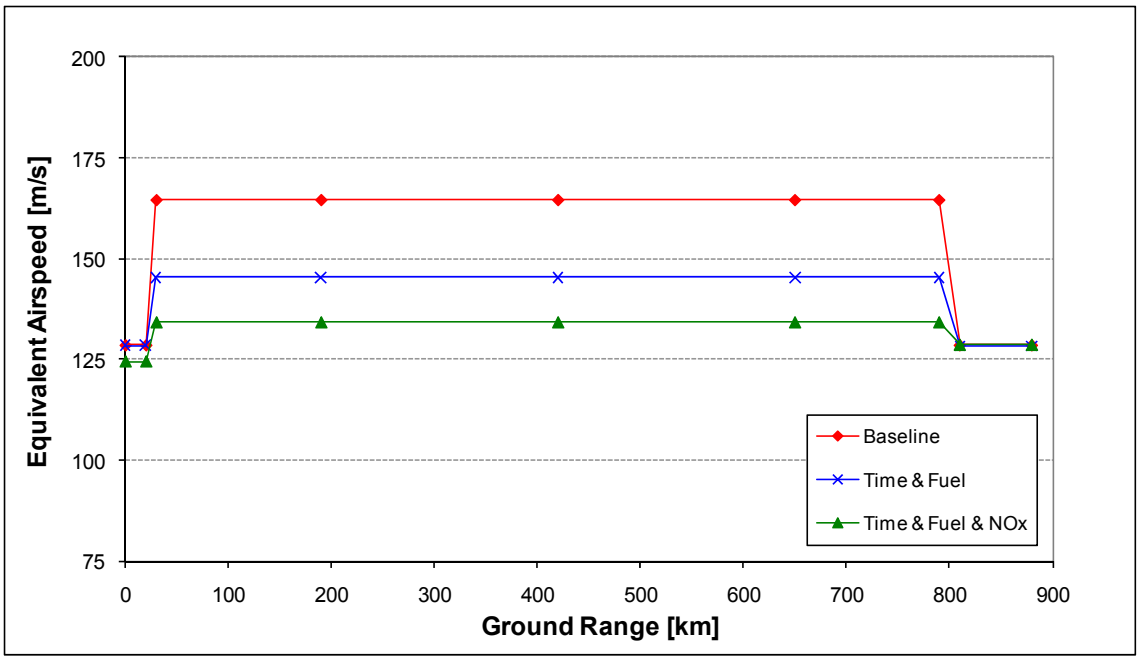


Figure 6-47. Case Study 5 – Equivalent airspeed (EAS)

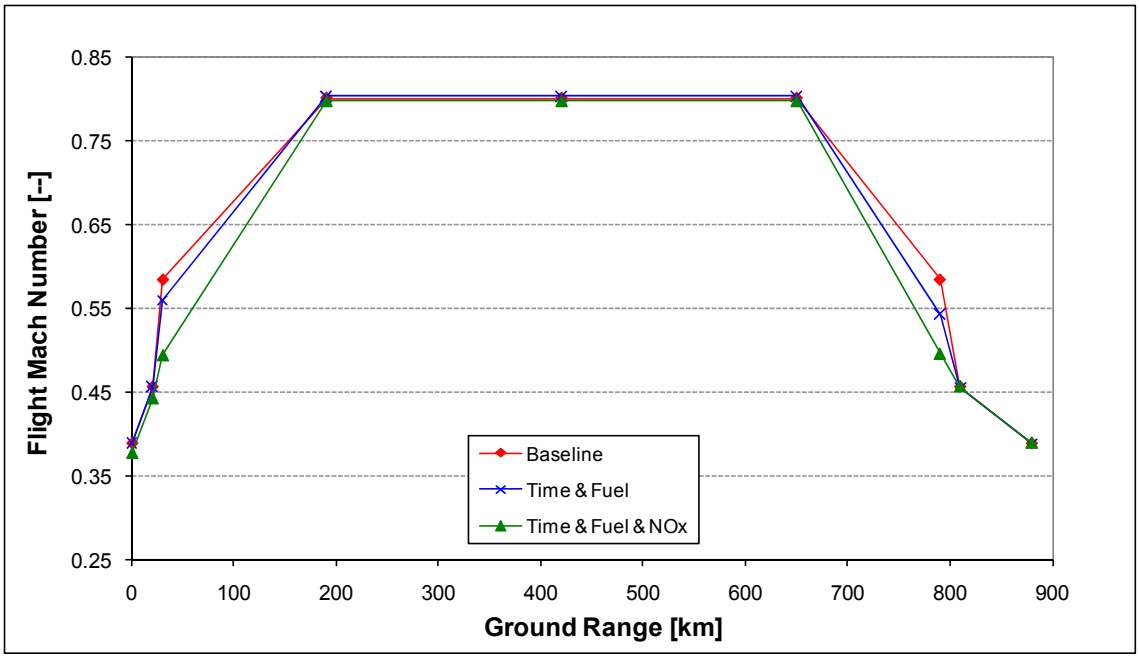


Figure 6-48. Case Study 5 – Flight Mach number

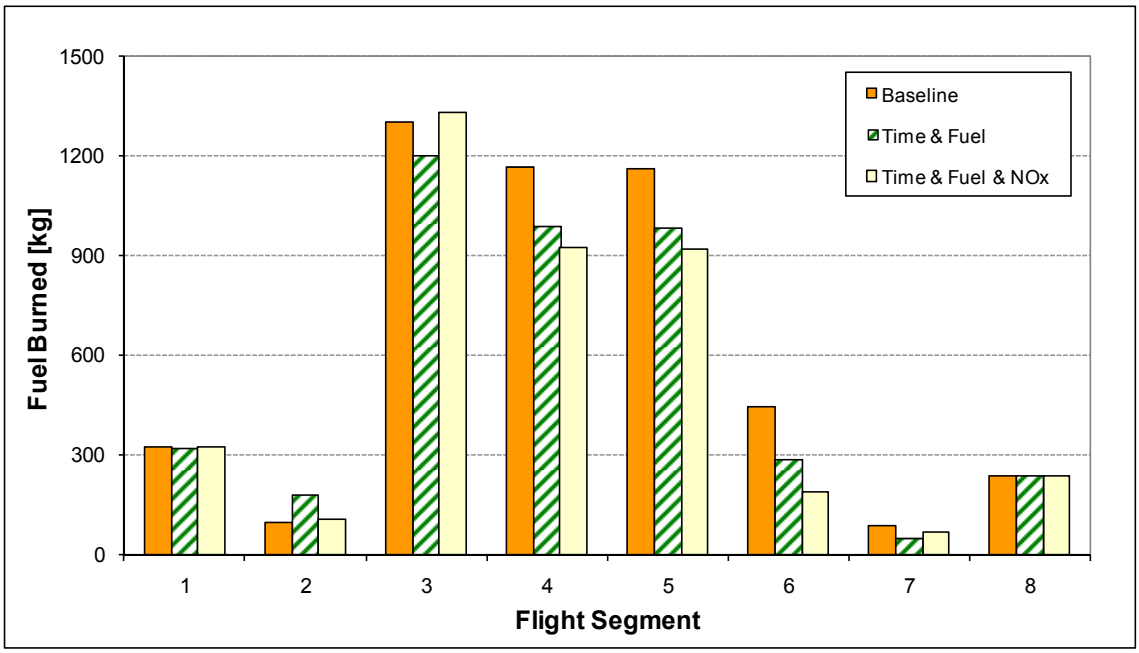


Figure 6-49. Case Study 5 – Fuel burned at each flight segment (segments – climb: 1-3; cruise: 4-5; descent: 6-8)

Regarding the low turbine entry temperatures mentioned before, which lead to reductions in the level of $NO_x$ emitted, Figure 6-50 illustrates that the TET values associated with the optimum trajectory computed including $NO_x$ emissions as one of its objectives are, in general, the lowest ones. This behaviour is expected, of course, because this parameter has a direct influence on the level of $NO_x$ emissions produced by

gas turbine combustors. Closing this section, Figure 6-51 shows graphically a comparison of the main results obtained when computing the two multi-objective optimum trajectories analysed in this fifth case study. Once again, this figure shows that the variations in $CO_2$ and $H_2O$ (species in chemical equilibrium) are directly proportional to the variations in the amount of fuel burned. Figure 6-51 also shows that, even though the optimum trajectories determined increase the total flight time, the total amount of fuel burned is largely reduced, which is a consequence of the lower engine thrust settings utilised to fly these trajectories.

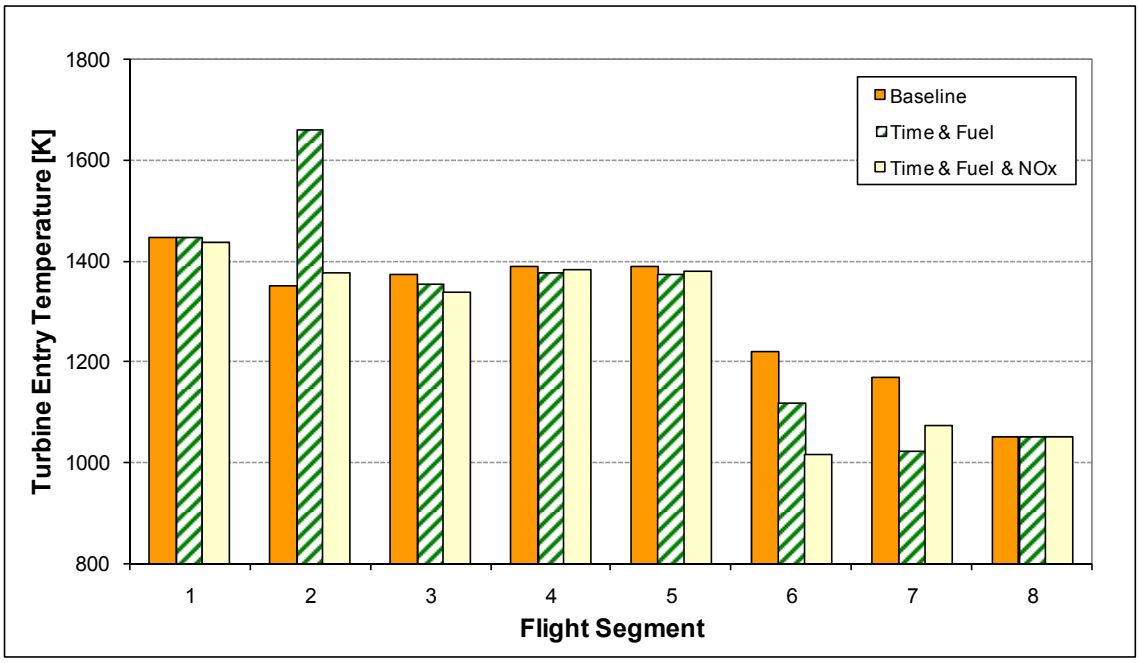


Figure 6-50. Case Study 5 – TET at each flight segment (segments – climb: 1-3; cruise: 4-5; descent: 6-8)

Finally, it is important to highlight once again that these multi-objective optimisation processes discussed in this case study were not performed to test the capabilities of Polyphemus, but to determine a reference trajectory which is used to optimise the preliminary design of aircraft propulsion systems. Accordingly, based on the results obtained from the multi-objective optimisation processes, it was decided to use the three-objective (flight time, fuel burned, and $NO_x$ emitted) optimised trajectory as the baseline trajectory for carrying the engine cycle optimisation assessments mentioned. The main reason behind this choice is related to the fact that both current aircraft cruise at similar altitudes, and this trajectory was obtained using all three objectives utilised in the cases studies described previously. The main results obtained

from these engine cycle optimisation-type processes will be described in the following chapter.

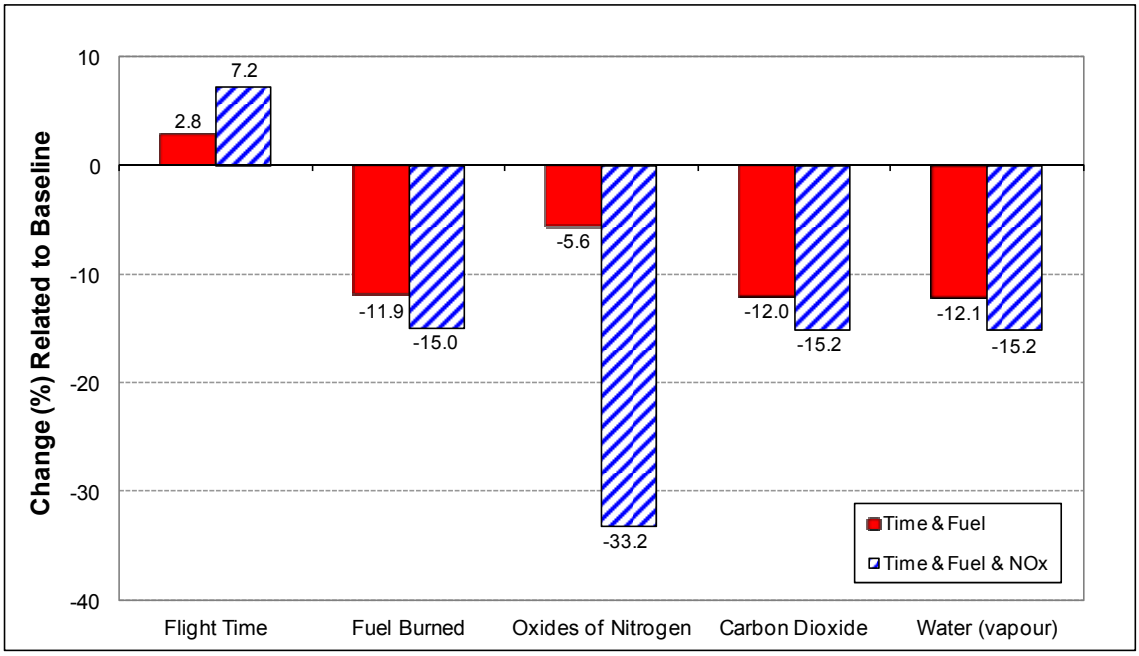


Figure 6-51. Case Study 5 – Optimum trajectories results (relative to baseline)

### 6.2.7 Case Study 6: Full Flight Profile Range Optimisation

#### 6.2.7.1 General Description

In this last case study, in order to illustrate other uses of Polyphemus, the range of one segment of a given aircraft trajectory has been utilised as one of the optimisation design variables. The optimisation problem analysed in this sixth and last case study can be briefly described as follows. First, imagine that there is an aircraft that flies between two cities (from point A to point B) without any stop (direct flight). Second, imagine that one wants to use the same aircraft/engine configuration to fly the same route, but this time having one stop for refuelling purposes. Finally, imagine that it is wanted to know the distance between the trajectory starting point (point A) and this intermediate stop (refuelling point), which is optimum according to given criteria. This last case study involved, then, the determination of the optimum distance between point A and this intermediate stop point which minimises the total flight time, fuel burned, and $NO_x$ emitted.

Similar to previous case studies, in order to afford greater visibility on the characteristics of the optimiser performance when assessing results, the number of segments characterising the whole flight profile (climb, cruise, and descent only) has been kept as small as possible in this case. Thus, as schematically represented in Figure 6-52, for this case study, the flight profile was divided into only ten segments: climb, segments 1, 2, 6, and 7; cruise, segments 3 and 8; and descent, segments 4, 5, 9, and 10. As before, for simplicity, the aircraft trajectory flight phases involving take-off and approach/landing have been not included in the optimisation processes. In addition, ISA conditions have been assumed and the FPA has been limited to values between 0 and 7.5deg during climb and cruise, and -7.5 and 0deg during descent. Accordingly, optimum trajectories which minimise the total flight time, fuel burned, and $NO_x$ emissions produced were determined.

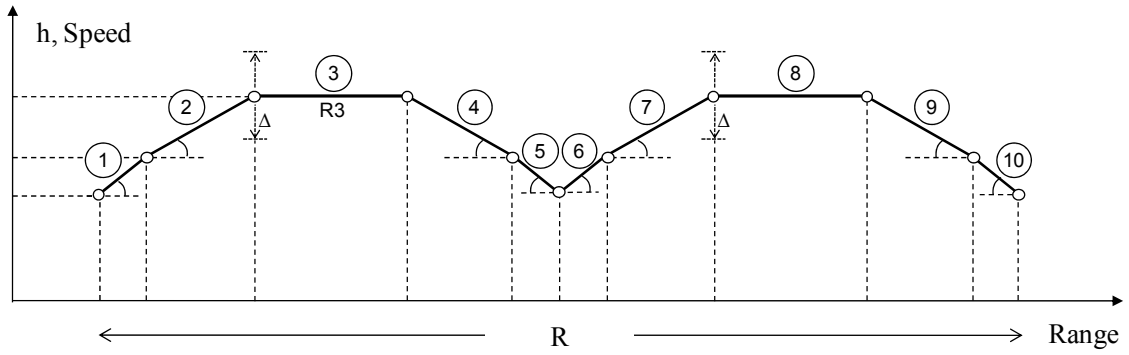


Figure 6-52. Schematic representation of flight profile for range optimisation

The arbitrary flight profile used as the reference or baseline trajectory in this last case study can be described as follows:

- 1st segment: Climb at constant EAS, 250kts EAS or 128.6m/s, from 1,500ft (457m) up to 10,000 ft (3,048m)
- 2nd segment: Simultaneous acceleration to 320kt EAS (164.6m/s) and climb from 10,000 ft (3,048m) up to 25,341ft (7,724m), where (cruise) Mach number is equal to 0.8
- 3rd segment: Cruise at 25,341ft (level flight) at constant M (0.80)
- 4th segment: Simultaneous deceleration to 250kt EAS (128.6m/s) and descent from 25,341ft (7,724m) to 10,000 ft (3,048m)

- 5th segment: Descent at constant EAS, 250kts EAS or 128.6m/s, from 10,000 ft (3,048m) to 1,500ft (457m)
- 6th segment: Climb at constant EAS, 250kts EAS or 128.6m/s, from 1,500ft (457m) up to 10,000 ft (3,048m)
- 7th segment: Simultaneous acceleration to 320kt EAS (164.6m/s) and climb from 10,000 ft (3,048m) up to 25,341ft (7,724m), where (cruise) Mach number is equal to 0.8
- 8th segment: Cruise at 25,341ft (level flight) at constant M (0.80)
- 9th segment: Simultaneous deceleration to 250kt EAS (128.6m/s) and descent from 25,341ft (7,724m) to 10,000 ft (3,048m)
- 10th segment: Descent at constant EAS, 250kts EAS or 128.6m/s, from 10,000 ft (3,048m) to 1,500ft (457m)

In Table 6-12 the values of the main parameters (altitude, aircraft speed, and ground range covered) that characterise the ten-segment reference trajectory described above are summarised. All design variables used in this last case study are also indicated in this table. As observed in this Table 6-12, the lower and upper bounds of the range of permissible values of the three design variables associated with the initial EAS in segments 1, 5, and 10 corresponded to, respectively, the aircraft stall speed (89.0m/s EAS), and the maximum EAS permissible below 10,000ft (250kts EAS or 128.6m/s according to ATC restrictions). The lower and upper bounds of the range of permissible values of the final EAS in segments 2 and 7 corresponded to the equivalent airspeeds that yield Mach numbers of about 0.8 at the lowest and highest permissible altitudes associated with the beginning of segments 3 and 8. In turn, the range of values in which the initial altitude in segments 3 and 8 can be varied when optimising the trajectories was established in such a way to allow cruise altitudes between 20,000ft (6,096m) and 40,000ft (12,192m).

Finally, as mentioned before, the range of segment 3 (R3) was also used as a design variable in this case study. The limits in which this design variable can vary were established in such a way to avoid segments 3 and 8 having a zero length. It means that only segments 3 and 8 had a variable range during the optimisation processes. Consequently, in order to keep fixed the distance separating the initial city pair (point A

to point B), when optimising R3, R8 (range of segment 8) was calculated as the difference between 1200km (sum of reference values of R3 and R8) and the value of R3 randomly generated.

Table 6-12. Case Study 6 – Baseline trajectory and design variables

| Seg. No. | $h_i$ [m] | $h_f$ [m] | $M_i$ [--] | $M_f$ [--] | $EAS_i$ [m/s] | $EAS_f$ [m/s] | R [km] | Design Variables |
|---|---|---|---|---|---|---|---|---|
| 1 | 457 | 3048 | -- | -- | 128.6 | 128.6 | 30 | $89.0 \leq EAS_i \leq 128.6$ |
| 2 | 3048 | 7724 | -- | -- | 128.6 | 164.6 | 150 | $117.1 \leq EAS_f \leq 184.6$ |
| 3 | 7724 | 7724 | 0.80 | 0.80 | -- | -- | 600 | $6096 \leq h_i \leq 12192$; $10 \leq R3 \leq 1190$ |
| 4 | 7724 | 3048 | -- | -- | 164.6 | 128.6 | 150 | -- |
| 5 | 3048 | 457 | -- | -- | 128.6 | 128.6 | 70 | $89.0 \leq EAS_i \leq 128.6$ |
| 6 | 457 | 3048 | -- | -- | 128.6 | 128.6 | 30 | -- |
| 7 | 3048 | 7724 | -- | -- | 128.6 | 164.6 | 150 | $117.1 \leq EAS_f \leq 184.6$ |
| 8 | 7724 | 7724 | 0.80 | 0.80 | -- | -- | 600 | $6096 \leq h_i \leq 12192$ |
| 9 | 7724 | 3048 | -- | -- | 164.6 | 128.6 | 150 | -- |
| 10 | 3048 | 457 | -- | -- | 128.6 | 128.6 | 70 | $89.0 \leq EAS_i \leq 128.6$ |

In a similar fashion to the implicitly constrained case studies analysed before, implicit constraints were also utilised in this last case study. These implicit constraints were related to the flight Mach number in segments 3 and 8. Accordingly, the allowable ranges of this parameter were established as being ± 0.5% of its nominal value, 0.8 in this case. Once again, it was not possible to use this parameter as an explicit constraint because it was not used as a design variable. Accordingly, optimum aircraft trajectories minimising the total flight time, fuel burned, and $NO_x$ emitted were computed, and the following section summarises the main results obtained.

#### 6.2.7.2 Results

The reference flight profile and the optimum trajectories computed in this last case study using Polyphemus are shown in Figure 6-53. Table 6-13 summarises, in turn, the results associated with these optimum trajectories when translated into quantitative terms. In terms of flight altitude, Figure 6-53 shows that the results obtained in this case are similar to those ones obtained in previous case studies. However, in Figure 6-53 it is also possible to see that the three optimum trajectories computed maximised the distance covered by segment 3. In other words, the optimisation processes led to the

maximisation of R3 and, consequently, to the minimisation of R8. In implies that (given the conditions imposed), in order to minimise the total flight time, fuel burned, or $NO_x$ emitted, the intermediate stop should be as near as possible to the original trajectory end point (point B). Saying differently, it implies that it is better to fly the whole trajectory without any stop than using an intermediate one. A brief analysis of the main reasons behind this finding is presented next.

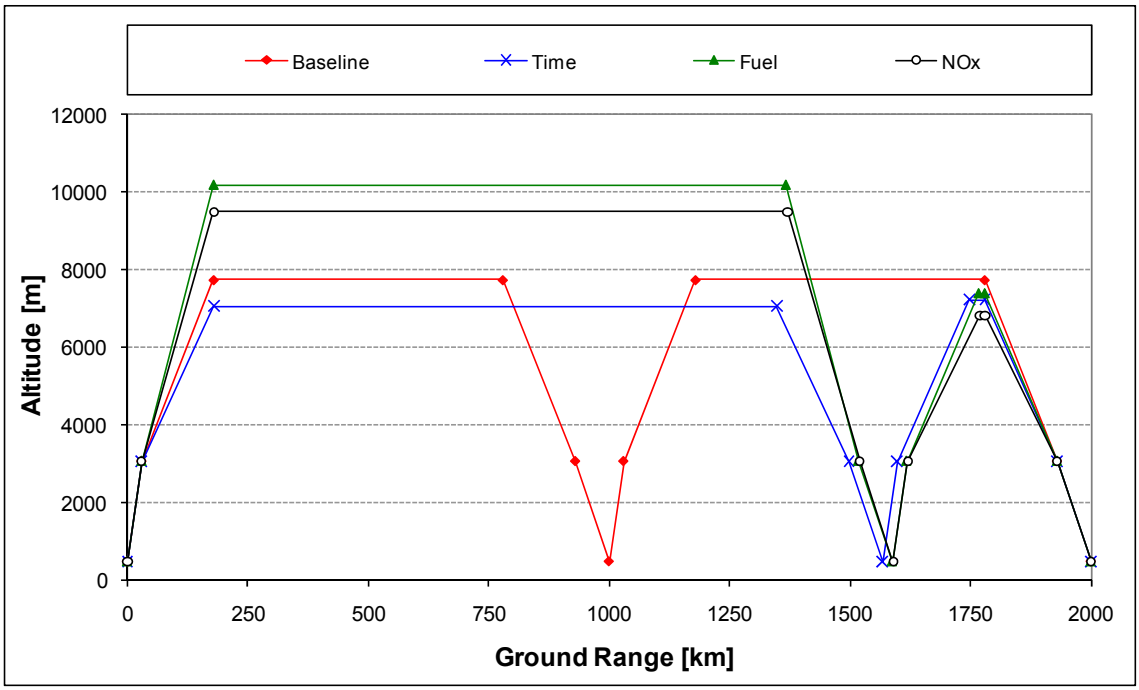


Figure 6-53. Case Study 6 – Baseline vs. Optimum trajectories

Table 6-13. Case Study 6 – Optimum trajectories results (relative to baseline)

| Objective Function/ Optimiser | Flight Time [%] | Fuel Burned [%] | $NO_x$ Emitted [%] |
|---|---|---|---|
| Time – Polyphemus | -0.9 | 5.6 | 20.9 |
| Fuel – Polyphemus | 2.6 | -11.7 | -26.8 |
| $NO_x$ – Polyphemus | 7.3 | -7.5 | -28.5 |

Consider for a moment only the fuel optimised trajectory. Then, reducing only the value of R3 from the optimum one (approximately equal to the highest permissible value, 1190km) to other sub-optimum values such as 900, 600, and 300km, different sub-optimum trajectories (e.g., Fuel, R3 = 900km; Fuel, R3 = 600km, etc.) can be computed. These new sub-optimum trajectories obtained by modifying only R3 in the fuel optimised trajectory are graphically illustrated in Figure 6-54. As expected, the total

fuel burned associated with these new sub-optimum trajectories is larger than the amount corresponding to the fuel optimised one (Figure 6-55). The main reason behind these results is associated with the fact that, as shown in Figure 6-56, as R3 decreases, the reduction in the fuel burned in segment 3 is smaller than the increase in the amount of fuel that is burned in segment 8. This aspect is clearly observed in Figure 6-56, which shows that the sum of the contributions of segment 3 and 8 to the total fuel burned increases with the decrease in the range of segment 3 (R3).

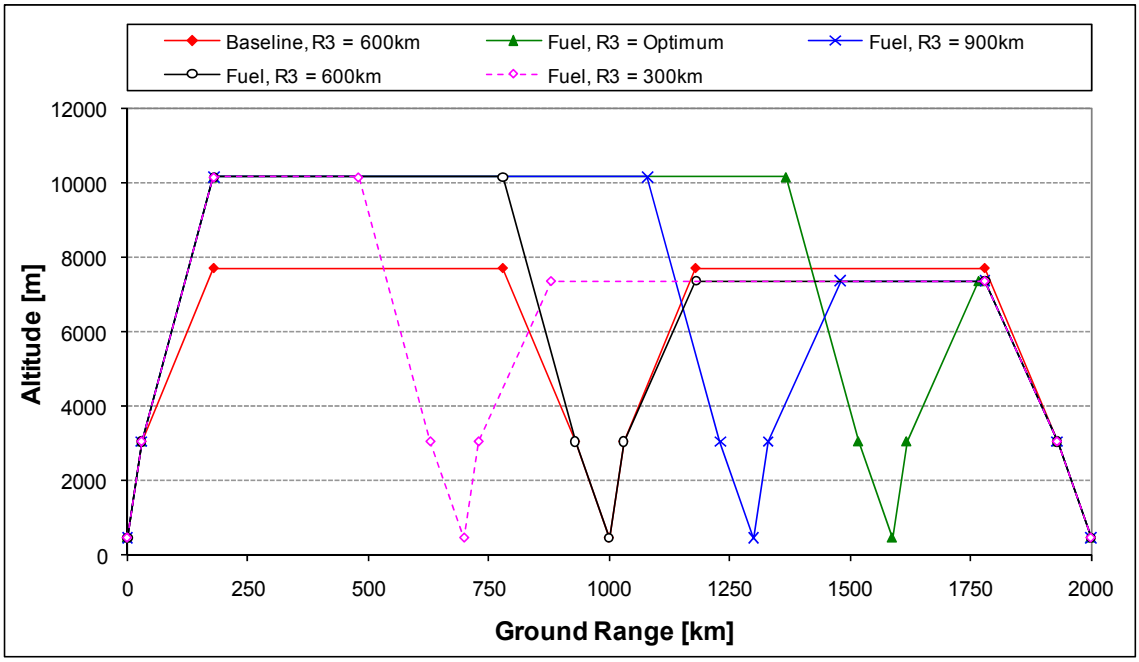


Figure 6-54. Case Study 6 – Flight profile (fuel trajectories: optimum vs. sub-optimum)

There are several factors that lead to the increase in the amount of fuel burned in segment 8 is larger that the reduction in this parameter in segment 3 as R3 decreases. Two of these main factors are the flight altitude and the aircraft weight in segment 8. Because of the lower cruise altitude in segment 8, the aircraft total drag in this segment is higher than in segment 3. Consequently, the thrust being required to fly this segment is higher. This implies in turn a higher fuel burn. Even though segments 3 and 8 cruise altitudes were equal, because of the higher aircraft weight in segment 8 (higher aircraft weight means higher lift and, consequently, higher drag and, in turn, higher engine thrust setting), the amount of fuel burned in segment 8 would be higher than the corresponding one in segment 3. These factors lead to the increase in total fuel burned with the decrease in the range of segment 3, as observed in Figure 6-55 and Figure 6-56.

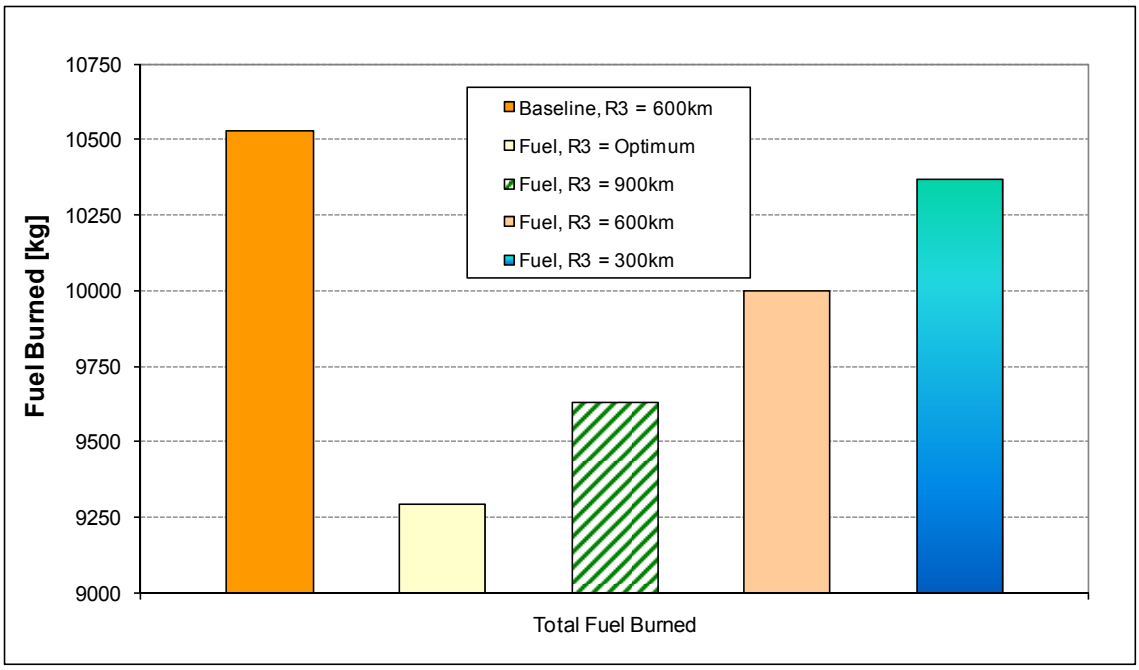


Figure 6-55. Case Study 6 – Total fuel burned (fuel trajectories: optimum vs. sub-optimum)

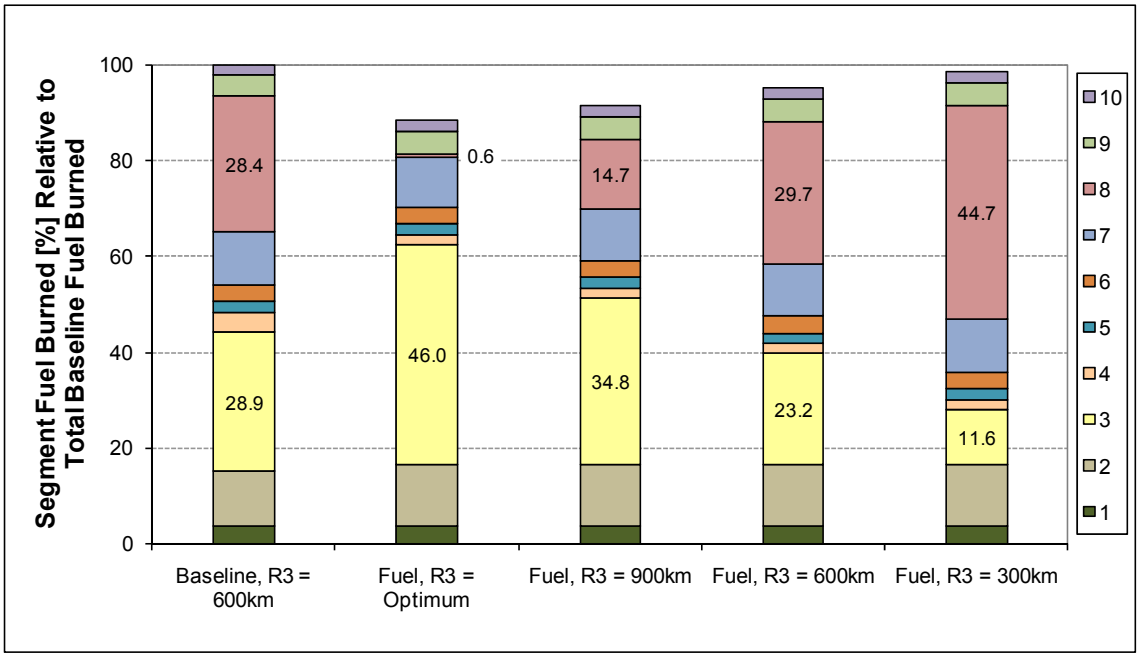


Figure 6-56. Case Study 6 – Relative fuel burned (fuel trajectories: optimum vs. sub-optimum)

For completeness, Figure 6-57 shows the main parameters characterising the sub-optimum trajectories discussed before relative to the baseline trajectory considered in this case study. The decrease in flight time and increase in $NO_x$ emitted as R3 decreases observed in Figure 6-57 are a consequence of, respectively, the higher TAS and engine thrust setting utilised to fly segment 8 when compared to segment 3.

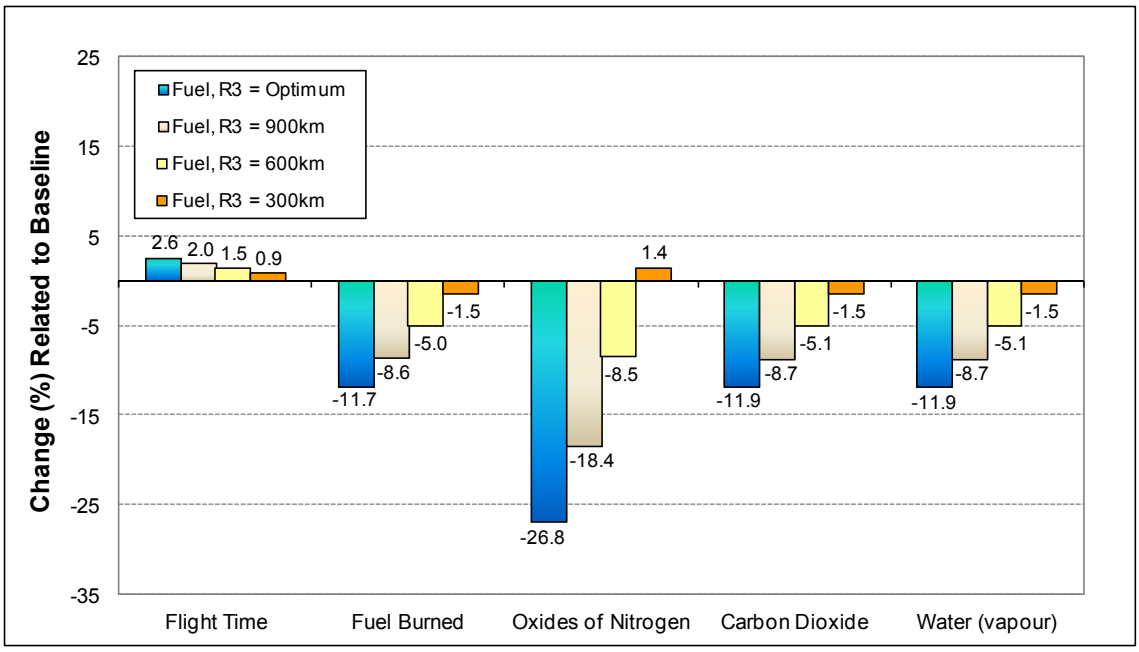


Figure 6-57. Case Study 6 – Fuel optimum and sub-optimum trajectories results

Similar analyses to that one carried out for the case of the fuel optimised trajectory can be performed for the other two cases related to the flight time and $NO_x$ emissions optimised trajectories. In this sense, Figure 6-58 and Figure 6-59 show, respectively, the relative contribution, in terms of flight time and $NO_x$ emissions, of the trajectory segments to the total flight time and $NO_x$ emitted as R3 decreases. As illustrated in these figures, the results obtained for the other two optimised trajectories (flight time and $NO_x$ emissions) follow the same pattern observed in the case of the fuel optimised trajectory discussed before. Even though it is not possible to note in Figure 6-58, there is a small increase in the total flight time as R3 decreases (due to the TAS in segment 8 is slightly lower than the corresponding one in segment 3), which yield that the value of the optimum R3 tends to the highest permissible one as observed in Figure 6-53.

The results associated with the $NO_x$ emitted trajectories (Figure 6-59) are very similar to the case involving the minimisation of the fuel burned (Figure 6-56). Thus, as observed in Figure 6-59, the sum of the $NO_x$ contributions of segment 3 and 8 to the total $NO_x$ emitted increases with the decrease in the range of segment 3 (R3). This is, of course, a direct consequence of the higher engine thrust settings and, in turn, turbine entry temperatures, utilised to fly segment 8 when compared to segment 3 (as R3 decreases). The comparisons performed above between the optimum trajectories

computed in this case study and the sub-optimum ones determined by reducing the range of segment 3 attempted to explain the main reasons why the (computed) optimum values of R3 have a tendency to their highest permissible value (Figure 6-53). Thus, no further explanations about this point will be given in the remaining of this section.

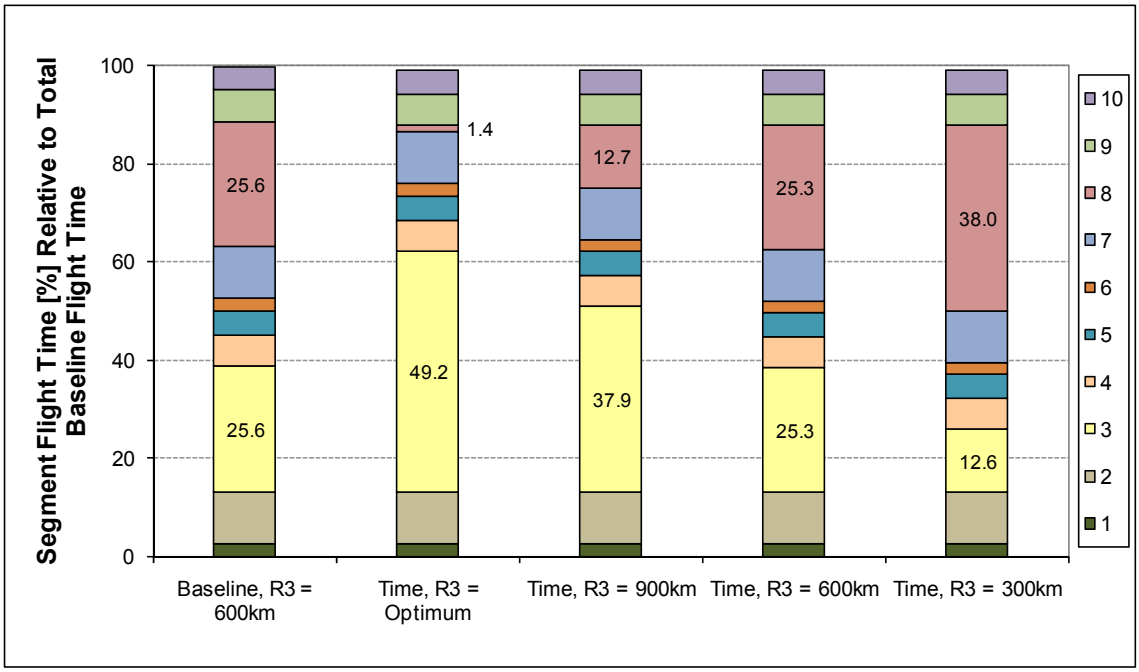


Figure 6-58. Case Study 6 – Relative flight time (time trajectories: optimum vs. sub-optimum)

Returning to the optimum results determined in this last case study, the minimisation of the total flight time implies, as highlighted before and illustrated in Figure 6-60, the maximisation of the TAS. Consequently, when determining the minimum flight time optimised trajectory, the optimiser suggests a solution where the aircraft flies all segments below 10,000ft at the highest EAS permissible (Figure 6-61), which was fixed at 128.6m/s due to ATC restrictions. This is conceptually correct, of course, because these segments are flown at fixed altitudes, where TAS increases with the increase in EAS, Eq. (6-10).

The equivalent airspeeds at TOC and the cruise altitudes for minimum flight time are established as a result of the compromise between increasing the final altitude of segments 2 and 7 and decreasing the cruise altitudes in segments 3 and 8. This compromise needs to be achieved at some stage because, firstly, TAS increases with the increase in both flight altitude and EAS (end of segments 2 and 7); and, secondly, for a given Mach number the TAS increases with the decrease in altitude (speed of sound is

the highest at sea level – Figure 6-1) – segments 3 and 8. In addition, because of the larger distance covered by the cruise segments 3 and 8, they have a larger influence on the total flight time than that one associated with the climb segments (2 and 7). This is reflected in the fact that the aircraft has a tendency to cruise at low altitude levels, as it can be verified in Figure 6-53. For completeness, Figure 6-62 shows the flight Mach number variation along the whole aircraft trajectories. This figure shows that all trajectories computed fulfilled the requirement of the implicit constraints imposed (flight Mach number at cruise, segments 3 and 8, ~ 0.8).

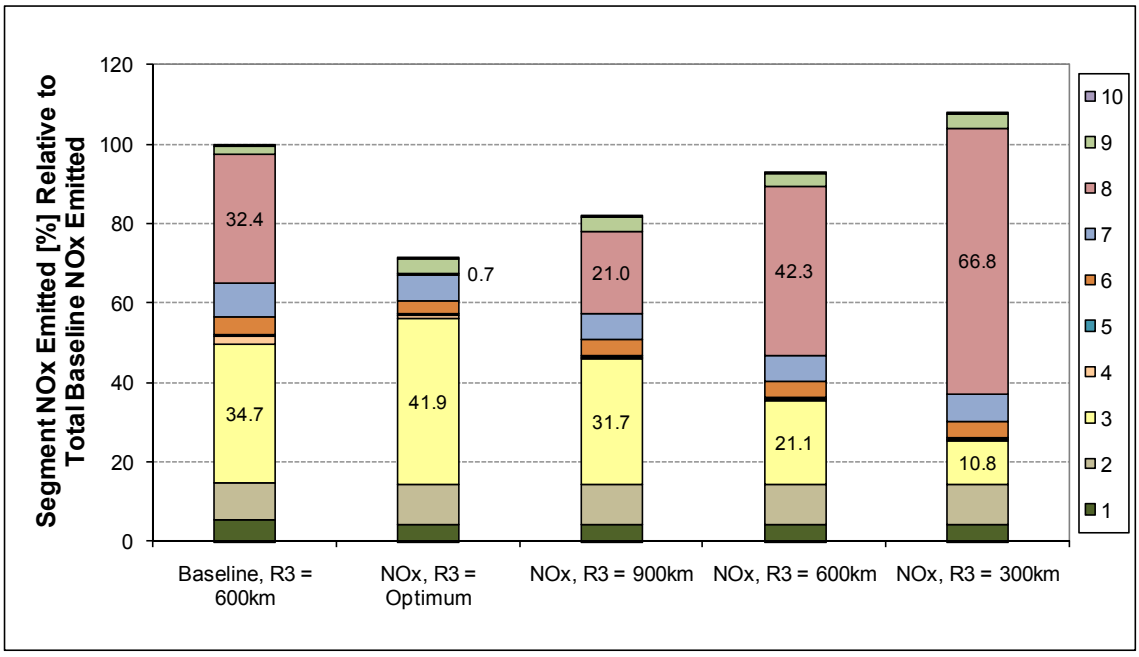


Figure 6-59. Case Study 6 – Relative $NO_x$ emitted ($NO_x$ trajectories: optimum vs. sub-optimum)

The results associated with the fuel and $NO_x$ emissions optimised trajectories obtained in this last case study are similar, in terms of flight altitudes and speeds, to those ones obtained when optimising the whole flight profile described in the fourth case study analysed in this chapter. Consequently, only a brief description of the results obtained in this case will be presented in this section. Thus, Figure 6-53 and Figure 6-60 show that in order to reduce the total fuel burned the optimiser suggests flying mostly slower and higher than the reference trajectory (at least the first part of the original trajectory). In particular, as shown in Figure 6-61, it suggests flying all segments below 10,000ft at or near the highest EAS permissible (fixed at 128.6m/s). As highlighted before, these results are partially due to the minimisation of the overall change in the aircraft kinetic energy (maximisation of the initial aircraft TAS) required.

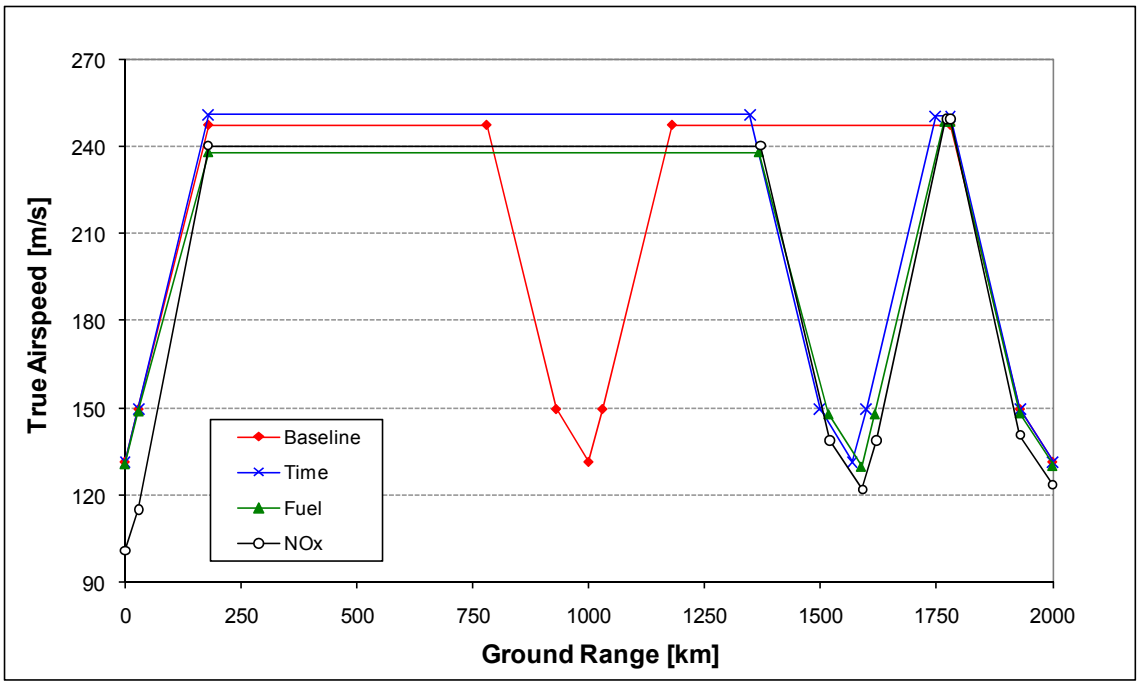


Figure 6-60. Case Study 6 – True airspeed (TAS)

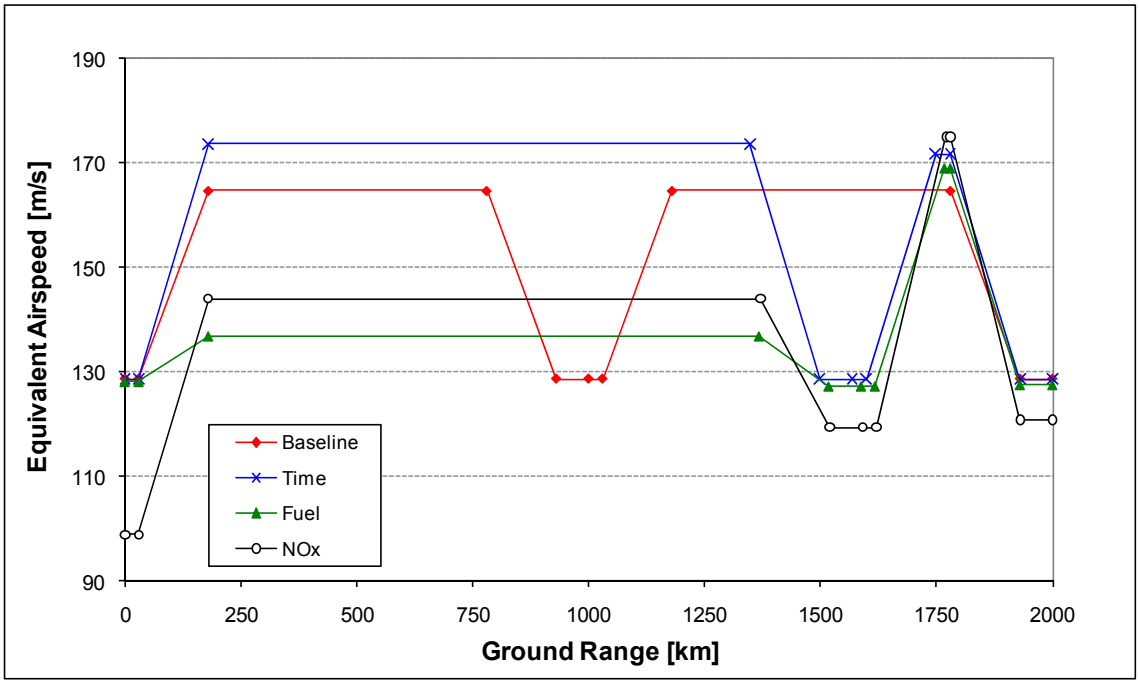


Figure 6-61. Case Study 6 – Equivalent airspeed (EAS)

It was indicated before in this chapter that, during the optimisation processes, a compromise between aircraft flight altitude and speed, which directly affect the changes in the aircraft mass, is achieved at some stage, and the result of this compromise is characterised by the fuel optimised trajectories determined. Thus, Figure 6-63 illustrates

the fuel burned associated with one of these compromised trajectories (i.e., fuel optimised trajectory), as well as the other two optimum trajectories computed in this last case study. In this figure it is interesting to note that the fuel optimised trajectory proposes a second segment affording a greater fuel burn (relative to the baseline) in order to gain height which, then, originates a fuel burn in segment 3 such that summing this amount to the fuel burned in segment 8 produces an overall lower fuel burn (see Figure 6-56).

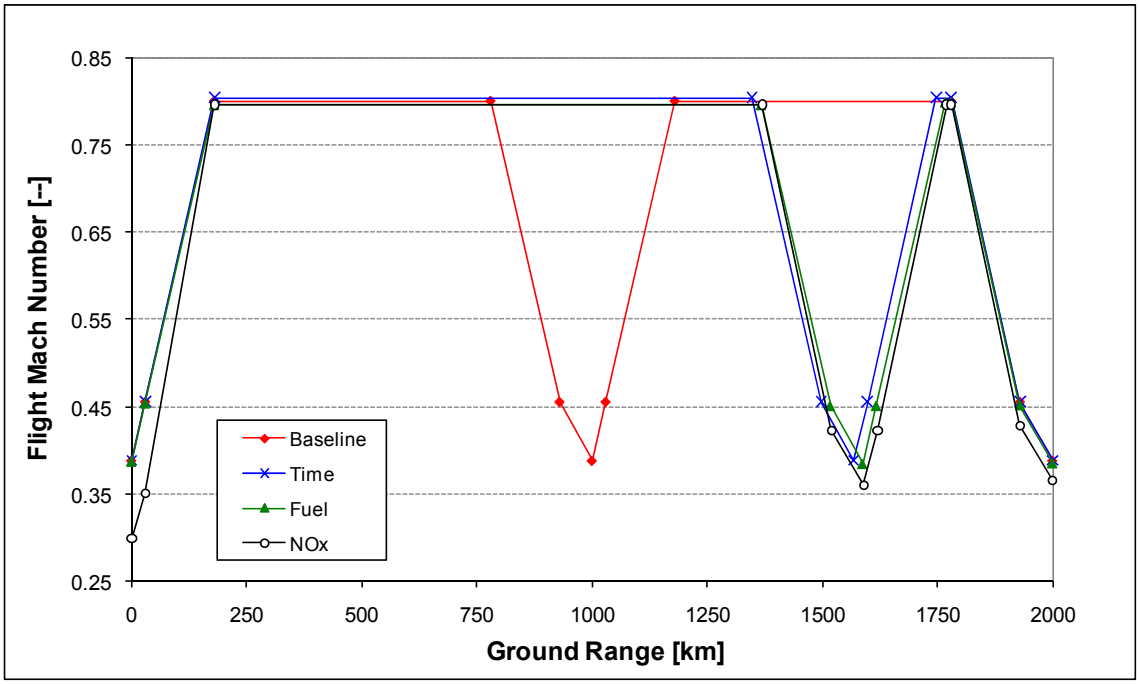


Figure 6-62. Case Study 6 – Flight Mach number

Similar to the fuel optimised trajectory, the flight profile optimised for minimum $NO_x$ emissions is flown mostly slower and higher than the baseline trajectory utilised (Figure 6-53 and Figure 6-60). In general terms, these relative lower speeds and higher altitudes utilised to fly the $NO_x$ emissions optimised trajectory result in reductions in the thrust required to fly the trajectory segments. These lower requirements in engine thrust are, in turn, translated into lower engine TET values (Figure 6-64) and, consequently, into lower levels of $NO_x$ emissions. In Figure 6-64 it is also possible to see that almost all TET values associated with the $NO_x$ emissions optimised trajectory are lower than those TET values corresponding to the baseline trajectory. This is expected, naturally, because TET directly influences the level of $NO_x$ emissions produced by gas turbine combustors.

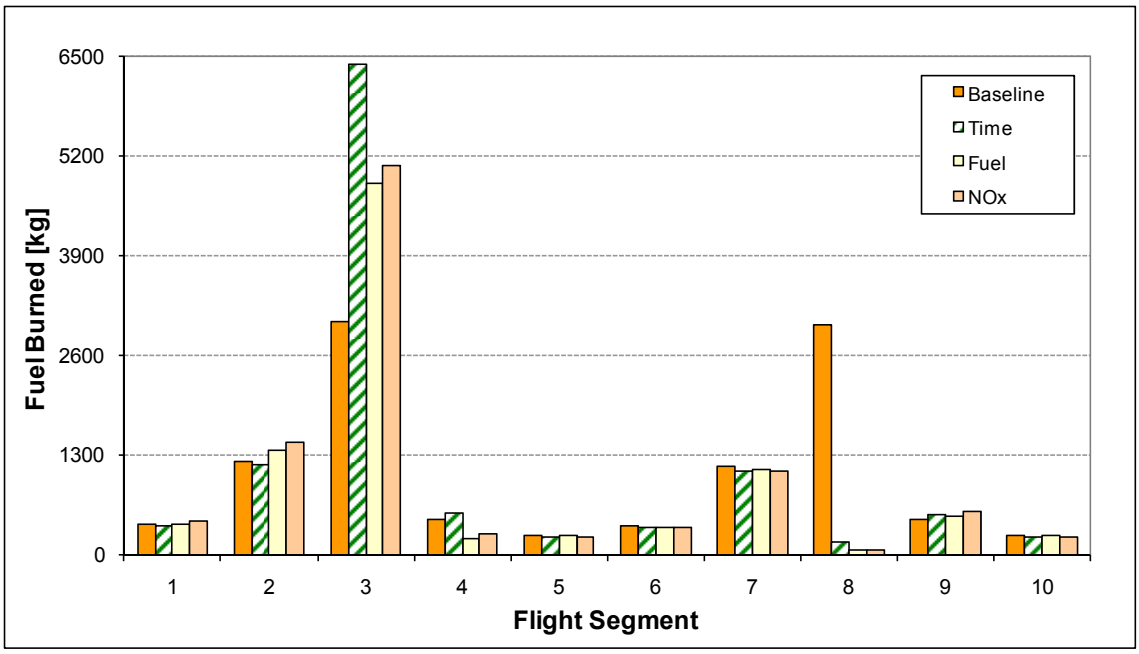


Figure 6-63. Case Study 6 – Fuel burned at each flight segment (segments – climb: 1,2,6,7; cruise: 3,8; descent: 4,5,9,10)

Figure 6-65 shows in turn a comparison of the main results associated with the three optimum trajectories analysed in this last case study. Once again, it is possible to see in this figure that the variations in $CO_2$ and $H_2O$ (species in chemical equilibrium) are directly proportional to the variations in the amount of fuel burned. Figure 6-65 also shows that even though the $NO_x$ emissions optimised trajectory increases the total flight time, as a consequence of the lower engine thrust settings utilised to fly this trajectory, the total amount of fuel burned is also reduced. Similar to other case studies analysed before, Figure 6-65 shows that the flight time optimised trajectory produce a relatively high increase in the amount of $NO_x$ emitted. This result is related to both the increase in the total fuel burned, and the relatively high TET values (Figure 6-64) used to fly this trajectory.

The results described in this last case study highlighted the fact that it is better (in terms of flight time, fuel burned, and $NO_x$ emitted) to fly the original aircraft trajectory without any stop (for refuelling) than using an intermediate one. However, the objective of this exercise was to determine the optimum distance, according to given criteria, between this intermediate stop and the initial or final point of the original trajectory. Obviously, the optimisation processes did not produce the results initially expected. It is

believed that one of the main reasons relates to way in which the initial aircraft weight was defined in this case study.

In this particular case, it was assumed that the initial fuel on board (i.e., fuel at the beginning of the original trajectory) was enough for flying from point A to point B (start and end points of original trajectory) regardless of the location of the intermediate stop point. It means that the initial aircraft weight was always constant at point A. Since the main reason for having this intermediate point is for refuelling purposes (i.e., the initial fuel on board is not enough for flying the whole original trajectory), it is recognised that the approach utilised in this particular case was not entirely realistic. Even so the results obtained in this case study are useful since they allow the illustration of other uses of Polyphemus, which was the main objective of this case study. These results also open a door for deeper analyses to be carried out in future. Consequently, further work should include the consideration of an initial fuel on board that varies proportionally to the distance to be flown. This is not a trivial task, however, once the fuel to be burned is initially unknown; and, in some situations, this is an optimisation parameter. A simple approach would involve the use of iterative processes; but of course it might considerably increase the computational time.

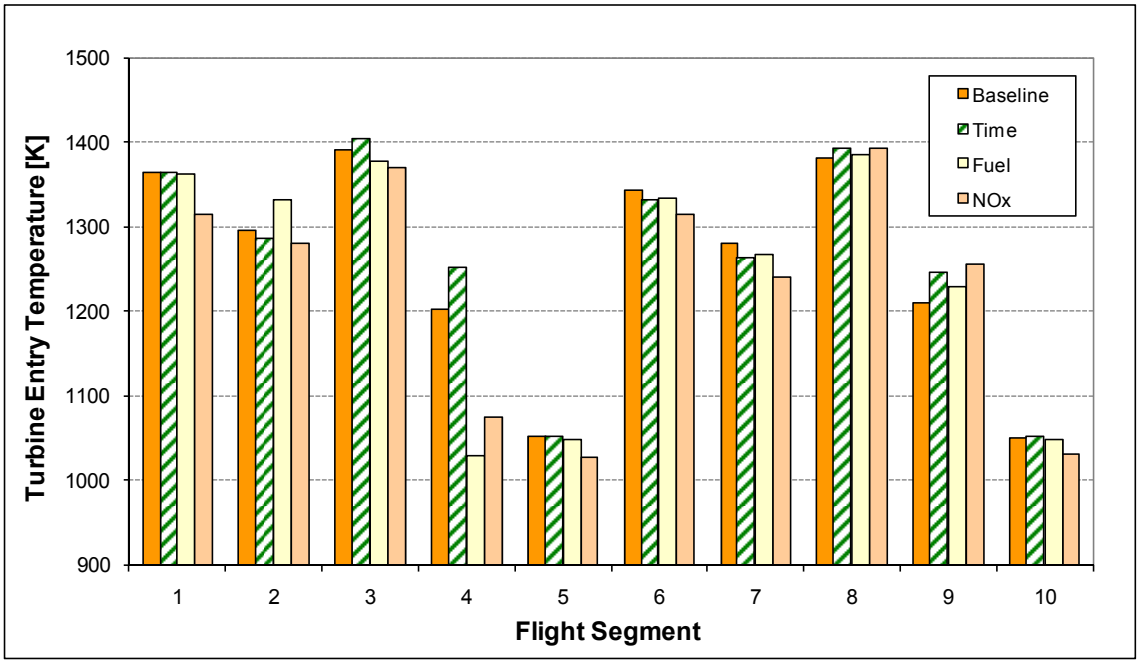


Figure 6-64. Case Study 6 – TET at each flight segment (segments – climb: 1,2,6,7; cruise: 3,8; descent: 4,5,9,10)

This case study involving the optimisation of the range of one segment of a given aircraft trajectory constitutes the last case study analysed in this chapter. It completes the set of case studies analysed in this work as part of the optimisation of aircraft propulsion systems from an operational point of view. The following chapter will involve the description of cases studies related, again, to the optimisation of aircraft propulsion systems, but this time from the point of view of their preliminary design. Engine cycle optimisation-type processes will be thus carried out and their main results presented and discussed.

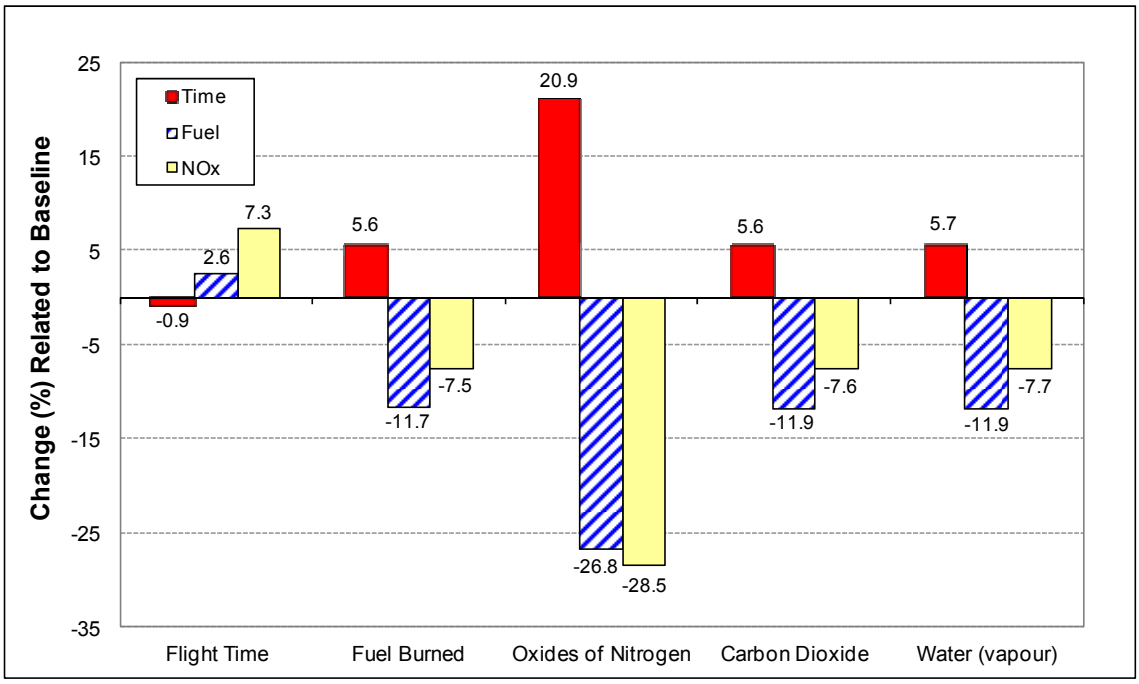


Figure 6-65. Case Study 6 – Optimum trajectories results (relative to baseline)

# 7 Evaluation and Optimisation of Propulsion Systems Part B: Engine Cycle Optimisation

The second part of the main results obtained from the processes of evaluation and optimisation of environmentally friendly aircraft propulsion systems is detailed in this chapter. Initially, general considerations about the different cases studies analysed are briefly highlighted. Aircraft propulsion systems are then optimised from the propulsion system design point of view. More specifically, aircraft engine cycle optimisation-type processes are carried out for a fixed aircraft flight profile (i.e., aircraft trajectory). The main results of these optimisation processes are subsequently presented and discussed.

## 7.1 General Considerations

Reducing the impact of commercial aviation on the environment through the introduction of new (mostly innovative) aircraft/engine configurations constitutes an alternative for medium and long term. This is because the timescale from new aircraft/engine concepts to be brought to operational readiness is a lengthy one. Even so it is worth pursuing these avenues because both these technologies are more likely to produce more drastic reductions in the environmental impact of commercial aircraft operations, and they allow the growth of this industry in a sustainable manner. In the particular case of aircraft engines, one of the very first stages of the analysis of new engine concepts involves the engine preliminary design. In this stage, based on the engine requirements (in terms of thrust, size, weight, performance, etc.), an initial estimation of the main parameters that characterise a new engine design is carried out. This initial estimation of the parameters characterising the design is directly linked to the operating conditions of the working fluid (i.e., pressures, temperatures, mass flow rates, etc.) at the engine design point condition. In other words, the thermodynamic cycle (and its associated processes) under which the engine operates has a large influence on the definition of the configuration of the new designed engine.

Thus, in the beginning of the engine design process the designer has essentially two options of path to follow. First, the designer can use a conventional design approach and find engine parameters (including those main ones that characterise the engine cycle) that allow the design of an engine which merely satisfies its requirements; or, second, due to the fact that often there will be more than one acceptable design, the designer can try to determine the best of the many acceptable designs available. Obviously, the determination of the best design involves an optimisation process. This is exactly the type of processes that have been performed in this research project. Accordingly, in this work engine cycle optimisation-type processes have been carried out as an attempt to both illustrate other uses of Polyphemus, and comply with one of the objectives of this work initially proposed, rather than determine optimum engine cycles which accurately represent real engines utilised in practical applications. The following sections briefly describe, among others, the optimisation strategy utilised as well as the main parameters used as design variables, constraints, and optimisation criteria during the optimisation processes. All optimisation processes carried out included these parameters unless otherwise explicitly indicated when describing the specific case studies analysed.

### 7.1.1 Optimisation Strategy

In general, two broad optimisation strategies can be adopted for the optimisation of the preliminary design of aircraft/engine configurations. First, both the aircraft/engine configuration and its associated flight profile (flight trajectory) can be optimised simultaneously. In this approach, the optimisation of the flight profile is usually treated as a sub-optimisation process. In other words, during the optimisation process, for each aircraft/engine configuration evaluated (potential optimum design) an optimum flight profile according to a given criterion (or given criteria) is determined. Depending on several aspects such as the fidelity of the computational models utilised in the optimisation process (for the simulation of different aircraft/engine disciplines including aerodynamics, performance, weight, emissions, cost, etc.), the type of optimisation technique utilised, the complexity involved in the definition of the optimisation problem (in terms of design variables, constraints, and performance parameters), and the level of

discretisation of the flight profile, among others, the determination of an optimum design following this optimisation strategy can involve a huge computational time. However, due to the simultaneous optimisation of both the aircraft/engine configuration and the flight trajectory, this approach allows the production of more representative results than the second simplified approach described next.

As mentioned above, the second optimisation strategy constitutes a simplification of the first one and involves the optimisation of the aircraft/engine configuration considering that the aircraft flight profile is fixed. The main advantage of this second approach relates to fact that it greatly reduces the computational time involved in the optimisation process. As expected, this reduction in the computational time is directly proportional to the same aspects indicated previously such as fidelity of the computational models, optimisation technique type, trajectory optimisation problem complexity, and flight profile discretisation level, among others. In the engine cycle optimisation-type processes performed in this work, this second optimisation strategy was utilised. The main reason behind this choice is associated with the fact that natural limitations in computational time were present during the development of this work. This was supported by the fact that optimum trajectories (for a fixed aircraft/engine configuration) had already been determined (as described in Chapter 6), and it was not the purpose of the case studies analysed in this chapter to optimise other aircraft trajectories.

The main parameters characterising the aircraft trajectory utilised in the optimisation processes described in this chapter are highlighted in Table 7-1. This aircraft trajectory corresponds to the three-objective (flight time, fuel burned, and $NO_x$ emitted) optimised trajectory obtained from the multi-objective optimisation processes carried out in the fifth case study analysed in the previous chapter (Chapter 6). The referred trajectory has been considered fixed and has been used as the baseline trajectory for performing the engine cycle optimisation-type processes described in this chapter. The following sections outline the main features of the optimisation problem analysed in this chapter through a description of the parameters utilised as design variables, constraints, and optimisation criteria during the optimisation processes performed.

Table 7-1. Fixed aircraft trajectory – Characteristic parameters

| Seg. No. | $h_i$ [m] | $h_f$ [m] | $M_i$ [--] | $M_f$ [--] | $EAS_i$ [m/s] | $EAS_f$ [m/s] | R [km] |
|---|---|---|---|---|---|---|---|
| 1 | 457 | 3048 | -- | -- | 124.5 | 124.5 | 20 |
| 2 | 3048 | 3606 | -- | -- | 124.5 | 134.1 | 10 |
| 3 | 3606 | 10411 | -- | -- | 134.1 | 134.1 | 160 |
| 4 | 10411 | 10411 | 0.80 | 0.80 | -- | -- | 230 |
| 5 | 10411 | 10411 | 0.80 | 0.80 | -- | -- | 230 |
| 6 | 10411 | 3659 | -- | -- | 134.1 | 134.1 | 140 |
| 7 | 3659 | 3048 | -- | -- | 134.1 | 128.6 | 20 |
| 8 | 3048 | 457 | -- | -- | 128.6 | 128.6 | 70 |

### 7.1.2 Computational Models

For carrying out the engine cycle optimisation-type processes described in this chapter the same computational models used for optimising aircraft trajectories (Chapter 6) have been utilised. This means that the same three computational models schematically represented in Figure 6-8, i.e., aircraft performance simulation model (APM), engine performance simulation model (TurboMatch), and emissions prediction model (Hephaestus), have been also used in this particular case. The main difference relates to the fact that, instead of determining characteristic parameters of aircraft trajectories that are optimum according to given criteria; in the case studies described in this chapter, the main parameters that characterise optimum (according to given optimisation criteria) engine cycles have been determined.

### 7.1.3 Design Variables

In the engine cycle optimisation-type processes carried out in this work, and whose main results are summarised in this chapter, the following cycle parameters have been utilised as main design variables: overall pressure ratio (OPR), bypass ratio (BPR), and turbine entry temperature (TET). These cycle parameters were chosen because they characterise the design of any turbofan engine – the particular type of engine (cycle) optimised in this work. In the optimisation processes, however, OPR was not directly used as a design variable. Instead, it was represented by the other three parameters that

characterise OPR in two-spool or three-spool (turbofan) engines: fan pressure ratio (FPR), booster or intermediate pressure compressor pressure ratio (IPCPR), and high pressure compressor pressure ratio (HPCPR).

Top of climb (TOC) has been utilised in this work as the design point (DP) condition of the engines. Consequently, due to the aircraft trajectory flight phase involving take off (TO) was not included in the analyses carried out, an additional design variable, TET at TO, was utilised in the optimisation processes. This last design variable was included in order to estimate parameters (detailed in the following section) which will allow determining whether (or not) a given engine design satisfies the engine requirements at TO (off design, OD) conditions. Table 7-2 summarises then the design variables (and their corresponding engine condition) utilised in the different case studies analysed in this work, unless otherwise explicitly indicated.

Table 7-2. Summary of design variables

| No. | Design Variable | Engine Condition |
|---|---|---|
| 1 | FPR | DP |
| 2 | IPCPR | DP |
| 3 | HPCPR | DP |
| 4 | BPR | DP |
| 5 | TET | DP |
| 6 | TET | TO |

### 7.1.4 Implicit Constraints

In the different engine cycle optimisation-type processes performed in this work, the following implicit constraints were imposed:

- Thrust Ratio (TR) – The ratio of TO thrust to cruise (TOC in this case) thrust. TR is usually a requirement dictated by the airframe on which the engine is installed [89]. Even so, in practice some adjustment in TO thrust is possible as TO field length varies. Once the aircraft trajectory utilised in the optimisation processes did not include the TO phase, it was necessary to use this parameter as a constraint in order to guarantee that an optimised engine is able to provide the required engine thrust at TO. Thus, in the

computations, a lower limit for the TR of 4.5 was utilised. This value reflects the performance of a typical turbofan powering a mid-sized, single-aisle, twin turbofan airliner (MTOW ≈ 72,000kg) and delivering thrust levels of about 25kN at TOC and 112.5kN at TO.

- Compressor Delivery Temperature (CDT) at TO (CDTTO) – This constraint reflects the level of technology, in terms of material capability, of the last stages of the HPC. This is one of the main limiters to the level of OPR that can be achieved in conventional turbofan engines. Excessive values of CDTTO would require the use of especial materials for the disc and blades of the HPC rear stages (which could increase the engine weight). Additionally, they could also cause cooling problems due to the high temperatures of the cooling flows used for cooling the high pressure turbine (HPT) components. In the optimisation processes carried out in this work, an upper limit for the CDTTO of 950K was considered.
- Blade Height of the last stage of the high pressure compressor (HPC) at TO (HBLTO) – Because of some limitations in the aircraft performance model utilised, constant overall engine/nacelle dimensions were considered during the optimisation processes. This was made possible through the use of a fixed overall (engine) inlet mass flow rate at DP. Thus, high values of OPR and BPR will require eventually small blades at the rear of the HPC, which are known to be characterised by high aerodynamic losses because of the low Reynolds numbers, and the comparatively thick boundary layers on the annulus walls and high tip clearances [89]. In addition, because of their size, small blades may present manufacturing problems. Consequently, it was necessary to constraint the HBLTO values. In this work, this parameter was estimated assuming a flow Mach number (0.3) and a compressor hub/tip ratio (0.9) at the HPC delivery section, and making use of the "swallowing function", Eq. (7-1) [126], which for an isentropic flow and a given gas is dependent only on the flow Mach number. In Eq. (7-1), W represents the mass flow rate, T the temperature, P the pressure, A the flow area, M the flow Mach number, R the specific gas constant, and $\gamma$ the ratio of specific

heats of the gas. In the computations, a lower limit for the HBLTO of 15mm was utilised.

$$\frac{W\sqrt{T}}{AP} = M\sqrt{\frac{\gamma}{R}}\left\{1 + \frac{\gamma - 1}{2}M^2\right\}^{\frac{-(\gamma+1)}{2(\gamma-1)}} \tag{7-1}$$

Table 7-3 summarises the general implicit constraints used in the different engine cycle optimisation-type processes carried out in this work, unless otherwise explicitly indicated. In this last case, a proper explanation of the additional constraints utilised will be provided.

Table 7-3. Summary of implicit constraints

| No. | Implicit Constraint | Limit |
|---|---|---|
| 1 | TR | ≥ 4.5 |
| 2 | CDTTO | ≤ 950K |
| 3 | HBLTO | ≥ 15mm |

According to these generic implicit constraints, the fact that the aircraft is able to fly the reference flight trajectory using a given engine design is the only criterion determining (internally) the validity of that design. Consequently, it is recognised that some variations in net thrust at DP and/or TO could exist as a result of the optimisation processes. However, considering the main purpose of the engine cycle optimisation-type processes performed in this work, it does not constitute a critical aspect. It is worth emphasising that these parameters (i.e., net thrust at DP and/or TO) were not initially constrained mainly because of the gradual approach, in terms of addition of complexities (e.g., number of implicit constraints), followed in this work.

### 7.1.5 Performance Parameters

Performance parameters are those parameters used for establishing the criterion (or criteria) of comparison of several acceptable designs which ultimately allows the determination and/or selection of the best design from many acceptable ones. As indicated previously, this criterion, with respect to which the design is optimised, when expressed as a function of the design variables, is known as the criterion or merit or

objective function. Due to some limitations in the optimisation algorithms utilised in this work when dealing with multi-objective optimisation problems, only single-objective engine cycle optimisation-type processes were carried out and their results summarised in this chapter. This means that in the optimisation processes only single-objective functions were utilised. Since they have a direct influence on the environmental impact of commercial aircraft operations, two of the three objective functions utilised in this case, fuel burned and $NO_x$ emitted, were the same as in the case of the optimisation of aircraft trajectories (Chapter 6). The third objective function involved the specific fuel consumption (SFC) in cruise (Cruise SFC), which was computed averaging the SFC corresponding to segments 4 and 5 considered as cruise in the reference aircraft trajectory utilised (c.f., Table 7-1). As expected, in this case it was not possible to use the flight time as an objective function once the aircraft trajectory and flight speeds were fixed, i.e., constant flight time. Based on these considerations, several optimum engine cycles minimising separately these three objective functions, cruise SFC, fuel burned, and $NO_x$ emitted, were determined and the main results are summarised in the case studies described in the following sections.

## 7.2 Engine Cycle Optimisation Case Studies

This section summarises through the use of case studies the main results obtained from the different engine cycle optimisation-type processes performed using the Polyphemus optimiser. In all case studies analysed it has been considered that the aircraft flight profile is fixed. As described in the previous section, the main design variables utilised involved characteristic parameters associated with the thermodynamic cycle of aircraft engines. The minimisation of cruise SFC, fuel burned, and $NO_x$ emitted were considered as the objective functions. The methodology followed in terms of sequence of computations for optimising a given engine cycle was similar to the corresponding one used for optimising aircraft trajectories.

### 7.2.1
### Summary of Case Studies

It is relevant to note that the main objective of the engine cycle optimisation-type processes carried out in this work was the illustration of other uses of Polyphemus, rather than the determination of optimum engine cycles which accurately represent real engines utilised in practical applications. Thus, simplifications have been introduced into all optimisation processes not only when defining the aircraft flight trajectory (e.g., small number of trajectory segments, limited number of flight phases, standard atmospheric conditions, etc.), but also when modelling the different engine configurations (e.g., constant nacelle/engine dimensions and weight, limited number of map of characteristics for compressors and turbines, simplified algorithms for pollutant formation, etc.). Consequently, when analysing the results obtained from the optimisation processes, it is considered that general trends are more reliable than absolute values.

In the engine cycle optimisation-type processes performed, the following main hypotheses were utilised:

- Atmospheric conditions correspond to ISA conditions.
- Aircraft flight altitudes and speeds are constant at each flight segment, i.e., aircraft flight profile is fixed.
- Aircraft configuration (dimensions, weight, etc.) is fixed. In other words, the aircraft is not resized during the optimisation processes. This hypothesis is mainly based on the fact that the aircraft performance model utilised can handle only fixed aircraft/engine configurations.
- Aircraft engine (nacelle + engine) dimensions and weight remain constant during the optimisation processes regardless of the variations in the engine thermodynamic cycle characteristic parameters. This was hypothesised partially because engine weight models were not used in this work
- Total aircraft weight (aircraft empty weight + engine weight + fuel on-board) at the beginning of the flight profile is constant. It implies that fuel on-board is enough for flying the flight profile using any engine design. This hypothesis avoids the use of iterative processes during the optimisation of the engine cycles.

Accordingly, three different cases studies, each of them involving the optimisation of a given aircraft engine cycle, were separately analysed. A brief description of these case studies is presented below:

- *Case Study 1: Two-Spool Turbofan Optimisation.* In the first case study, engine cycle optimisation-type processes involving a two-spool turbofan engine with separate exhausts were carried out. The two-spool engine optimised corresponded to the same aircraft engine utilised for performing the aircraft trajectory optimisation processes described in the previous chapter. The parameters used as design variables and (implicit) constraints in this case corresponded to the same generic ones described in Section 7.1.
- *Case Study 2: Three-Spool Turbofan Optimisation.* Optimisation-type processes involving a three-spool turbofan engine cycle with separate exhausts were performed in the second case study. DP and TO conditions corresponded to the same conditions utilised as such in the first case study. The three-spool baseline engine was designed by matching the engine model performance with the performance of the (two-spool) engine used as baseline in the first case study. The design variables and (implicit) constraints utilised were also the same generic ones described in Section 7.1.
- *Case Study 3: Intercooled Recuperated Turbofan Optimisation.* In the third and last case study, the thermodynamic cycle of an intercooled recuperated two-spool turbofan engine with separate exhausts was optimised. DP and TO conditions in this case also corresponded to the same conditions used as such in the first case study. The intercooled recuperated baseline engine was designed by matching the engine model performance with the performance of the first case study baseline engine. Besides the generic design variables and (implicit) constraints described in Section 7.1, and additional constraint, i.e., net thrust at DP, was imposed in this case.

In addition to the optimisation processes performed as part of the case studies mentioned above, in order to compare the three engine cycles analysed in these case studies, other optimisation processes were carried out. In these processes, in order to allow a fairer comparison among the engine cycles, additional implicit constraints were

imposed when required. These constraints related to the net thrust at DP and TO. The main results obtained from this comparison process are presented and discussed in the last section of this chapter.

## 7.2.2
## Case Study 1: Two-Spool Turbofan Optimisation

### 7.2.2.1
### General Description

The first case study analysed in this work related to engine cycle optimisation-type processes involved the optimisation of a two-spool turbofan engine with separate exhausts (Figure 7-1). Table 7-4 details the main parameters characterising the two-spool engine used as the reference (baseline) engine in this first case study. In this table, W represents the overall (engine) inlet (air) mass flow rate. This two-spool engine corresponds to the same aircraft engine utilised for performing the aircraft trajectory optimisation processes described in the previous chapter.

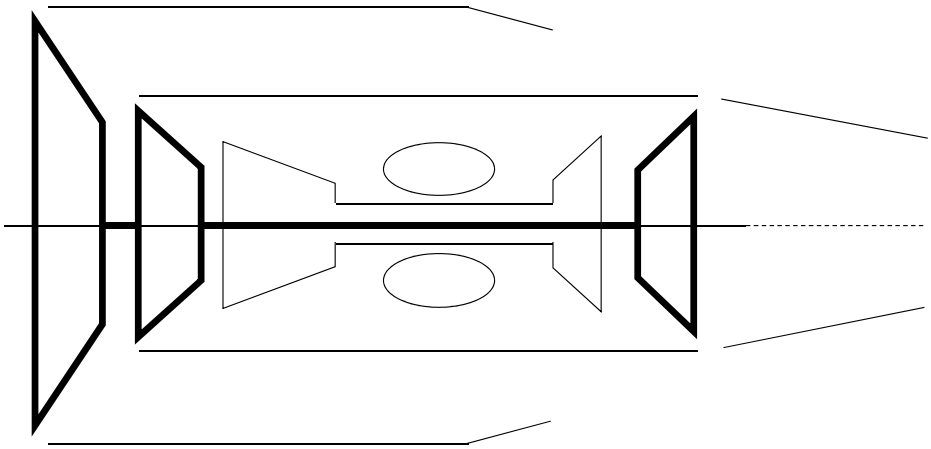

Figure 7-1. Case Study 1 – Schematic of a two-spool (turbofan) engine with separate exhausts

In Table 7-4 it is possible to observe that the engine condition used as DP condition corresponded to TOC (10,668m [35,000ft], M0.8, ISA), implying in this way that TO (Sea Level [S/L], M0.0, ISA+30°C) was treated as an OD engine condition. For the design of this baseline engine (Table 7-4), an iterative process involving engine simulations at DP and OD point conditions was utilised in order to match the performance of the model with data obtained from the public domain for an aircraft engine (high BPR, two spool turbofan engine with separate exhausts) used in similar

applications. When necessary, educated guesses were made for some characteristic parameters (component efficiencies, bleeding flows, pressure losses, etc.), which were required for the modelling of the engine.

The design variables and (implicit) constraints utilised in this first case study, as well as their ranges of permissible values considered, are detailed in Table 7-5. As it can be observed in this table, these parameters are the same generic ones described as design variables and (implicit) constraints in the general considerations section preceding these case studies. In Table 7-5, a double hyphen representing a given parameter limit (lower or upper bound) indicates that this limit has not been considered in the optimisation processes.

Table 7-4. Case Study 1 – Baseline engine characteristic parameters

| DP: TOC (10,668m [35,000ft], M0.8, ISA) | | |
|---|---|---|
| Parameter | Unit | Value |
| W | [kg/s] | 180.0 |
| BPR | [--] | 5.46 |
| FPR | [--] | 1.80 |
| IPCPR | [--] | 1.81 |
| HPCPR | [--] | 10.0 |
| OPR | [--] | 32.6 |
| TET | [K] | 1340 |
| FN | [kN] | 25.1 |
| SFC | [mg/Ns] | 17.0 |
| OD: TO (S/L , M0.0, ISA+30°C) | | |
| Parameter | Unit | Value |
| TET TO | [K] | 1600 |
| FN TO | [kN] | 121.4 |

Finally, it is important to highlight that in order to take into account the state of the art associated with the design of the main components of aircraft engines, namely compressors and turbines, appropriate component efficiencies which attempt to reflect the current level of technology in this field have been assumed. These component efficiencies at DP remained constant during all optimisation processes performed. The polytropic efficiencies assumed were equal to: 0.93 in the particular case of the fan, 0.91 for the IPC and HPC, 0.88 for the HPT, and 0.90 for the low pressure turbine (LPT). Considering what was mentioned above, engine cycle optimisation-type processes determining optimum engine cycles which minimise cruise SFC, fuel burned,

and $NO_x$ emitted were carried out in this first case study. The following section summarises the main results obtained.

Table 7-5. Case Study 1 – Design variables and Constraints

| Parameter Type | Parameter Name | Parameter Unit | Lower Bound | Upper Bound |
|---|---|---|---|---|
| Design Variable | FPR | [--] | 1.1 | 1.9 |
| Design Variable | IPCPR | [--] | 2.0 | 5.0 |
| Design Variable | HPCPR | [--] | 5.0 | 20.0 |
| Design Variable | BPR | [--] | 2.0 | 15.0 |
| Design Variable | TET | [K] | 1200 | 1800 |
| Design Variable | TET TO | [K] | 1200 | 1900 |
| Constraint | TR | [--] | 4.5 | -- |
| Constraint | CDTTO | [K] | -- | 950 |
| Constraint | HBLTO | [mm] | 15 | -- |

#### 7.2.2.2 Results

The main parameters characterising the thermodynamic cycle of the baseline engine and those cycles associated with the optimum engines computed in this first case study are shown in Figure 7-2. These same parameters when expressed in relative terms using the characteristic parameters of the baseline engine are illustrated in Figure 7-3. Figure 7-4 shows, in turn, a comparison of the main results associated with these three optimised engines determined in this first case study. As it can be observed in this figure, the three optimum engines computed originated (relatively) significant reductions in cruise SFC (~ -8%), fuel burned (~ -7%), and $NO_x$ emitted (~ -70%). In order to have a better understanding of the nature of the optimised engines computed in this case study, a brief analysis of each of them will be presented separately next.

As it is well known, the rate of consumption of fuel in an aircraft engine is usually expressed in terms of SFC, which is defined as the engine fuel mass flow rate divided by the net thrust produced by the engine. Consequently, the minimisation of SFC (or cruise SFC in this particular case) implies, for a given net thrust, the minimisation of the fuel mass flow rate; or, for a given fuel mass flow rate, the maximisation of the engine net thrust. Consider for the sake of simplicity a turbofan with mixed exhausts whose BPR and overall inlet air mass flow rate are fixed. Consider as well that one wants to minimise the SFC of this turbofan assuming that the engine fuel mass flow rate is

constant. An increase in the OPR (by increasing only the compression system pressure ratio and keeping for simplicity the FPR constant) results then in an increase in CDT, and, consequently, in TET (fixed fuel mass flow rate). Even though this process changes the temperature ratios in the compression and turbine systems, because the addition of heat (fuel mass flow rate) remains constant, the temperature at the nozzle inlet is also constant. However, the pressure at this section (nozzle inlet) increases once the OPR increases faster than the turbine expansion ratio does. This increase in nozzle inlet pressure yields increases in the net thrust (because of the higher jet gas velocity), and consequently, reductions in the engine SFC. Similar trends can be observed in the case of turbofans with separate exhausts. Therefore, a way of reducing the SFC in turbofans involves the simultaneous increase in OPR and TET.

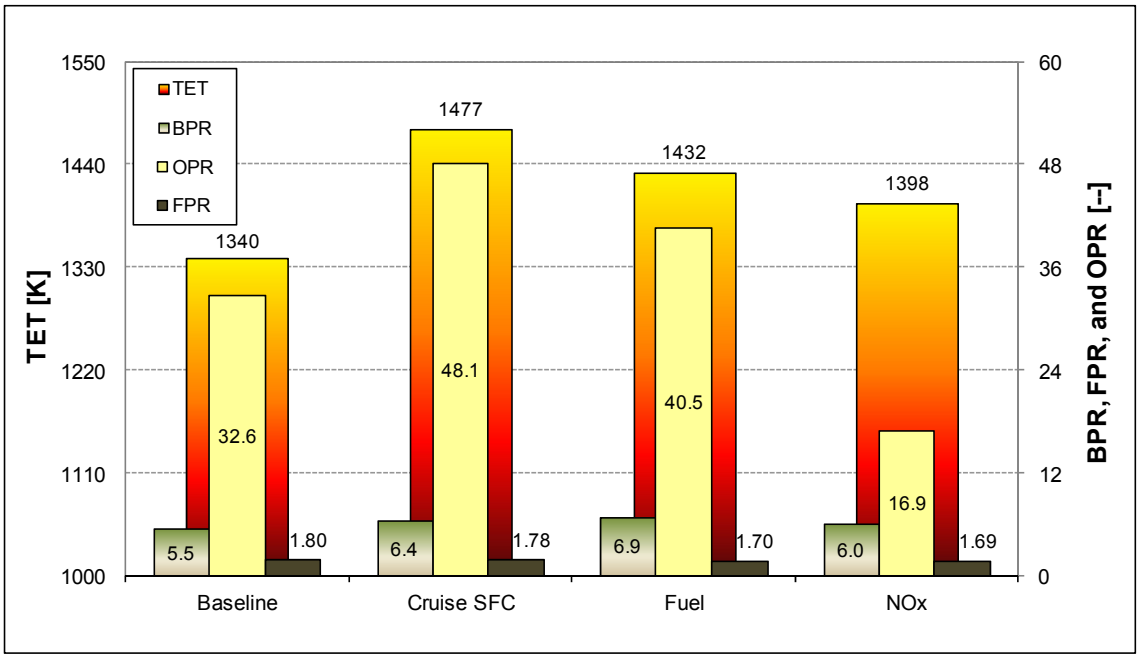


Figure 7-2. Case Study 1 – Characteristic parameters of engine cycles (baseline and optimum)

For a given aircraft speed (cruise speed for instance) and fuel type, the SFC of a turbofan engine can be also expressed as being inversely proportional to both thermal efficiency and propulsive efficiency. It means that increases in these efficiencies yield reductions in SFC. Increases in OPR and TET have a favourable effect on thermal efficiency. Thus, high values of OPR and TET improve the engine thermal efficiency, and, consequently, they reduce its SFC. This is, of course, in accordance with the analysis carried out previously for the case of a mixed turbofan.

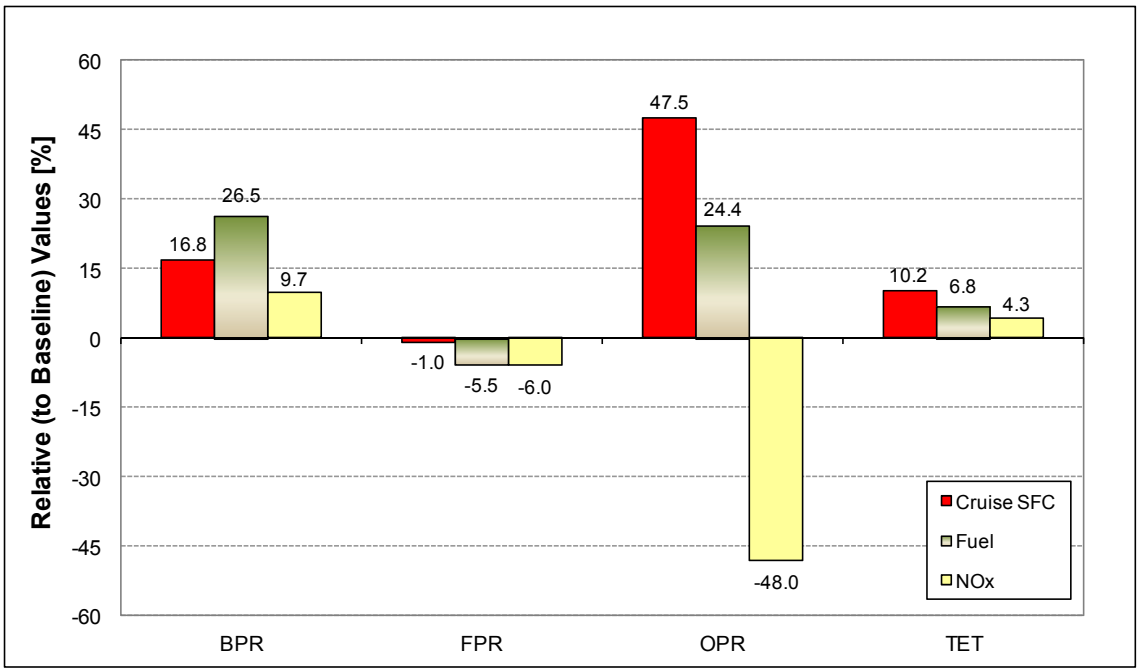


Figure 7-3. Case Study 1 – Relative (to baseline) parameters of optimum engine cycles

In the previous analysis involving a mixed turbofan, it was assumed, among others, that the engine BPR is fixed. Thus, due to that fact that for a given BPR there is an optimum FPR which minimises SFC (see reference [127] for discussion about this topic), for simplicity in the analysis, it was assumed that only the compression system pressure ratio changed. For a given OPR, however, SFC decreases with the increase in the BPR of the turbofan engine. This is originated because as BPR rises, the optimum FPR decreases, so does (in general) the jet gas velocity, yielding in this way an improvement in the engine propulsive efficiency. This increase in propulsive efficiency leads to those reductions in SFC observed as BPR increases.

In the particular turbofan engine being optimised in this case study however, the engine BPR cannot be increased indefinitely. The main reason why this cannot happen is related to the constraints imposed when defining the optimisation problem. In this case, due to fact that the overall inlet air mass flow rate is fixed, increases in BPR imply reductions in engine core mass flow rate. This is, in turn, translated into higher OPR and/or TET values to cope with the higher work required from the core flow to move the larger amount of air that bypasses the core engine. Thus, in this case – as it happens when OPR and TET are increased for better thermal efficiency – better compressor and turbine materials are required to cope with the increases in both CDT and TET. In addition, very high values of OPR and BPR will also require eventually small blades at

the rear of the HPC. Therefore, parameters such as the HBLTO need to be checked during the engine optimisation processes.

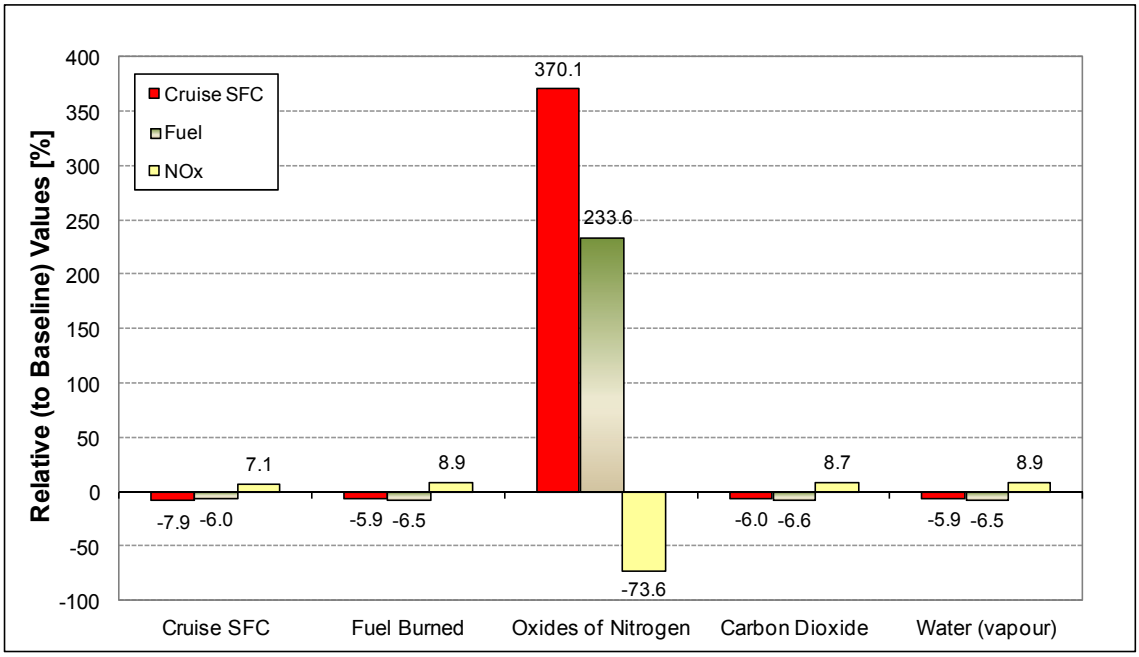


Figure 7-4. Case Study 1 – Optimum engine cycles results (relative to baseline)

Summarising what was discussed previously, the cruise SFC optimised engine is characterised by relatively high values of TET and OPR, which contribute to the improvement of the engine thermal efficiency, and, consequently, to the reduction of the engine cruise SFC. Regarding the engine BPR, the results suggest that this parameter has been increased only to an extent in which the reduced core flow can cope with the work required by the fan under conditions of maximum OPR, which seems to have been established by restrictions in the maximum value of CDT (at TO) allowed in the process. Engine TET, in turn, seems to be a compromise between increasing its value in order to augment the engine thermal efficiency and, hence, SFC; and reducing it in order to diminish the propulsive efficiency degradations, and, consequently, the increases in SFC. All these complex interactions among the main parameters characterising the thermodynamic cycle of turbofan engines yielded the results discussed above, and particularly illustrated in Figure 7-2 and Figure 7-4. For completeness, Figure 7-5 shows the SFC for each segment of the aircraft trajectory. As expected, segments 4 and 5 are among the segments with the lowest SFC values. This is an obvious result once the cruise SFC optimisation involved the minimisation of a

parameter which was computed averaging the SFC corresponding to these two segments considered as cruise in the optimisation processes.

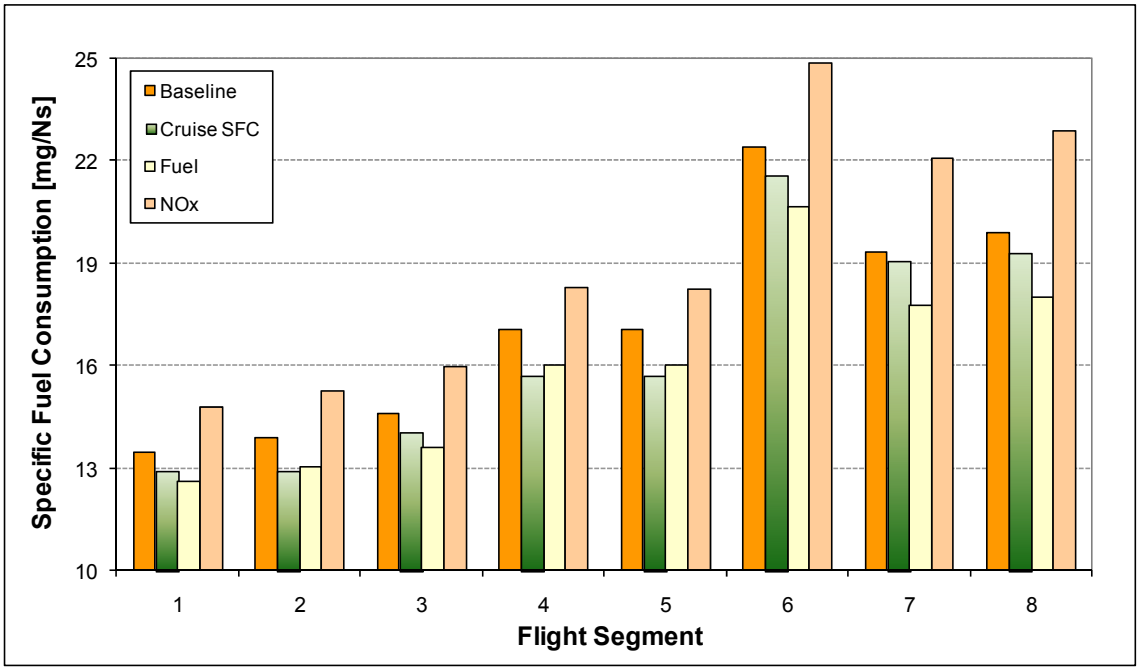


Figure 7-5. Case Study 1 – SFC at each trajectory segment

The results associated with the fuel optimised engine are similar to those ones obtained for the case in which the cruise SFC was minimised. This is expected, of course, once the objective functions are similar as well. The biggest difference between these two functions relates to the fact that, when optimising for minimum fuel burned, the SFC corresponding to all trajectory segments is minimised and not only the SFC in cruise, as it happens when optimising for minimum cruise SFC. Strictly speaking, minimisation of fuel burned implies minimisation of fuel mass flow rate (fixed aircraft speeds, and hence segment flight times). However, due to the direct relationship between SFC and fuel mass flow rate, minimisation of fuel burned can be also regarded as minimisation of SFC at all trajectory segments. Therefore, the main parameters driving the cruise SFC optimisation discussed before also play an important role when designing a turbofan engine for minimum fuel burned.

It was mentioned above that one way in which the SFC of a turbofan engine can be reduced is by increasing its BPR. It was also highlighted that the BPR cannot be indefinitely increased because it has a direct influence on the core flow, and, consequently, on the OPR and TET required for its operation in order to deliver the

work demanded by the engine fan. Thus, starting from a cruise SFC optimised engine (and using the same hypotheses utilised when analysing a mixed turbofan above), if OPR is slightly reduced, the net thrust produced by the engine also decreases slightly and the (cruise) SFC suffers a small penalty. This small decrease in OPR also results in a decrease in CDT (and HBL), and, consequently, in TET. In other words, it creates a room for increasing BPR without violating the constraints imposed on CDT (and HBL). This type of behaviour is also reflected at OD point conditions, such as TO, which is the engine condition associated with some of the main constraints imposed in this work.

The results obtained in the case of the fuel optimised engine seem to suggest what was just mentioned above. The OPR of the turbofan engine is slightly modified (reduced), which leads to a small increase in the cruise SFC; and, at the same time, the engine BPR is slightly increased, which yields improvements in the engine propulsive efficiency and SFC reductions in almost all the remaining segments of the flight trajectory. This aspect can be clearly observed in Figure 7-5, which shows that, when compared to the cruise SFC optimised engine, the engine optimised for minimum fuel burned presents a slightly higher SFC in cruise segments 4 and 5, and lower SFC in the remaining segments, except in segment 2. These results are reflected in the fuel that is burned at each flight segment, as illustrated in Figure 7-6. In this figure it is possible to see that the fuel optimised engine presents the lowest fuel consumption in all trajectory segments (except in cruise segments 4 and 5, where the cruise SFC optimised engine does), which consequently results in the lowest overall fuel burned.

As discussed in Chapter 3, $NO_x$ can be produced by four main mechanisms: thermal NO, $N_2O$ mechanism, prompt NO, and fuel NO. Depending on several factors including engine operating conditions and fuel type, one or more of these mechanisms can be more relevant than the others when determining the level of $NO_x$ emitted. Since optimisation problems involving engine cycle parameters is the main discussion topic in this chapter, the analyses are mainly focused on the engine operating conditions and their influence on the formation of $NO_x$ inside the engine combustion chamber. For the sake of brevity, only the main parameters directly or indirectly related to the engine operating conditions that affect $NO_x$ emissions are discussed. These parameters include flame temperature, combustor air inlet temperature, and combustor air inlet pressure.

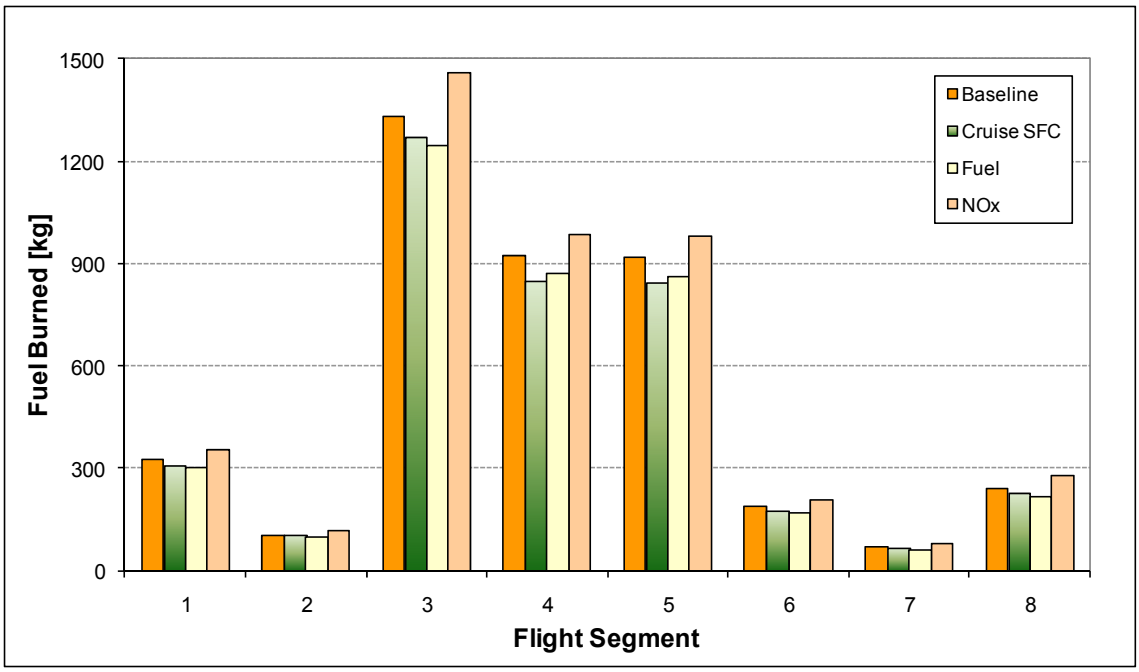


Figure 7-6. Case Study 1 – Fuel burned at each trajectory segment

$NO_x$ emissions present an exponential dependence on flame temperature [56], especially above around 1,800K, where the thermal NO mechanism is dominant. Under these circumstances, a significant amount of $NO_x$ is formed in the high temperature regions of the flame as well as in the post flame gases. Two of the main factors that affect the flame temperature are the fuel-air-ratio (FAR) and the temperature of the reactants, in particular, the combustor air inlet temperature. As FAR approaches to its stoichiometric value, the flame temperature becomes higher and higher. FAR depends, obviously, on the amount of fuel and air entering to the combustor. The amount of fuel directly influences, in turn, TET. In other words, under a given set of operating conditions, TET determines the amount of fuel required for the normal operation of the engine. In general, because of the direct influence of temperature on $NO_x$ formation, in order to reduce the level of $NO_x$ emitted, it is necessary to keep TET as low as possible.

Combustor air inlet temperature directly influences the temperature of the flame. In other words, increases in air inlet temperature produces increases in flame temperature as well. This happens because as air inlet temperature increases, the combustion efficiency also increases, and, at the same time, the surrounding air/gasses do not suck the heat out of the flame as quickly as they would do if they were at lower temperatures. This results in higher flame temperatures as air inlet temperature increases. Therefore, it is expected that increases in air inlet temperature augment

significantly the level of $NO_x$ emitted. This is confirmed by the results to be discussed later.

As literature highlights [56], the level of pressure dependence of $NO_x$ formation is related to the temperature of the flame. Thus, at relatively low temperatures in which some of the mechanisms of $NO_x$ formation such as prompt NO and $N_2O$ mechanism predominate, the level of $NO_x$ emitted is largely independent of pressure. However, at relatively high temperatures in which thermal $NO_x$ has a dominant effect, $NO_x$ formation exhibits a square root dependence on pressure. Therefore, the continuous trend toward engines of higher OPR and, consequently, lower SFC, tends to exacerbate the $NO_x$ problem (at least in conventional aircraft engines), since higher OPR results in higher combustor air inlet temperature, and consequently, higher flame temperature and $NO_x$ emissions.

Accordingly, a conventional engine optimised for minimum $NO_x$ emissions is expected to be characterised by both a relatively low (combustor) air inlet temperature (i.e., a low CDT and, consequently, a low OPR), and a relatively low (combustor) air inlet pressure (i.e., a low OPR). At the same time, the $NO_x$ optimised engine is expected to be operated using as low TET values as possible. All these aspects are confirmed by the results obtained in this first case study for the case in which the engine is optimised for minimum $NO_x$ emissions. Thus, as it can be observed in Figure 7-2, the $NO_x$ optimised engine presents the lowest OPR and TET of the three optimum engines computed. In addition, the engine BPR is slightly lower than those ones corresponding to the other two optimised engines. This allowed that the reduced OPR core flow provides the work demanded by the engine fan.

As expected, the relatively low OPR and TET characterising the $NO_x$ optimised engine worsened its SFC. This is reflected in the high values of SFC (Figure 7-5), and, consequently, fuel burned (Figure 7-6) characterising each aircraft trajectory segment. As it can be verified in Figure 7-5 and Figure 7-6, when compared to the other engines computed, the engine optimised for minimum $NO_x$ presents the highest SFC and fuel burned values at each segment of the trajectory. Even so, as illustrated in Figure 7-7, the $NO_x$ optimised engine TET values at each flight segment are the lowest ones. This, of course, translated into low $NO_x$ emissions at each flight segment, and, consequently, in the lowest overall $NO_x$ emissions characterising this optimised engine. On the contrary,

as observed in Figure 7-4, the relatively high OPR and TET values characterising the cruise SFC and fuel optimised engines produce significant increases in $NO_x$ emissions, and reductions in fuel burned.

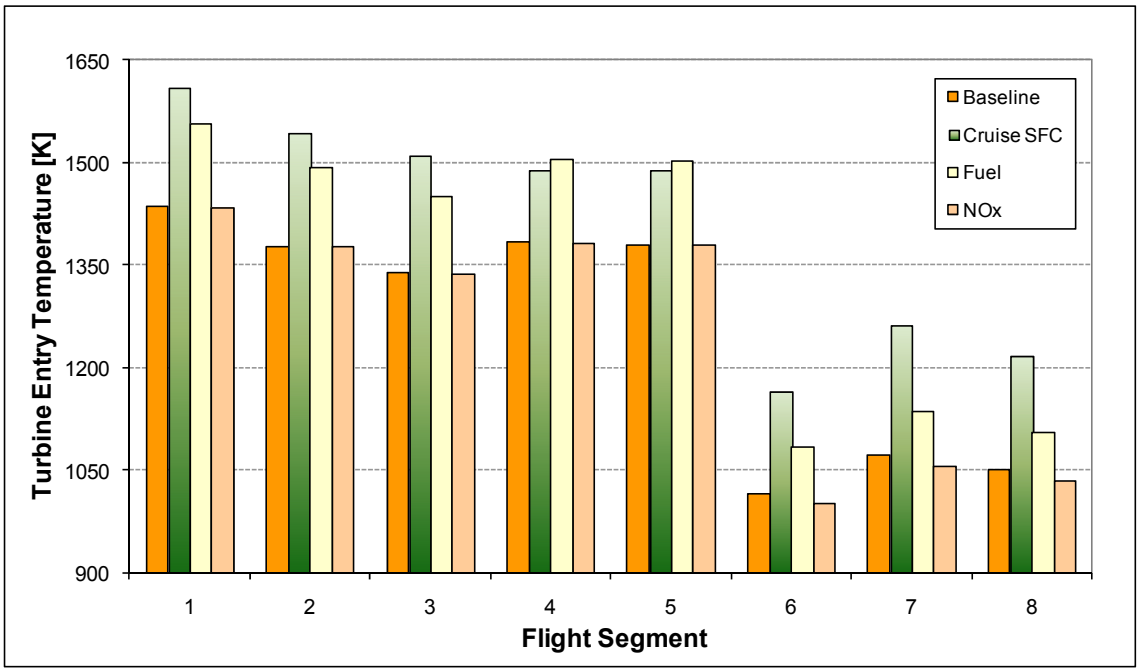


Figure 7-7. Case Study 1 – TET at each trajectory segment

Closing this first case study, Table 7-6 summarises, quantitatively, the main results associated with the three optimum engine cycles analysed in this first case study. In this table (and in the subsequent ones utilised in this chapter in order to summarise optimum engine cycles results), all parameters correspond to DP conditions. Exceptions to this rule are those parameters whose name finishes with 'TO' (e.g., CDTTO, HBLTO, etc.), which of course correspond to TO conditions. There are two aspects that it is worth highlighting in Table 7-6. The first one relates to the IPCPR and HPCPR associated with the $NO_x$ optimised engine. As observed in Table 7-6, the values of these parameters correspond to their respective minimum permissible values – lower bounds imposed as explicit constraints (design variables) during the optimisation processes. Thus, it seems that the optimisation process, in this particular case, converged when it was not possible to further reduce these pressure ratios. FPR could not have been reduced arbitrarily, of course, because of its link with BPR, and, consequently, with the thrust required to flight the aircraft trajectory. The second aspect regards to the CDTTO associated with both cruise SFC and fuel optimised engine cycles. Table 7-6 shows that

these two optimum engine cycles present CDTTO values close to the highest permissible value (950K). These results suggest that the optimisation of OPR and BPR in these engines was mainly driven by the value of the CDTTO parameter, which was implicitly constrained in all optimisation processes performed. Similar analyses to those ones carried out in this first case study will be performed in the remaining case studies described in this chapter.

Table 7-6. Case Study 1 – Summary of optimum engine cycles results

| Parameter | Unit | Baseline | Cycle Optimisation for Minimum: | | |
|---|---|---|---|---|---|
| | | | Cruise SFC | Fuel | $NO_x$ |
| FPR | [--] | 1.80 | 1.78 | 1.70 | 1.69 |
| IPCPR | [--] | 1.8 | 4.4 | 2.4 | 2.0 |
| HPCPR | [--] | 10.0 | 6.1 | 9.8 | 5.0 |
| BPR | [--] | 5.5 | 6.4 | 6.9 | 6.0 |
| TET | [K] | 1340 | 1477 | 1432 | 1398 |
| TR | [--] | 4.8 | 4.5 | 5.4 | 5.9 |
| CDTTO | [K] | 862 | 949 | 948 | 786 |
| HBLTO | [mm] | 23 | 18 | 19 | 30 |
| OPR | [--] | 32.6 | 48.1 | 40.5 | 16.9 |
| FN | [kN] | 25.1 | 26.3 | 23.9 | 27.7 |

## 7.2.3 Case Study 2: Three-Spool Turbofan Optimisation

### 7.2.3.1 General Description

The two-spool engine analysed in the first case study was an obvious choice once this aircraft engine was utilised when performing the aircraft trajectory optimisation processes described in the previous chapter. However, in order to select the other engines to be evaluated and/or optimised in this chapter, it was necessary to establish a basic criterion or criteria for carrying out this selection process. Accordingly, it was decided to analyse in the remaining case studies only some of the potential engines that could be eventually used in regional aircraft configurations similar to that one being studied in this work. Consequently, given the current hard market conditions, it seems likely that configurations usually reserved for large aircraft engines, such as three-spool configurations, will be also utilised for relatively smaller engines. Thus, in the second

case study analysed in this work, engine cycle optimisation-type processes involving the optimisation of a three-spool turbofan engine (Figure 7-8) with separate exhausts were performed. Table 7-7 details the main parameters characterising the three-spool engine used as the reference or baseline engine in this second case study. As it can be verified in this table, DP (10,668m [35,000ft], M0.8, ISA) and TO (Sea Level [S/L], M0.0, ISA+30°C) conditions in this second case study corresponded to the same conditions utilised as such in the first one.

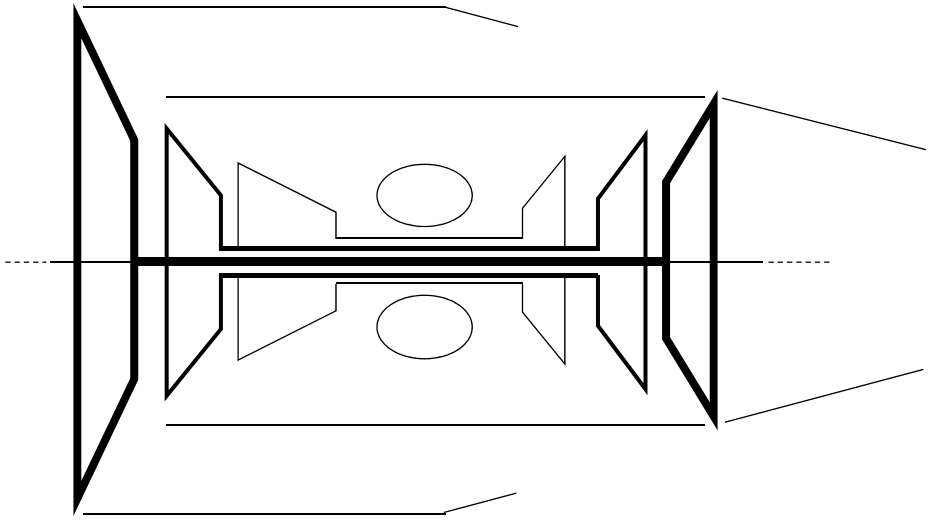

Figure 7-8. Case Study 2 – Schematic of a three-spool (turbofan) engine with separate exhausts

Table 7-7. Case Study 2 – Baseline engine characteristic parameters

| DP: TOC (10,668m [35,000ft], M0.8, ISA) | | |
|---|---|---|
| Parameter | Unit | Value |
| W | [kg/s] | 180.0 |
| BPR | [--] | 5.46 |
| FPR | [--] | 1.70 |
| IPCPR | [--] | 4.38 |
| HPCPR | [--] | 4.38 |
| OPR | [--] | 32.6 |
| TET | [K] | 1412 |
| FN | [kN] | 25.2 |
| SFC | [mg/Ns] | 17.1 |
| OD: TO (S/L , M0.0, ISA+30°C) | | |
| Parameter | Unit | Value |
| TET TO | [K] | 1655 |
| FN TO | [kN] | 121.7 |

For the design of this three-spool baseline engine (Table 7-7), an iterative process involving engine simulations at DP and OD point conditions was utilised in order to match the engine model thrust requirements with those associated with the (two-spool) engine used as baseline in the first case study. In addition, when necessary, educated guesses were made for some engine characteristic parameters required for the modelling of the engine. It is also possible to see in Table 7-7 that, due to fact that the fan and IPC may have different rotational speeds, the IPCPR and HPCPR of the designed three-spool baseline engine are similar. In addition, the values of W, BPR, and OPR are the same ones utilised for the design of the two-spool baseline engine used in the first case study.

In a similar fashion to the first case study, Table 7-8 summarises the design variables and (implicit) constraints utilised in this second case study, as well as the ranges of permissible values considered. As it can be observed in this table, these parameters are the same generic ones described as design variables and (implicit) constraints in the general considerations section preceding these case studies. In Table 7-8, a double hyphen representing a given parameter limit (lower or upper bound) indicates, as customary, that this limit has not been considered in the optimisation.

Table 7-8. Case Study 2 – Design variables and Constraints

| Parameter Type | Parameter Name | Parameter Unit | Lower Bound | Upper Bound |
|---|---|---|---|---|
| Design Variable | FPR | [--] | 1.1 | 1.9 |
| Design Variable | IPCPR | [--] | 2.0 | 15.0 |
| Design Variable | HPCPR | [--] | 2.0 | 15.0 |
| Design Variable | BPR | [--] | 2.0 | 15.0 |
| Design Variable | TET | [K] | 1200 | 1800 |
| Design Variable | TET TO | [K] | 1200 | 1900 |
| Constraint | TR | [--] | 4.5 | -- |
| Constraint | CDTTO | [K] | -- | 950 |
| Constraint | HBLTO | [mm] | 15 | -- |

One aspect to highlight in Table 7-8 relates to the ranges of permissible values associated with both IPCPR and HPCPR. As it can visualised in this table, when compared to the first case study (Table 7-5), the ranges of permissible values associated with these parameters were slightly modified in order to reflect the fact that these parameters may have similar values (i.e., similar order of magnitude). This is a

consequence of the fact that, in three-spool configurations, the engine fan and IPC usually rotate at different rotational speeds. Finally, similarly to the first case study, the polytropic efficiencies assumed in this case were equal to: fan 0.93, IPC and HPC 0.91, HPT 0.88, IPT 0.89, and LPT 0.90. Accordingly, engine cycle optimisation-type processes determining optimum engine cycles which minimise cruise SFC, fuel burned, and $NO_x$ emitted were performed in this second case study, and the following section summarises the main results obtained.

### 7.2.3.2 Results

Figure 7-9 (absolute) and Figure 7-10 (relative) illustrate the main thermodynamic cycle parameters associated with both the baseline and the optimum engines determined in this second case study. In Figure 7-11, in turn, a comparison of the main results associated with the three optimised engines computed in this case study is shown. As visualised in this last figure, the cruise SFC optimised engine yielded only an small improvement in cruise SFC (~ -1.5%), while the other two optimum engines computed originated, similarly to the two-spool case, relatively significant reductions in fuel burned (~ -8%) and $NO_x$ emitted (~ -95%).

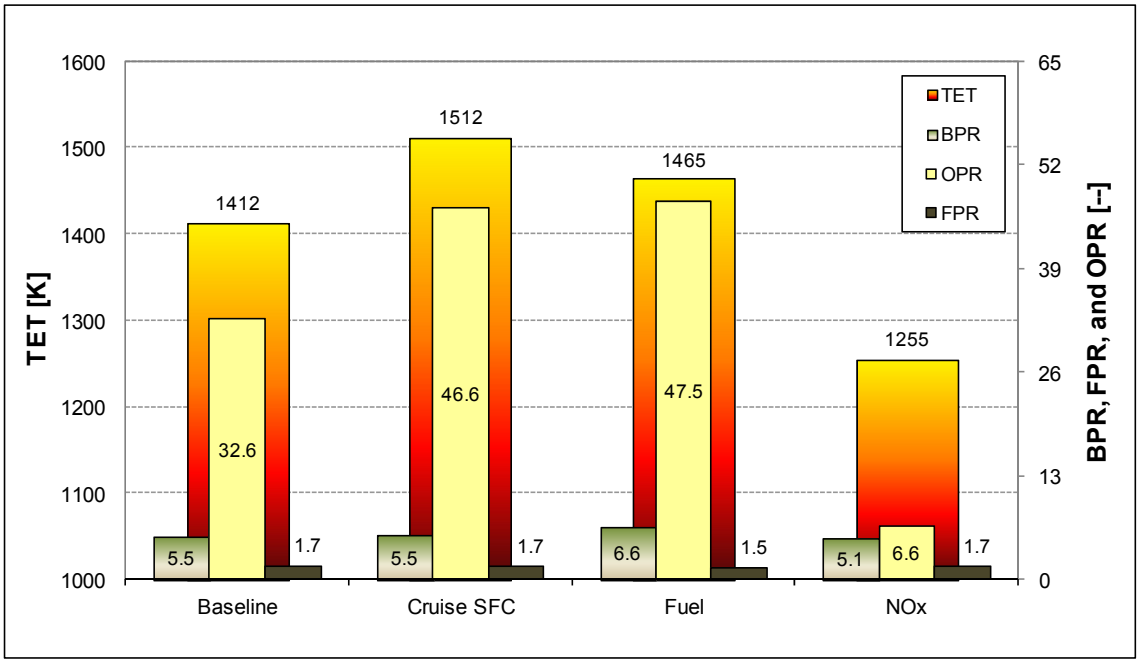


Figure 7-9. Case Study 2 – Characteristic parameters of engine cycles (baseline and optimum)

From the analyses carried in the first case study, it was concluded that high values of OPR and TET are the main characteristics of cruise SFC optimised engines. It was also indicated there that there is a tendency to increase BPR in this type of engines. However, it seemed that BPR is increased only to a point in which the reduced core flow can cope with the work required by the engine fan without violating the constraints (e.g. CDTTO, HBLTO, etc.) imposed when defining the optimisation problem. Therefore, as it happened in the first case study, the three-spool engine optimised for minimum cruise SFC is characterised by relatively high values of TET and OPR (Figure 7-9), which contribute to the improvement of the engine thermal efficiency, and, consequently, to the reduction of the engine cruise SFC. In addition, TET seems to be a compromise between increasing its value for a better thermal efficiency and, hence, a lower SFC; and reducing it in order to avoid significant reductions in propulsive efficiency, and, consequently, increases in engine SFC.

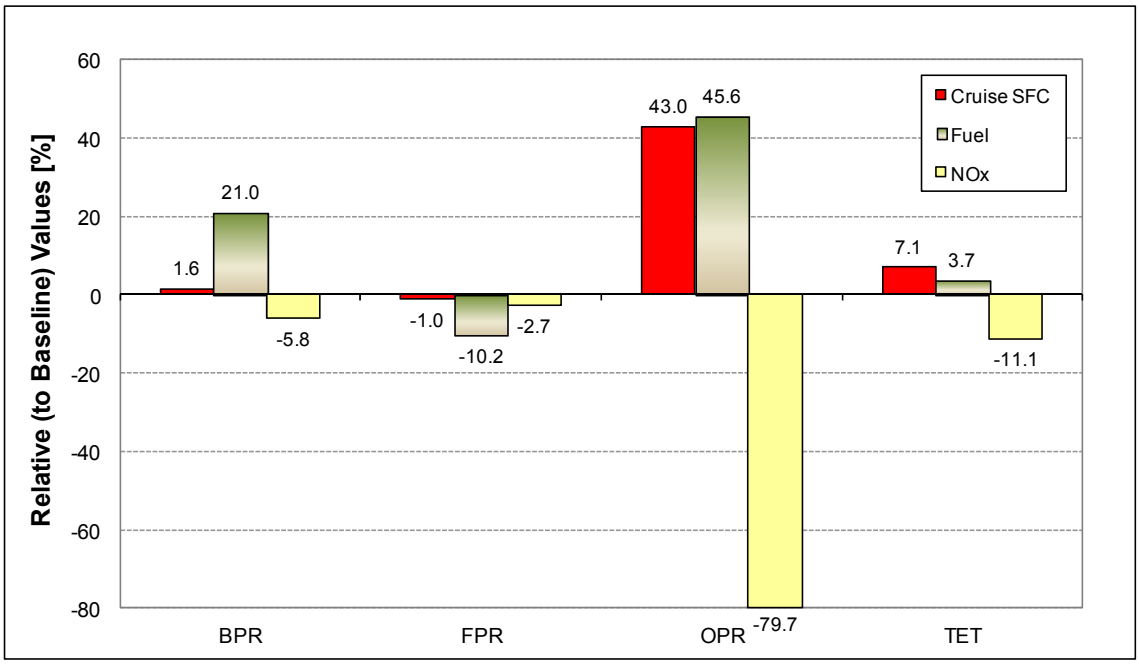


Figure 7-10. Case Study 2 – Relative (to baseline) parameters of optimum engine cycles

Because BPR increases generally lead to improvements in propulsive efficiency and, consequently, reductions in SFC, the BPR associated with the cruise SFC optimised engine is slightly higher than the baseline engine BPR (Figure 7-10). These results suggests that even though this parameter has been increased, its increase has been restricted such that the reduced core flow is able to provide the work required by

the engine fan under conditions of maximum OPR, which seems to have been established by restrictions in the maximum value of CDT (at TO conditions) allowed in the process. Similarly to the first case study, the complex interactions among the main thermodynamic cycle parameters characterising turbofan engines yielded the results obtained in this case, and particularly illustrated in Figure 7-9 and Figure 7-11. For completeness, Figure 7-12 shows the SFC for each segment of the aircraft trajectory. As expected, segments 4 and 5 (originating cruise SFC) exhibit the lowest SFC values.

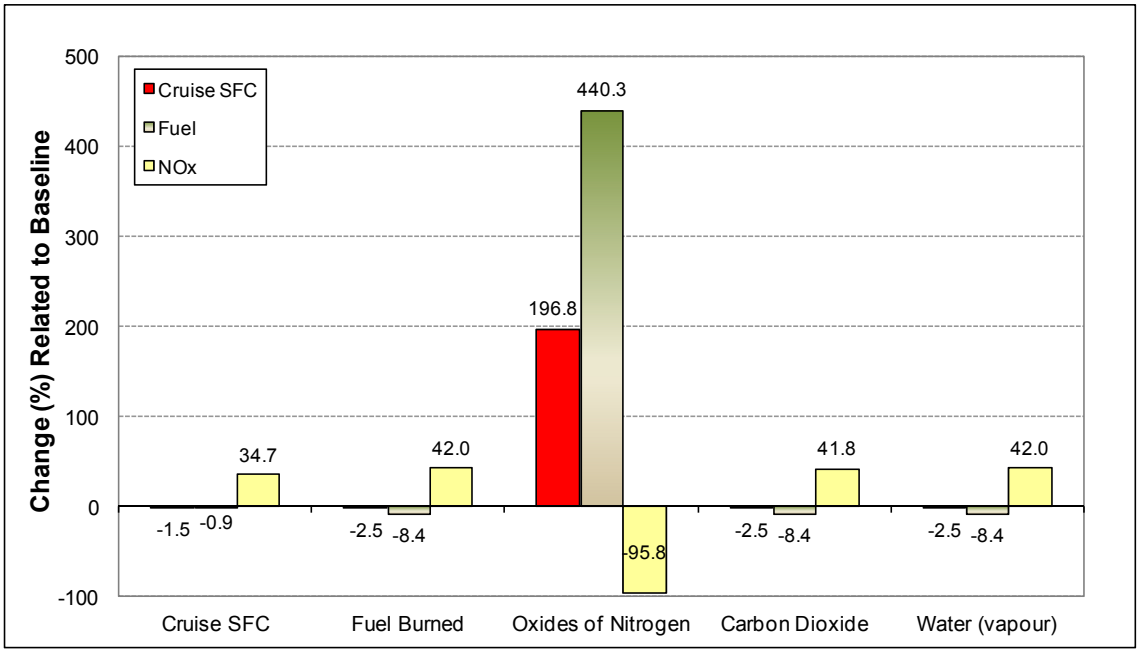


Figure 7-11. Case Study 2 – Optimum engine cycles results (relative to baseline)

At least in terms of OPR and TET, the fuel optimised engine is similar to the engine designed for minimum cruise SFC. Both are characterised by relatively high values of OPR and TET. As mentioned before, because the objective functions are similar as well, this is an expected result. The main difference between these two functions is associated with the fact that, when optimising for minimum fuel burned, the SFC corresponding to all trajectory segments is minimised and not only the SFC in cruise, as it happens when engines are optimised for minimum cruise SFC. Consequently, fundamentally, the main parameters driving the cruise SFC optimisation also drive the engine optimisation processes for minimum fuel burned.

From the cruise SFC optimised engine results discussed above, it is possible to conclude that, in order to minimise cruise SFC, values of engine OPR and BPR are determined such that the core flow is able to provide the work required by the engine

fan (without violating any constraint) at TO conditions. At this point, it is important to emphasise, once again, that the restrictions imposed on CDT (and HBL) corresponded to TO conditions. Thus, because TO is treated as an OD point condition, it means that for a given engine design the engine component characteristics ultimately determine the values of CDT (and HBL). In other words, two engine designs having the same OPR, TET, BPR, etc., may still have different values of CDT (and HBL) at TO conditions, if they use different turbomachinery maps.

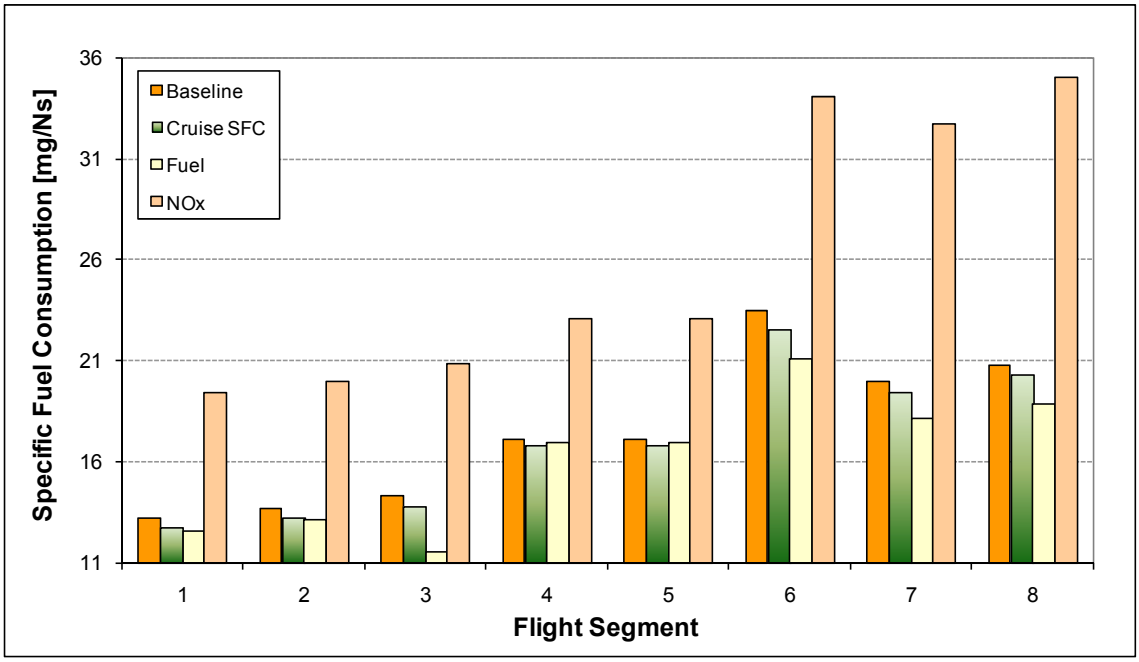


Figure 7-12. Case Study 2 – SFC at each trajectory segment

Therefore, when optimising an engine for minimum fuel burned, starting for simplicity from a cruise SFC optimised engine; the results seem to indicate that OPR needs to be modified such that it creates a room for increasing BPR without violating the constraints imposed on CDT (or HBL). To do so, in the first case study analysed in this chapter, it was observed that the OPR of the two-spool engine was slightly reduced. Unlike the first case study, in this second one, as illustrated in Figure 7-9, the OPR of the three-spool engine is slightly increased, which allows increases in the engine BPR without violating any constraint. This BPR increase yields in turn improvements in the engine propulsive efficiency; and, as observed in Figure 7-12, SFC reductions in all segments of the flight trajectory (except in cruise segments 4 and 5, where the cruise SFC optimised engine does). As expected, these results are reflected in the fuel that is

burned at each flight segment, as illustrated in Figure 7-13. Similarly to the first case study, in this last figure it is possible to see that the fuel optimised engine presents the lowest fuel consumption in all trajectory segments (except in cruise segments 4 and 5, where the cruise SFC optimised engine does), which yields, consequently, the lowest overall fuel burned.

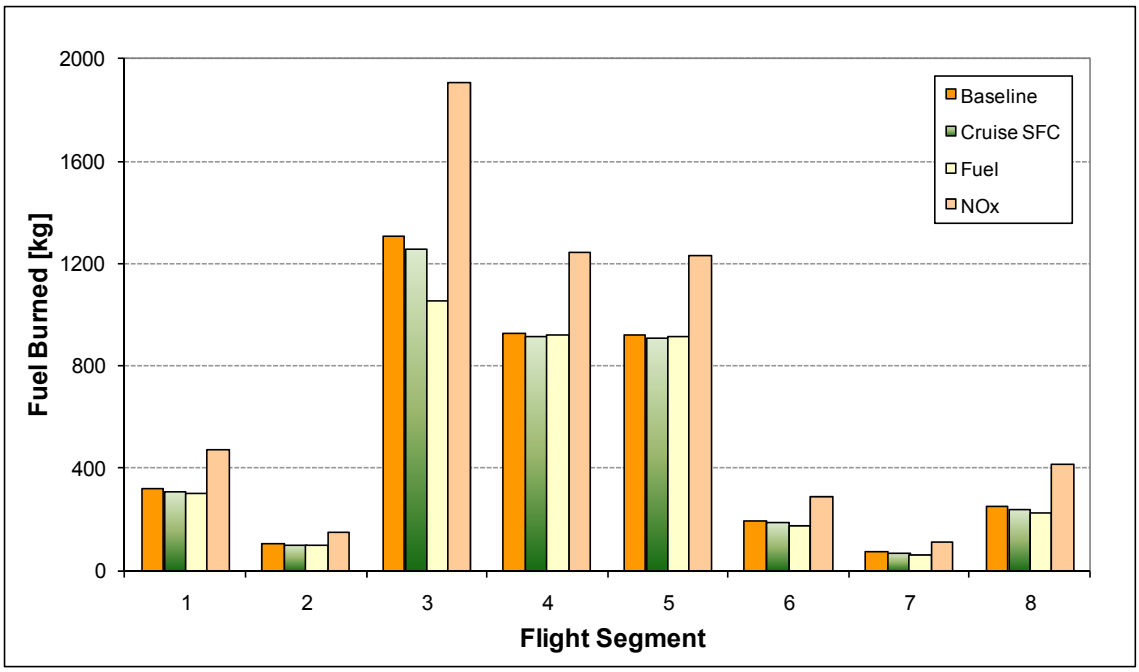


Figure 7-13. Case Study 2 – Fuel burned at each trajectory segment

Based on the analyses performed in the first case study about engine cycle optimisation-type processes and minimisation of $NO_x$ emissions, it was concluded that conventional engines optimised for minimum $NO_x$ emissions are expected to be characterised by both a relatively low (combustor) air inlet temperature (i.e., a low CDT and, consequently, a low OPR), and a relatively low (combustor) air inlet pressure (i.e., a low OPR). In addition, relatively low values of TET constitute also a characteristic of $NO_x$ optimised engines. As in the first case study, all these aspects are also confirmed by the results obtained in this second one for the engine optimised for minimum $NO_x$ emissions. Thus, as it can be verified in Figure 7-9, the $NO_x$ optimised engine presents the lowest OPR and TET of the three optimum engines computed. In addition, the engine BPR is lower than not only those values of BPR corresponding to the other two optimised engines, but also the baseline engine BPR. The considerable reduction in OPR (Figure 7-9 and Figure 7-10) seems to have been compensated by this BPR

decrease, which allowed that the reduced OPR core flow is able to generate the work required for driving the engine fan.

The significant reductions in OPR and TET observed in the case of the $NO_x$ optimised engine produced, as expected, huge increases in the engine SFC associated with each aircraft trajectory segment (Figure 7-12), and, consequently, in the corresponding fuel burned (Figure 7-13). In a similar fashion to the first case study, Figure 7-12 and Figure 7-13 show that, when compared to the other engines computed, the engine optimised for minimum $NO_x$ presents the highest SFC and fuel burned values at each segment of the flight trajectory. Even so, Figure 7-14 shows that the $NO_x$ optimised engine presents the lowest TET values at each flight segment. The relatively low values of OPR, TET and BPR characterising the engine optimised for minimum $NO_x$ are, therefore, mainly responsible for the low levels of $NO_x$ emitted at each flight segment; and, consequently, for the lowest overall $NO_x$ emissions that characterises this optimum engine. Unlike this result and similar to what was observed in the first case study analysed before, Figure 7-11 illustrates that the relatively high OPR and TET values associated with both cruise SFC and fuel optimised engines produce significant increases in $NO_x$ emissions and reductions in the total amount of fuel burned.

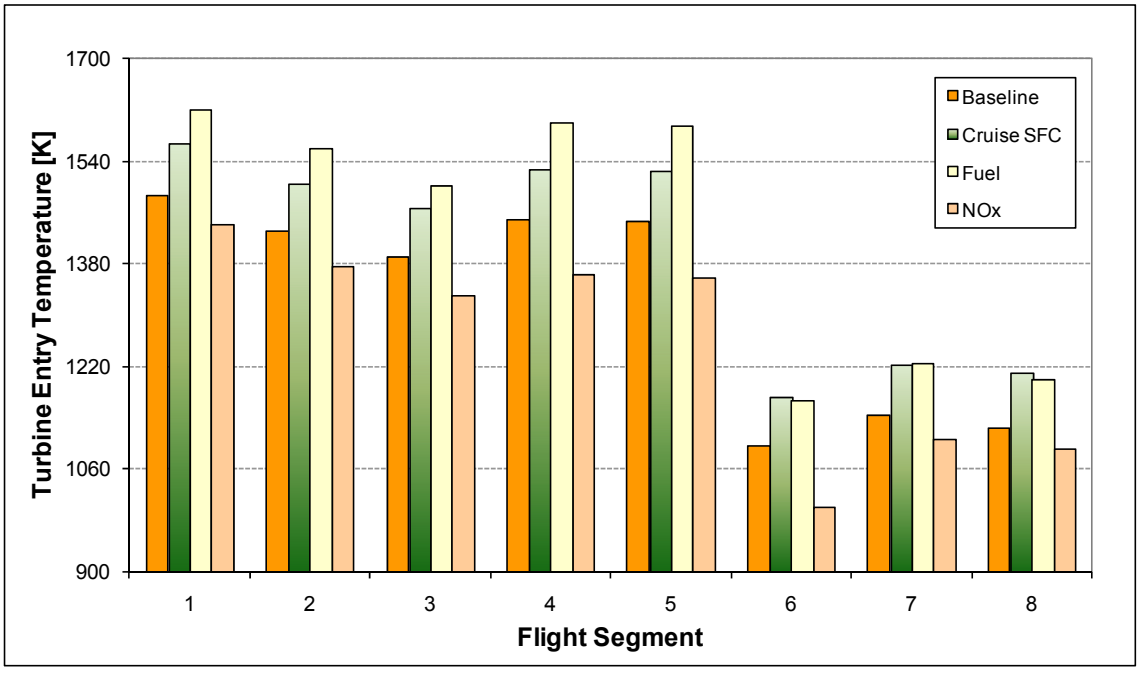


Figure 7-14. Case Study 2 – TET at each trajectory segment

Closing this section, Table 7-9 summarises, in quantitative terms, the main results associated with the baseline and the three optimum engine cycles analysed in this second case study. Similar to first case study, Table 7-9 shows that the $NO_x$ optimised engine presents IPC and HPC pressure ratios that correspond to their respective minimum permissible values – lower bounds imposed as explicit constraints (design variables) during the optimisation processes. It suggests in turn that convergence was achieved when it was not possible to further reduce these pressure ratios. In this table it is also possible to see that both cruise SFC and fuel optimised engine cycles present CDTTO values that roughly correspond to their highest permissible value (950K). This seems to suggest that the optimisation of these engine cycles was mainly driven by this limitation imposed on the CDTTO (implicitly constrained) parameter. Similar analyses to those ones carried out in these two first case studies will be performed in the following one which involves a more innovative engine cycle.

Table 7-9. Case Study 2 – Summary of optimum engine cycles results

| Parameter | Unit | Baseline | Cycle Optimisation for Minimum: | | |
|---|---|---|---|---|---|
| | | | Cruise SFC | Fuel | $NO_x$ |
| FPR | [--] | 1.70 | 1.68 | 1.53 | 1.65 |
| IPCPR | [--] | 4.4 | 4.4 | 3.5 | 2.0 |
| HPCPR | [--] | 4.4 | 6.2 | 8.9 | 2.0 |
| BPR | [--] | 5.5 | 5.5 | 6.6 | 5.1 |
| TET | [K] | 1412 | 1512 | 1465 | 1255 |
| TR | [--] | 4.8 | 4.5 | 4.7 | 6.6 |
| CDTTO | [K] | 871 | 950 | 949 | 591 |
| HBLTO | [mm] | 23 | 20 | 18 | 47 |
| OPR | [--] | 32.6 | 46.6 | 47.5 | 6.6 |
| FN | [kN] | 25.2 | 26.4 | 21.1 | 21.6 |

## 7.2.4 Case Study 3: Intercooled Recuperated Turbofan Optimisation

### 7.2.4.1 General Description

As highlighted in literature [128-130], the need of more affordable and economic engines along with the gradual tightening of environmental regulations exert constantly pressure on the aviation industry for evaluation and future utilisation of novel engine

concepts, whose main characteristic are their high efficiency (low fuel consumption) and environmental friendliness. In general terms, there are mainly three innovative (or unconventional) engine concepts that have been extensively studied in recent years for future aircraft applications: intercooled recuperated (ICR) engines, geared turbofans, and open rotors. All these three concepts have their advantages and disadvantages. For instance, when compared to conventional engines, open rotors are more fuel efficient (mainly due to their higher propulsive efficiency), but noise can be a problem; and geared turbofans, although having also a higher fuel efficiency and being quieter, the additional complexity and weight associated with the use of a gearbox constitute issues that need to be addressed carefully. From these three relatively novel engine cycles, due to mainly the work developed in the first part of this research project, the ICR engine concept was selected for carrying out the optimisation processes performed as part of this third and last case study analysed in this chapter.

In general, in addition to the processes present in conventional aircraft engines, an ICR engine involves, as schematically illustrated in Figure 7-15, intercooling and recuperation processes. The cooling of the air during the compression process, on one hand, reduces the compression work required, which in turn results in an increased engine thrust. However, due to fact that as a result of this process the CDT also decreases, an additional amount of heat input will be required. Thus, because the increase in engine thrust cannot offset this additional amount of heat added, the thermal efficiency and fuel consumption are penalised in cycles with intercooling. Recuperation, on the other hand, has the effect of increasing the efficiency of the cycle at the expense of a small reduction in the engine output. Therefore, when intercooling and recuperation are complementarily utilised, their benefits increase and improvements in both engine thrust and thermal efficiency can be obtained. All these effects contribute to the reduced engine SFC, which is the main characteristic of this type of engines, i.e., ICR engines.

As expected, ICR engines also present some drawbacks that are worth mentioning before describing the specific ICR engine optimised in this case study. The main downsides associated with this type of engines relate to the inherent additional complexities involved when using the heat exchangers. These include the increase in engine weight and more likely in engine dimensions, the additional pressure losses caused by the use of the heat exchangers, and the dependence of the intercooling and

recuperation systems' performance on the engine operating conditions. A previous work [55] showed that the benefits of the use of ICR engines – in terms of fuel burned and gaseous emissions – depend on both the performance of the intercooling and recuperation systems (namely heat exchangers' effectiveness and pressure losses), and the changes in engine weight and nacelle dimensions. More specifically, these gains decrease as both the referred (intercooling and recuperation systems') performance decreases, and the engine weight and nacelle dimensions increase. Thus, when carrying out the optimisation of the particular ICR engine analysed in this case study, some simplifications in the modelling of the engine and its associated systems were introduced.

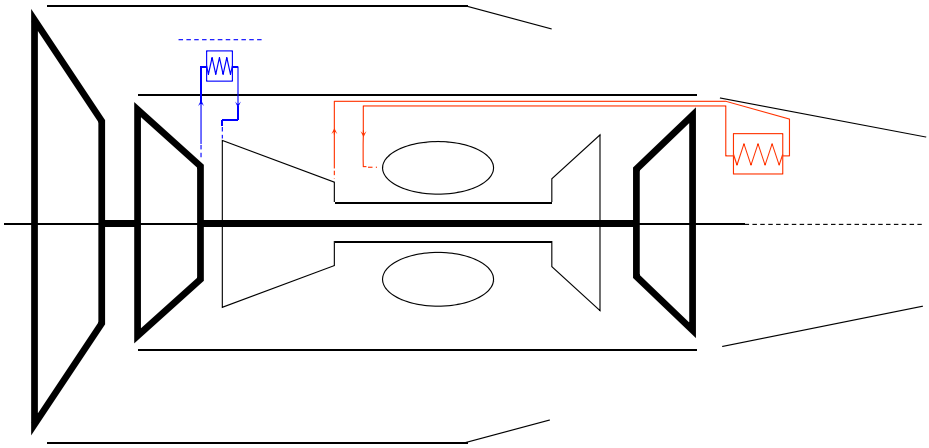

Figure 7-15. Case Study 3 – Schematic of an ICR (two-spool turbofan) engine with separate exhausts

In this case study, it was assumed that: (i) the use of the intercooling and recuperation systems does not imply variations in the dimensions of the nacelle; (ii) the ICR engine is 50% heavier than a conventional one used for similar purposes; (iii) the heat exchangers produce additional pressure losses of 3% (each one); and (iv) the heat exchangers' effectiveness is about 90%. The first assumption is coherent with what is being considered in all cases studies analysed in this chapter. That is, due to some limitations in the aircraft performance model utilised in this work, the overall engine dimensions (including nacelle dimensions) remain constant during the optimisation processes. The increase in the engine weight was directly translated as an increase in the aircraft MTOW. The setting of the pressure losses and effectiveness associated with the heat exchangers used in this particular case was carried following a similar methodology to that one used in previous studies [129,130]. These assumptions

attempted to reflect in general a typical scenario where this type of engines might be utilised. Taking into account these aspects, an ICR engine, which was used as the reference or baseline engine in this third case study, was initially designed. Table 7-10 details the main parameters characterising this engine.

Table 7-10. Case Study 3 – Baseline engine characteristic parameters

| DP: TOC (10,668m [35,000ft], M0.8, ISA) | | |
|---|---|---|
| Parameter | Unit | Value |
| W | [kg/s] | 180.0 |
| BPR | [--] | 5.46 |
| FPR | [--] | 1.70 |
| IPCPR | [--] | 1.92 |
| HPCPR | [--] | 10.0 |
| OPR | [--] | 32.6 |
| TET | [K] | 1280 |
| FN | [kN] | 25.4 |
| SFC | [mg/Ns] | 17.2 |
| OD: TO (S/L , M0.0, ISA+30°C) | | |
| Parameter | Unit | Value |
| TET TO | [K] | 1510 |
| FN TO | [kN] | 120.4 |

As shown in Table 7-10, DP (10,668m [35,000ft], M0.8, ISA) and TO (Sea Level [S/L], M0.0, ISA+30°C) conditions in this third case study corresponded to the same conditions utilised as such in the first two case studies analysed in this chapter. Similar to the second case study, for the design of this baseline ICR engine (Table 7-10), an iterative process involving engine simulations at DP and OD point conditions was utilised in order to match the engine model thrust requirements with those associated with the (two-spool) engine used as baseline in the first case study. As customary, when necessary, educated guesses were made for some engine characteristic parameters required for the modelling of the engine. In Table 7-10 it is also possible to see that the values of W, BPR, and OPR are the same ones (and roughly them in the case of the OPR split in the compression system) utilised for the design of the two-spool baseline engine used in the first case study.

Table 7-11 summarises, in turn, the design variables and (implicit) constraints utilised in this third and last case study, as well as the ranges of permissible values considered. As it can be observed in this table, all these parameters, except one of them,

are the same parameters utilised in the optimisation processes of the two-spool engine performed in the first case study. The only additional parameter present in this table (last row) corresponds to the engine net thrust at DP. The rationale behind the inclusion of this constraint is because, for this particular type of optimisation problems, the larger the number of (implicit) constraints, the more meaningful the outcomes of the optimisation studies.

Table 7-11. Case Study 3 – Design variables and Constraints

| Parameter Type | Parameter Name | Parameter Unit | Lower Bound | Upper Bound |
|---|---|---|---|---|
| Design Variable | FPR | [--] | 1.1 | 1.9 |
| Design Variable | IPCPR | [--] | 2.0 | 5.0 |
| Design Variable | HPCPR | [--] | 5.0 | 20.0 |
| Design Variable | BPR | [--] | 2.0 | 15.0 |
| Design Variable | TET | [K] | 1200 | 1800 |
| Design Variable | TET TO | [K] | 1200 | 1900 |
| Constraint | TR | [--] | 4.5 | -- |
| Constraint | CDTTO | [K] | -- | 950 |
| Constraint | HBLTO | [mm] | 15 | -- |
| Constraint | FN | [kN] | 25.2 | 25.7 |

The only criterion determining (internally) the validity of a given engine design was so far the ability of the aircraft to fly the (fixed) reference flight trajectory utilised. Although respecting all constraints imposed, following this approach however, the optimisation processes at some stage could yield unrealistic solutions which present very low or very high values of net thrust at DP and/or TO. Therefore, in this third case study, in order to reduce the probability of determining such solutions, an additional constraint, i.e., FN at DP, was imposed. As illustrated in Table 7-11, the range of permissible values in which this constraint was allowed to vary corresponded to ±1% of its nominal value (25.4kN, Table 7-10). It is important to highlight that this constraint was not included in the two first case studies analysed above mainly because of the gradual approach, in terms of addition of complexities, followed in this work. Finally, similar to the first two cases studies analysed in this chapter, polytropic efficiencies (fan 0.93, IPC and HPC 0.91, HPT 0.88, and LPT 0.90) were assumed for the main components of the ICR engine. Accordingly, engine cycle optimisation-type processes determining optimum ICR engine cycles which minimise cruise SFC, fuel burned, and

$NO_x$ emitted were performed. The following section summarises the main results obtained.

### 7.2.4.2 Results

The main thermodynamic cycle parameters associated with both the baseline and the optimum engines determined in this case study are shown in Figure 7-16. These same parameters when expressed in relative terms using the characteristic parameters of the baseline engine are illustrated in Figure 7-17. In Figure 7-18, in turn, a comparison of the main results associated with the three optimised engines computed in this case study is shown. As observed in this last figure, all three optimum engines computed yield, similarly to the two-spool case, relatively significant reductions in cruise SFC (~ -12%), fuel burned (~ -14%) and $NO_x$ emitted (~ -65%). A brief analysis of the results associated with each of these optimum engines determined in this case study is presented next.

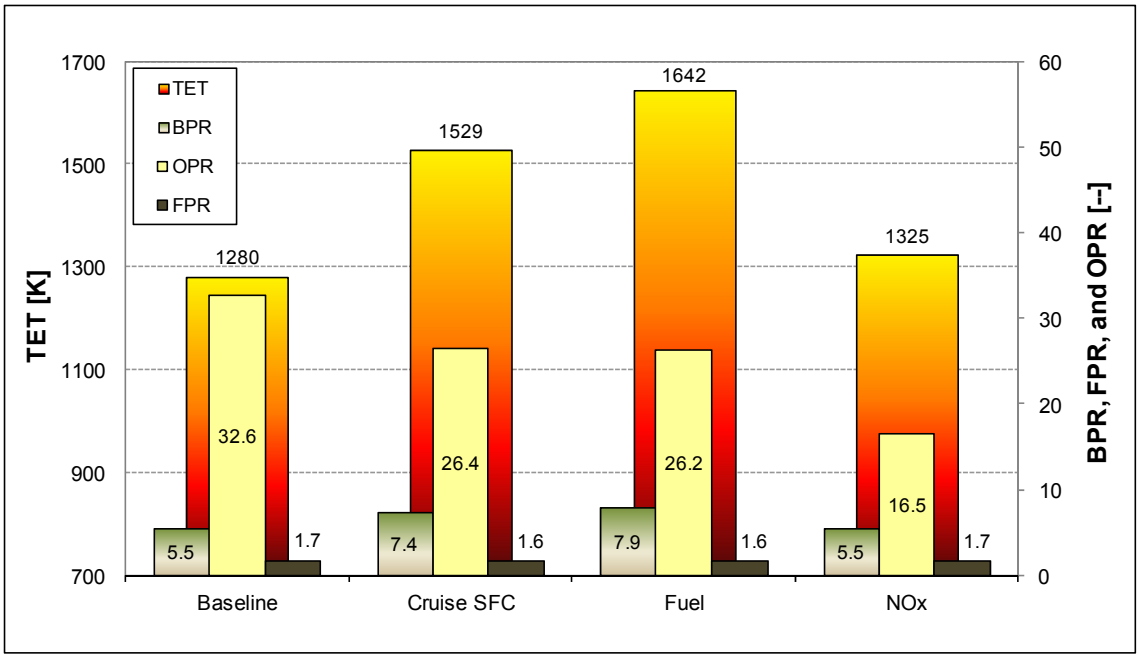


Figure 7-16. Case Study 3 – Characteristic parameters of engine cycles (baseline and optimum)

Based on the analyses of the results associated with conventional (two- or three-spool) engines carried out above, it was concluded that SFC optimised engines are characterised by relatively high values of OPR and TET; and, at the same time, relatively high values of BPR. This is only partially true in the case of ICR engines

optimised for minimum cruise SFC because of the intercooling and recuperation systems used in this type of engines. As highlighted in references [127,128], unlike conventional engines, ICR engines offer higher efficiencies, and hence lower SFC values, with lower values of OPR. This is because the larger the difference between the temperatures of the hot and cold flows, the more effective the heat exchange process. In the case of the recuperation system used in ICR engines, this implies that the larger the difference between the turbine exit temperature and CDT, the better. This difference can be made larger by increasing the turbine exit temperature, through increases in TET for instance; and/or by reducing CDT. Reductions in CDT can be in turn achieved by reducing OPR and/or by using intercooling processes. However, due to the fact that intercooling on its own results in increases in SFC, a relatively low OPR is one of the main characteristics of ICR engines.

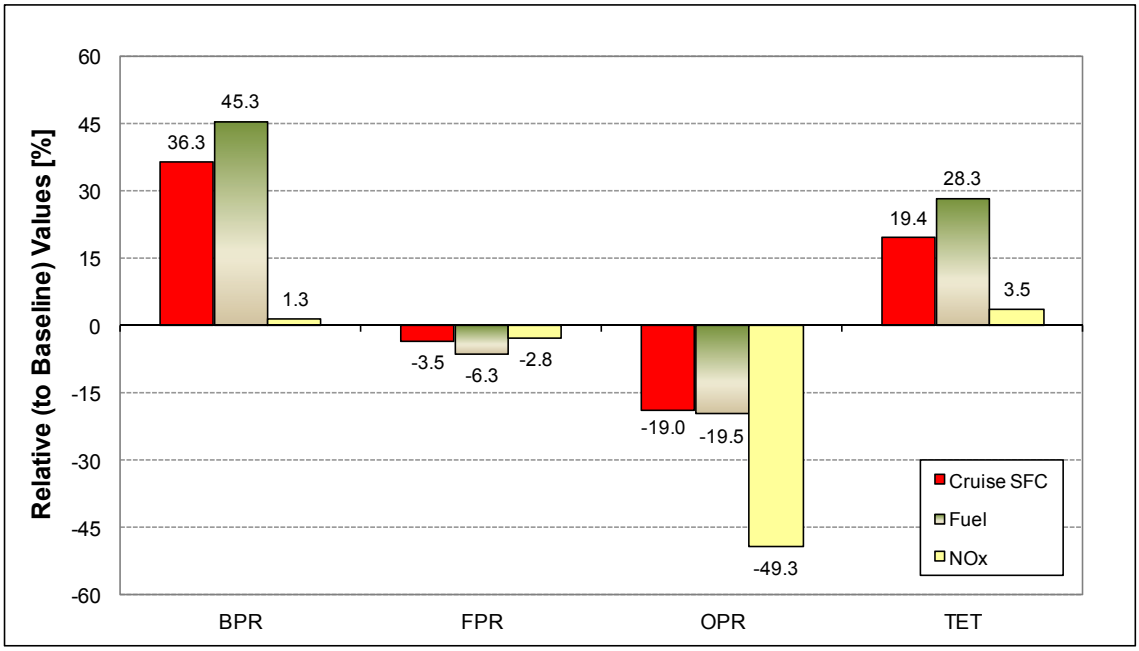


Figure 7-17. Case Study 3 – Relative (to baseline) parameters of optimum engine cycles

Therefore, as it can be observed in Figure 7-16, the ICR engine optimised for minimum cruise SFC is characterised by a relatively high value of TET and a moderate value of OPR. These two aspects contribute to the improvement of the engine thermal efficiency and the effectiveness of the heat exchange processes and, consequently, to the reduction of the engine cruise SFC. TET seems to be a compromise between increasing its value to improve thermal efficiency and heat exchange's effectiveness and, hence, SFC; and reducing it to avoid significant reductions in propulsive efficiency that can

worsen SFC. In addition, because increases in BPR yield improvements in propulsive efficiency and, consequently, reductions in SFC, the BPR associated with the cruise SFC optimised engine is higher than the baseline engine BPR (Figure 7-16 and Figure 7-17). Another aspect that may have a certain contribution to the increase in BPR is the reduction in compression work originated by both the reduction in OPR and the use of an intercooling process. For completeness, Figure 7-19 shows the SFC for each segment of the aircraft flight trajectory. As expected, when compared to the corresponding SFC values associated with the other engines (baseline and optimum), segments 4 and 5 (yielding cruise SFC) exhibit the lowest SFC values.

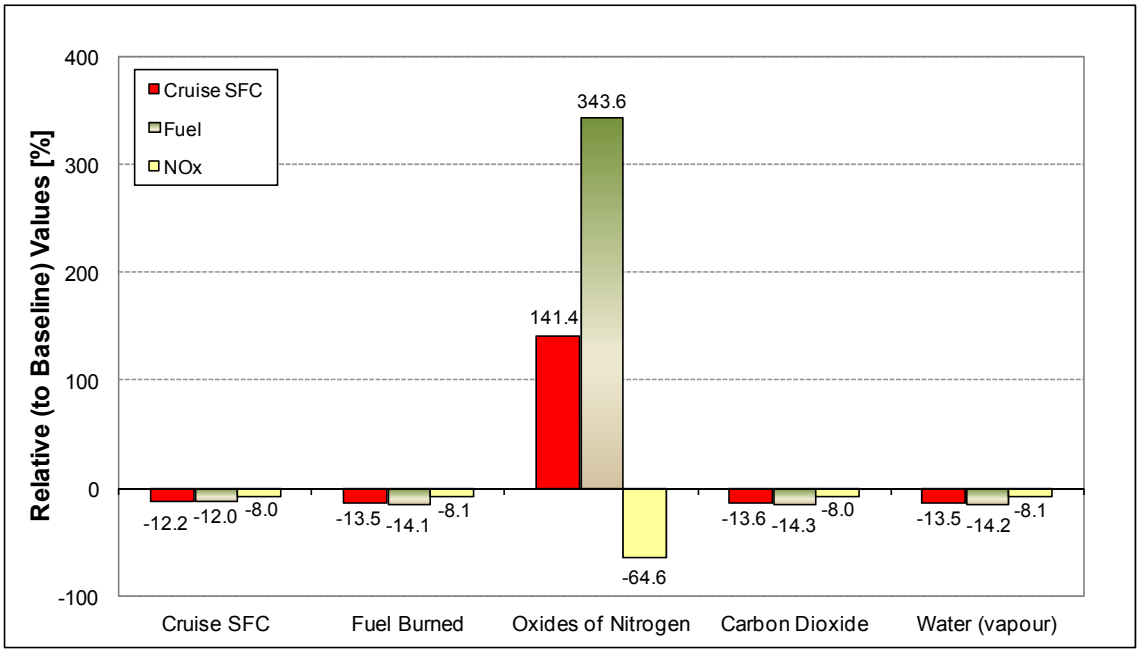


Figure 7-18. Case Study 3 – Optimum engine cycles results (relative to baseline)

In terms of OPR and TET, the ICR engine optimised for minimum fuel burned is similar to the engine designed for minimum cruise SFC (both are characterised by relatively high values of TET and moderated values of OPR). This is expected because the objective functions utilised in these two cases are similar as well. As already highlighted, the big difference between these two functions relates to the fact that, when optimising for minimum fuel burned, unlike cruise SFC optimisation (optimisation of SFC in cruise only), the SFC corresponding to all trajectory segments is minimised. Thus, in general, the main parameters driving the cruise SFC optimisation also drive the minimum fuel burned optimisation processes. Therefore, as observed in Figure 7-16, the

ICR engine optimised for minimum fuel burned is also characterised by relatively high values of TET and BPR, as well as moderate values of OPR.

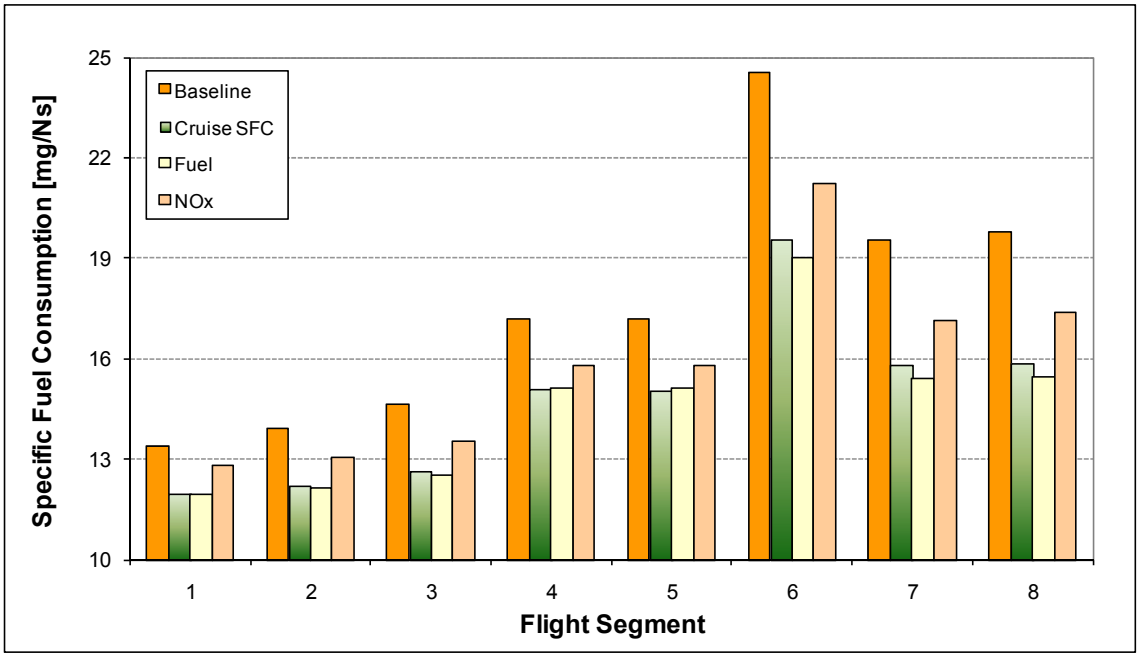


Figure 7-19. Case Study 3 – SFC at each trajectory segment

Regarding specifically the engine BPR, when compared to the other optimum engines computed in this case study, the results (Figure 7-16 and Figure 7-17) show that the engine optimised for minimum fuel burned presents the highest BPR. This behaviour can be attributed to the improvements in engine propulsive efficiency (main contributors to the reduction in SFC and, consequently, in fuel burned) originated from the increases in BPR. These results are consistent with those associated with conventional engines, as shown in Figure 7-2 and Figure 7-9. The relatively high value of BPR used in this particular optimised engine, together with the relatively high value of TET and moderate OPR, originates SFC reductions in almost all segments of the flight trajectory. Figure 7-19 shows that this ICR engine, i.e., fuel optimised, presents the lowest values of SFC in all trajectory segments, except in cruise segments 4 and 5, where the cruise SFC optimised engine does. As expected, these SFC results are reflected in the fuel that is burned at each flight segment, as illustrated in Figure 7-20. In this last figure it is possible to observe that the fuel optimised ICR engine presents the lowest fuel consumption in all trajectory segments, except in those segments where the

cruise SFC optimised engine does. This fact of course leads to the lowest overall fuel burned that characterises this particular ICR engine.

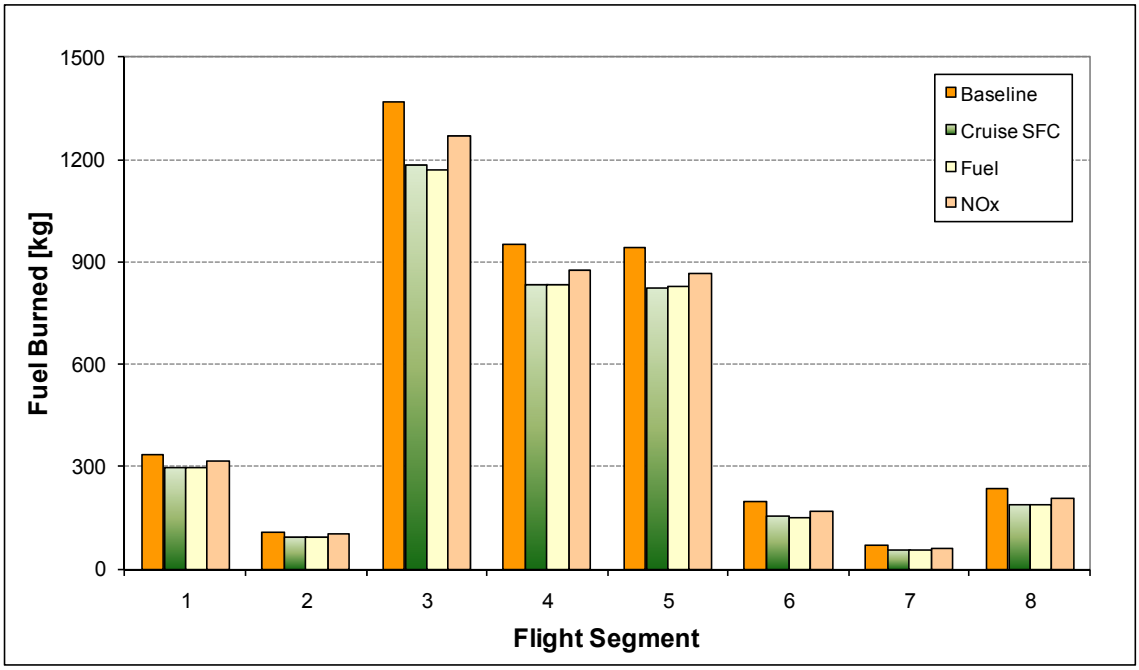


Figure 7-20. Case Study 3 – Fuel burned at each trajectory segment

The analyses performed previously about engine cycle optimisation-type processes and minimisation of $NO_x$ emissions determined that conventional engines optimised for minimum $NO_x$ emissions are expected to be characterised by relatively low values of combustor air inlet temperature, combustor air inlet pressure, and TET. In the case of ICR engines, air inlet temperature is mainly related to both CDT (and hence to OPR) and TET (through the recuperation system utilised). Air inlet pressure, in turn, is directly related to OPR. Accordingly, low values of combustor air inlet temperature and pressure mean low values of OPR and TET. Observing the results shown in Figure 7-16, it is possible to see that relatively low values of OPR and TET is indeed one of the characteristics of the engine optimised for minimum $NO_x$ emissions. Thus, as shown in this figure, the $NO_x$ optimised engine presents the lowest OPR and TET of the three optimum engines computed. However, when compared to the baseline case, this optimum engine presents a slightly higher value of TET. It seems that this value is a consequence of the additional constraint (FN at DP) imposed in this case. Even so, the $NO_x$ optimised engine produces significant reductions (~ -65%) in the level of $NO_x$ emitted (Figure 7-18). It seems then that OPR has a dominant effect on $NO_x$ emissions

in this particular case. Regarding the engine BPR, the results show that this parameter is roughly the same as in the case of baseline engine and lower than those values of BPR corresponding to the other two optimised engines.

The significant reduction in OPR characterising the $NO_x$ optimised engine results in relatively high values of SFC at each trajectory segment (Figure 7-19); and, consequently, fuel burned (Figure 7-20). Similar to previous case studies, Figure 7-19 and Figure 7-20 show that, when compared to the other optimum engines determined in this case study, the engine optimised for minimum $NO_x$ presents the highest SFC and fuel burned values at each segment of the flight trajectory. Even so, Figure 7-21 shows that this optimised engine presents the lowest TET values at the last trajectory flight segments. In the initial ones, its TET values are comparable to those ones associated with the baseline engine. These relatively low values of OPR and TET characterising the engine optimised for minimum $NO_x$ lead to the lowest overall $NO_x$ emissions that qualify this optimum engine. Unlike this result, Figure 7-18 shows that the relatively high TET values associated with both cruise SFC and fuel optimised engines (Figure 7-16 and Figure 7-21) produce significant increases in $NO_x$ emissions.

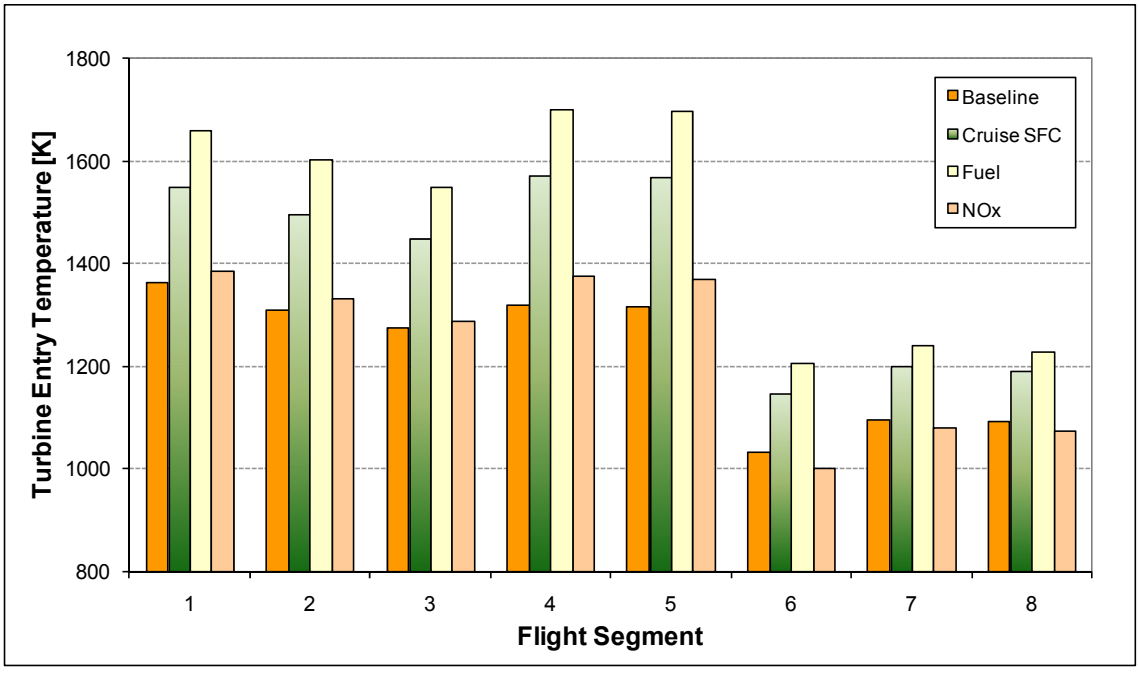


Figure 7-21. Case Study 3 – TET at each trajectory segment

Finally, Table 7-12 summarises, quantitatively, the main results associated with the baseline and the three optimum engine cycles analysed in this third and last case

study. In this table it is possible to see that the $NO_x$ optimised engine present IPCPR and HPCPR values which correspond to their respective minimum permissible ones – lower bounds imposed as explicit constraints (design variables) during the optimisation processes – suggesting, in turn, that convergence was achieved when it was not possible to further reduce these parameters. Table 7-12 also shows that the optimum engines computed present, as expected, FN values which are within their range of permissible values (±1% of its nominal value, 25.4kN). Closing this chapter, the following section describes a simple comparison of the three engine configurations analysed in this work.

Table 7-12. Case Study 3 – Summary of optimum engine cycles results

| Parameter | Unit | Baseline | Cycle Optimisation for Minimum: | | |
|---|---|---|---|---|---|
| | | | Cruise SFC | Fuel | $NO_x$ |
| FPR | [--] | 1.70 | 1.64 | 1.59 | 1.65 |
| IPCPR | [--] | 1.9 | 3.2 | 3.1 | 2.0 |
| HPCPR | [--] | 10.0 | 5.0 | 5.3 | 5.0 |
| BPR | [--] | 5.5 | 7.4 | 7.9 | 5.5 |
| TET | [K] | 1280 | 1529 | 1642 | 1325 |
| TR | [--] | 4.7 | 5.4 | 4.7 | 5.4 |
| CDTTO | [K] | 735 | 870 | 920 | 834 |
| HBLTO | [mm] | 23 | 21 | 21 | 30 |
| OPR | [--] | 32.6 | 26.4 | 26.2 | 16.5 |
| FN | [kN] | 25.4 | 25.6 | 25.3 | 25.2 |

### 7.2.5 Further Results

During a typical engine cycle optimisation process, in order to understand the influence of particular cycle parameters on the optimum results, initially only a limited number of design variables and constraints, as well as objective functions (mostly only one) are usually utilised. Design variables and constraints are then gradually added to the optimisation processes. Eventually, not only single-objective but also multi-objective optimisation processes are carried out involving all relevant design variables and constraints. This approach allows the understanding of the importance of key engine cycle parameters, as well as it enables the determination of realistic optimum engine cycles satisfying the engine requirements.

The main objective of the optimisation processes performed in the case studies described in this chapter was the illustration of other uses of Polyphemus and the evaluation of their mathematical performance rather than the determination of realistic engine cycles. Thus, in these case studies, only a limited number of design variables and constraints, as well as objective functions (single-objective) were utilised. This allowed greater visibility about the characteristics of the optimiser performance when assessing results. This, of course, would have proved more difficult if a larger number of design variables, constraints, and objective functions had been utilised. Consequently, the optimisation processes described so far in this chapter constitute typical examples of those processes that are carried out only in the initial stages of an engine cycle optimisation. When analysing different engine cycles it is important to find a means of comparing the different results obtained. Therefore, it has been decided to include in the final part of this chapter results showing a comparison of the three engine cycles analysed before. This section summarises the results associated with the referred comparison process.

Due to the simplifications introduced when carrying out the engine cycle optimisation-type processes described above, mainly in terms of constraints, it has been necessary to slightly increase the number of implicit constraints utilised so far for performing the comparison of the engine cycles mentioned. The main reason for the utilisation of these additional constraints was to allow a fairer comparison process. The process of addition of constraints was similar to that one used in the case of the ICR engine discussed before. Thus, in the cases of the two- and three-spool engines, the additional constraints considered related to the net thrust, FN, at DP and TO. In the case of the ICR engine, in turn, because FN at DP had been already considered as a constraint, only FN at TO was added. The ranges of permissible values in which these two additional constraints were allowed to vary corresponded to ±1% of their corresponding nominal values. These nominal values were taken, in turn, from the respective values of FN at DP and TO (c.f., Table 7-4, DP: 25.1kN, TO: 121.4kN) associated with the baseline two-spool engine, which was also considered as reference or baseline engine in this comparison process. For brevity, only one of the three objective functions usually utilised in the previous analyses, fuel, was used in the single-objective optimisation processes carried out in this work for comparison

purposes. All other details associated with the optimisation of each particular engine configuration and described in the previous case studies remained the same, and they will not be repeated here. The only big difference was associated with the increase in the number of implicit constraints as just highlighted.

The main thermodynamic cycle parameters associated with both the two-spool baseline engine and the three engine configurations optimised for minimum fuel burned are shown in Figure 7-22. These same parameters when expressed in relative terms using the characteristic parameters of the two-spool baseline engine are illustrated in Figure 7-23. In Figure 7-24, in turn, the main results associated with the three optimised engine configurations are shown. As observed in this last figure, the three-spool fuel optimised engine yielded only a relatively small reduction in the total amount of fuel burned (~ -1.7%), while the other two optimum engines computed led to relatively significant reductions in this parameter, i.e., two-spool ~ -8.7%, and ICR ~ -10.6%.

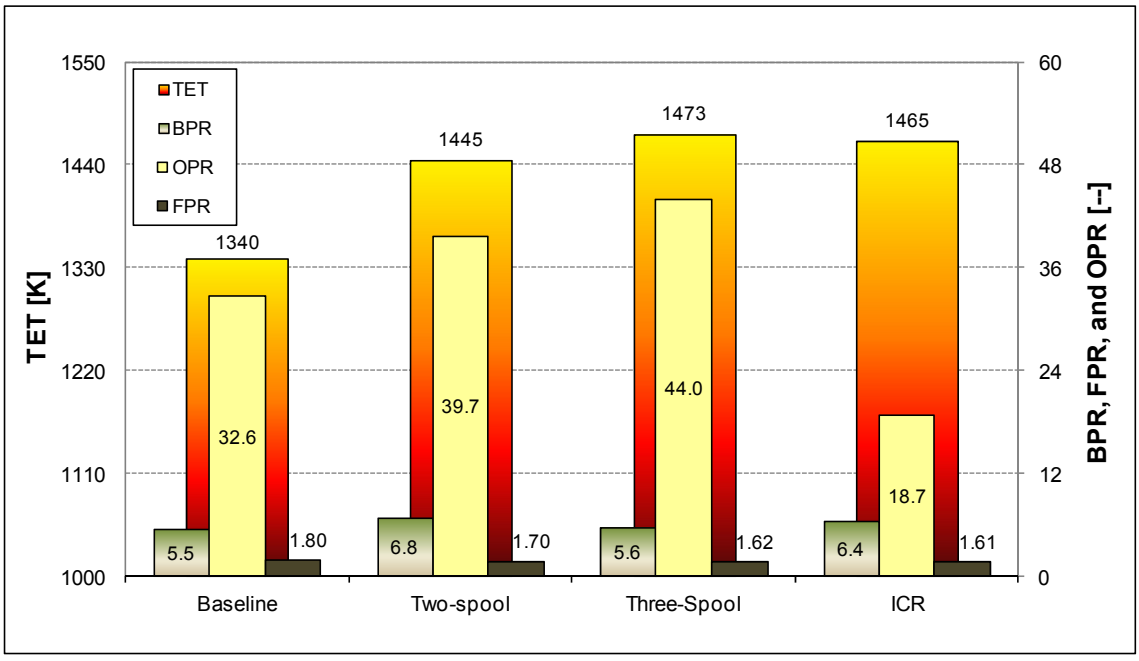


Figure 7-22. Comparison of engines – Characteristic cycle parameters

Figure 7-22 illustrates that conventional (two- and three spool) engines are characterised by relatively high values of OPR and TET. This is an expected result after what was discussed about this type of configurations in the two first case studies described in this chapter. Unlike these results, the ICR engine is characterised by a moderate value of OPR. However, as it happens in the case of conventional engines, a

relatively high value of TET is also a characteristic of minimum fuel burned ICR optimised engines. The main reason behind these moderate values of OPR in ICR engines, as mentioned before, relates to the presence of the intercooling and recuperation systems, which require relatively low values of OPR in order to maximise the benefits associated with their utilisation.

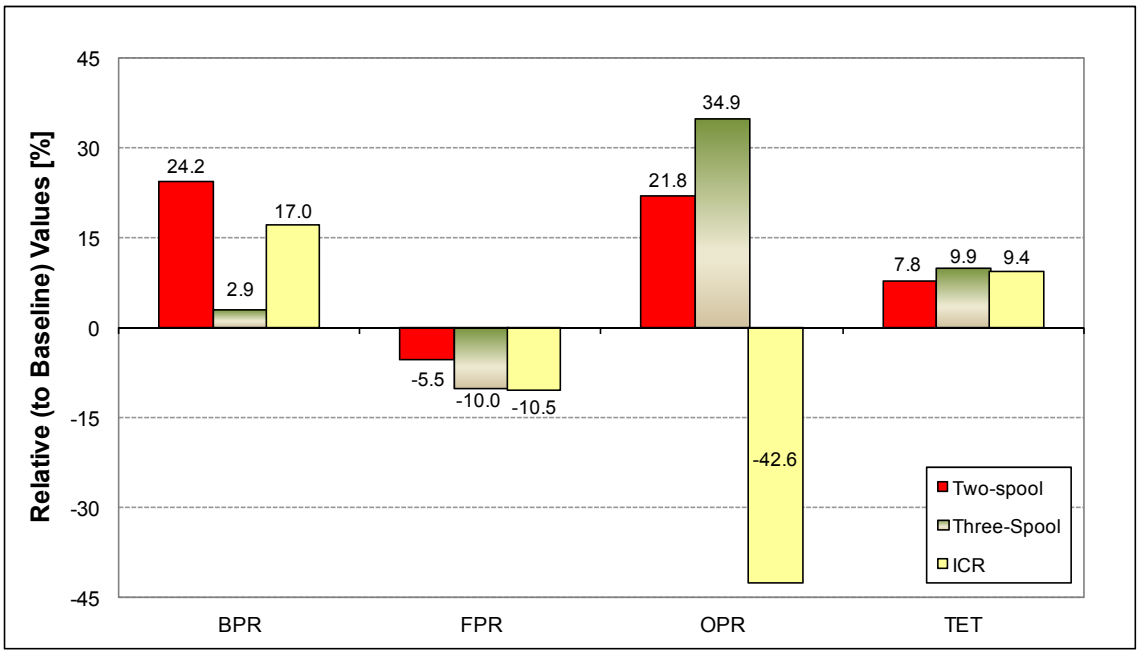


Figure 7-23. Comparison of engines – Relative (to baseline) cycle parameters

Regarding the engine BPR, the results (Figure 7-22 and Figure 7-23) show that there is a tendency to increase this parameter in order to reduce the fuel burned. This is expected, of course, once increases in BPR lead to improvements in engine propulsive efficiency; and, consequently, reductions in SFC. Then, due to the fact that when optimising for minimum fuel burned, the SFC corresponding to all trajectory segments is minimised (including the SFC in cruise), it is natural to expect that fuel optimised engines are characterised by relatively high values of BPR. Thus, as particularly observed in Figure 7-23, when compared to the two-spool baseline engine, the three optimum engines computed present higher values of BPR. In the particular case of the ICR engine, it seems that the reduction in compression work as a result of both the reduction in OPR and the use of an intercooling process also contributes to the large increase in BPR associated with this engine.

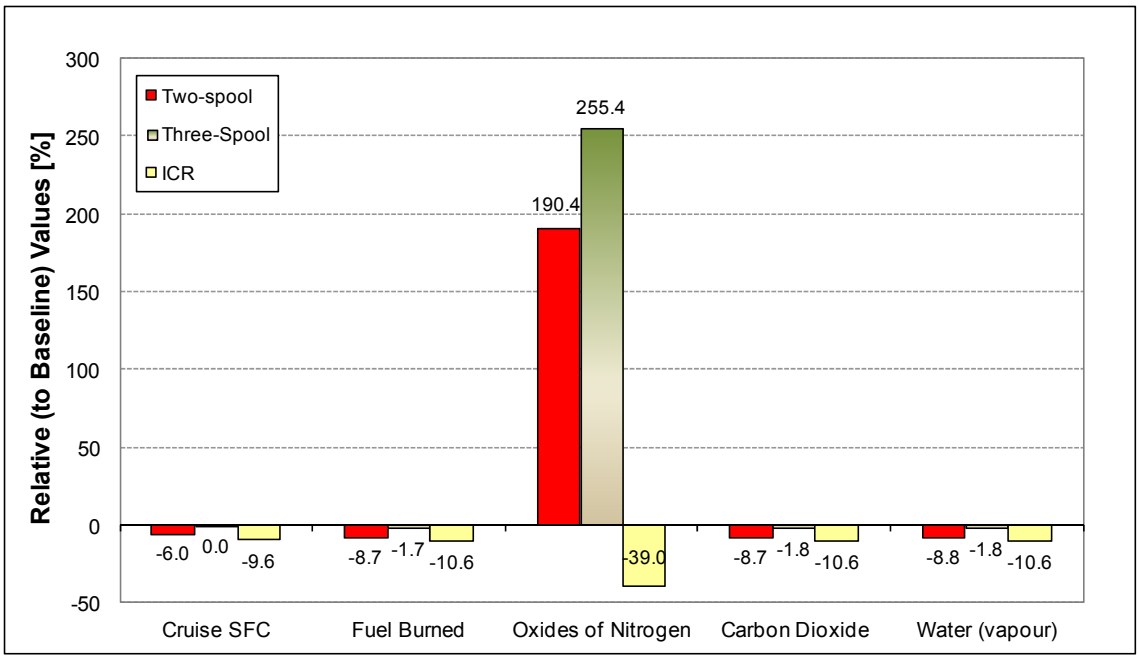


Figure 7-24. Comparison of engines – Optimum engine cycles results (relative to baseline)

Comparing specifically the results corresponding to the three engine configurations optimised for minimum fuel burned, it is possible to see from Figure 7-22 and Figure 7-23 that the conventional engines present OPR and TET values which are roughly comparable. The relatively high TET value associated with the ICR engine seems to be related to its recuperation system which requires as high TET values as possible. In addition, the TET values characterising each engine configuration seem to be obtained from a compromise between increasing its value for a better thermal efficiency (and heat exchange's effectiveness in ICR engines) and, hence, a lower SFC; and reducing it in order to avoid important reductions in propulsive efficiency, worsening in this way SFC. The relatively low value of OPR characterising the ICR engine is, of course, a requirement of the intercooling and recuperation systems used in this type of engines. Thus, in terms of compression stages and cooling flow, it seems that an ICR engine is 'simpler' than conventional ones; but it also has of course all the other complexities associated with the use of the heat exchangers present in this type of engine configurations.

Looking at the overall results obtained from the optimisation processes the conventional three-spool engine optimised for minimum fuel presents, on one hand, the smallest reduction in fuel burned (Figure 7-24). Because of the simplifications introduced into the optimisation processes, it is not possible to determine with certainty

the reasons behind the differences (in terms of fuel burned reduction) between the results obtained for the conventional two- and three-spool engines. Further optimisation work involving higher fidelity computational tools able to model, for instance, changes in engine weight and dimensions as the engine thermodynamic cycle varies should help to clarify this point. The ICR engine, on the other hand, yields the largest reduction in this parameter. This last result can be attributed to both the relatively lower SFC characterising an ICR engine, and its improved part-load performance. This characteristic SFC can also be observed in Figure 7-24. Regarding $NO_x$ emissions, Figure 7-24 shows that the ICR engine produces a smaller amount of this pollutant when compared to the other optimised engines. The relatively low values of OPR characterising ICR engines are partially responsible for this relatively low amount of $NO_x$ emissions. Closing this chapter, Table 7-13 summarises in quantitative terms the main results associated with both the two-spool baseline engine, and the three engine configurations optimised for minimum fuel burned analysed in this section.

Table 7-13. Comparison of engines – Summary of optimum engine cycles results

| Parameter | Unit | Baseline | Cycle Optimisation for Minimum Fuel | | |
|---|---|---|---|---|---|
| | | | Two-spool | Three-spool | ICR |
| FPR | [--] | 1.80 | 1.70 | 1.62 | 1.61 |
| IPCPR | [--] | 1.8 | 2.6 | 4.3 | 2.2 |
| HPCPR | [--] | 10.0 | 9.0 | 6.3 | 5.3 |
| BPR | [--] | 5.5 | 6.8 | 5.6 | 6.4 |
| TET | [K] | 1340 | 1445 | 1473 | 1466 |
| TET TO | [K] | 1600 | 1715 | 1722 | 1692 |
| TR | [--] | 4.8 | 4.8 | 4.8 | 4.8 |
| CDTTO | [K] | 862 | 911 | 950 | 884 |
| HBLTO | [mm] | 23 | 20 | 20 | 26 |
| OPR | [--] | 32.6 | 39.7 | 44.0 | 18.7 |
| FN | [kN] | 25.1 | 24.9 | 24.9 | 25.3 |
| FN TO | [kN] | 121.4 | 120.5 | 120.4 | 121.1 |

Almost all results illustrated in Table 7-13 were already discussed. Therefore, the only aspect to highlight in this table relates to the values of FN at DP and TO. As mentioned before, these parameters were used as implicit constraints in this particular case. Table 7-13 shows that the optimum engines computed present, as expected, FN values which are within their range of permissible values. Finally, the comparison process of engine cycles described in this last section closes this chapter dealing with

engine cycle optimisation-type processes. This chapter provided a flavour of the type of analyses that can be carried out in this field of optimisation of engine cycles using optimisation algorithms such as those utilised in this work, i.e., Polyphemus.

# 8
# Conclusions and Further Work

The main conclusions drawn from the present research work as well as some proposals for further work are summarised in this chapter.

## 8.1
## Conclusions

The aim of this research work was to develop a methodology to evaluate and quantify aircraft/engines design trade-offs originated as a consequence of addressing conflicting objectives such as low environmental impact and low operating costs. More specifically, in this work it was mainly intended to evaluate and optimise both aircraft flight trajectories and aircraft engine cycles taking into account multidisciplinary aspects such as performance, gaseous emissions, and economics, among others. It was also an objective of this project to use different computational tools currently available at Cranfield University, and, when necessary, to develop new computational tools or to introduce modifications to the existent ones, in order to perform the tasks proposed in this project.

The main contributions of this work to knowledge broadly comprise the following:

- Development of an environmental-based methodology for carrying out both aircraft trajectory optimisation processes, and engine cycle optimisation-type ones.
- Development of an advanced, innovative gas turbine emissions prediction software suitable to be integrated into multi-disciplinary optimisation frameworks, e.g., aircraft trajectory optimisation framework under development.

- Development and/or adaptation of a suitable optimiser with a library of optimisation algorithms (i.e., Polyphemus) to be integrated into multi-disciplinary optimisation frameworks.
- Evaluation and optimisation of aircraft propulsion systems from two different perspectives, operation (aircraft trajectories) and preliminary design (engine cycles).
- Determination and assessment of optimum and 'greener' aircraft trajectories and aircraft engine cycles using a multi-disciplinary optimisation tool, including, among others, Polyphemus and the gas turbine emissions prediction model developed.

Based on its objectives and contributions, it is concluded that the present research project was successfully completed. In general, the development of the research project followed its normal path, and all objectives associated with the project, including its expected results, were successfully achieved.

Regarding the specific work developed in this project, it is worth indicating that an initial literature review was carried out in the first part of this research work. This review was oriented to the establishment of the state-of-the-art of the different approaches considered so far to reduce the environmental impact of aircraft operations. Literature basically indicates that, in order to reduce the aircraft climate impact, the number of aircraft operations must be reduced, the type of aircraft must be changed, and/or the aircraft operational rules and procedures must be changed. From a practical perspective, it is concluded that a combination of last two alternatives seems to be the most feasible route to the achievement of the goal.

The different processes involving the evaluation and optimisation of environmentally friendly aircraft propulsion systems carried out in this work included the use of several computational packages/models developed at Cranfield University over the years, and eventually other new ones developed according to the need of this particular project. In this sense, as part of the familiarisation process with the computational tools already available at Cranfield University, simulation processes using these tools were initially performed.

A new computational tool for modelling the formation of pollutants in gas turbine combustors was developed and the details of its development and implementation were

described in this thesis. Details of both the development of generic reactors models intended to simulate particular combustor regions, and the different mechanisms utilised to estimate the level of emissions produced from a given combustor, in terms of $NO_x$, CO, UHC, and soot/smoke, were described as well. The gaseous emissions prediction model developed allows the reliable calculation of emissions trends from current and potential future aircraft gas turbine combustors.

In order to provide insight into the results that can be obtained using the emissions prediction software developed, a verification exercise of the model was carried out involving the simulation of a typical two-spool high bypass ratio turbofan using a conventional combustor. Based on the results obtained from the simulations, it is concluded that in general the emission trends observed in practice are sufficiently well reproduced, and in a computationally efficient manner for its subsequent incorporation in optimisation processes. Additionally, from experience obtained during the development of the computational model, it is concluded that it is particularly important to represent accurately the different combustor regions in order to obtain reasonable results, which present a satisfactory level of agreement with experimental data.

In order to carry out the processes of evaluation and optimisation of environmentally friendly aircraft propulsion systems intended in this work, it was decided to develop and implement a suitable optimiser with a library of optimisation algorithms, Polyphemus. Different numerical methods that could be used for this purpose were firstly reviewed, and a suitable optimisation technique, i.e., Genetic Algorithms, was initially selected. In order to have the background required, the main principles governing the selected optimisation technique were next reviewed. The referred optimisation algorithms were then developed and/or adapted and this thesis described their current status. The Polyphemus optimiser was subsequently utilised to analyse several case studies involving both aircraft trajectory optimisation processes, and engine cycle optimisation-type ones.

Before carrying out the different aircraft trajectory optimisation processes, an appropriate methodology was developed. This methodology mainly involved the definition of the aircraft trajectory optimisation problem, and more specifically, the identification of the parameters used as design variables, (implicit) constraints, and objective functions. Since all optimisation processes performed were limited to vertical

profiles, only three parameters, flight altitude, aircraft speed, and range, were used to define a given segment-based aircraft trajectory. In the trajectory optimisation processes, the range was usually kept constant (optimisation between city pairs). Thus, in general, only flight altitude and aircraft speed were used as design variables or constraints. Flight time, fuel burned, and $NO_x$ emitted were considered as the main objective functions.

The definition of the aircraft trajectory optimisation problem allowed, in turn, the identification of both the computational models required for the trajectory optimisation processes, and the different parameters to be exchanged among them. After being successfully used in several optimisation processes, it is concluded that the trajectory optimisation methodology developed was robust and well conceived for the type of optimisation processes carried out in this work. In particular, the definition of the aircraft trajectory problem was flexible enough, which allowed the realistic representation of flight procedures utilised currently in practice.

In this work, several aircraft trajectory optimisation processes involving both climb and whole (climb, cruise, and descent) flight profiles were carried out and their main results were presented and discussed. These flight profiles were assessed as part of several cases studies where complexities (in terms of operational constraints, number of segments, number of trajectory flight phases, etc.) were gradually included. Since, in general, the results obtained using Polyphemus and other commercially available optimisation algorithms presented a satisfactory level of agreement (average discrepancies of about 2%), it is concluded that its development is proceeding in the correct direction and should continue in order to improve its capabilities for identifying and efficiently computing optimum and ‘greener’ aircraft trajectories, which help to minimise the impact of commercial aircraft operations on the environment.

Regarding the trajectory optimisation results, it is important to start highlighting that the main objective of the different case studies analysed was the evaluation of the mathematical performance of Polyphemus rather than the determination of realistic aircraft trajectories. Accordingly, due to the fact that in general these different case studies provided solutions mathematically and conceptually correct, it is concluded that the approach utilised in this work for carrying out the aircraft trajectory optimisation

processes is a valid one. This of course provides the necessary motivation for continuing with the development of Polyphemus.

A number of optimum vertical aircraft flight profiles which minimise total flight time, fuel burned, and $NO_x$ emissions were computed in this work. A detailed summary of these optimum results is extensive. Thus, only their general trends and the main conclusions drawn from them are briefly indicated next. Minimisation of flight time means maximisation of true airspeed. For the minimisation of the total flight time, Polyphemus suggests then that the aircraft should fly using the highest possible true airspeed. In order to minimise the fuel burned during a given flight profile, in turn, the total energy required during the process must be minimised. This originates that profiles optimised for minimum fuel burned are characterised by relative low speeds and high altitudes. Accordingly, in order to reduce the fuel burned, Polyphemus suggests flying mostly slower and higher than the minimum time flight profiles.

Regarding the flight profiles optimised for minimum $NO_x$ emissions, it has been observed that they are generally flown similarly to the fuel optimised ones, i.e., mostly slower and higher than the minimum time flight profiles. Generally the relative lower speeds and higher altitudes utilised to fly these trajectories result in reductions in the thrust required to fly their segments. These lower thrust requirements are then translated into lower engine TET values, which ultimately reduce the level of $NO_x$ emissions produced. Overall it is concluded that, although the optimum flight profiles determined corresponded to hypothetical ones, the results provided numerical solutions that enabled the understanding of the performance of Polyphemus, which was the main objective of these optimisation processes.

In this work, as an attempt to illustrate other uses of Polyphemus, different engine cycle optimisation-type processes were also performed. These optimisation processes were mainly focused on the evaluation of the mathematical performance of Polyphemus rather than on the determination of realistic engine cycles. Simplifications were then introduced into these processes when both defining the aircraft flight trajectory and modelling the different engine configurations analysed. Accordingly, several optimum engine cycles minimising separately three objective functions, cruise SFC, fuel burned, and $NO_x$ emitted, were determined.

The optimum engine cycles results show that conventional two- or three-spool engines optimised for minimum cruise SFC and fuel burned are characterised by relatively high values of TET and OPR. A relatively high BPR is also a characteristic of this type of optimised engines. Since these parameters directly influence the level of $NO_x$ emitted, conventional (two- or three-spool) engines optimised for minimum $NO_x$ emissions are characterised by relatively low values of OPR and TET. ICR engines optimised for both minimum cruise SFC and minimum fuel burned are also characterised by relatively high values of TET, but only moderate OPR values. Further reductions in OPR characterise minimum $NO_x$ emissions ICR optimised engines. Regarding BPR specifically, the ICR engine results are consistent with those associated with conventional engines.

The engine cycle optimisation-type processes carried out yielded optimum results that reflect the general trends that could be expected when optimising according to the objective functions used in this work (i.e., cruise SFC, fuel burned, and $NO_x$ emissions). It is concluded then that Polyphemus is also suitable for carrying out this type of optimisation processes. Thus it is expected that these algorithms can be used in future for determining both optimum and 'greener' aircraft trajectories, and realistic aircraft engine cycles which help to optimise the preliminary design of this type of engines.

Finally, based on the results obtained from the different evaluation and optimisation processes carried out involving aircraft trajectories and engine cycles, it is concluded that there is indeed a feasible route to reduce the environmental impact of commercial aviation through the introduction of changes in the aircraft operational rules and procedures and/or in the aircraft/engine configurations. The magnitude of these reductions needs to be determined yet through careful consideration of more realistic aircraft trajectories and the use of higher fidelity computational models. In order to realistically estimate the magnitude of these reductions, eventually the computations will need to be extended to the entire fleet of aircraft. They will also need to include different operational scenarios involving partial replacements of old aircraft with new environmentally friendly ones.

## 8.2 Further Work

Further work needs to be developed in different research areas that are directly or indirectly related to the work developed in this research project. From these research areas, three of them deserve a special attention: modelling of formation of pollutants in gas turbine combustors, development and implementation of optimisation algorithms, and evaluation and optimisation of aircraft trajectories and engine cycles.

Even though the gaseous emissions prediction model developed in this work allows the reliable calculation of emissions trends from current and potential future aircraft gas turbine combustors, it is possible to improve its capabilities such that its absolute results reflect a better level of agreement with experimental data. This can be done through the inclusion (in the modelling process) of other phenomena that occur inside gas turbine combustors such as flow recirculation and fuel evaporation.

Flow recirculation patterns can be included through the direct modelling of the flow recirculation inside the combustor, or through the use of a stochastic representation of the combustor residence time. Either way, it would allow increases in the residence time in certain regions of the combustor which, in turn, would reduce the level of underestimation observed in some of the results obtained from the simulations. The modelling of fuel evaporation on the other hand may allow a more reliable prediction of pollutants such as CO and UHC, which are direct or indirect dependent on the level of completion of the combustion process. However, simplicity must be always a key feature of the model in order to both avoid significant increases in the level of uncertainties in the results obtained, and allow the production of results in a computationally efficient manner (i.e., model usable in optimisation processes).

Due to the modular approach followed during its development, the emissions prediction model developed can easily be expanded such that it allows the modelling of different types of gas turbine combustors, other than conventional ones. This could be done through both the incorporation of other generic reactors modelling particular regions of gas turbine combustors and/or particular phenomena occurring inside them, and the inclusion of features that allow the modelling of different types of fuel. This would allow eventually the simulation of combustors utilised not only in aircraft engines, but also in gas turbines utilised in industrial applications. For instance, the

emissions model can be extended to potential future aircraft gas turbine combustors based on novel concepts such as those of Lean Direct Injection (LDI) and Lean Pre-vaporised Premixed combustion (LPP).

Regarding optimisation algorithms in general, it is worth highlighting that the primary factor driving the initial stages of the development/adaptation of the optimiser (or optimisation algorithms) used in this work was its (their) robustness. Thus, since GAs are in general more robust than other traditional optimisation techniques, GAs-based optimisation routines developed in the past at Cranfield University were selected as the basis for the development and/or adaptation of Polyphemus. Since the suitability of Polyphemus for carrying out different optimisation processes (in particular aircraft trajectory optimisation ones) has been proved through the different cases studies analysed in this work, the next step in the development of this optimiser is naturally related to the improvement of its performance. Since Polyphemus already includes several algorithms for each of the main phases associated with a GAs-based optimisation, one way of improving the performance of this optimiser would involve the incorporation of other more efficient algorithms capable to better perform the same tasks as well as result in a lower computational time.

Other additional enhancements can also be introduced in future to further improve the performance of Polyphemus. These improvements include the use of both adaptive GAs (e.g., 'master-slave' configurations), which would allow the use of optimum GAs parameters (e.g., population size, crossover ratio, and mutation ratio, etc.) during the optimisation processes; and Pareto optimality-based concepts (Pareto fronts), which would improve its capabilities when performing multi-objective optimisation processes. Eventually, the GAs-based optimiser used in this work could be hybridised with other techniques including expert systems (which guide genetic operators more directly towards better strings), response surfaces (which construct objective function's approximate models to reduce full-cost functions evaluations), and neural networks (which act as pre-processors of GAs determining sub-regions in the search space where the optimum is likely to be found), among others.

The development and implementation of other optimisation algorithms based on different optimisation techniques also constitutes an important aspect that needs to be considered. As any optimisation tool, it is important that Polyphemus provides the user

with different alternatives of optimisation methods that could be used for a particular optimisation problem. Some of these methods will be of course appropriate only for specific types of optimisation problems. In these cases however it is likely that these methods will produce solutions faster than other more robust ones such as the GAs-based one currently available. Particular optimisation methods that might be interesting to implement are those ones associated with hill climbing approaches. These methods could include not only simplified ones which make use of the objective function value only (e.g., direct search methods), but also other more complex ones involving partial derivatives of the objective function (e.g., gradient and Newton methods). The availability of different optimisation methods would allow the comparison of their performance when applied to specific optimisation problems. It would provide at the same time the required basis for hybridising the current algorithm (i.e., GAs) with these other techniques if necessary. It is expected that these hybrid processes are able to yield eventually more accurate optimum solutions and in a more computationally efficient manner.

Finally, in regard to the evaluation and optimisation of aircraft trajectories and engine cycles, there are two main sub-areas in which further work needs to be developed. These areas relate to the definition of the optimisation problem (in particular the aircraft trajectory optimisation one) and the computational models utilised in the optimisation processes. The way in which the aircraft trajectory problem was defined in this work was robust and well conceived for the type of optimisation processes carried out here. Its flexibility allowed the realistic representation of flight procedures utilised currently in practice. Since in this work only theoretical aircraft trajectories were computed, in order to determine more realistic ones, some modifications in the aircraft trajectory problem definition need to be introduced.

These modifications are necessary because the computation of realistic trajectories will eventually require a very large number of trajectory segments. According to the current approach, this will imply the use of a very large number of design variables, which can negatively affect the performance of the optimisation algorithms. Thus, some sort of translation module will be required in order to ‘translate’ the parameters directly used in the optimisation processes as design variables (or constraints) into those ones directly defining the aircraft trajectory (e.g., flight altitudes), and vice versa. This

translation process can be carried out using for instance ‘spline’ functions, which represent and characterise, partially or entirely, the different flight phases associated with aircraft flight profiles. In order to determine optimum and realistic aircraft trajectories, this modified approach will also need to be extended eventually from the two-dimensional space utilised in this work to the three-dimensional one.

Once the aircraft trajectory optimisation problem is properly defined, the next step may involve the optimisation of other two- and three-dimensional flight profiles including not only separate flight phases, but also whole flight profiles; and taking into account a number of physical, operational, and environmental constraints. In order to carry out these processes, other computational models will also be required. These computational packages would model several other aspects related to commercial aircraft operations such as aircraft and engine noise, weather conditions, formation of contrails, and environmental impact, as well as flight corridors, airports, and ATC constraints, among others. In addition, other well known optimisers such as Isight [95] could also be utilised for testing and validating the results obtained from the evaluation and optimisation processes performed using the optimisation tool in development.

Similarly, in the case of the evaluation and optimisation of engine cycles, several other evaluation and optimisation processes can be carried out including other (gradually added) design variables and constraints. New computational models or modified ones can also be utilised in these processes. Both an engine weight model, and an aircraft performance model taking into account variations in the engine (nacelle) size, constitute typical examples of computational models that need to be included when optimising engine cycles. Additionally, both the engine (or aircraft/engine) configuration and its associated flight profile (flight trajectory) can eventually be optimised simultaneously. In other words, during the optimisation processes, for each engine (or aircraft/engine) configuration evaluated (potential optimum design), an optimum flight profile according to given criteria can be determined. At the end of the day, it is expected that following optimisation processes similar to those ones described in this work is possible to determine optimum and realistic engine cycles, which constitute ‘greener’ engine (cycle) designs that help to reduce the impact of commercial aircraft operations on the environment.

# 9
# References


1 Boeing Commercial Airplanes, Market Analysis, 2009, "Boeing Current Market Outlook 2009 to 2028", <www.boeing.com/cmo> , (accessed 16th August, 2009).

2 Riddlebaugh, and Stephen, M., (edit.), 2007, "Research & Technology 2006", NASA/TM – 2007-214479, NASA Glenn Research Center, Cleveland, Ohio, US.

3 Clarke, J. P., 2003, "The Role of Advanced Air Traffic Management in Reducing the Impact of Aircraft Noise and Enabling Aviation Growth", *Journal of Air Transport Management*, Vol. 9, No. 3, pp. 161-165.

4 Green, J. E., 2003, "Civil Aviation and the Environmental Challenge", *The Aeronautical Journal*, Vol. 107, No. 1072, pp. 281-299.

5 Brooker, P., 2006, "Civil Aircraft Design Priorities: Air Quality? Climate Change? Noise?", *The Aeronautical Journal*, Vol. 110, No. 1110, pp. 517-532.

6 PARTNER – Partnership for AiR Transportation Noise and Emissions Reduction, <web.mit.edu/aeroastro/partner/>, (accessed 18th August, 2009).

7 Clean Sky JTI (Joint Technology Initiative), <www.cleansky.eu>, (accessed 18th August, 2009).

8 Diedrich, A., Hileman, J., Tan, D., Willcox, K., and Spakovszky, Z., 2006, "Multidisciplinary Design and Optimization of the Silent Aircraft", AIAA 2006-1323, 44th AIAA Aerospace Sciences Meeting, Reno, Nevada, US.

9 Hileman, J. I., Spakovszky, Z. S., Drela, M., and Sargeant, M. A., 2006, "Aerodynamic and Aeroacoustic Three-Dimensional Design for a 'Silent' Aircraft", AIAA 2006-241, 44th AIAA Aerospace Sciences Meeting, Reno, Nevada, US.

10 Hileman, J. I., Reynolds, T. G., De La Rosa Blanco, E., Law, T. R., and Thomas, S., 2007, “Development of Approach Procedures for Silent Aircraft”, AIAA 2007-451, 45th AIAA Aerospace Sciences Meeting, Reno, Nevada, US.

11 Crichton, D., De La Rosa Blanco, E., Law, T. R., and Hileman, J. I., 2007, “Design and Operation for Ultra Low Noise Take-Off”, AIAA 2007-456, 45th AIAA Aerospace Sciences Meeting, Reno, Nevada, US.

12 Kim, H. D., Berton, J. J., and Jones, S. M., 2006, “Low Noise Cruise Efficient Short Take-Off and Landing Transport Vehicle Study”, AIAA 2006-7738, 6th AIAA Aviation Technology, Integration and Operations Conference, Wichita, Kansas, US.

13 Leifsson, L. T., Mason, W. H., Schetz, J. A., Haftka, R. T., and Grossman, B., 2006, “Multidisciplinary Design Optimization of Low-Airframe-Noise Transport Aircraft”, AIAA 2006-0230, 44th AIAA Aerospace Sciences Meeting, Reno, Nevada, US.

14 Atkins, E. M., Xue, M., 2004, “Noise-Sensitive Final Approach Trajectory Optimization for Runway-Independent Aircraft", *Journal of Aerospace Computing, Information, and Communication*, Vol. 1, No. 7, pp. 269-287.

15 Xue, M., Atkins, E. M., 2005, “Three-Dimensional Segmented Trajectory Optimization for Runway-Independent Aircraft”, AIAA 2005-0909, 43rd AIAA Aerospace Sciences Meeting, Reno, Nevada, US.

16 Xue, M., Atkins, E. M., 2006, “Terminal Area Trajectory Optimization Using Simulated Annealing”, AIAA 2006-1473, 44th AIAA Aerospace Sciences Meeting, Reno, Nevada, US.

17 Escarti, F., 2007, “Boeing Research and Technology Europe: Can Europe Compete as a Research Location?”, Final Conference of the European Commission LocoMotive Project, Hamburg, Germany. Available at <www. locomotive-project.org>.

18 Visser, H. G., and Wijnen, R. A. A., 2001, “Optimization of Noise Abatement Departure Trajectories”, *Journal of Aircraft*, Vol. 38, No. 4, pp. 620-627.

19 Visser, H. G., and Wijnen, R. A. A., 2001, “Optimization of Noise Abatement Arrival Trajectories”, AIAA 2001-4222, AIAA Guidance, Navigation, and Control Conference and Exhibit, Montreal, Canada.

20 Wijnen, R. A. A., and Visser, H. G., 2003, “Optimal Departure Trajectories with Respect to Sleep Disturbance”, *Aerospace Science and Technology*, Vol. 7, No. 1, pp. 81-91.

21 Visser, H. G., 2005, “Generic and Site-Specific Criteria in the Optimization of Noise Abatement Trajectories”, *Transportation Research, Part D: Transport and Environment*, Vol. 10, No. 5, pp. 405-419.

22 Quehl, J., and Basner, M., 2006, “Annoyance from Nocturnal Aircraft Noise Exposure: Laboratory and Field-Specific Dose-Response Curves”, *Journal of Environmental Psychology*, Vol. 26, No. 2, pp. 127-140.

23 Barkana, A., and Cook, G., 1976, “An Aircraft Noise Pollution Model for Trajectory Optimization”, *IEEE Transactions on Aerospace and Electronic Systems*, Vol. AES-12, No. 2, pp. 109-116.

24 Norgia, L., 1999, “A Graphical Optimization of Take-Off Noise Abatement Procedures for Subsonic Aircraft”, *Journal of Sound and Vibration*, Vol. 222, No. 3, pp. 489-501.

25 Green, S. M., and Vivona, R. A., 2001, "En route Descent Advisor Concept for Arrival Metering", AIAA 2001-4114, AIAA Guidance, Navigation, and Control Conference, Montreal, Canada.

26 Coppenbarger, R. A., Lanier, R., Sweet, D., and Dorsky, S., 2004, "Design and Development of the En Route Descent Advisor (EDA) for Conflict-Free Arrival Metering", AIAA 2004-4875, AIAA Guidance, Navigation, and Control Conference, Providence, RI, US.

27 Mueller, K. T., Bortins, R., Schleicher, D. R., Sweet, D., and Coppenbarger, R. A., 2004, "Effect of Uncertainty on (EDA) Predictions," AIAA 2004-6347, AIAA 4th Aviation Technology, Integration, and Operations (ATIO) Forum, Chicago, IL, US.

28 Hagelauer, P., and Mora-Camino, F., 1998, "A Soft Dynamic Programming Approach for On-Line Aircraft 4D-Trajectory Optimization", *European Journal of Operational Research*, Vol. 107, No. 1, pp. 87-95.

29 Zaporozhets, O. I., and Tokarev, V. I., 1998, "Predicted Flight Procedures for Minimum Noise Impact", *Applied Acoustics*, Vol. 55, No. 2, pp. 129-143.

30 Ponater, M., Pechtl, S., Sausen, R., Schumann, U., and Hüttig, G., 2006, "Potential of The Cryoplane Technology to Reduce Aircraft Climate Impact: A State-of-the-art Assessment", *Atmospheric Environment*, Vol. 40, No. 36, pp. 6928-6944.

31 Antoine, N. E., and Kroo, I. M., 2005, "Framework for Aircraft Conceptual Design and Environmental Performance Studies", *AIAA Journal*, Vol. 43, No.10, pp. 2100-2109.

32 Antoine, N. E., Kroo, I. M., Willcox, K., and Barter, G., 2004, "A Framework for Aircraft Conceptual Design and Environmental Performance Studies", AIAA-2004-4314, 10th AIAA/ISSMO Multidisciplinary Analysis and Optimization Conference, Albany, NY, US.

33 Le Dilosquer, M., 1998, "Influence of Subsonic Aero Engine Design and Flight Routes on Atmospheric Pollution", Ph.D. Thesis, School of Mechanical Engineering, Cranfield University, UK.

34 Laskaridis, P., 2004, "Performance Investigations and Systems Architectures for the More-Electric Aircraft", Ph.D. Thesis, School of Engineering, Cranfield University.

35 Laskaridis, P., Pilidis, P., and Kotsiopoulos, P., 2005, "An Integrated Engine-Aircraft Performance Platform for Assessing New Technologies in Aeronautics", ISABE-2005-1165, Munich, Germany.

36 Green, J. E., 2003, "Civil Aviation and the Environmental Challenge", *The Aeronautical Journal*, Vol. 107, No. 1072, pp. 281-299.

37 Filippone, A., 2007, "On the Benefits of Lower Mach Number Aircraft Cruise", *The Aeronautical Journal*, Vol. 111, No. 1122, pp. 531-542.

38 Nangia, R. K., 2006, “Operations and Aircraft Design towards Greener Civil Aviation using Air-to-Air Refuelling”, *The Aeronautical Journal*, Vol. 110, No. 1113, pp. 705-721.

39 Nangia, R. K., 2007, “‘Greener’ Civil Aviation using Air-to-Air Refuelling – Relating Aircraft Design Efficiency and Tanker Offload Efficiency”, *The Aeronautical Journal*, Vol. 111, No. 1123, pp. 589-592.

40 Moss, J. B., 2001, “Predictive Methods for Gas Turbine Combustor Emissions”, IMechE Seminar Publications on Gas Turbine Pollutant Emissions, Professional Engineering Publishing, London, UK.

41 Allaire, D. L., Waitz, I. A., and Willcox, K. E., 2007, “A Comparison of Two Methods for Predicting Emissions from Aircraft Gas Turbine Combustors”, GT2007-28346, Proceedings of GT2007, ASME Turbo Expo 2007: Power for Land, Sea and Air, Montreal, Canada.

42 Visser, W. P. J., and Kluiters, S. C. A, 1998, “Modeling the Effects of Operating Conditions and Alternative Fuels on Gas Turbine Performance and Emissions”, RTO AVT Symposium on Gas Turbine Performance and Emissions, Lisbon, Portugal.

43 Shakariyants, S. A., van Buijtenen, J. P., Visser, W. P. J., and Tarasov, A., 2006, "A Multidisciplinary Aero-Engine Exhaust Emission Study", Proceedings of GT2006, ASME Turbo Expo 2006: Power for Land, Sea and Air, Barcelona, Spain.

44 Mohamed, H., Ticha, H. B., and Mohamed, S., 2004, “Simulation of Pollutant Emissions from a Gas-Turbine Combustor”, *Combustion Science and Technology*, Vol. 176, No. 5, pp. 819-834.

45 Aksit, I. M., 1995, “A Stochastic Model for Aircraft Gas Turbine Combustor Emissions”, Ph.D. Thesis, School of Mechanical Engineering, Cranfield University.

46 Gordon, S., and McBride, B. J., 1994, “Computer Program for Calculation of Complex Chemical Equilibrium Compositions and Applications. I. Analysis”,

NASA Reference Publication 1311, National Aeronautics and Space Administration, Lewis Research Center, Ohio, US.

47 McBride, B. J., and Gordon, S., 1996, "Computer Program for Calculation of Complex Chemical Equilibrium Compositions and Applications. II. Users Manual and Program Description", NASA Reference Publication 1311, National Aeronautics and Space Administration, Lewis Research Center, Ohio, US.

48 Hammond, D. C. JR., and Mellor, A.M., 1971, "Analytical Calculations for the Performance and Pollutant Emissions of Gas Turbine Combustors", *Combustion Science and Technology*, Vol. 4, pp.101-112.

49 Hammond, D. C. JR., and Mellor, A. M., 1973, "Analytical Predictions of Emissions from and Within an Allison J-33 Combustor", *Combustion Science and Technology*, Vol. 6, pp. 279-286.

50 Mellor, A. M., 1976, "Gas Turbine Engine Pollution", *Progress in Energy and Combustion Science*, Vol. 1, pp. 111-133.

51 Fletcher, R. S., and Heywood, J. B., 1971, "A Model for Nitric Oxide Emissions from Aircraft Gas Turbine Engines", AIAA Paper 71-123, AIAA 9th Aerospace Sciences Meeting, New York, US.

52 Williams, F. A., 1985, *Combustion Theory*, 2nd Edition, Benjamin/Cummings Pub. Co, California, US.

53 Sturgess, G. J., 1998, "An Account of Fuel/Air Unmixedness Effects on $NO_x$ Generation in Gas Turbine Combustors", IECEC-98-353, 33rd Intersociety Engineering Conference on Energy Conversion, Colorado Springs, US.

54 Sturgess, G. J., Zelina, J., Shouse, D., and Roquemore, W., 2005, "Emissions reduction technologies for military gas turbine engines", *Journal of Propulsion and Power*, Vol. 21, No. 2, pp. 193-217.

55 Celis, C., Mohseni, M., Kyprianidis, K., Sethi, V., Ogaji, S., Haslam, A., and Pilidis, P., 2008, "Multidisciplinary Design Optimisation of Aero Engines: Environmental Performance-based Methodology", International Symposium on Compressor & Turbine Flow Systems − Theory & Application Areas, SYMKOM'08, Lodz, PL.

56 Lefebvre, A. H., 1998, *Gas Turbine Combustion*, Taylor and Francis, 2nd Edition, London, UK.

57 Bowman, C. T., 1992, "Control of Combustion-Generated Nitrogen Oxide Emissions: Technology Driven by Regulation," Twenty-Fourth Symposium (International) on Combustion/The Combustion Institute, Sydney, Australia.

58 Miller, J. A., and Bowman, C. T., 1989, "Mechanism and Modelling of Nitrogen Chemistry in Combustion", *Progress in Energy and Combustion Science*, Vol. 15, pp. 287-338.

59 Heywood, J. B., Fay, J. A., and Linden, L. H, 1971, "Jet Aircraft Air Pollutant Production and Dispersion," *AIAA Journal*, Vol. 9, No. 5, pp. 841-850.

60 De Soete, G. G., 1975, "Overall Reaction Rates of NO and N2 Formation from Fuel Nitrogen", 15th Symposium (International) on Combustion/The Combustion Institute, Tokyo, Japan.

61 FLUENT, Flow Modeling Software, "FLUENT 6.2 User's Guide", Fluent Inc., Lebanon, NH, US.

62 Westenberg, A. A., 1971, "Kinetics of NO and CO in Lean, Premixed Hydrocarbon-Air Flames", *Combustion Science and Technology*, Vol. 4, pp.59-64.

63 Dryer, F. L., and Glassman, I., 1973, "High-Temperature oxidation of CO and CH4", 14th Symposium (International) on Combustion/The Combustion Institute, PA, US.

64 Edelman, R. B., and Fortune, O. F., 1969, "A Quasi- Global Chemical Kinetic Model for the Finite Rate Combustion of Hydrocarbon Fuels with Application to Turbulent Burning and Mixing in Hypersonic Engines and Nozzles", 7th AIAA Aerospace Sciences Meeting, New York, US.

65 Rizk, N. K., and Mongia, H. C., 1994, "Emissions Predictions of Different Gas Turbine Combustors", AIAA-94-0118, 32nd AIAA Aerospace Sciences Meeting & Exhibit, Reno, NV, US.

66 Nagle, J., and Strickland-Constable, R. F., 1962, "Oxidation of Carbon between 1000-2000ºC', Proceedings of 5th Conference on Carbon, Pergamon Press, NY, US, pp. 154-164.

67 Appleton, J. P., 1973, "Soot Oxidation Kinetics at Combustion Temperatures", Atmospheric Pollution by Aircraft Engines, AGARD-Conference Proceedings-125, Paper 20, Neuilly Sur Seine, France.

68 Villasenor, R. and Kennedy, I. M., 1992, "Soot Formation and Oxidation in Laminar Diffusion Flames," Twenty-Fourth Symposium (International) on Combustion/The Combustion Institute, Sydney, Australia.

69 Girling, S. P., 1988, "Gas Turbine Smoke Measurement: A Smoke Generator for the Assessment of Current and Future Techniques", Proceedings Combustion and Fuels in Gas Turbine Engines, Paper 20, AGARD, Neuilly Sur Seine, France.

70 Palmer, J. R., 1999, The TurboMatch Scheme for Gas-Turbine Performance Calculations, User's Guide, Cranfield University, Cranfield, UK.

71 Gunston, B. (Edt.), 2007, *Jane's Aero Engines*, Issue 21, Jane's Information Group.

72 General Electric Aviation home page <http://www.geaviation.com>.

73 United Kingdom Civil Aviation Authority (Updated 07 April 2008), "ICAO Engine Emissions Databank", <http://www.caa.co.uk>.

74 Rizk, N. K., and Mongia, H. C., 1993, "Semianalytical Correlations for $NO_x$, CO, and UHC Emissions", *Journal of Engineering for Gas Turbine and Power*, Vol. 115, No. 3, pp.612-619.

75 Walsh, G. R., 1975, *Methods of Optimization*, John Wiley, London, UK.

76 Schwefel, H. P., 1981, *Numerical Optimization of Computer Models*, John Wiley, Chichester, UK.

77 Bunday, B. D., 1984, *Basic Optimisation Methods*, Edward Arnold, London, UK.

78 Fletcher, R., 1987, *Practical Methods of Optimization*, 2nd Edition, John Wiley, Chichester, UK.

79 Everitt, B., 1987, Introduction to Optimization Methods and their Application in Statistics, Chapman and Hall, London, UK.

80 Krotov, V. F., 1996, *Global Methods in Optimal Control Theory*, Marcel Dekker, New York, US.

81 Rao, S. S., 1996, *Engineering Optimization: Theory and Practice*, 3rd Edition, John Wiley, New York, US.

82 Betts, J., 1998, "Survey of Numerical Methods for Trajectory Optimization", *Journal of Guidance, Control, and Dynamics*, Vol. 21, No. 2, pp. 193-207.

83 Russell, S., and Norvig, P., 2003, *Artificial Intelligence: A Modern Approach*, 2nd Edition, Prentice Hall, New Jersey, US.

84 Quagliarella, D., 1998, Genetic Algorithms and Evolution Strategy in Engineering and Computer Science, Recent Advances and Industrial Applications, John Wiley & Sons, Ltd., Chichester, UK.

85 Koza, J. R., 1992, Genetic Programming: On the Programming of Computers by Means of Natural Selection, MIT Press, Cambridge, MA, US.

86 Gulati, A., 2001, "An Optimization Tool for Gas Turbine Engine Diagnostics", Ph.D. Thesis, School of Engineering, Cranfield University.

87 Rogero, J. M., 2002, "A Genetic Algorithms-based Optimisation Tool for the Preliminary Design of Gas Turbine Combustors", Ph.D. Thesis, School of Mechanical Engineering, Cranfield University.

88 Sampath, S., 2003, "Fault Diagnostics for Advanced Cycle Marine Gas Turbine Using Genetic Algorithms", Ph.D. Thesis, School of Engineering, Cranfield University.

89 Whellens, M. W., 2003, "Multidisciplinary Optimisation of Aero-Engines Using Genetic Algorithms and Preliminary Design Tools", Ph.D. Thesis, School of Engineering, Cranfield University.

90 Hargraves, C. R., and Paris, S.W., 1987, "Direct Trajectory Optimization Using Nonlinear Programming and Collocation", *Journal of Guidance, Control, and Dynamics*, Vol. 10, No. 4, pp. 338-342.

91 Schultz, R. L., 1990, "Three-Dimensional Trajectory Optimization for Aircraft", *Journal of Guidance, Control, and Dynamics*, Vol. 13, No. 6, pp. 936-943.

92 Betts, J. T., and Cramer, E. J., 1995, “Application of Direct Transcription to Commercial Aircraft Trajectory Optimization”, *Journal of Guidance, Control, and Dynamics*, Vol. 18, No. 1, pp.151-159.

93 Casanova, D., 2000, “On Minimum Time Vehicle Manoeuvring: The Theoretical Optimal Lap”, Ph.D. Thesis, School of Mechanical Engineering, Cranfield University.

94 MATLAB®, *The Language of Technical Computing*, Version 7.7 (R2008b), The MathWorks, Inc., <www.mathworks.com>.

95 Isight, SIMULIA-Dassault Systèmes (DS), < www.simulia.com >.

96 Ogaji, S.O.T., Pilidis, P., and Sethi, V., 2008, “Power Plant Selection in a Carbon Constrained World: The TERA (Techno-economic Environmental Risk Analysis)”, 2nd International Symposium on Jet Propulsion and Power Engineering, 2008-ISJPPE-0006, Guilin, China.

97 Ogaji, S.O.T., Pilidis, P., and Sethi, V., 2008, “Advanced Power Plant Selection: The TERA (Techno-economic Environmental Risk Analysis) Framework”, 19th ISABE Conference, ISABE-2009-1115, Montreal, Canada.

98 Goldberg, D., and Sastry, K., 2007, *Genetic Algorithms: The Design of Innovation*, 2nd Edition, Springer, New York, US.

99 Luger, G. F., 2005, Artificial Intelligence: Structures and Strategies for Complex Problem Solving, 5th Edition, Addison-Wesley, Harlow, UK.

100 Haupt, R. L., and Haupt, S. E., 2004, *Practical Genetic Algorithms*, 2nd Edition, John Wiley & Sons Inc., Chichester, UK.

101 Callan, R., 2003, *Artificial Intelligence*, Palgrave Macmillan, New York, US.

102 Goldberg, D. E., 2002, The Design of Innovation: Lessons from and for Competent Genetic Algorithms, Kluwer Academic Publishers, Norwell, MA, US.

103 Gen, M., and Cheng, R., 2000, *Genetic Algorithms and Engineering Optimization*, John Wiley & Sons Inc., Chichester, UK.

104 Goldberg, D. E., 1989, Genetic Algorithms in Search, Optimization and Machine Learning, Addison-Wesley, Reading, MA, US.

105 Whitley, D., 1989, "The GENITOR Algorithm and Selection Pressure: Why Rank-based Allocation of Reproductive Trials is Best", Proceedings of the 3rd International Conference on Genetic Algorithms, Morgan Kaufmann Publishers Inc., San Francisco, CA, US.

106 Davis, L., editor, 1991, *Handbook of Genetic Algorithms*, Van Nostrand Reinhold, New York, US.

107 Eshelman, L. J., and Schaffer, J. D., 1993, "Real-coded Genetic Algorithms and Interval-schemata", Whitley, D. L. (Editor), *Foundations of Genetic Algorithms*, Vol. 2, Morgan Kaufmann Publishers, San Francisco, US.

108 Deb, K., and Agrawal, R. B., 1994, "Simulated Binary Crossover for Continuous Search Space Export", *Complex Systems*, Vol. 9, pp. 1-34.

109 Michalewicz, Z., 1996, *Genetic Algorithms + Data Structures = Evolution Programs*, 3rd Edition, Springer-Verlag, New York, US.

110 Eiben, A. E., and Smith, J. E., 2003, *Introduction to Evolutionary Computing*, Springer-Verlag, New York, US.

111 Michalewicz, Z., 1995, "A Survey of Constraint Handling Techniques in Evolutionary Computation Methods", Proceedings of the 4th Annual Conference on Evolutionary Programming, MIT Press, Cambridge, MA, US.

112 Deb, K. 2000, "An Efficient Constraint Handling Method for Genetic Algorithms", *Computer Methods in Applied Mechanics and Engineering*, Vol. 186, No. 2-4, pp. 311-338.

113 Wienke, D., Lucasius, C. B., and Kateman, G., 1192, "Multicriteria Target Vector Optimization of Analytical Procedures Using a Genetic Algorithm. Part I. Theory, Numerical Simulation and Application to Atomic Emission Spectroscopy", *Analytica Chimica Acta*, 265, pp. 211-225.

114 Rogero, J. M., and Rubini, P. A., 2003, "Optimisation of Combustor Wall Heat Transfer and Pollutant Emissions for Preliminary Design Using Evolutionary

Techniques", *Proceedings of the Institution of Mechanical Engineers, Part A: Journal of Power and Energy*, 217(6), pp. 605-614.

115 Hartley, S. J., 1998, *Concurrent Programming: The Java Programming Language*, Oxford University Press, New York, US.

116 Lowry, J. T., 1999, *Performance of Light Aircraft*, American Institute of Aeronautics and Astronautics, Inc., Reston, VA, US.

117 National Aeronautics and Space Administration, NASA, 1976, "U.S. Standard Atmosphere", NASA-TM-X-74335, U.S. Government Printing Office, Washington, US.

118 Gracey, W, 1980, "Measurement of Aircraft Speed and Altitude", NASA Langley Research Center, Report No. L-12610, NASA-RP-1046.

119 Saarlas, M., 2007, *Aircraft Performance*, John Wiley & Sons, Inc., Hoboken, New Jersey, US.

120 Houghton, E. L., and Carpenter, P. W., 2003, *Aerodynamics for Engineering Students*, 5th Edition, Butterworth-Heinemann, Oxford, UK.

121 Filippone, A., 2006, *Flight Performance of Fixed and Rotary Wing Aircraft*, First Edition, Butterworth-Heinemann, Oxford, UK.

122 Long, R. F, 2009, "An Aircraft Performance Model for Trajectory Optimisation", School of Engineering, Cranfield University, UK (unpublished).

123 Celis, C, Moss, B., and Pilidis, P., 2009, "Emissions Modelling for the Optimisation of Greener Aircraft Operations", GT2009-59211, Proceedings of GT2009, ASME Turbo Expo 2009, Power for Land, Sea and Air, Orlando, Florida, USA.

124 Celis, C., Long, R., Sethi, V., and Zammit-Mangion, D., 2009, "On Trajectory Optimisation for Reducing the Impact of Commercial Aircraft Operations on the Environment", ISABE-2009-1118, 19th Conference of the International Society for Air Breathing Engines, Montréal, Canada.

125 Zolata, H., 2009, "Development of a Multi-Disciplinary Aircraft Trajectory Optimisation Simulation Framework", M.Sc. Thesis, School of Engineering, Cranfield University, UK.

126 Ramsden, K, W., 2007, *Turbomachinery*, Course's lecture notes, School of Engineering, Cranfield University, UK.

127 Saravanamuttoo, H. I. H., Rogers, C. F. G., Cohen, H., and Straznicky, P. V., 2009, *Gas Turbine Theory*, 6th Edition, Pearson Prentice Hall, Harlow, England.

128 Boggia, S., and Rüd, K., 2005, "Intercooled Recuperated Gas Turbine Engine Concept", AIAA 2005-4192, 41st AIAA/ASME/SAE/ASEE Joint Propulsion Conference & Exhibit, Tucson, Arizona, US.

129 Fanourakis, E., 2006, "Inter-cooled Recuperated Aero-Engine: Feasibility Investigation", M.Sc. Thesis, School of Engineering, Cranfield University, UK.

130 Scialo', S., E., 2007, "Performance Simulation and Investigation of an Intercooled Recuperated Aeroengine", M.Sc. Thesis, School of Engineering, Cranfield University, UK.

# 10
# Appendices

## Appendix A
## List of Publications

Scientific Journals:

- Celis, C., Sethi, V., Zammit-Mangion, D., and Singh, R., 2010, "Theoretical Optimal Trajectories for Reducing the Environmental Impact of Commercial Aircraft Operations", Article submitted to the *Journal of Aerospace Science and Technology*.
- Celis, C., Sethi, V., Singh, R., and Pilidis, P, 2010, "On Optimisation of Environmentally Friendly Aircraft Engine Cycles", Article submitted to the *ASME Journal of Engineering for Gas Turbines and Power*.
- Sethi, V., Ogaji, S., Singh, R., Pilidis, P, Celis, C., Di Lorenzo, G., and Zammit-Mangion, D., 2010, "Energy Plant Selection and Asset Management: The TERA (Technoeconomic Environmental Risk Analysis)", Article submitted to the *ASME Journal of Energy Resources Technology*.

Conference and Proceedings:

- Zolata, H., Celis, C., Sethi, V., Singh, R., and Zammit-Mangion, D., 2010, "A Multi-Criteria Simulation Framework for Civil Aircraft Trajectory Optimisation", Abstract submitted to the ASME International Mechanical Engineering Congress & Exposition, Vancouver, Canada.

- Ogaji, S., Sethi, V., Pilidis, P, Singh, R., Celis, C., Di Lorenzo, G., and Zammit-Mangion, D., 2010, "Power Plant Selection and Deployment: The TERA (Technoeconomic Environmental Risk Analysis)", Paper submitted to the 5th ETN (European Turbine Network) International Gas Turbine Conference, The Future of Gas Turbine Technology, Brussels, Belgium.
- Goulos, I., Pachidis, V., Celis, C, D'Ippolito, R., Stevens, J., 2010, "Simulation Framework Development for Aircraft Mission Analysis", GT2010-23379, Proceedings of GT2010, ASME Turbo Expo 2010, Power for Land, Sea and Air, Glasgow, UK.
- Celis, C., Long, R., Sethi, V., and Zammit-Mangion, D., 2009, "On Trajectory Optimisation for Reducing the Impact of Commercial Aircraft Operations on the Environment", ISABE-2009-1118, 19th Conference of the International Society for Air Breathing Engines, Montréal, Canada.
- Celis, C, Moss, B., and Pilidis, P., 2009, "Emissions Modelling for the Optimisation of Greener Aircraft Operations", GT2009-59211, Proceedings of GT2009, ASME Turbo Expo 2009, Power for Land, Sea and Air, Orlando, Florida, USA.
- Celis, C, Moss, B., and Pilidis, P., 2009, "Towards a Larger Reduction of the Environmental Impact of Commercial Aircraft Operations: An Emissions Prediction Model for Gas Turbine Combustors", 3rd AlBan Conference - Oporto 2009, Oporto, Portugal.
- Celis, C., Mohseni, M., Kyprianidis, K., Sethi, V., Ogaji, S., Haslam, A., and Pilidis, P., 2008, "Multidisciplinary Design Optimization of Aero Engines: Environmental Performance-based Methodology", International Symposium on Compressor & Turbine Flow Systems − Theory & Application Areas, SYMKOM'08, Lodz, PL.

## Appendix B
## Kinetic Model of Thermal NO and N2O Mechanism

The thermal NO formation rate is predicted according to the extended Zeldovich mechanism [51, 56-58]:

$$N_2 + O \Leftrightarrow NO + N \qquad \text{R1} \qquad (10\text{-}1)$$

$$N + O_2 \Leftrightarrow NO + O \qquad \text{R2} \qquad (10\text{-}2)$$

$$N + OH \Leftrightarrow NO + H \qquad \text{R3} \qquad (10\text{-}3)$$

and the $N_2O$ contribution to the formation of NO according to [51,59]:

$$H + N_2O \Leftrightarrow N_2 + OH \qquad \text{R4} \qquad (10\text{-}4)$$

$$O + N_2O \Leftrightarrow N_2 + O_2 \qquad \text{R5} \qquad (10\text{-}5)$$

$$O + N_2O \Leftrightarrow NO + NO \qquad \text{R6} \qquad (10\text{-}6)$$

Then from Eq. (10-1):

$$\frac{d[N]}{dt} = -k_{1f}[N][NO] + k_{1b}[N_2][O] \qquad (10\text{-}7)$$

$$\frac{d[NO]}{dt} = -k_{1f}[N][NO] + k_{1b}[N_2][O] \qquad (10\text{-}8)$$

$$\frac{d[N_2]}{dt} = k_{1f}[N][NO] - k_{1b}[N_2][O] \qquad (10\text{-}9)$$

$$\frac{d[O]}{dt} = k_{1f}[N][NO] - k_{1b}[N_2][O] \qquad (10\text{-}10)$$

from Eq. (10-2):

$$\frac{d[N]}{dt} = -k_{2f}[N][O_2] + k_{2b}[NO][O] \qquad (10\text{-}11)$$

$$\frac{d[O_2]}{dt} = -k_{2f}[N][O_2] + k_{2b}[NO][O] \qquad (10\text{-}12)$$

$$\frac{d[NO]}{dt} = k_{2f}[N][O_2] - k_{2b}[NO][O] \tag{10-13}$$

$$\frac{d[O]}{dt} = k_{2f}[N][O_2] - k_{2b}[NO][O] \tag{10-14}$$

from Eq. (10-3):

$$\frac{d[N]}{dt} = -k_{3f}[N][OH] + k_{3b}[NO][H] \tag{10-15}$$

$$\frac{d[OH]}{dt} = -k_{3f}[N][OH] + k_{3b}[NO][H] \tag{10-16}$$

$$\frac{d[NO]}{dt} = k_{3f}[N][OH] - k_{3b}[NO][H] \tag{10-17}$$

$$\frac{d[H]}{dt} = k_{3f}[N][OH] - k_{3b}[NO][H] \tag{10-18}$$

from Eq. (10-4):

$$\frac{d[H]}{dt} = -k_{4f}[H][N_2O] + k_{4b}[N_2][OH] \tag{10-19}$$

$$\frac{d[N_2O]}{dt} = -k_{4f}[H][N_2O] + k_{4b}[N_2][OH] \tag{10-20}$$

$$\frac{d[N_2]}{dt} = k_{4f}[H][N_2O] - k_{4b}[N_2][OH] \tag{10-21}$$

$$\frac{d[OH]}{dt} = k_{4f}[H][N_2O] - k_{4b}[N_2][OH] \tag{10-22}$$

from Eq. (10-5):

$$\frac{d[O]}{dt} = -k_{5f}[O][N_2O] + k_{5b}[N_2][O_2] \tag{10-23}$$

$$\frac{d[N_2O]}{dt} = -k_{5f}[O][N_2O] + k_{5b}[N_2][O_2] \tag{10-24}$$

$$\frac{d[N_2]}{dt} = k_{5f}[O][N_2O] - k_{5b}[N_2][O_2] \tag{10-25}$$

$$\frac{d[O_2]}{dt} = k_{5f}[O][N_2O] - k_{5b}[N_2][O_2] \tag{10-26}$$

and from Eq. (10-6):

$$\frac{d[O]}{dt} = -k_{6f}[O][N_2O] + k_{6b}[NO][NO] \tag{10-27}$$

$$\frac{d[N_2O]}{dt} = -k_{6f}[O][N_2O] + k_{6b}[NO][NO] \tag{10-28}$$

$$\frac{d[NO]}{dt} = k_{6f}[O][N_2O] - k_{6b}[NO][NO] \tag{10-29}$$

$$\frac{d[NO]}{dt} = k_{6f}[O][N_2O] - k_{6b}[NO][NO] \tag{10-30}$$

Summing equations (10-8), (10-13), (10-17), (10-29), and (10-30), as well as assuming equilibrium concentrations for $O_2$, $N_2$, O, OH, and H,

$$\frac{d[O_2]_e}{dt} = \frac{d[N_2]_e}{dt} = \frac{d[O]_e}{dt} = \frac{d[OH]_e}{dt} = \frac{d[H]_e}{dt} = 0 \tag{10-31}$$

the rate of formation of NO is given by:

$$\begin{aligned}\frac{d[NO]}{dt} &= -k_{1f}[N][NO] + k_{1b}[N_2]_e.[O]_e + k_{2f}[N][O_2]_e - k_{2b}[NO][O]_e \\ &+ k_{3f}[N][OH]_e - k_{3b}[NO][H]_e + 2k_{6f}[O]_e.[N_2O] - 2k_{6b}[NO][NO]\end{aligned} \tag{10-32}$$

Then defining:

$$\begin{aligned}R_1 &= k_{1f}[N]_e.[NO]_e \\ R_2 &= k_{2f}[N]_e.[O_2]_e \\ R_3 &= k_{3f}[N]_e.[OH]_e \\ R_4 &= k_{4f}[H]_e.[N_2O]_e\end{aligned} \tag{10-33}$$

$$R_5 = k_{5f}[O]_e.[N_2O]_e$$

$$R_6 = k_{6f}[O]_e.[N_2O]_e$$

and,

$$\alpha = \frac{[NO]}{[NO]_e} \; ; \; \beta = \frac{[N]}{[N]_e} \; ; \; \gamma = \frac{[N_2O]}{[N_2O]_e} \tag{10-34}$$

the following terms can be expressed as:

$$\begin{aligned} &-k_{1f}[N][NO] + k_{1b}[N_2]_e.[O]_e = -k_{1f}[N][NO].\frac{[NO]_e}{[NO]_e}.\frac{[N]_e}{[N]_e} + k_{1b}[N_2]_e.[O]_e \\ &= -\alpha.\beta.R_1 + R_1 \end{aligned} \tag{10-35}$$

$$\begin{aligned} &k_{2f}[N][O_2]_e - k_{2b}[NO][O]_e = k_{2f}[N][O_2]_e.\frac{[N]_e}{[N]_e} - k_{2b}[NO][O]_e.\frac{[NO]_e}{[NO]_e} \\ &= \beta.R_2 - \alpha.R_2 \end{aligned} \tag{10-36}$$

$$\begin{aligned} &k_{3f}[N][OH]_e - k_{3b}[NO][H]_e = k_{3f}[N][OH]_e.\frac{[N]_e}{[N]_e} - k_{3b}[NO][H]_e.\frac{[NO]_e}{[NO]_e} \\ &= \beta.R_3 - \alpha.R_3 \end{aligned} \tag{10-37}$$

$$\begin{aligned} &2k_{6f}[O]_e.[N_2O] - 2k_{6b}[NO][NO] \\ &= 2k_{6f}[O]_e.[N_2O].\frac{[N_2O]_e}{[N_2O]_e} - 2k_{6b}[NO][NO].\frac{[NO]_e}{[NO]_e} \\ &= 2\gamma.R_6 - 2\alpha^2.R_6 \end{aligned} \tag{10-38}$$

From equations (10-35) – (10-38) in (10-32):

$$\frac{d[NO]}{dt} = -\alpha\left(\beta.R_1 + R_2 + R_3 + 2\alpha.R_6\right) + R_1 + \beta\left(R_2 + R_3\right) + 2\gamma.R_6 \tag{10-39}$$

Assuming steady state conditions for N and $N_2O$,

$$\begin{aligned} &\frac{d[N]}{dt} = -k_{1f}[N][NO] + k_{1b}[N_2][O] - k_{2f}[N][O_2] + k_{2b}[NO][O] \\ &- k_{3f}[N][OH] + k_{3b}[NO][H] = 0 \\ &= -\beta\left(\alpha.R_1 + R_2 + R_3\right) + R_1 + \alpha\left(R_2 + R_3\right) = 0 \end{aligned} \tag{10-40}$$

and

$$\frac{d[N_2O]}{dt} = -k_{4f}[H][N_2O] + k_{4b}[N_2][OH] - k_{5f}[O][N_2O] + k_{5b}[N_2][O_2]$$
$$- k_{6f}[O][N_2O] + k_{6b}[NO][NO] = 0 \qquad (10\text{-}41)$$
$$= -\gamma(R_4 + R_5 + R_6) + R_4 + R_5 + \alpha^2.R_6 = 0$$

Therefore:

$$\beta = \frac{K_1 + \alpha}{1 + \alpha.K_1} \text{ and } \gamma = \frac{1 + \alpha^2.K_2}{1 + K_2} \qquad (10\text{-}42)$$

where

$$K_1 = \frac{R_1}{R_2 + R_3} \text{ and } K_2 = \frac{R_6}{R_4 + R_5} \qquad (10\text{-}43)$$

Substituting Eq. (10-42) in (10-39), one has:

$$\frac{d[NO]}{dt} = 2(1 - \alpha^2)\left\{\frac{R_1}{1 + \alpha K_1} + \frac{R_6}{1 + K_2}\right\} \qquad (10\text{-}44)$$

but

$$[NO] = \frac{\rho Y_{NO}}{\overline{M}_{NO}} \qquad (10\text{-}45)$$

therefore,

$$\frac{dY_{NO}}{dt} = \frac{2\overline{M}_{NO}}{\rho}(1 - \alpha^2)\left\{\frac{R_1}{1 + \alpha K_1} + \frac{R_6}{1 + K_2}\right\} \qquad (10\text{-}46)$$

In the equations indicated previously, [] represents concentration of species or elements, and the subscript ‘e’ represents in turn equilibrium values.

## Appendix C
## Kinetic Model of Carbon Monoxide (CO)

The modelling of carbon monoxide (CO) emissions is carried out assuming that during combustion all fuel first reacts instantaneously to CO and $H_2O$:

$$C_xH_y + \frac{1}{\phi}\left(\frac{x}{2}+\frac{y}{4}\right)\left(O_2 + \frac{X_{N_2}}{X_{O_2}}N_2\right) \Leftrightarrow xCO + \frac{y}{2}H_2O + \frac{1}{\phi}\left(\frac{x}{2}+\frac{y}{4}\right)\left(\frac{X_{N_2}}{X_{O_2}}\right)N_2 + \left(\frac{1}{\phi}-1\right)\left(\frac{x}{2}+\frac{y}{4}\right)O_2 \tag{10-47}$$

From a volumetric analysis of the combustion products (Eq. (10-47)), the initial number of moles, molar fraction, and mass fraction of CO, can be expressed as:

$$n_{CO} = x,$$

$$X_{CO} = \frac{x}{\left(\frac{x}{2}+\frac{y}{4}\right)\left(1+\frac{1}{\phi}+\frac{1}{\phi}\frac{X_{N_2}}{X_{O_2}}\right)} \tag{10-48}$$

$$Y_{CO} = \left\{\frac{x}{\left(\frac{x}{2}+\frac{y}{4}\right)\left(1+\frac{1}{\phi}+\frac{1}{\phi}\frac{X_{N_2}}{X_{O_2}}\right)}\right\}\left(\frac{\overline{M}_{CO}}{\overline{M}_g}\right)$$

Thus the CO initial concentration is given by,

$$[CO]_0 = \frac{\rho Y_{CO}}{\overline{M}_{CO}} \tag{10-49}$$

Once the CO initial concentration is established, the CO conversion (oxidation) proceeds according to [62,63]:

$$CO + OH \Leftrightarrow CO_2 + H \qquad \text{R7} \tag{10-50}$$

Then from Eq. (10-50):

$$\frac{d[CO]}{dt} = -k_{7f}[CO].[OH] + k_{7b}[CO_2].[H] \tag{10-51}$$

$$\frac{d[OH]}{dt} = -k_{7f}[CO].[OH] + k_{7b}[CO_2].[H] \tag{10-52}$$

$$\frac{d[CO_2]}{dt} = k_{7f}[CO].[OH] - k_{7b}[CO_2].[H] \tag{10-53}$$

$$\frac{d[H]}{dt} = k_{7f}[CO].[OH] - k_{7b}[CO_2].[H] \tag{10-54}$$

Assuming equilibrium conditions for OH and H,

$$[OH] = [OH]_e \text{ and } [H] = [H]_e \tag{10-55}$$

Thus,

$$\frac{d[OH]}{dt} = \frac{d[OH]_e}{dt} = 0 \text{ and } \frac{d[H]}{dt} = \frac{d[H]_e}{dt} = 0 \tag{10-56}$$

Then from Eq. (10-56):

$$\begin{aligned} \frac{d[OH]}{dt} = \frac{d[H]}{dt} = 0 &= -k_{7f}[CO]_e.[OH]_e + k_{7b}[CO_2]_e.[H]_e \\ \Rightarrow k_{7b} &= k_{7f}\frac{[CO]_e.[OH]_e}{[CO_2]_e.[H]_e} \end{aligned} \tag{10-57}$$

Also, from carbon conservation,

$$[CO] + [CO_2] = [CO]_e + [CO_2]_e \tag{10-58}$$

Finally, from equations (10-55), (10-57), and (10-58) in (10-51), the rate of CO oxidation can be written as, in terms of CO concentration:

$$\frac{d[CO]}{dt} = -k_{7f}[OH]_e\left[1 + \frac{[CO]_e}{[CO_2]_e}\right]([CO] - [CO]_e) \tag{10-59}$$

or, in terms of mass fraction:

$$\frac{dY_{CO}}{dt} = -k_{7f}\left(\frac{\overline{M}_{CO}}{\rho}\right)[OH]_e\left[1+\frac{[CO]_e}{[CO_2]_e}\right]([CO]-[CO]_e) \qquad (10\text{-}60)$$

Equation (10-59) or (10-60) is integrated (e.g., (10-61)) along all the reactors used to model a particular combustion chamber.

$$[CO] = [CO]_e + ([CO]_0 - [CO]_e)\exp\left\{-k_{7f}[OH]_e\left[1+\frac{[CO]_e}{[CO_2]_e}\right]t\right\} \qquad (10\text{-}61)$$

## Appendix D
## Kinetic Model of Unburned Hydrocarbons (UHC)

Unburned hydrocarbons (UHC) are modelled following the methodology described in [64]. It is assumed that the fuel initially reacts according to:

$$C_{12}H_{23} + 6O_2 \Leftrightarrow 12CO + 11.5H_2 \qquad \text{R8} \qquad (10\text{-}62)$$

The quasi-global reaction rate for Eq. (10-62) – reaction R8,

$$\frac{dY_{C_{12}H_{23}}}{dt} = -2\times10^5\left(\frac{\overline{M}^{0.5}_{C_{12}H_{23}}}{\overline{M}_{O_2}}\right)\left(\frac{9T}{1000}-\frac{1}{2}\right)P^{0.3}Y_{O_2}\exp\left(\frac{-6914.947}{T}\right)\left(Y_{C_{12}H_{23}}\right)^{0.5} \qquad (10\text{-}63)$$

is then integrated – as shown in Eq. (10-64) – along all the reactors used to simulate a given combustor chamber.

$$Y_{C_{12}H_{23}}{}^{0.5} = Y_{C_{12}H_{23_0}}{}^{0.5} - 10^5\left(\frac{\overline{M}^{0.5}_{C_{12}H_{23}}}{\overline{M}_{O_2}}\right)\left(\frac{9T}{1000}-\frac{1}{2}\right)P^{0.3}Y_{O_2}\exp\left(\frac{-6914.947}{T}\right)\left(t-t_0\right) \qquad (10\text{-}64)$$

For determining the UHC initial concentration (or mass fraction, $Y_{C_{12}H_{23_0}}$), it is assumed that the fuel entering to the first reactor(s) evaporates instantaneously. Then through a balance of mass and energy between fuel and air entering to the first reactor(s), the UHC initial amount(s) is (are) calculated.

## Appendix E
## Kinetic Model of Soot/smoke

Soot formation:

According to Rizk and Mongia [65], the rate of soot formation ($S_f$), in mg soot/kg gas, is expressed as (omitting the term for soot oxidation):

$$S_f = 0.0145\left(\frac{\phi FAR_s}{\dot{m}_a T}\right)P^2\left(18 - H_{cont}\right)^{1.5} \tag{10-65}$$

Then dividing this expression by the soot density and multiplying by the total mass flow rate of the gas passing through the combustion chamber (and converting the units of mass, from mg to kg, and pressure, from kPa to atm), $S_f$ can be calculated as, in $m^3$ soot/s:

$$S_f = 1.4887\times10^{-4}\left(\frac{\phi FAR_s}{\dot{m}_a T}\right)P^2\left(18 - H_{cont}\right)^{1.5}\left(\frac{\dot{m}_{g_t}}{\rho_{soot}}\right) \tag{10-66}$$

In equations (10-65) and (10-66), the hydrogen content ($H_{cont}$) in a hydrocarbon fuel of the form $C_xH_y$ (e.g., $C_{12}H_{23}$) is estimated according to:

$$\%H = H_{cont} = \frac{y\left(\overline{M}_H\right)}{x\left(\overline{M}_C\right) + y\left(\overline{M}_H\right)}\times 100\% \tag{10-67}$$

Soot oxidation:

The two major soot oxidation species are considered to be oxygen molecules ($O_2$) and hydroxyl radical (OH). The rate of soot oxidation ($W'_{O_2}$), in kg soot/$m^2$.s, due to $O_2$ is determined from the Nagle and Strickland-Constable formula [66]:

$$W'_{O_2} = 12\left\{\left[x_s\left(\frac{k_A p_{O_2}}{1 + k_Z p_{O_2}}\right)\right] + \left[k_B p_{O_2}\left(1 - x_s\right)\right]\right\} \tag{10-68}$$

where,

$$x_s = \left( \frac{1}{1 + \frac{k_T}{k_B p_{O_2}}} \right) \tag{10-69}$$

The temperature dependence in Eq. (10-68) occurs via the reaction rate constants $k_A$, $k_B$, $k_Z$, and $k_T$, which in this case they are taken from [67]:

$$\begin{aligned} k_A &= 200.0 \times \exp(\frac{-15098.0}{\mathrm{T}}) \quad \text{, kg-mol/m}^2\text{.s.atm} \\ k_B &= 4.46 \times 10^{-2} \exp(\frac{-7650.0}{\mathrm{T}}) \quad \text{, kg-mol/m}^2\text{.s.atm} \\ k_T &= 1.51 \times 10^{6} \exp(\frac{-48817.0}{\mathrm{T}}) \quad \text{, kg-mol/m}^2\text{.s} \\ k_Z &= 21.3 \times \exp(\frac{2063.0}{\mathrm{T}}) \quad \text{, 1/atm} \end{aligned} \tag{10-70}$$

Assuming soot particles are of spherical shape and the particle size distribution is mono-dispersed, the soot volume fraction ($f_v$), in $m^3$ soot/$m^3$, can be expressed as:

$$f_v = \frac{\pi}{6} d^3 N \tag{10-71}$$

where $N$ is the soot number density ($1/m^3$). Similarly, the total surface area of a cloud of $N$ soot particles, $A_s$, which is the soot surface area per unit volume of space, is given by:

$$A_s = \pi . d^2 N \tag{10-72}$$

or in terms of $f_v$:

$$A_s = \pi^{1/3} . 6^{2/3} . N^{1/3} . f_v^{\,2/3} \tag{10-73}$$

Then the rate of soot oxidation due to $O_2$ ($W_{O_2}$), in $m^3$ soot/$m^3$.s, is given by:

$$W_{O_2} = \frac{A_s W_{O_2}^{'}}{\rho_{soot}} = \pi^{1/3} . 6^{2/3} . f_v^{\,2/3} . N^{1/3} . W_{O_2}^{'} / \rho_{soot} \tag{10-74}$$

Following the same approach used in [68], the OH oxidation of soot is calculated as [68],

$$W_{OH} = 10.14.\theta.f_v^{2/3}.N^{1/3}.X_{OH}.T^{-1/2} \qquad (10\text{-}75)$$

where $\theta$ is the collision efficiency (assumed 0.2 in this work).

The overall rate of soot oxidation is the sum of the terms given by equations (10-74) and (10-75), in $m^3$ soot/$m^3$.s. In the equations described above, a suitable average value (of the order of $10^{18}m^{-3}$) is adopted for $N$. In turn, $f_v$ is computed as the difference between the amount of soot formed and oxidised in the previous calculation step.

Smoke number:

Using the soot volume fraction ($f_v$) at the end of the combustor chamber, the particulate (smoke) mass loading ($PML$) – the mass of particulate per unit of standard volume – is calculated as follows, in µg/l:

$$PML = 10^6 f_v \rho_{soot} \left(\frac{P_{std}}{P}\right)\left(\frac{T}{T_{std}}\right) \qquad (10\text{-}76)$$

where the standard pressure ($P_{std}$) and temperature ($T_{std}$) are considered are being equal to 1.0atm and 273.15K, respectively. Finally, the $PML$ is converted into Smoke Number (SN) using the correlation presented in [69]. For the sake of completeness, this correlation is reproduced here in Figure 10-1.

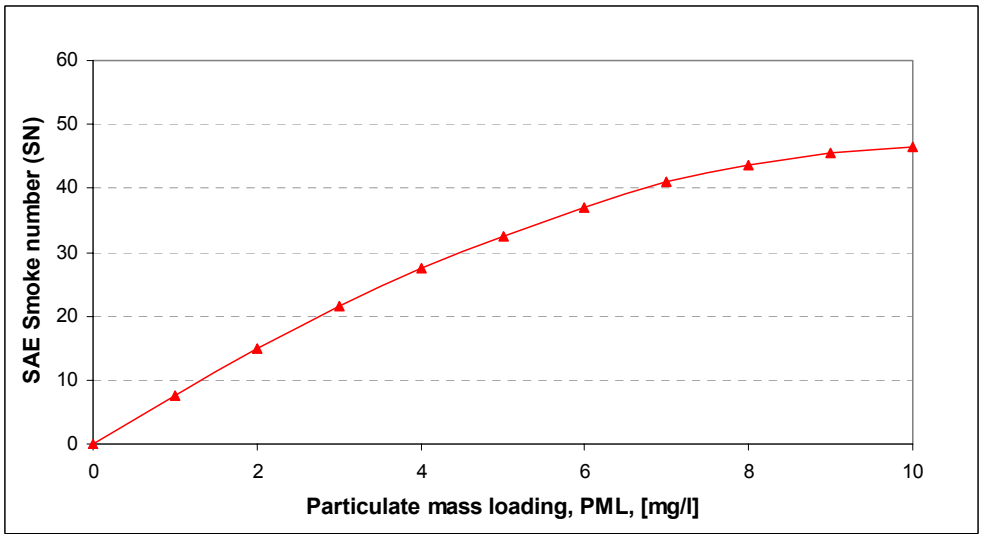


Figure 10-1. SAE Smoke number (SN) vs. Particulate mass loading (PML) [69]

## Appendix F
## Emission Model – Sensitivity Analysis of Parameters

Results obtained from a sensitivity analysis of the influence of the five model arbitrary parameters – F1 to F5 (see Figure 3-2 or Figure 10-2 ) – on the level of emissions produced are illustrated in the following plots. The results are presented in two groups: (i) high power setting and (ii) low power setting. In the high and low power setting groups, the influence of the model arbitrary parameters on the level of emissions produced in terms $NO_x$ and soot/smoke (main pollutants at engine high power settings), and in terms of CO and UHC, (main pollutants at engine low power settings) is illustrated, respectively.

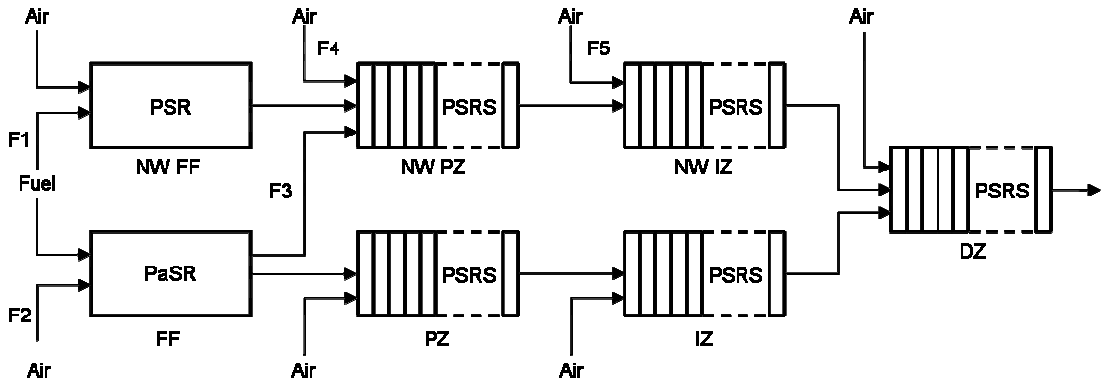


Figure 10-2. Conventional combustor – Multi-reactor model

In addition, the plots show variations in the equivalence ratio associated with specific regions of the combustor as a function of these model parameters (at engine high and low power settings). During the combustor simulations, each arbitrary parameter (e.g., F1) was varied separately, and the values of the remaining parameters (e.g., F2-F5) were kept constant (illustrated at the top of each plot). Emissions levels derived from the engine certification data [73] are also included for reference.

High power setting (~100%):

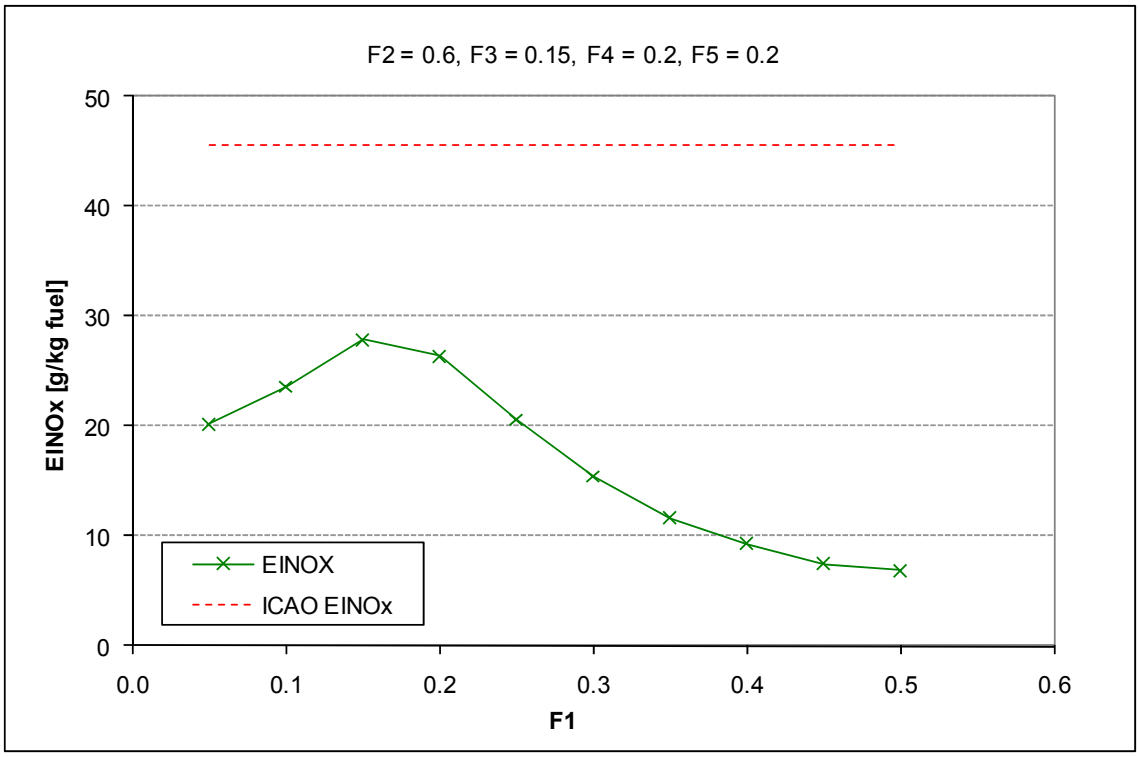


Figure 10-3. Influence of F1 on $NO_x$ emission index ($EINO_x$)

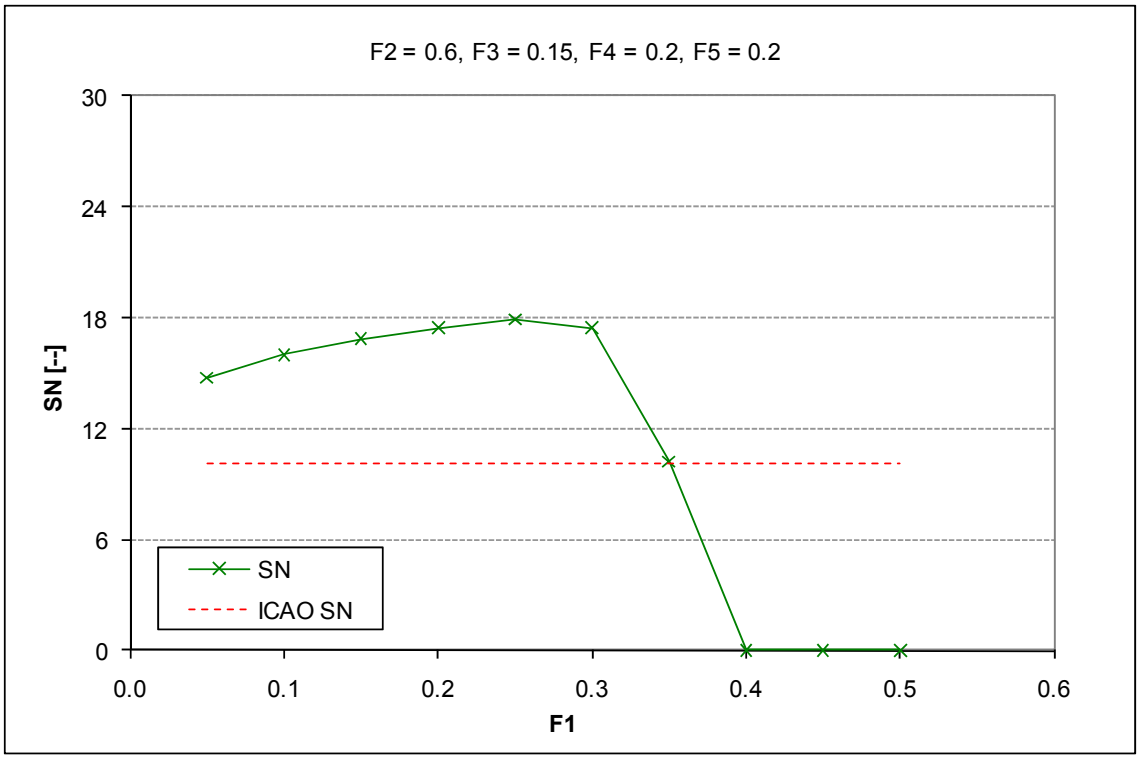


Figure 10-4. Influence of F1 on Smoke number (SN)

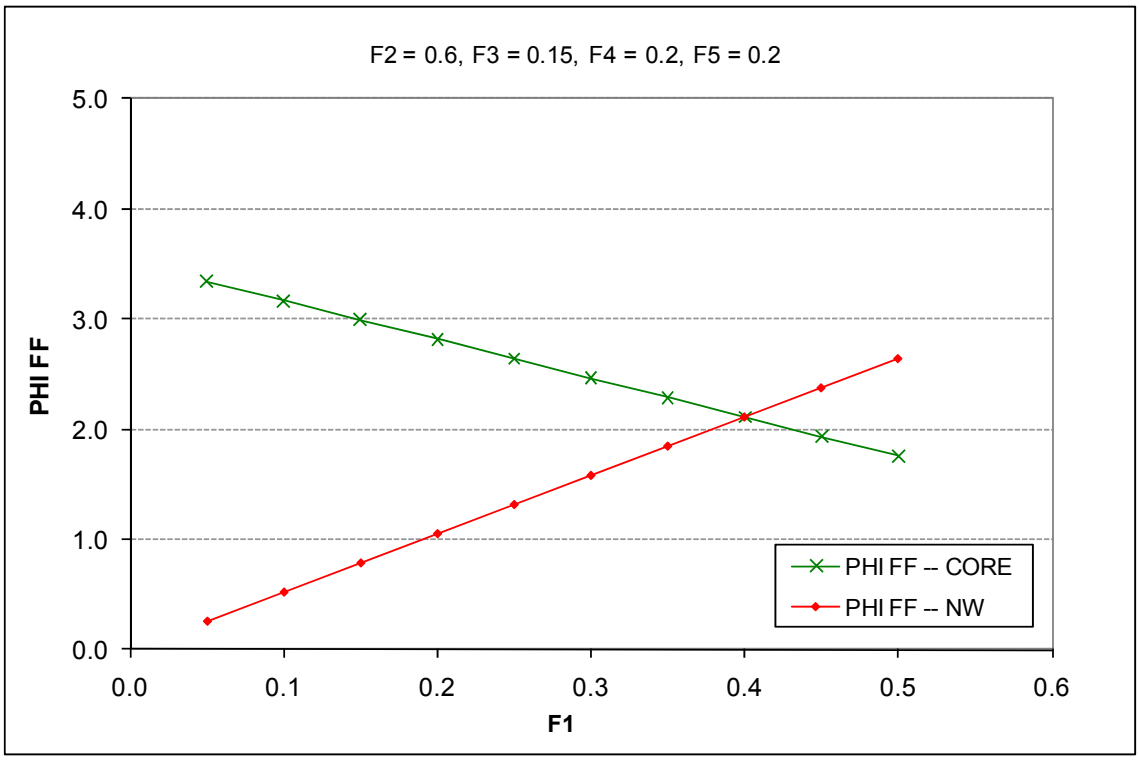


Figure 10-5. Influence of F1 on flame front equivalence ratio (PHI FF), high power

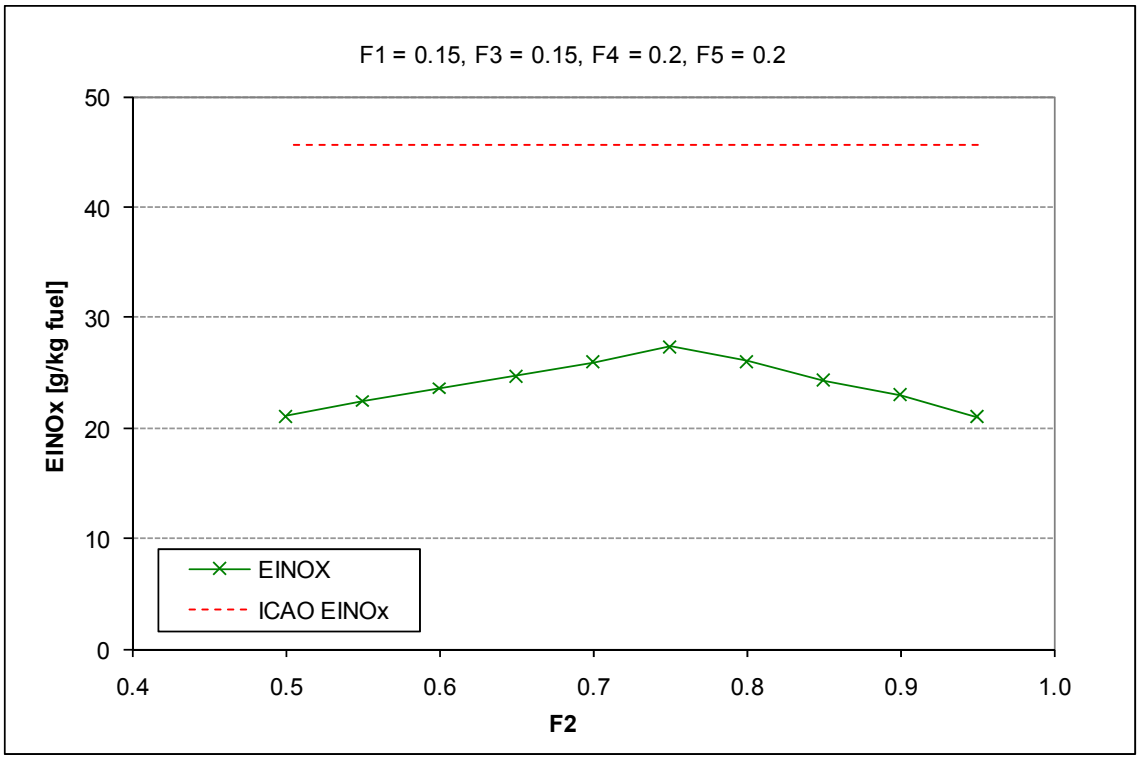


Figure 10-6. Influence of F2 on $NO_x$ emission index ($EINO_x$)

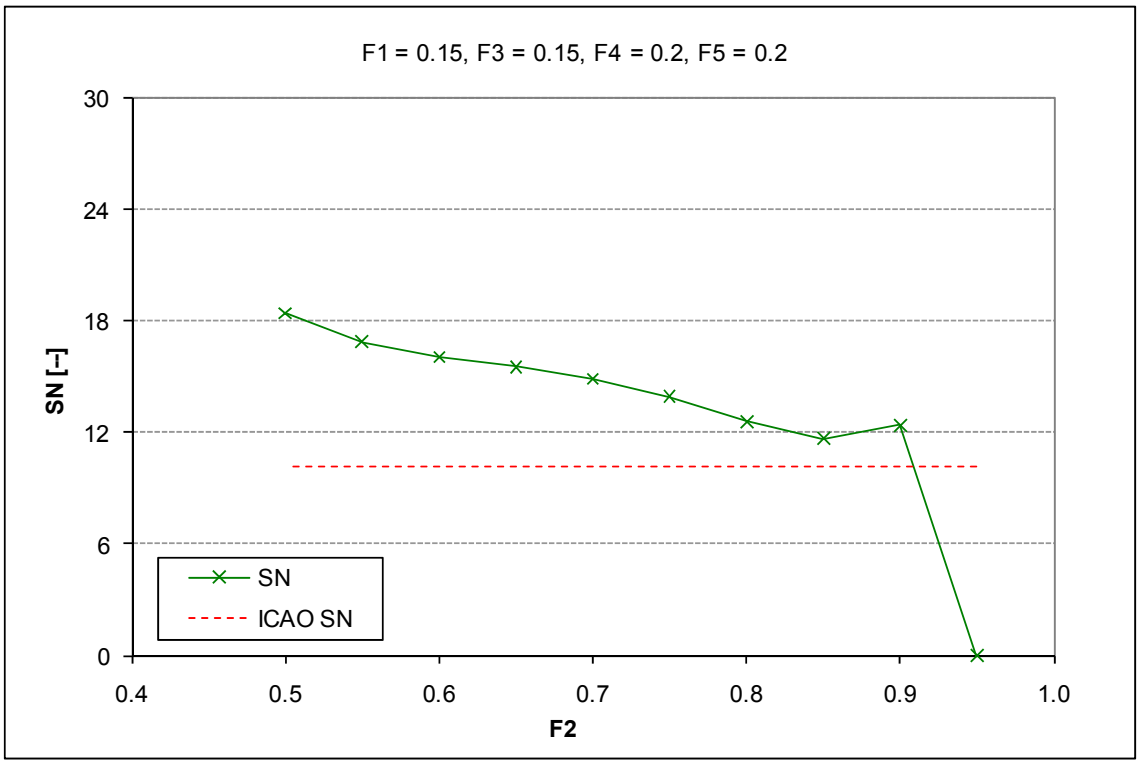


Figure 10-7. Influence of F2 on Smoke number (SN)

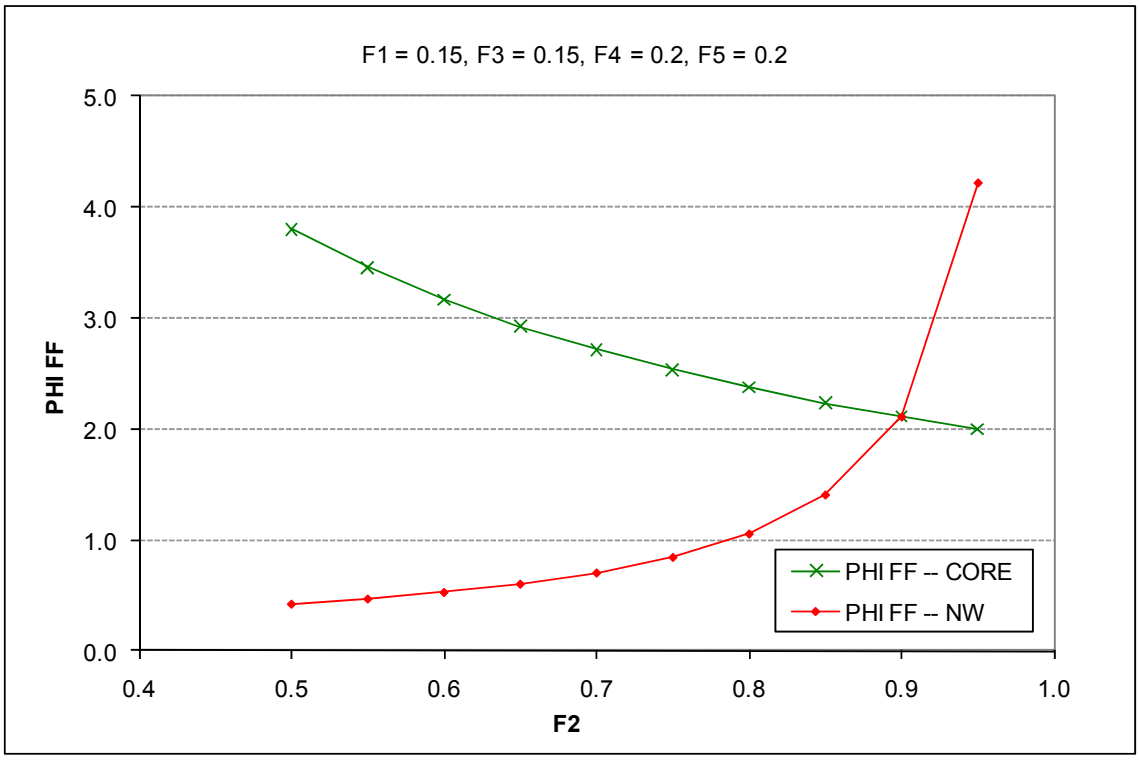


Figure 10-8. Influence of F2 on flame front equivalence ratio (PHI FF), high power

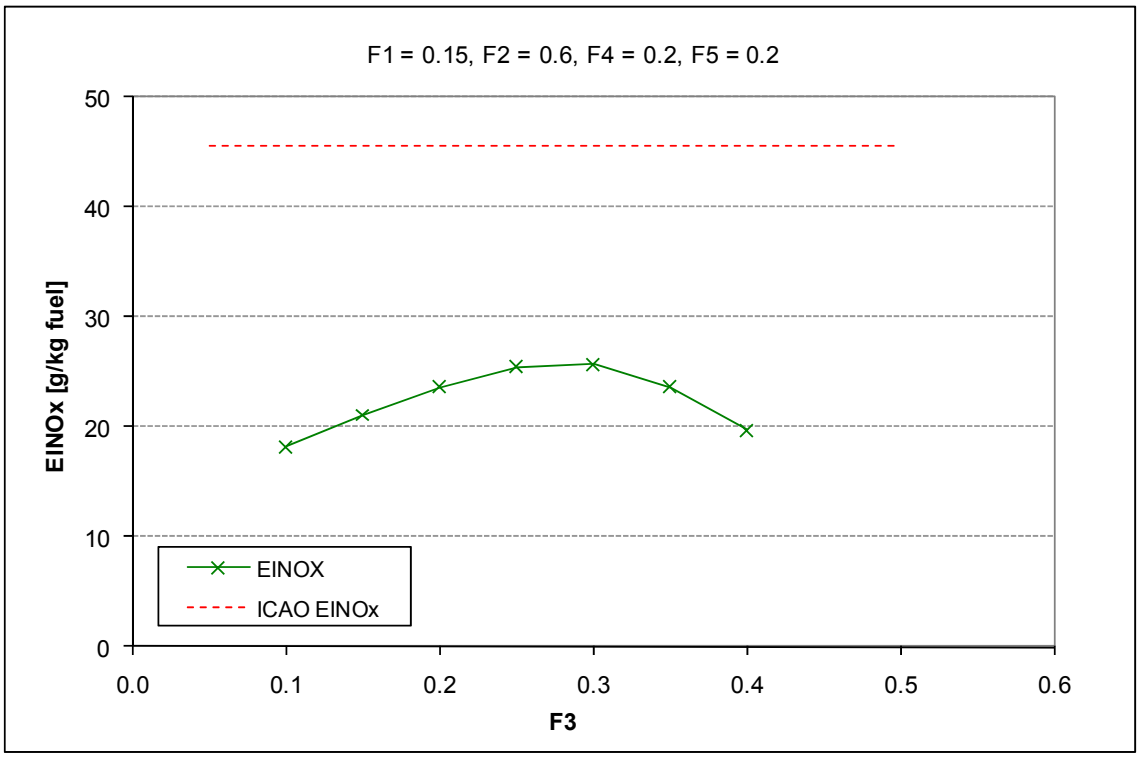


Figure 10-9. Influence of F3 on $NO_x$ emission index ($EINO_x$)

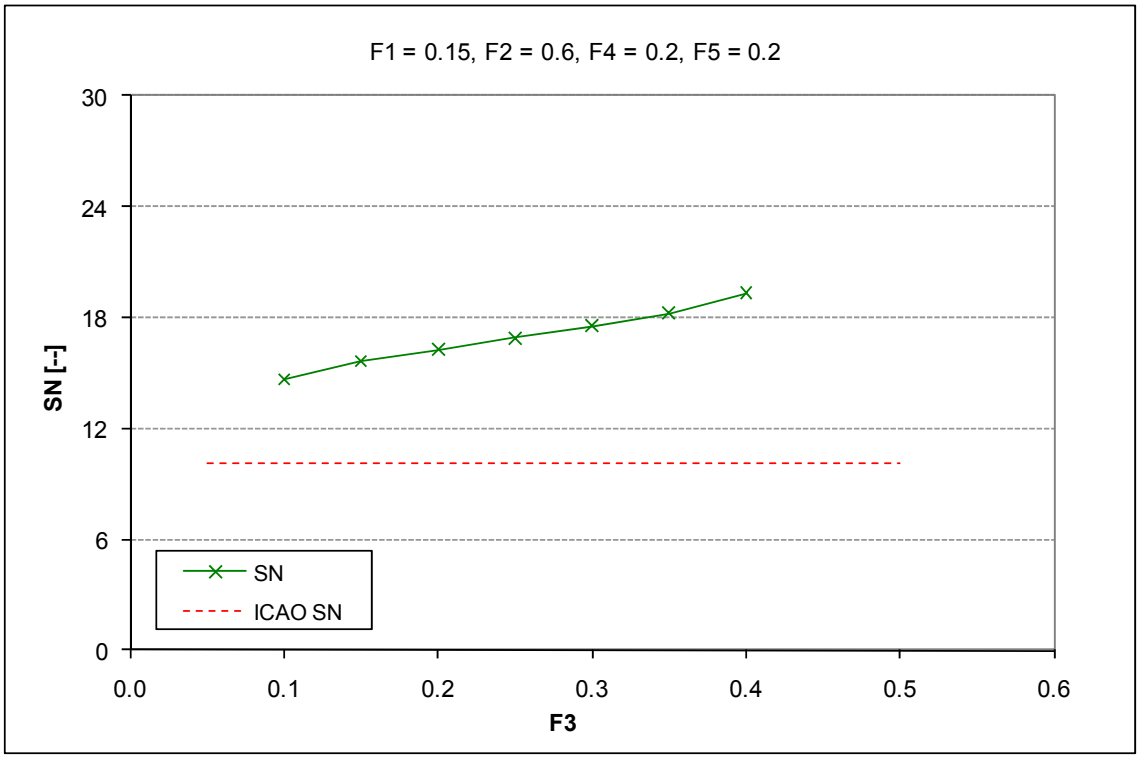


Figure 10-10. Influence of F3 on Smoke number (SN)

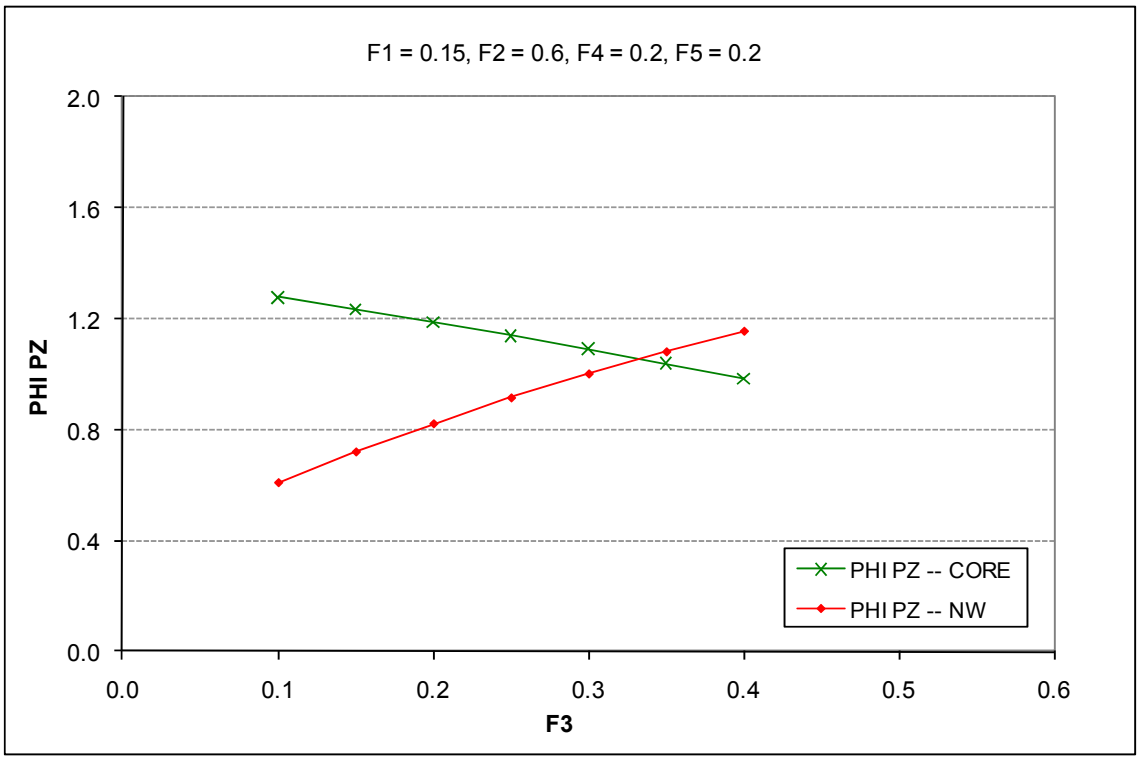


Figure 10-11. Influence of F3 on primary zone equivalence ratio (PHI PZ), high power

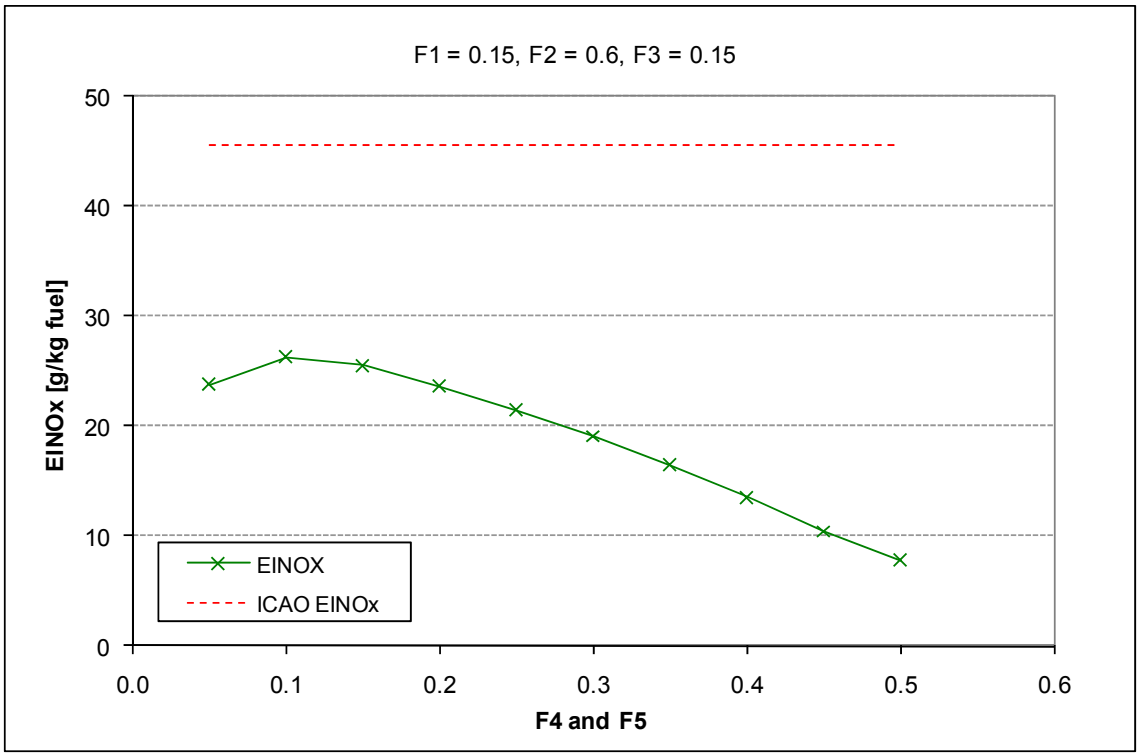


Figure 10-12. Influence of F4 & F5 on $NO_x$ emission index ($EINO_x$)

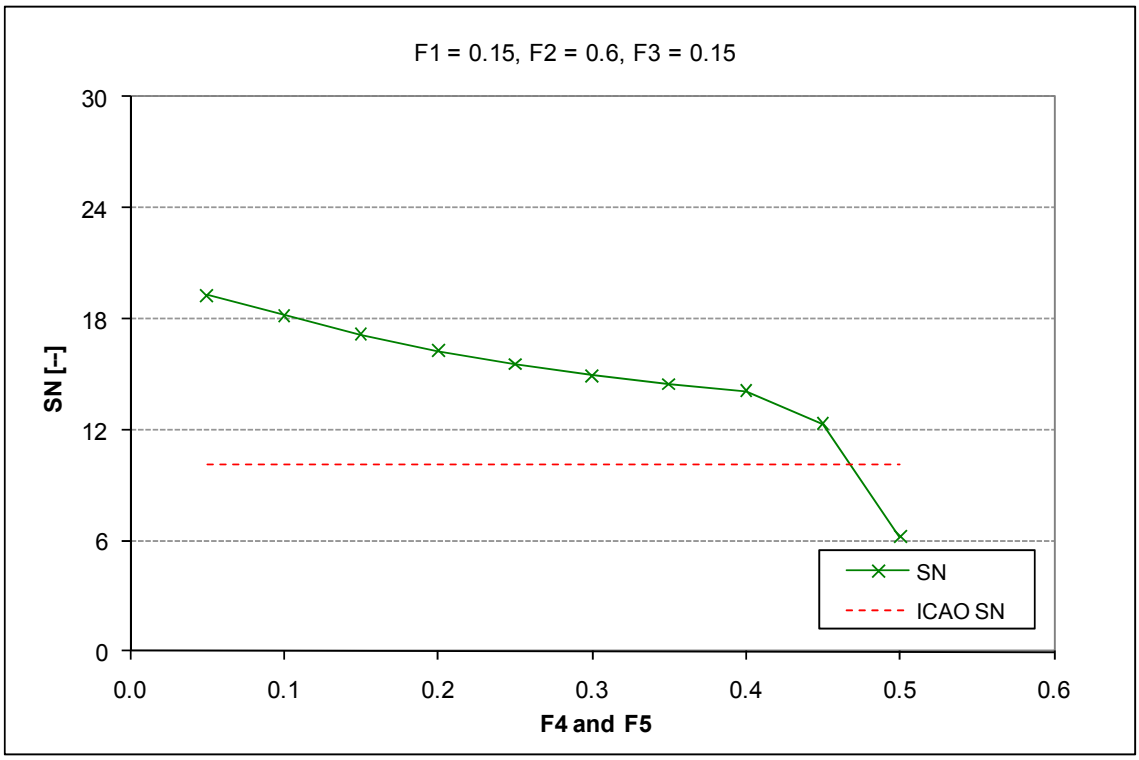


Figure 10-13. Influence of F4 & F5 on Smoke number (SN)

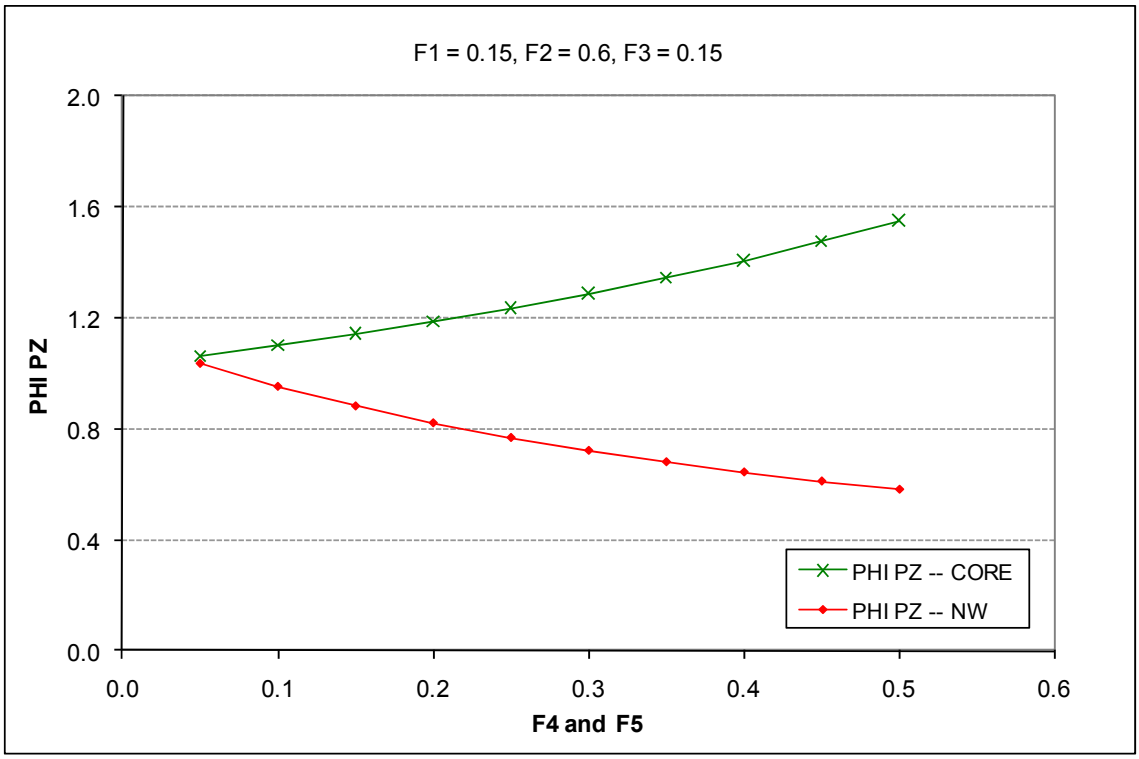


Figure 10-14. Influence of F4 & F5 on primary zone equivalence ratio (PHI PZ), high power

Low power setting (~11%):

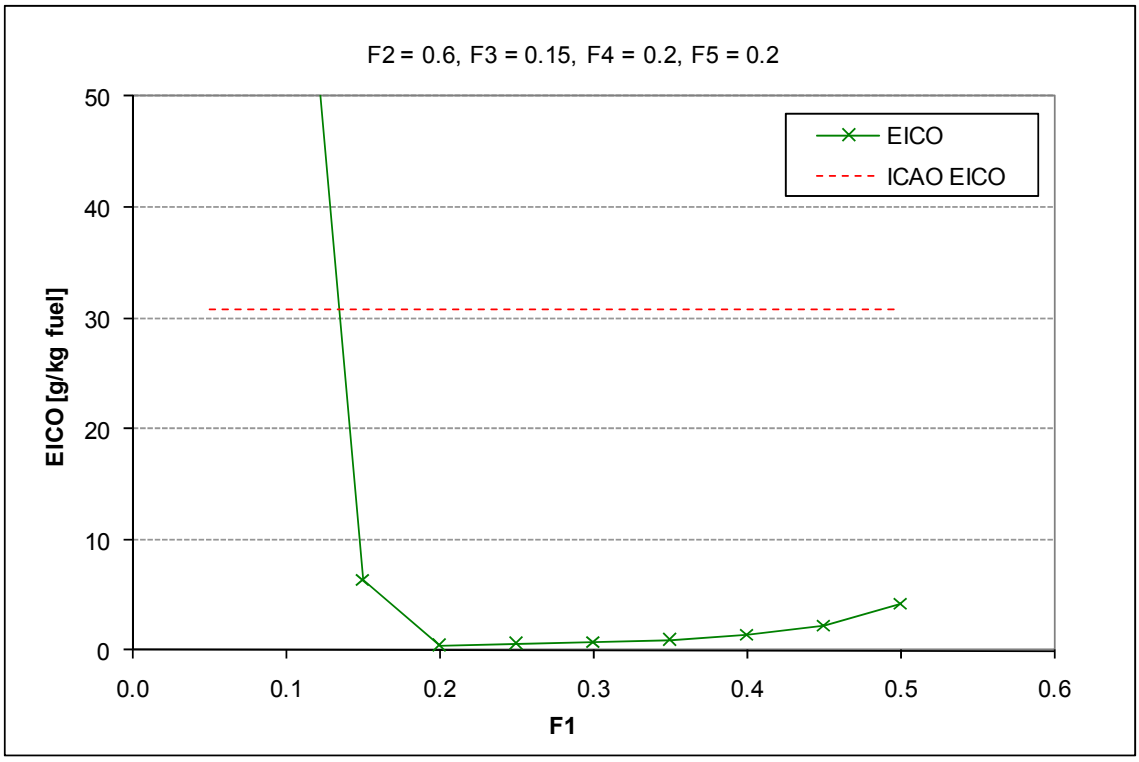


Figure 10-15. Influence of F1 on CO emission index (EICO)

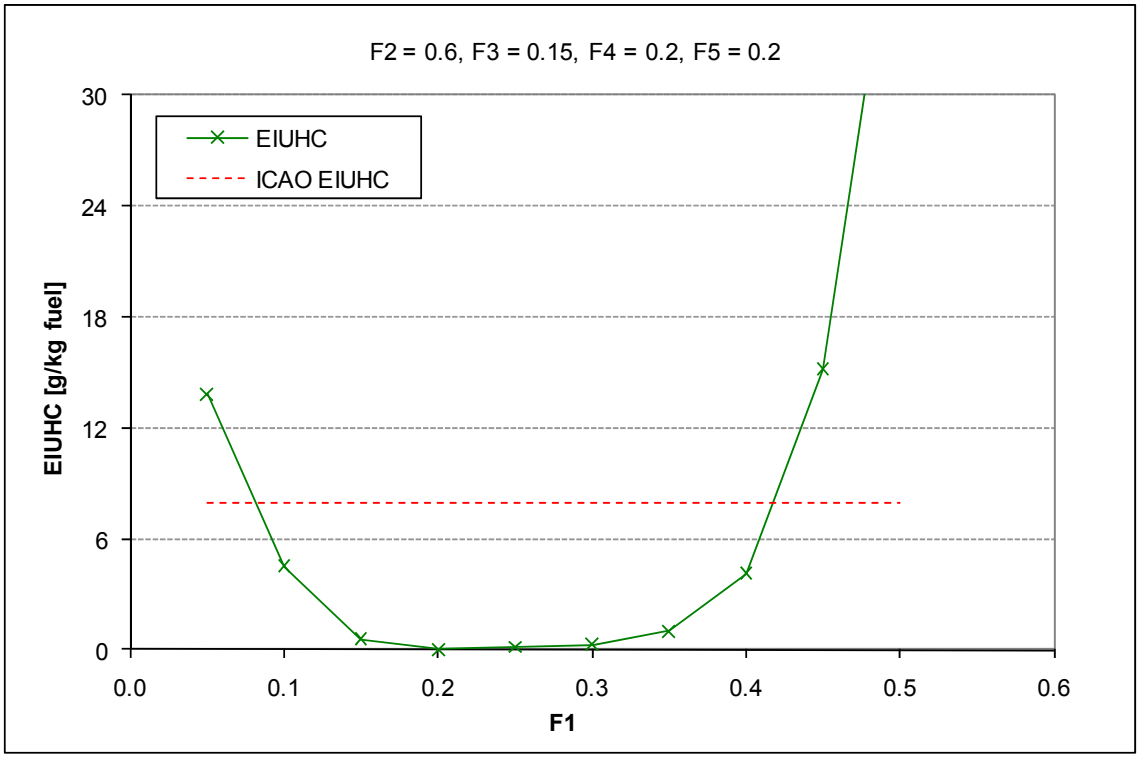


Figure 10-16. Influence of F1 on UHC emission index (EIUHC)

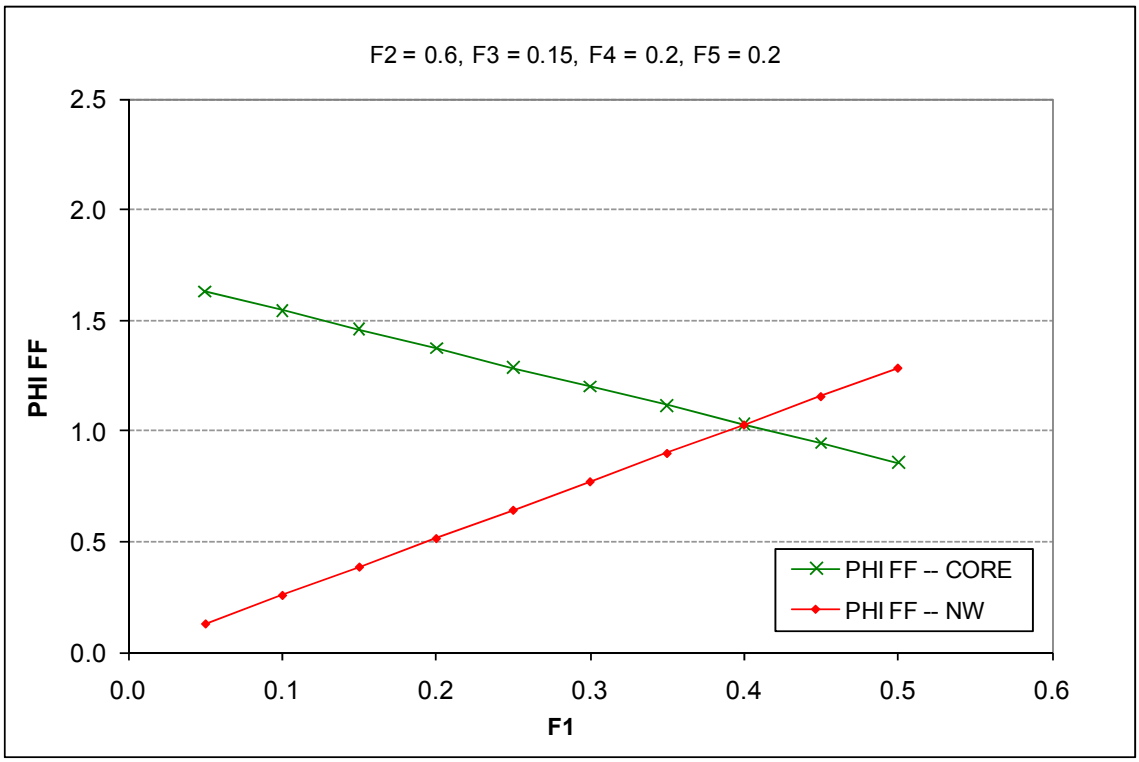


Figure 10-17. Influence of F1 on flame front equivalence ratio (PHI FF), low power

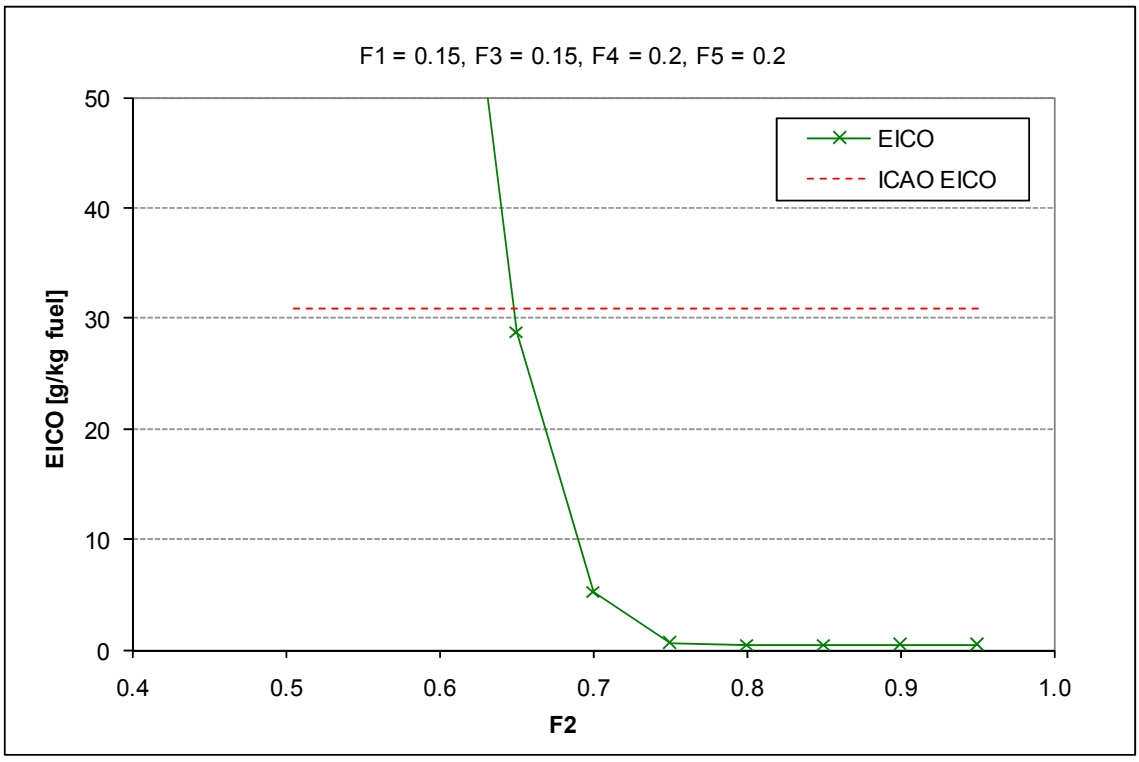


Figure 10-18. Influence of F2 on CO emission index (EICO)

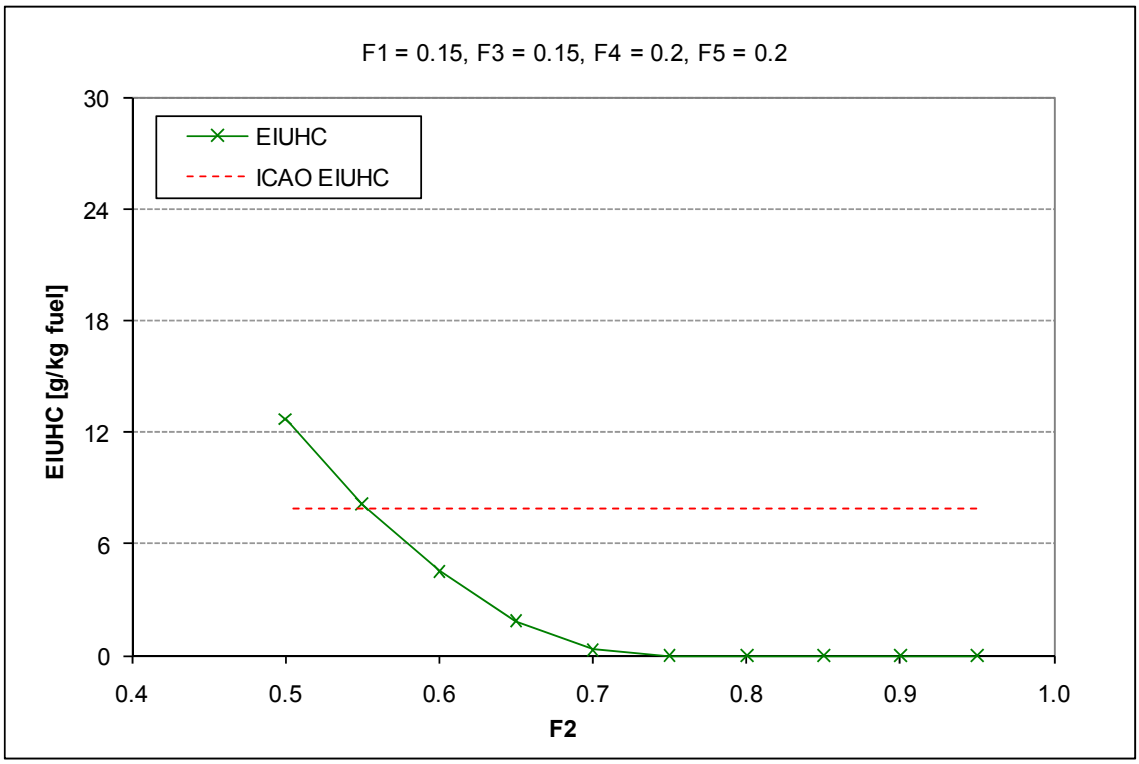


Figure 10-19. Influence of F2 on UHC emission index (EIUHC)

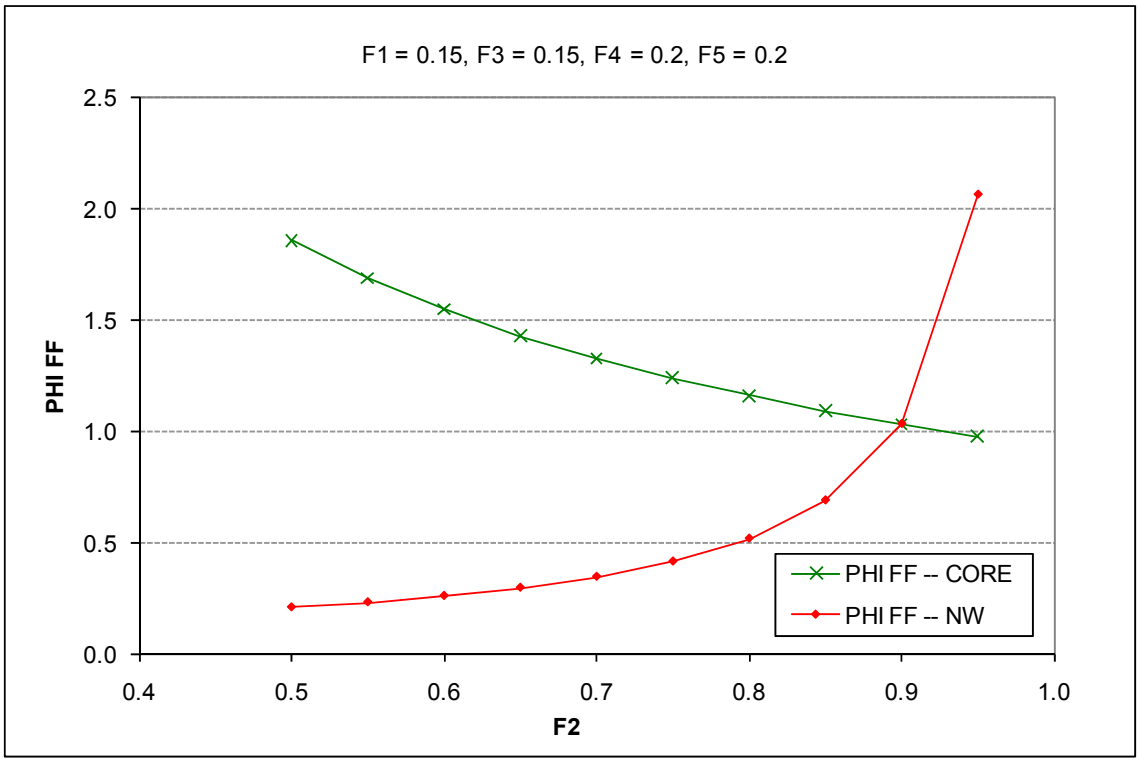


Figure 10-20. Influence of F2 on flame front equivalence ratio (PHI FF), low power

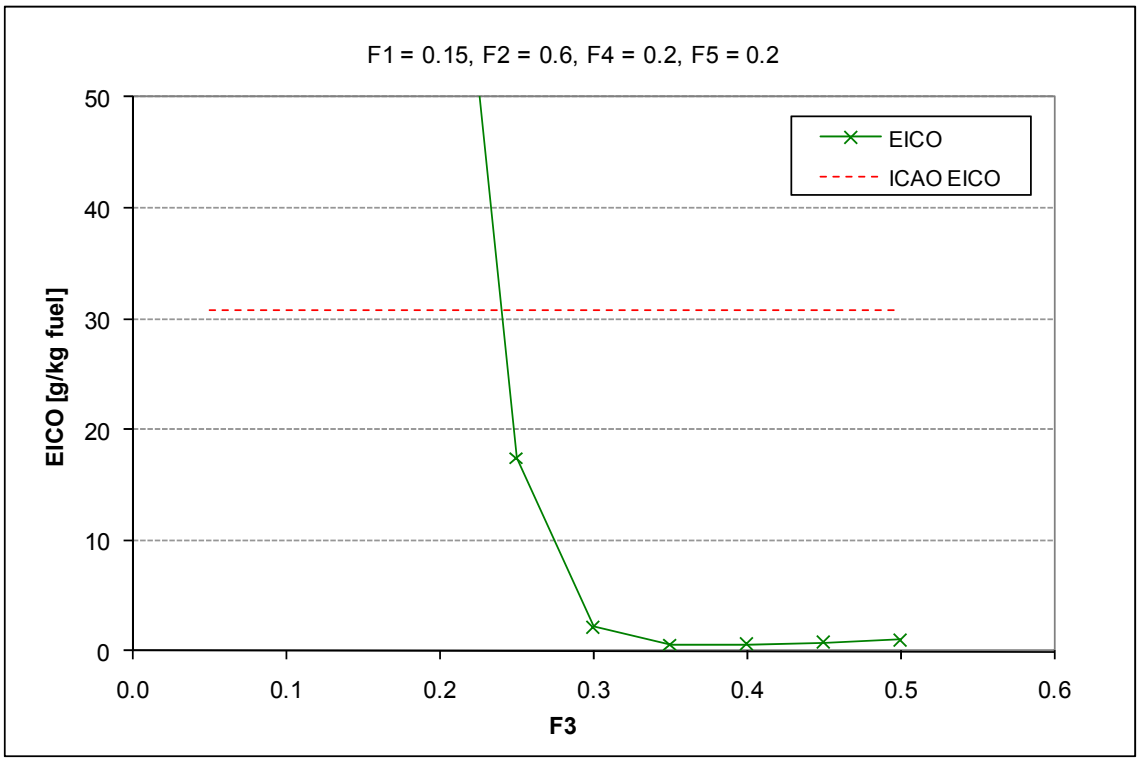


Figure 10-21. Influence of F3 on CO emission index (EICO)

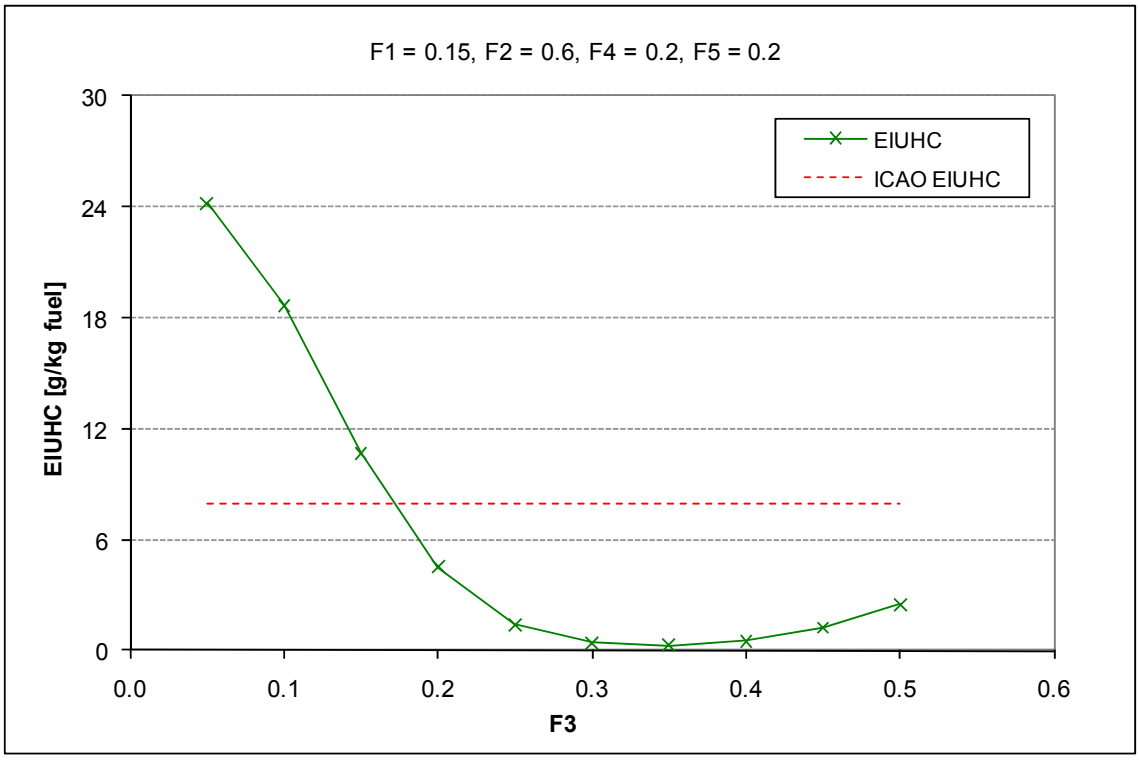


Figure 10-22. Influence of F3 on UHC emission index (EIUHC)

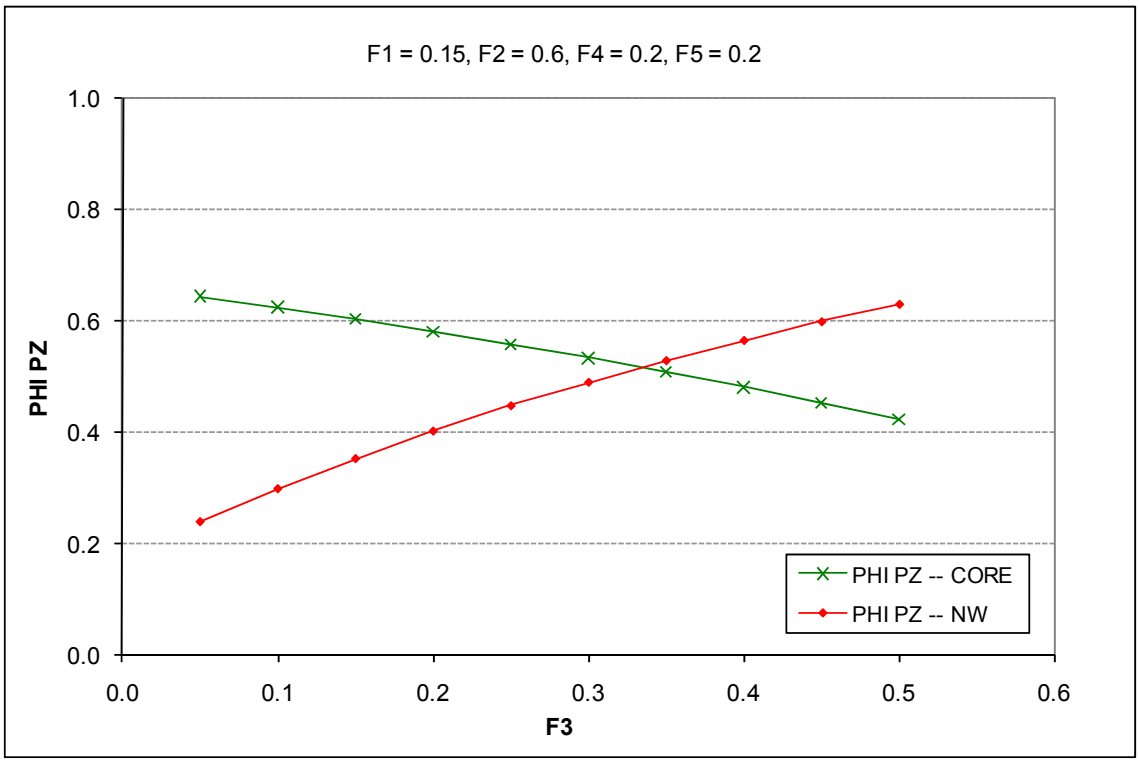


Figure 10-23. Influence of F3 on primary zone equivalence ratio (PHI PZ), low power

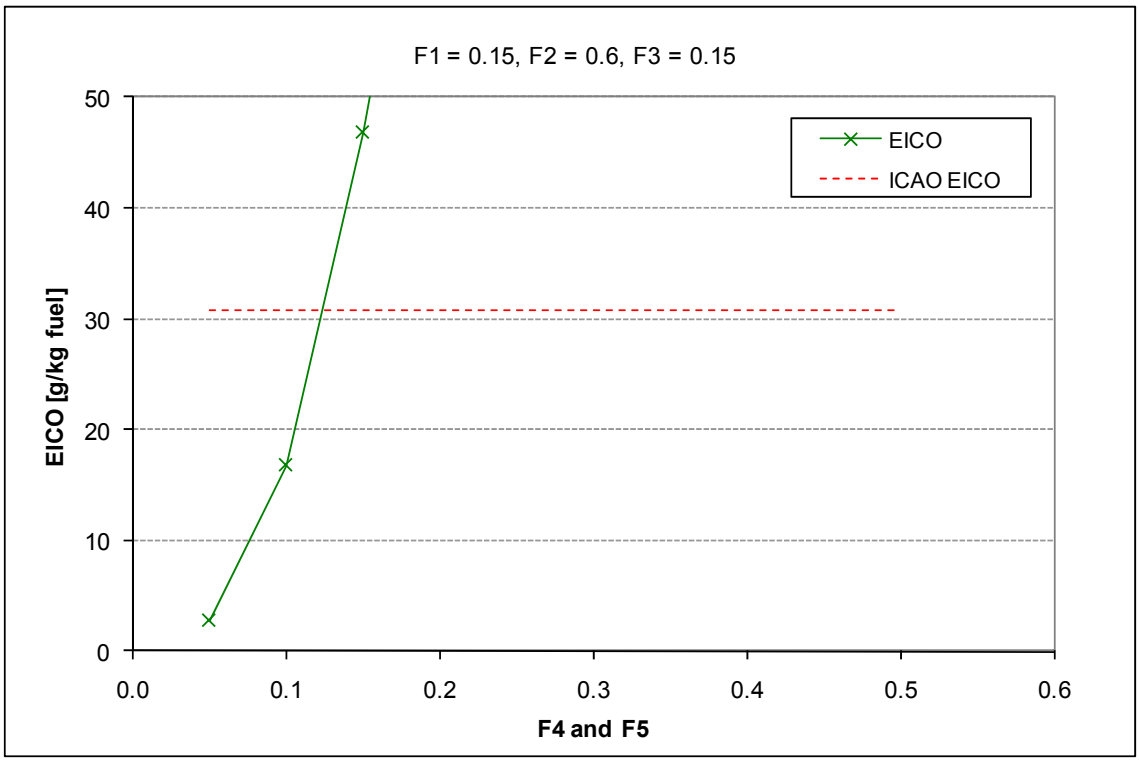


Figure 10-24. Influence of F4 & F5 on CO emission index (EICO)

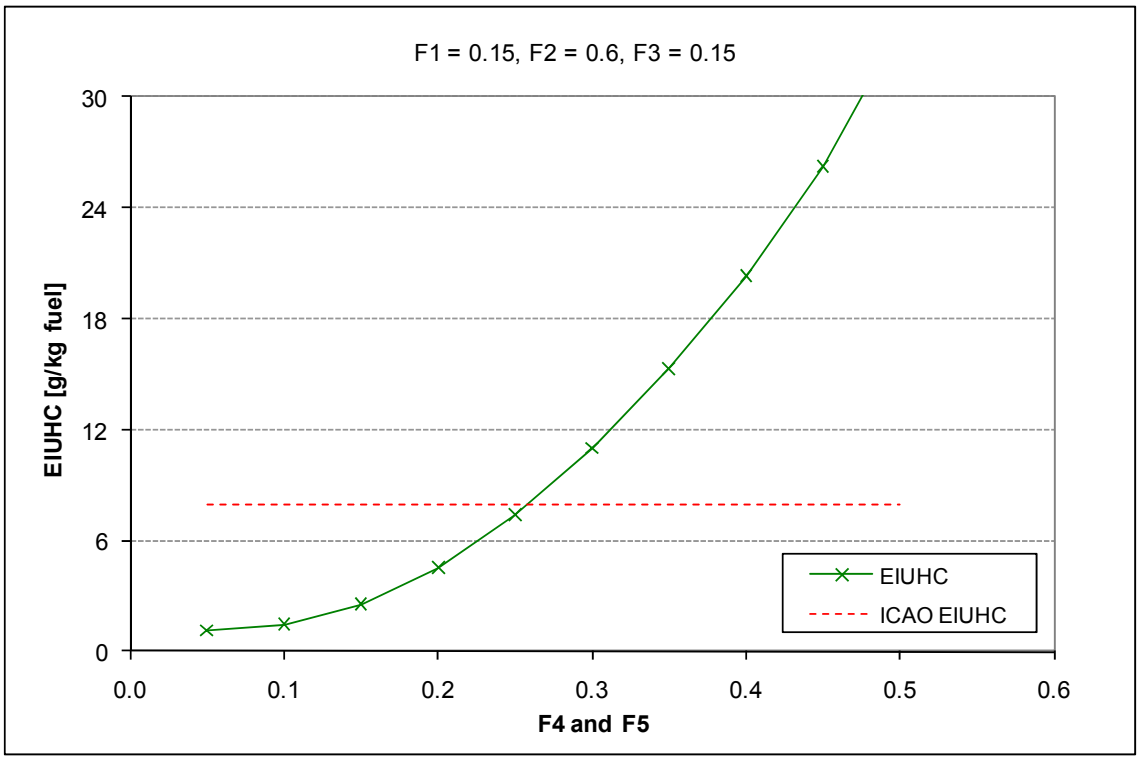


Figure 10-25. Influence of F4 & F5 on UHC emission index (EIUHC)

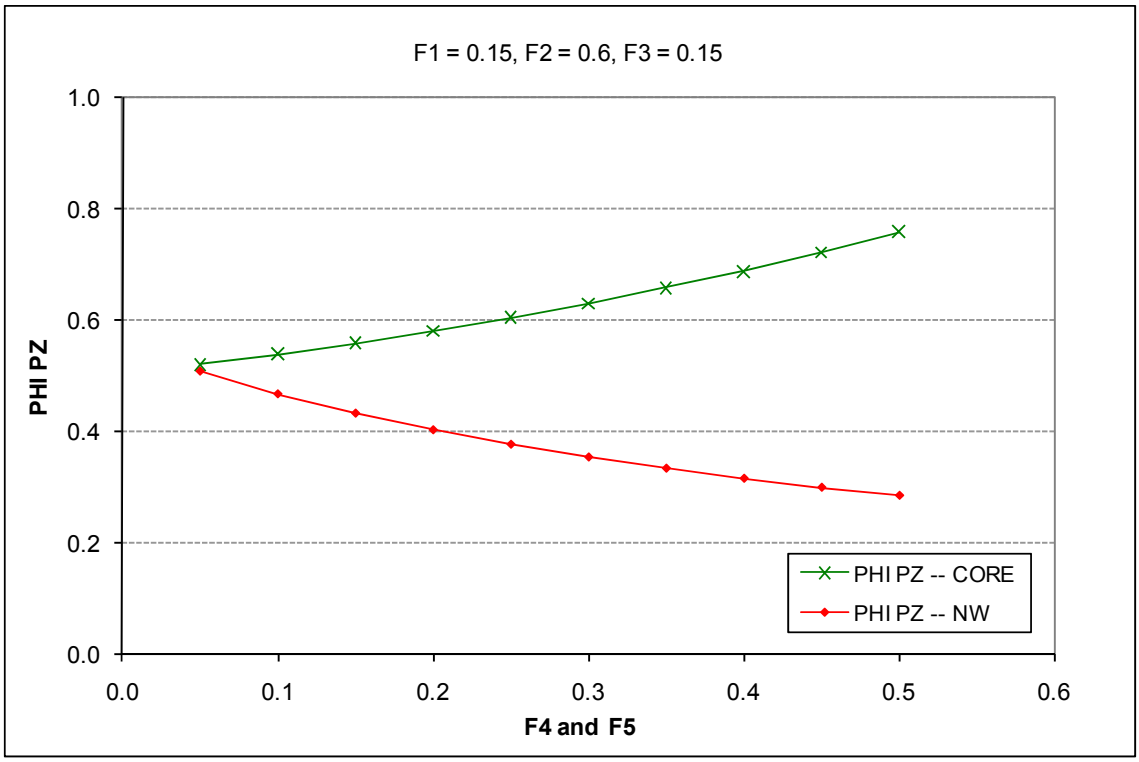


Figure 10-26. Influence of F4 & F5 on primary zone equivalence ratio (PHI PZ), low power

## Appendix G

## TurboMatch Iterative Process: TET Guess

As indicated in Chapter 6, in this work when optimising aircraft trajectories the engine operating conditions are iteratively calculated based on the net thrust required for flying a given trajectory segment. In this appendix, additional details about how to estimate the initial turbine entry temperature (TET) guess necessary to start this iterative process is described.

In general, there are three factors that directly affect the level of power (in terms of net thrust, FN) produced by an aircraft engine. These are the flight conditions, the throttle setting, and the air mass flow passing through the engine. The flight conditions can be characterised by both the ambient conditions, directly related to the flight altitude, and the speed of the aircraft. Ambient conditions are mainly characterised by temperature ($T_{amb}$) and pressure ($P_{amb}$). Aircraft speed, in turn, is directly related to flight Mach number (M). The engine throttle setting controls the amount of fuel consumed by the engine, and it has consequently a direct relation to TET. Finally, the air mass flow passing through the engine can be associated to the engine nozzle area ($A_{noz}$). Different approaches can be used to correlate the main parameters that control the engine thrust described above. One of them involves the creation of dimensionless parameters as illustrated in Figure 10-27.

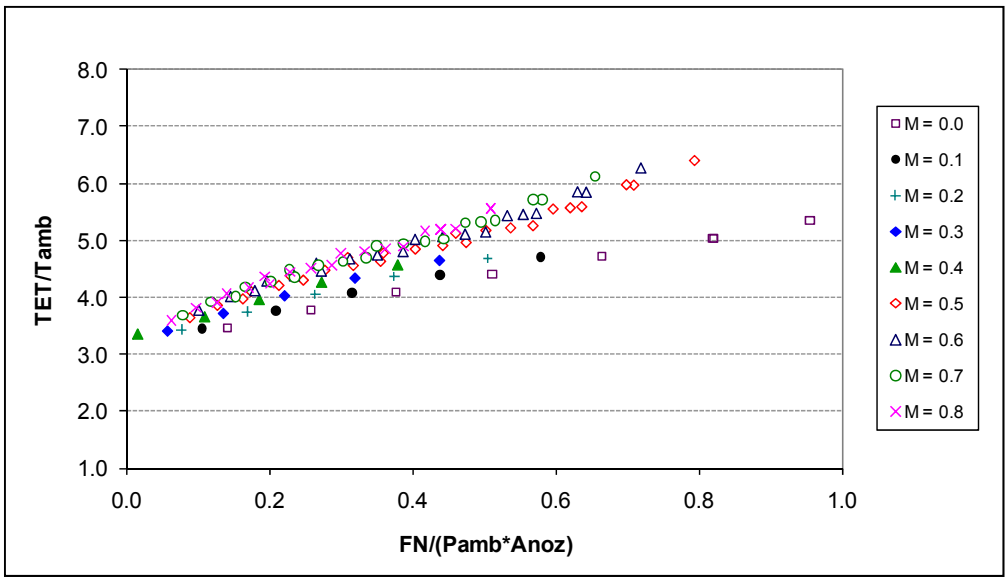


Figure 10-27. Interrelation of parameters controlling aircraft engine thrust

In Figure 10-27 it is possible to observe that if TET and net thrust are transformed into dimensionless parameters using the ambient conditions and the nozzle area, several curves describing their interrelationship can be obtained, each one related to a particular flight Mach number. This expected results come from the fact that, for a given flight condition (both ambient conditions and Mach number constant), as TET increases the net thrust produced by the engine increases as well (considering that the nozzle area is constant). Ideally, it would be desirable to have only one curve describing the interrelationship between the dimensionless parameters illustrated in Figure 10-27. That would avoid the use of interpolation processes when the flight number is different to those values associated with these curves. In this ideal situation, knowing the flight conditions and the nozzle area, TET could be readily estimated. Thus, in this work the whole exercise involved finding a suitable factor as a function of Mach number, $FactM = f(M)$, which allows merging all curves shown in Figure 10-27 into a single one.

Different functions for $FactM$ were initially tested without so many encouraging results. At the end, a function was devised for this factor which involves the flight Mach number at engine design point conditions ($M_{DP}$), the actual flight Mach number (M), and the ratio of the specific heats of the air (γ), as follows:

$$FactM = 1 + \left( \left( \frac{M}{M_{DP}} \right)^{\frac{(\gamma-1)}{2}} \right) \qquad (10\text{-}77)$$

When used this $FactM$ in conjunction with the dimensionless parameters illustrated in Figure 10-27, all curves corresponding to Mach numbers different from zero merge into a single one. However, as shown in Figure 10-28, a Mach number equal to zero also has its own curve. In conclusion, the $FactM$ devised does not generate a single curve as initially expected; but instead it generates two curves, one corresponding to M 0.0 and the other corresponding to Mach numbers different from zero. The fact of using two curves instead of one for estimating TET is not really a problem because there is no additional computational burden required. It simply means that, depending on the values of the flight Mach number, one of the two curves will be utilised.

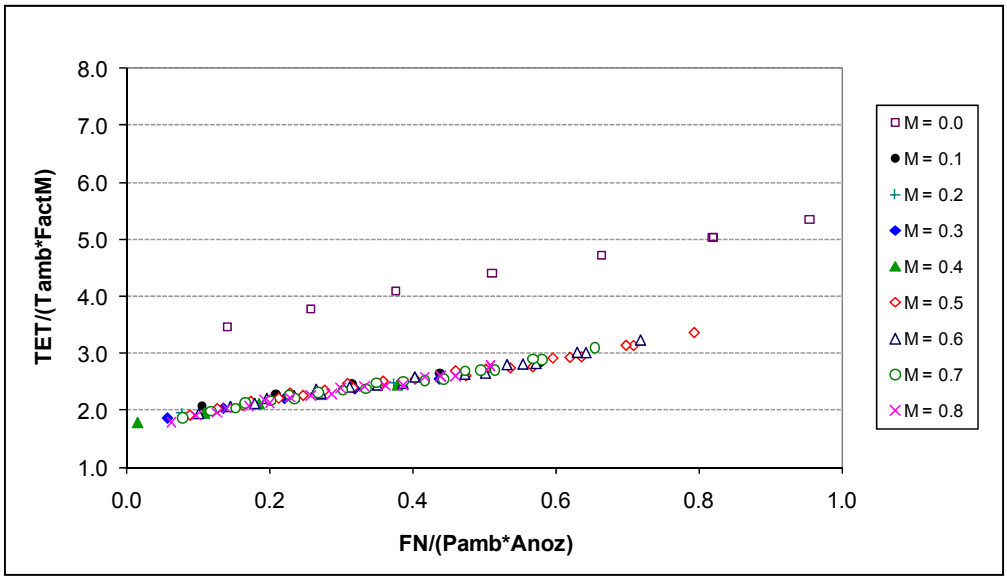


Figure 10-28. Flight Mach number factor (FactM)

The next step in the process then involved determining the expressions that characterise the pair of curves generated. These expressions are illustrated in Figure 10-29, and explicitly indicated in the following equation,

$$y = \begin{cases} -0.464251x^2 + 2.774257x + 3.087466, & M = 0 \\ 0.083974x^2 + 1.825285x + 1.786250, & M \neq 0 \end{cases} \quad (10\text{-}78)$$

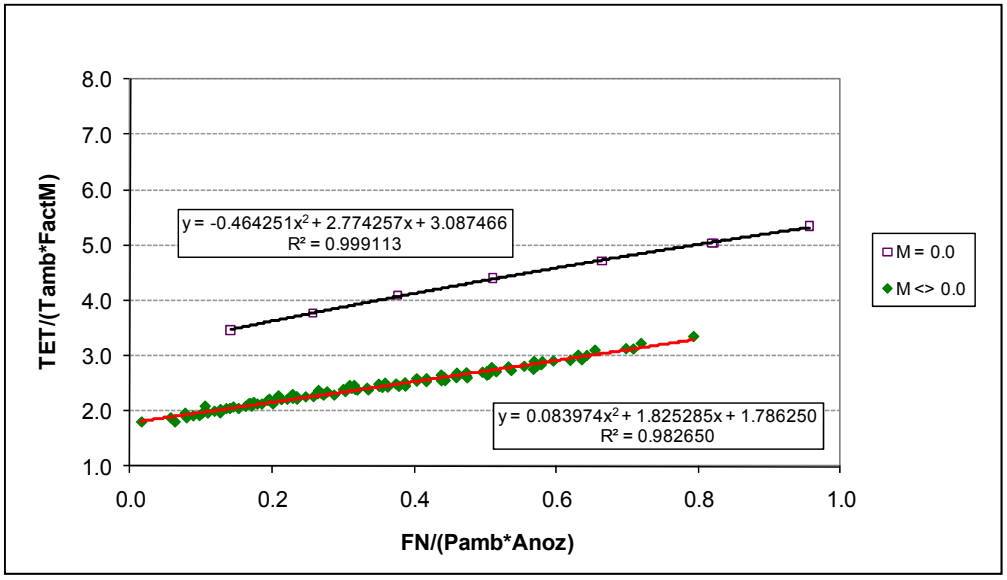


Figure 10-29. Simplified representation of main aircraft engine parameters interrelation

In Eq. (10-78) and Figure 10-29, $x$ is given by,

$$x = \frac{FN}{(P_{amb} * A_{noz})} \tag{10-79}$$

and $y$ by,

$$y = \frac{TET}{(T_{amb} * FactM)} \tag{10-80}$$

In order to illustrate the usefulness of the expressions derived, comparisons between TET values calculated using Eq. (10-78) and the corresponding ones computed using TurboMatch were performed for a variety of flight conditions and engine thrusts. Values of Mach number analysed ranged from 0.0 to 0.8, flight altitude from 0.0 to 10668m, and TET from 1,100 to 1,500K. The results of these comparisons are summarised in Figure 10-30, which shows the relative difference (in %) between the estimated TET values ($TET_{cal}$) and those computed by TurboMatch (TET). As it can be seen in this figure, the average error associated with the estimation of TET according to the expressions derived above, Eq. (10-78), is about 1.5%, which is a more than acceptable TET value for starting a iterative process. Finally, it is worth emphasising that even though the methodology followed in order to obtain Eq. (10-78) can be applied to any aircraft engine, the actual expression derived is only valid for the particular engine utilised in the trajectory optimisation processes carried out in this work.

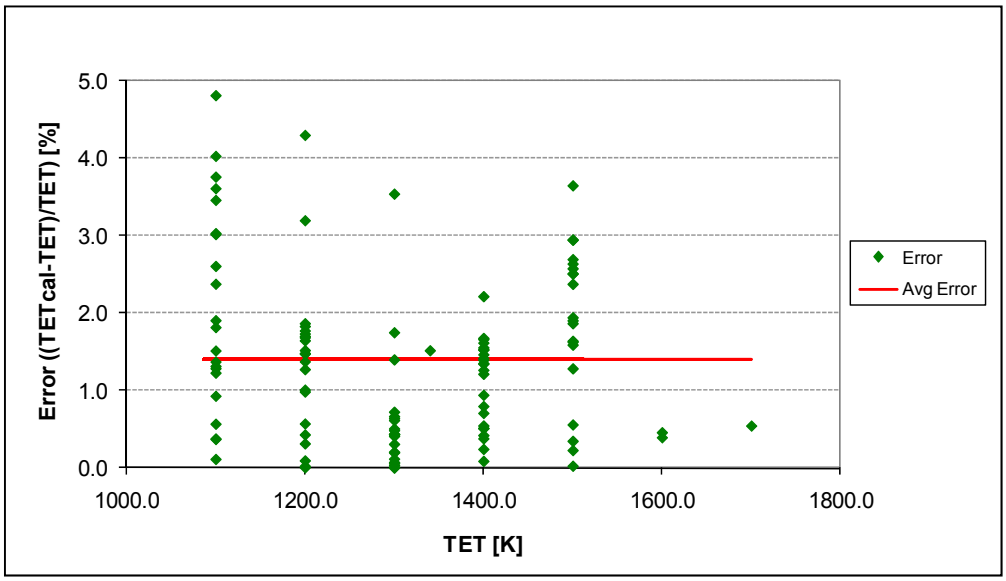


Figure 10-30. TET guesses and their associated errors